



Durabilité des composites carbone/époxy pour applications pales d'hydroliennes

Nicolas Tual

► To cite this version:

Nicolas Tual. Durabilité des composites carbone/époxy pour applications pales d'hydroliennes. Génie mécanique [physics.class-ph]. Université de Bretagne occidentale - Brest, 2015. Français. NNT : 2015BRES0057 . tel-01285006v2

HAL Id: tel-01285006

<https://hal.science/tel-01285006v2>

Submitted on 21 Dec 2018

HAL is a multi-disciplinary open access archive for the deposit and dissemination of scientific research documents, whether they are published or not. The documents may come from teaching and research institutions in France or abroad, or from public or private research centers.

L'archive ouverte pluridisciplinaire **HAL**, est destinée au dépôt et à la diffusion de documents scientifiques de niveau recherche, publiés ou non, émanant des établissements d'enseignement et de recherche français ou étrangers, des laboratoires publics ou privés.



université de bretagne
occidentale



THÈSE / UNIVERSITÉ DE BRETAGNE OCCIDENTALE

sous le sceau de l'Université européenne de Bretagne

pour obtenir le titre de

DOCTEUR DE L'UNIVERSITÉ DE BRETAGNE OCCIDENTALE

Mention : Génie mécanique

École Doctorale Des Sciences de la Mer

présentée par

Nicolas Tual

Préparée au Laboratoire Brestois de Mécanique
et des Systèmes et au Laboratoire
Comportement des Structures en Mer à l'Ifremer

**Durabilité des composites
carbone/époxy pour applications
pales d'hydroliennes**

*Durability of carbon/epoxy
composites for tidal turbine blade
applications*

Thèse soutenue le 9 Novembre 2015
devant le jury composé de :

Marie-Christine Lafarie

Professeur, ENSMA, Poitiers / *Examineur*

Frédéric Jacquemin

Professeur, Université de Nantes / *Rapporteur*

Xavier Colin

Professeur, ENSAM ParisTech/ *Rapporteur*

Dominique Perreux

Professeur, Université de Franche-Comté / *Examineur*

Bruno Castanié

Professeur, INSA de Toulouse / *Examineur*

Thomas Bonnemains

Maître de conférence, Université de Brest / *Examineur*

Nicolas Carrère

Enseignant chercheur HDR, LBMS ENSTA Bretagne / *Directeur de thèse*

Peter Davies

Ingénieur de recherche HDR, IFREMER / *Co-directeur de thèse*

Acknowledgment

Table of contents

Acknowledgment	3
Table of contents	4
Chapter I. General Introduction	9
1. Context of the study	10
1.1 Renewable marine energy, state of art	11
1.1.1 Tidal energy and Tidal turbines	11
1.1.2 Tidal turbine in the ocean environment.....	13
1.2 Composites for tidal turbine blade application	16
1.2.1 Composite materials: definition	16
1.2.2 Composites, a new possibility for tidal energy.....	17
1.3 Sea water ageing effects on composite materials	17
1.3.1 Damage in composites	22
1.4 Manufacturing process for tidal turbine blades	23
1.4.1 Blade composition	23
1.4.2 Vacuum infusion process	25
1.4.3 Resin transfer moulding process	25
1.4.4 Autoclave pre-preg process.....	26
2. Aims of the present study	28
Chapter II. Materials behaviour in the un-aged state	33
1. Materials of the study	37
1.1 Pre-preg material	37
1.2 RTM material	38
1.3 Infused material	39
1.4 RTM/Infusion resin	40
1.5 Choice of materials	41
1.6 Specimen preparation.....	42
2. Physico-chemical characterization	43
2.1 DSC	43
2.2 Density measurement.....	43
3. Mechanical characterization	46

3.1	Elastic properties	46
3.1.1	Tensile test procedure on 0° and 90° laminates	46
3.1.2	Test procedure and calculation on ±45° laminates	49
3.1.3	Four-point bending test.....	54
3.2	Viscoelastic behaviour	57
3.2.1	In-plane shear test on composites at different loading rates	58
3.2.2	In-plane shear creep test.....	58
3.3	Transverse crack kinetics test	59
3.3.1	Specimens preparation	59
3.3.2	Acoustic emission (AE)	60
3.3.3	Test procedure	61
3.3.4	Image processing.....	62
3.3.5	Results of intralaminar tensile cracking tests.....	63
3.4	Interlaminar fracture toughness	64
3.4.1	Double Cantilever Beam (DCB) test:.....	65
3.4.2	Interlaminar fracture toughness calculations and interpretation	68
3.4.3	Modified beam theory (MBT) method:	68
3.4.4	Compliance calibration (CC) method:	69
3.4.5	DCB results for the three unaged materials.	70
3.5	Out-of-plane strengths.....	72
4.	Microscopy observations.....	76
4.1	Optical microscopy.....	76
4.1.1	Infused composite	76
4.1.2	RTM composite	77
4.1.3	Pre-preg composite	78
4.2	Scanning electron microscopy (SEM)	80
4.2.1	SEM observation on Infused material in the unaged state	82
4.2.2	SEM observation on RTM material in the un-aged state	83
4.2.3	SEM observation on Pre-preg material in the unaged state	85
5.	Damage Modelling	87
5.1	Model based on physical parameters.	87
5.2	Damage model for the prediction of the crack density	88
5.3	Definition of the threshold of the damage	89
5.4	Definition of the effect of the damage	91
5.5	Definition of the kinetics of the damage development	92
5.6	Identification of the model	95
5.7	Validation on Carbon/Epoxy materials	96
5.8	Summary and conclusion on the damage model.....	99

Chapter III. Effects of sea water ageing on composite materials.....101

1.	Ageing in a marine environment: phenomena and mechanisms	105
1.1	The processes of water diffusion	105
1.1.1	Water diffusion mechanism	105
1.1.2	Sea water	106
1.2	The diffusion models.....	107
1.2.1	The Fickian approach.....	107
1.2.2	The Langmuir approach.....	110
1.3	Diffusion in composite materials	112
1.3.1	A first approach for diffusion in composites	113
1.3.2	Non Fickian diffusion in composites.....	115
1.4	Measurement of water concentration in polymers and composites	115
1.5	Temperature dependence of the diffusion process	116
2.	Accelerated sea water ageing	117
2.1	Necessity to accelerate ageing.....	117
2.2	Procedure and conditions used to accelerate ageing	117
3.	Characterisation of sea water ageing	120
3.1	Characterisation of the water diffusion into Pre-preg, RTM and Infused materials.....	120
3.1.1	Sea water diffusion neat epoxy resin	121
3.1.2	Sea water diffusion in three composite materials	123
3.1.3	Effect of material orientation on the diffusion process	127
3.1.4	Effect of composite thickness on the diffusion of seawater	129
3.2	Physico-chemical characterization.....	130
3.2.1	Change in Tg during ageing	130
3.3	Effect on elastic properties	131
3.3.1	Tensile properties of neat resin (40°C and 60°C)	131
3.3.2	Tensile properties of 0° and 90° laminates	133
3.3.3	Effect of sea water ageing on in-plane shear behaviour.....	136
3.4	Influence of ageing on viscoelastic properties.....	136
3.4.1	Tensile tests at different loading rates.....	136
3.4.2	Creep behaviour	137
3.5	Effect of sea water ageing on damage propagation	138
3.6	Effect on interlaminar fracture toughness.....	140
3.7	Effect of ageing on out of plane strength	142
3.8	Additional investigation on ageing	143
4.	Microscopy observation of ageing effects	145
4.1	Composite surface exposed to sea water	145

4.1.1	Infused material	145
4.1.2	Pre-preg material	147
4.1.3	RTM material	147
4.2	Fracture surface after longitudinal tensile tests.	148
4.2.1	Infused material	148
4.2.2	RTM material	150
4.3	Fracture surfaces after transverse tensile tests.	152
4.3.1	Infused transverse	152
4.3.2	RTM transverse	153
4.3.3	Pre-preg transverse	154
4.4	Interlaminar fracture surface after DCB test	156
4.4.1	Infused material	156
4.4.2	RTM material	158
4.4.3	Pre-preg	160
5.	Influence of manufacturing process	164
5.1	Influence of manufacturing process on the kinetic of diffusion	164
5.2	Effect of manufacturing process on properties after water ageing	167
5.2.1	Tensile longitudinal and transverse strength	167
5.2.2	Shear strengths and modulus	168
5.2.3	ILSS shear strength for UD and QI materials	169
5.3	A first conclusion on sea water ageing in composites for tidal turbine	171
	<i>Chapter IV. Multi-physics modelling of diffusion/damage</i>	<i>176</i>
1.	Water diffusion modelling in composites	179
1.1	Model presentation	179
1.2	Identification of model parameters	182
1.3	Sensitivity study of the model	185
1.3.1	Influence of mesh size on diffusion model	186
1.3.2	Influence of fibre content on diffusion model	187
1.4	Validation and optimisation of the model	188
1.4.1	A first comparison between FE calculation and experimental results	188
1.4.2	Investigation of fibre arrangement	189
1.4.3	Modelling diffusion on Infused and RTM materials at different temperature	193
1.4.4	Prediction of sea water diffusion on Infused material for lower temperature	195
1.5	Application to a tidal turbine blade	197
2.	Modelling of damage after sea water ageing	201
2.1	Model key elements after sea water ageing	201
2.2	Comparison between modelling and experimental results	202

3.	Modelling of damage/diffusion coupling.....	204
3.1	Modelling of damage/diffusion coupling.....	204
3.2	First experimental approach on damage/diffusion coupling.....	207
3.2.1	Experimental procedure.....	207
3.2.2	First results and additional investigations.....	209
Chapter V. General conclusion.....		214
1.	Conclusion	215
1.1	Effect of accelerated sea water ageing on different composites	215
1.2	Modelling composite long term behaviour.....	216
1.3	Material choice for tidal turbine blades.....	217
2.	Perspectives.....	218
2.1	Sea water ageing at lower temperature	218
2.2	Interface degradation and diffusion	218
2.3	Coupling diffusion under loading/damage/diffusion	219
2.4	Sea water ageing and fatigue.....	219
2.5	Composites protection, abrasion, impact, shock.....	220
Appendix Chapter II.....		223
Appendix Chapter III.....		226
Appendix Chapter IV		240
Appendix Chapter V		245
Figure table caption		246
Table caption		256
References		258

Chapter I. General Introduction

Table of contents

Acknowledgment	3
Table of contents	4
Chapter I. General Introduction	9
1. Context of the study	10
1.1 Renewable marine energy, state of art	11
1.1.1 Tidal energy and Tidal turbines	11
1.1.2 Tidal turbine in the ocean environment.....	13
1.2 Composites for tidal turbine blade application	16
1.2.1 Composite materials: definition	16
1.2.2 Composites, a new possibility for tidal energy.....	17
1.3 Sea water ageing effects on composite materials	17
1.3.1 Damage in composites	22
1.4 Manufacturing process for tidal turbine blades	23
1.4.1 Blade composition	23
1.4.2 Vacuum infusion process	25
1.4.3 Resin transfer moulding process	25
1.4.4 Autoclave pre-preg process.....	26
2. Aims of the present study	28

1. Context of the study

Seventy percent of the surface of the earth is covered by the oceans, and these marine resources represent an important potential source of energy. For instance the natural energy dissipated by ocean tides has been estimated to be approximately 25 000 TWh/year. As a comparison the world consumption of electricity in 2011 was estimated to be 17 800 TWh by the International Energy Agency [1]. As a consequence the potential to extract energy from the marine environment is gigantic. Naturally this theoretical potential is not totally exploitable for different reasons including environmental, economical, and technical limitations. Extraction of renewable marine energy requires specific technologies. In the past 10 years many marine energy structures have been developed but presently only a small number of mature technologies are emerging. These projects have been matured thanks to long R&D and prototype development and are now close to commercial exploitation. For tidal turbine technology, the blades are the central element in extracting the power of the sea. Special attention to their design, and in particular to material selection, is thus essential to ensure their durability in such a severe environment.

Contexte de l'étude

Soixante-dix pourcent de la surface de la terre sont recouverts par les océans, ces ressources marines représentent d'importantes sources potentielles d'énergies. Par exemple, l'énergie naturellement dissipée par les courants des marées a été estimée à environ 25 000 TWh par année. En comparaison la consommation mondiale en électricité a été évaluée à 17 800 TWh, par l'Agence Internationale de l'Energie en 2011 [1]. En conséquence, le potentiel pour extraire l'énergie marine est gigantesque. Naturellement, ce potentiel théorique n'est pas totalement exploitable pour différentes raisons, notamment pour des motifs environnementaux, économiques ou du fait de limitations techniques. L'extraction des énergies renouvelables des mers requiert des technologies spécifiques. Dans les dix dernières années, de nombreuses structures pour les énergies marines renouvelables ont été développées, mais actuellement peu de ces technologies ont abouti. Certains de ces projets ont réussi à émerger grâce à de longs procédés de R&D. Certains de ces prototypes développés sont proches des versions finales pour une future commercialisation. Pour les technologies hydroliennes, les pales sont les éléments centraux permettant l'extraction de la puissance de la mer. Une attention particulière pour leur conception ainsi que le choix de leurs matériaux sont ainsi nécessaires pour assurer leur durabilité dans un environnement aussi sévère.

1.1 Renewable marine energy, state of art

Renewable marine energy can be defined as the resource that can be extracted from the sea in order to produce a form of energy such as electricity without reducing the resource. These resources can be exploited in different forms using different technologies to produce electricity:

- Tidal current energy
- Waves energy
- Offshore wind energy
- Ocean thermal energy conversion

This list is not exhaustive but represents the main projects currently being developed. Other technologies are being evaluated, and many reviews describe marine renewable energy systems [2], [3], [4], [5]. However in this study we will only focus on tidal turbine devices.

1.1.1 Tidal energy and Tidal turbines

Tidal energy is the world's most predictable renewable energy source [6], [7], and with increasing demands on the earth's natural resources, it offers a reliable and sustainable opportunity for energy generation [8]. Tidal energy is produced by extracting the kinetic energy contained in flowing water resulting from the changing tides in order to turn a turbine to generate power. Tides are the rise and fall of sea levels, determined by the position of the moon and the sun and their gravitational pulls on the earth. There are generally two high and two low tides per day, but in some areas, there may only be one of each [9]. Factors that can impact on the scale of tides include the underwater landscape, water depths and the surrounding coastline.

Converting the power of the tides into energy is not a new idea, we have been using water to generate energy since Roman times through tide mills [10], [11], and more recently in 1966 with the Rance tidal power station, [12]. Today, tidal technology is developing rapidly, although the principle behind the different types of technologies is the same. Tidal plants, whether they are tidal turbine farms, tidal fences or tidal barrages, utilise the flow of water to turn turbines to generate electricity. However generation does not take place 24 hours a day, but tides rise and fall every day and can be reliably mapped many years in advance, making tidal energy a stable and predictable method of energy generation.

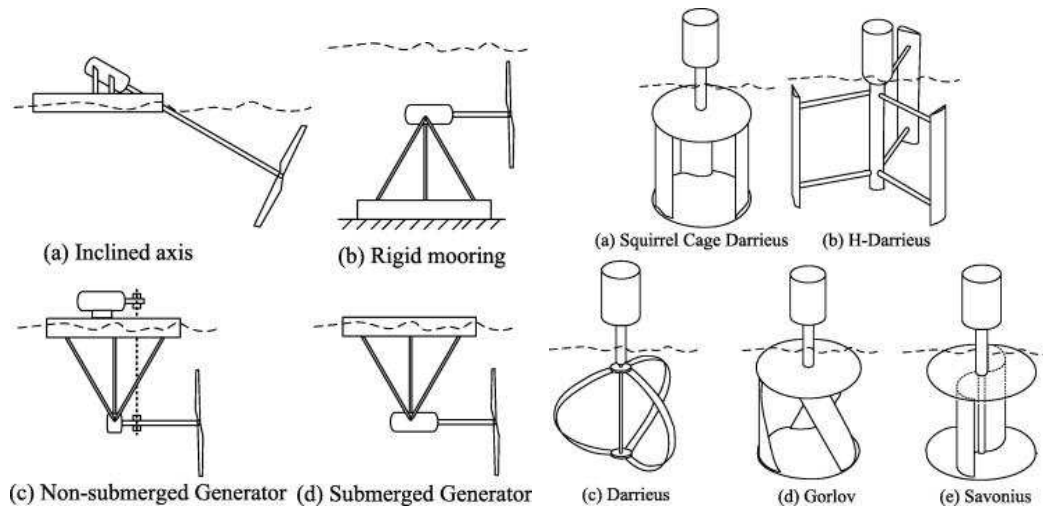


Figure 1: Illustration of possible technologies used for horizontal and vertical axis turbines [13].

Horizontal and vertical axis tidal turbines with different designs and technology have been widely developed in the last 10 years. These technologies use blades that are positioned either in parallel (horizontal) or perpendicular (vertical) to the direction of the flow of water [13] as illustrated in Figure 1. Most current designs are using blades that are connected to a central rotor shaft, linked to a gearbox, finally connected to the generator of electricity as shown for two recent technologies in Figure 2.



Figure 2: Sabella D10 Tidal turbine (a) and CoRMAT tidal turbine with 4 m RTM blades, courtesy of Airborne Marine and Nautricity Ltd (b).

Other systems, such as open-centre turbines have a different design, as presented in Figure 3. The blades are assembled on an inner-ring, this technology has been developed mainly by OpenHydro and DCNS. The turbine features a horizontal axis rotor, with power take-off through a

direct drive permanent magnet generator. It is principally composed of two components, the rotor, which is the only moving part in the turbine and the stator, which encompasses the majority of the generator components.



Figure 3: Example of open centre tidal turbine blade developed by OpenHydro and DCNS for the EDF project (a) [14] and the Bay of Fundy (b) [15].

The blades of horizontal or vertical turbines can also be enclosed within a duct. As for the blades, this duct requires development and material selection, for instance composites. Due to the enclosure, the ocean current is concentrated and streamlined so that the flow and power output from the turbines increases. Based on an overview of existing tidal current projects, most tidal turbine projects are based on horizontal axis technology (76%). Only 12% of current projects use vertical axis turbines, (review by International Renewable Energy Agency (IRENA) in 2014), [16].

Horizontal axis turbines are thus the main technologies in tidal energy converters and at first sight appear very similar to wind turbines from a concept and design point of view, but tidal turbines will evolve in very different environmental conditions [17].

1.1.2 Tidal turbine in the ocean environment

Choosing a tidal turbine exploitation site and environment is also crucial, and suitable tide velocity, site exposure to storms, and swell periodicity must all be considered [18], [19], [20]. Site bathymetry is also important in order to predict possible turbulence due to the seabed [21], [22]. Tidal turbine structures are subject to many forces such as ocean tides, waves, and storms but also to

various marine aggressions, such as sea water and corrosion. As water has a high density compared to air, applied loads on the tidal blade are considerable. It has been estimated [23] for a 1MW turbine operating in a 4.5 knot tide that 900 tons/s of water pass through the turbine rotor.

There have been some published studies on the design of tidal turbine blades, which estimate the applied loads as a function of the tide velocity and blade geometry, [24], [25], [26]. Structures for tidal energy must also be designed to withstand transient forces caused by turbulence and passing surface waves. Wave loads are one of the main contributors to fatigue loads of tidal turbine blades, [27]. As a consequence, mechanical loads on marine energy converters are cyclic (due to the motion of the waves for wave energy converters or the action of tides on tidal turbines). A thorough understanding of the fatigue behavior of the moving parts such as turbine blades is therefore essential. A previous study [28], [29], on glass/epoxy composites has highlighted the sensitivity of durability to the choice of components (fibre, resin, surface treatment of fibres).

The total kinetic power in a marine current turbine has a similar dependence to that of a wind turbine, and is governed by the following equation Eq.1. With ρ the density of the fluid, A is the area in contact with the fluid v is the effective flow velocity or the component of the fluid flow velocity perpendicular to the turbine and P is the energy flux.

$$P = \frac{1}{2} \rho A v^3 \quad \text{Eq. 1}$$

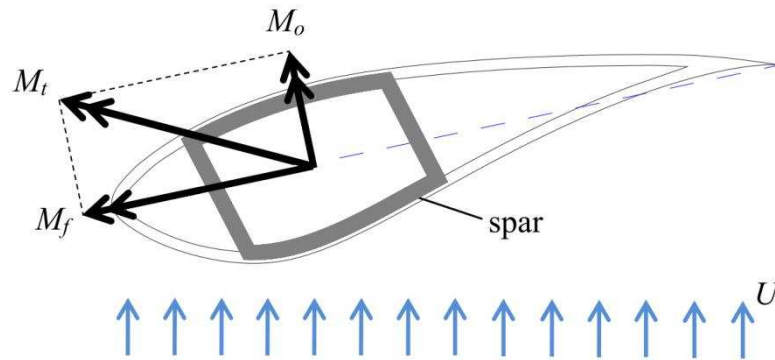


Figure 4: Blade cross-section at the root with acting bending moments: M_f – flap wise moment, M_o – in-plane moment and M_t – total moment, [30].

As a comparison, in the case of wind turbines centrifugal loads are dominating along the blade, and these forces tend to restrict bending. In tidal turbines, however, due to water density, it is the

bending loads which dominate. Figure 4 shows an example of the bending moment distribution in a specific tidal turbine blade cross-section with a spar box, [30] .

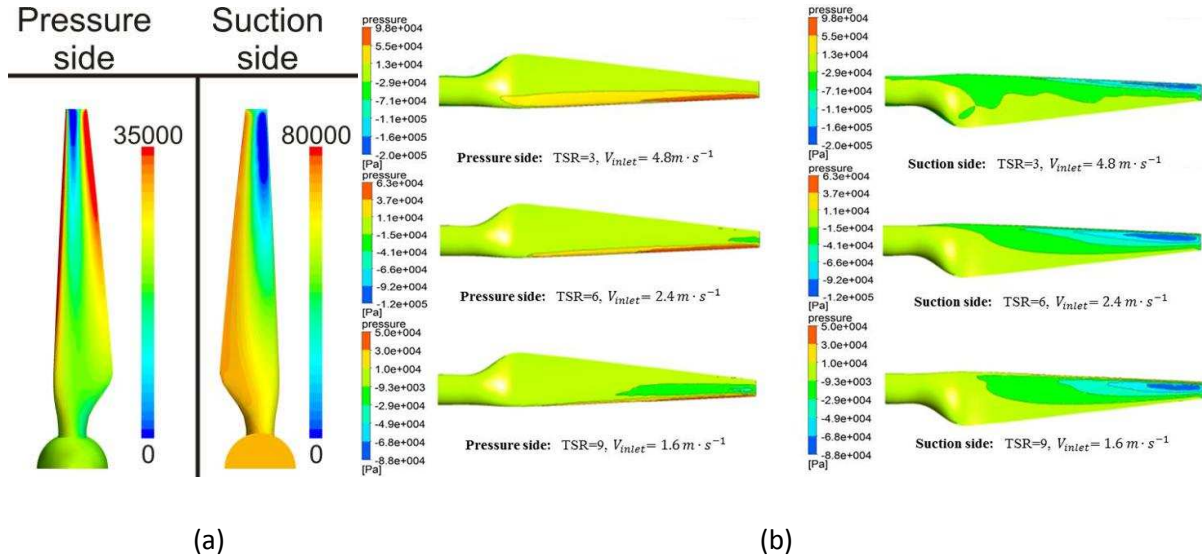


Figure 5: 10 m blade pressure for extreme operating condition [31] (a), and pressure on the blade surface (pressure and suction side) for different tide velocities [25] (b).

Marine turbine blades are relatively short and thick, in order to keep bending loads manageable. Because marine turbines are limited in terms of size (rotor diameter) and rotation is slow, there is little centrifugal force to react with the bending moment. Handling the load distribution in such complex structures evolving in a marine environment presents a real challenge. In different studies the authors have presented positive and negative pressure distributions on both tidal turbine blade sides. For instance Figure 5 illustrates the distributions for different loading cases. In Figure 5 (a) the blade is exposed to extreme operating conditions [31] while in Figure 5 (b) another blade design is loaded with different tide velocities [25]. As shown here, the pressure on the blade is non-uniformly distributed depending on operating conditions, tide velocity, side of the blade and design.

Composite materials are good candidates for tidal turbine blade applications. Inherently orthotropic, the blade can therefore be optimised to the loading, reducing weight, cost and improving efficiency of the turbine. Composite materials have excellent strength-to-weight properties, and the manufacturing process allows complex blade shapes to be produced.

1.2 Composites for tidal turbine blade application

Over the last 50 years composite materials have found many applications in the maritime domain, particularly in the yachting and offshore energy industries [32], [33], [34], [35], [36]. Composite materials are used in many marine structures and new applications are being developed. Tidal turbines offer an exciting opportunity to use these materials to exploit ocean current flows to generate energy.

1.2.1 Composite materials: definition

A composite material is a complex material resulting from the synergy of two or more components as presented in Figure 6. The new material created has a heterogenous nature but this material provides new properties which it is not possible to obtain with one component alone. In the general case composites are composed of two components, matrix and reinforcement. The matrix is the binding element of the material. The nature of the matrix is varied, it can be a thermoplastic or thermoset resin for instance polyester, vinylester and epoxy resin are widely used in the marine domain. The other main component of a composite material is the reinforcement, which is usually fibres for instance glass, carbon, polyester or aramid. This list of fibres is non-exhaustive, but for marine composite application glass and carbon fibres are widely used. Additionally some fillers can be added to enhance specific properties.

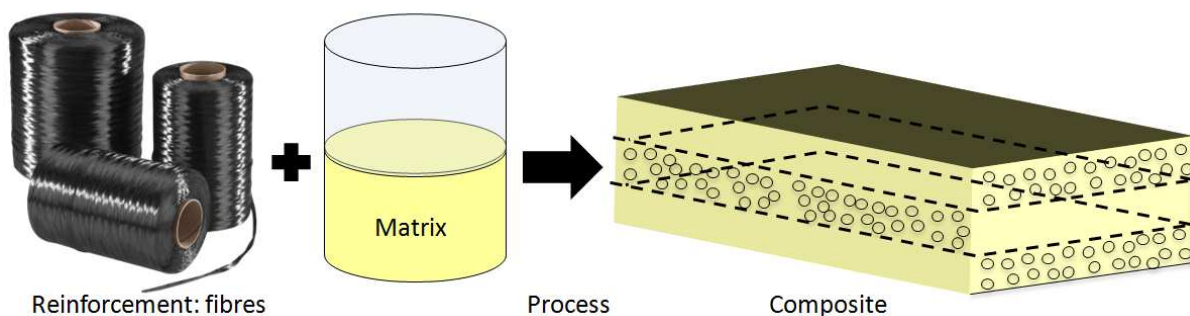


Figure 6: Composite reinforcement and matrix used for composite laminates.

The matrix serves to distribute the fibres and ensure the load transfer between them. In composite laminates the orientation of the fibres allows the material to respond to a complex load distribution in a structure, but this material orientation induces anisotropy in composite materials.

1.2.2 Composites, a new possibility for tidal energy

At the beginning of renewable marine energy development, some designers considered that it was necessary to produce marine rotors in steel, in order to ensure the stiffness of the structure. However, the production of compound-curved profiles in steel was very expensive. Moreover, steel is heavy and susceptible to corrosion induced by sea water.

The interest in the use of composite materials for tidal energy convertor structures is based on the potential improvements in hydrodynamic and structural performance. In addition to the advantages of high strength-to-weight and stiffness-to-weight ratios, the anisotropy of composites can be designed to allow three dimensional tailoring of the blade deformation [37]. The reliability of these components, in a very severe environment, is crucial to the profitability of tidal current energy systems and composite material offer good resistance to corrosion [35] and fatigue [38]. Some previous studies in the literature present the structural design procedure of tidal turbine blades using composite laminates [31], [39]. Other studies have described the characteristics and possibilities in order to apply composite materials to tidal turbine blade structures [40],[41].

The majority of tidal turbine developers (MCT SeaGen, Alstom/TGL, Atlantis, Sabella...) have preferred carbon fibre reinforced blades, and the composite thicknesses are very large, especially in the area of connection between blade and hub (tens of millimetres). Some developers have preferred glass reinforcement (OpenHydro/DCNS) or combinations of the two reinforcements. For both types of material it is essential to investigate the influence sea water on material behaviour [42], [43].

1.3 **Sea water ageing effects on composite materials**

The absorption of water molecules in polymer composites is known to have important effects on their final performance [44], [45], especially in their long-term exploitation [46], [47]. By the organic nature of the matrix resin, often an epoxy, long immersion in sea water can induce both physical and chemical changes [48]. Experimentally it is possible to measure the evolution of water concentration in polymer and composite materials [49]. There are various experimental methods but the simplest and most popular is based on sample weight measurements in the dry (w_0) then in wet (w) conditions throughout the immersion time of the samples. Then it is possible to determine the water mass fraction : $m = (w - w_0) / w_0$, and quantify the diffusion behaviour of water in the material

[48]. The kinetics of diffusion can change during the service life of composites in operation, damage due to the diversity of mechanical loads may impact and accelerate the diffusion of water inside the composite structures as damage can create new pathways for water entry [50], [51]. More details about the different water diffusion processes will be discussed in Chapter III. However, water molecules have a strong affinity with specific functional groups of cured epoxy [52]. Musto et al. [53] have described the interaction between water and specific epoxy resin groups. The analysis presented in Figure 7 highlights the interaction of water with interacting epoxy groups during sorption (water affects polar group species in the polymer by hydrogen bonding with these species). As presented, IR (Infrared) peaks shift during water sorption and the intensity of the absorbance changes, which is the consequence of the interaction between water molecules and the epoxy network [54]. It has been shown that some epoxy resin components are strongly hydrophilic, for instance the amine groups [55],[56], which play an important role in the curing process of many epoxy systems [57].

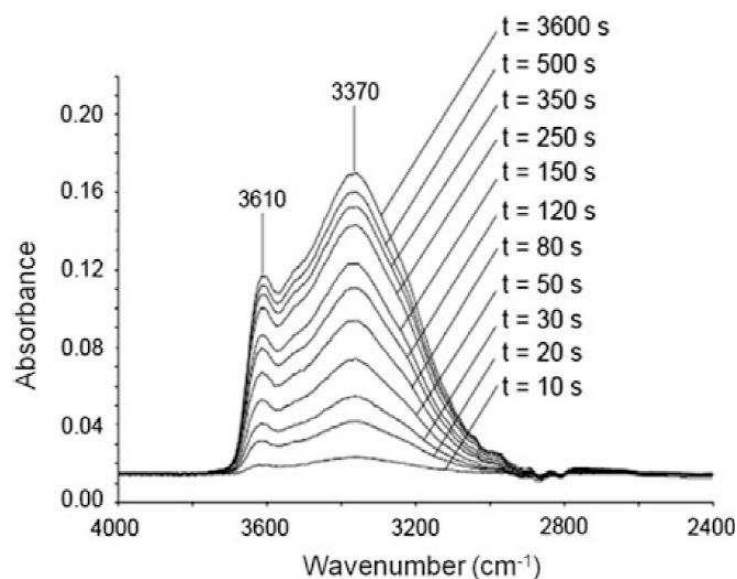


Figure 7: Example of subtraction Fourier transform infrared spectroscopy after different times of water exposure for epoxy resin [53].

Swelling and plasticization are the main physical consequences of water absorption on polymer structures, reviews can be found in the following references[58], [59], [60]. In the case of carbon fibre reinforced epoxy material, the ageing of the material will be mainly controlled by the matrix, which is highly sensitive to water compared to the carbon fibres.

Plasticization is a reversible phenomenon corresponding to a modification of the structure of the polymer and results in a lowering of the glass transition temperature (T_g) [53],[61]. This mechanism of polymer degradation is strongly linked to the T_g . The reduction of the T_g induces a reduction of the yield stress making plastic deformation easier. As a consequence, a reduction in moduli and failure stress and an increase in elongation at failure will appear in a polymer exposed to water.

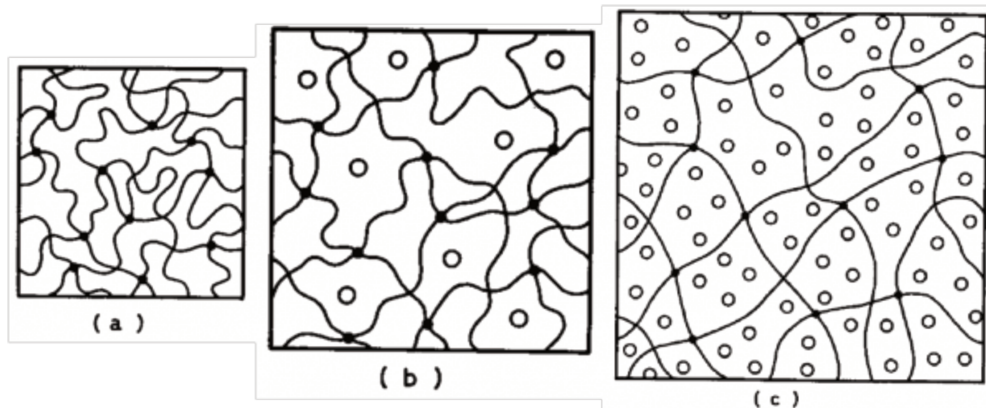


Figure 8: Representation of swelling due to water absorption between polymer chains at different steps of absorption, illustration from [62] (water molecules are represented by the black circles).

Swelling is caused by the penetration of water into polymers, as a consequence volume changes will occur. The Figure 8 illustrates the swelling phenomena induced by water entry in the polymer network [62]. Swelling acts as a negative pressure on the material, in the literature a hygroelasticity coefficient has been proposed in order to express swelling strain as a function of the mass of water absorbed,[63],[64],[65].

At the composite scale, swelling can create interfacial cracks and fibre/matrix debonding, [66]. However stresses induced by swelling may also reduce the residual stresses induced during curing and hence the combined effect may be beneficial [67]. For the case of unidirectional composites, swelling strain can only develop in the direction perpendicular to fibres. Some authors have shown that the swelling yield y/m , where $y = 100 (v - v_0)/v_0$ and m is the mass of water uptake, is low at low water activities and begins to increase at mass uptakes for an average value of 0.4–0.6 for various epoxy-carbon composites [68],[69].

Water also affects the composite fibre/matrix interface and may cause a loss of interfacial integrity [70]. The interaction between water and the composite interface can play an important role in the durability of composite materials, for instance by accelerating the diffusion process or

reducing the final strength of the material [71],[72]. The diffusion process at the fibre/matrix interface is different to matrix diffusion. Water molecules diffuse first into the interface region through the matrix, matrix micro-cracks and voids.

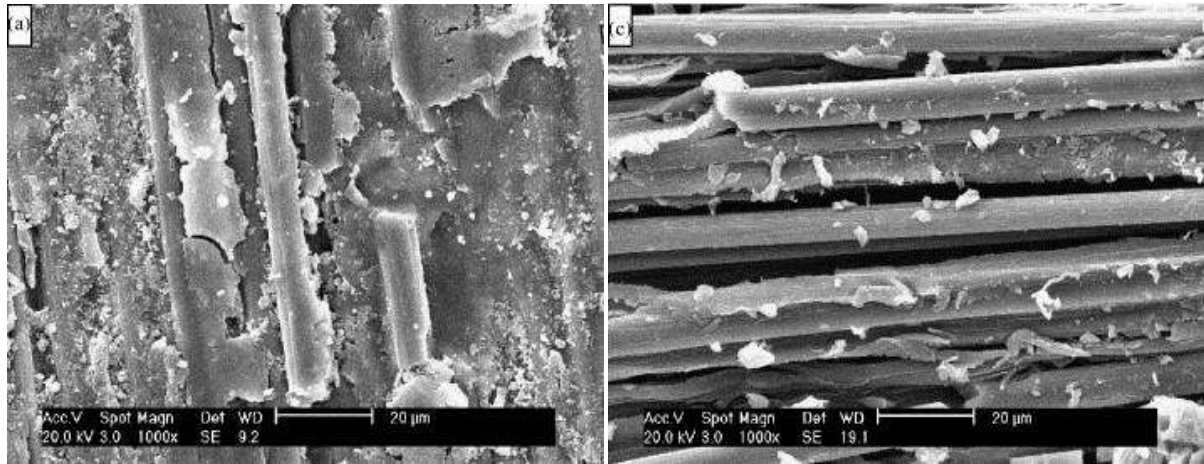


Figure 9: Shear fracture surfaces of the dry (a) and saturated specimens (c), saturated carbon/epoxy specimens were aged 37 days in distilled water [73].

The absorbed water molecules then diffuse along interfaces and through the matrix, inducing swelling phenomena in the matrix. As previously stated, the carbon fibres neither absorb water nor swell. As a result of the difference in expansion, internal stresses may appear in these interface regions. But at the same time, the absorbed water molecules weaken the fibre/matrix bonds by forming hydrogen bonds with carbon fibres, which disturb and weaken the fibre/matrix bonding. The internal stresses and interface weakening may eventually result in interface failure [73]. Figure 9 presents SEM fracture surface observations of carbon/epoxy materials before and after water ageing in water at 37°C, taken from the work of Luo et al. [73]. These reveal interface debonding by comparing the shear fracture surfaces of saturated specimens with dry samples.

The interface debonding caused by water ageing has been studied by many investigators. Komai et al. have shown that water absorption induced a loss in strength of the fibre/matrix interfaces of UD reinforced carbon/epoxy composites [74]. Selzer and Friedrich highlighted that fibre/matrix bonding weakens with increasing moisture content [75]. Buehler and Seferis have observed interface delamination, due to water absorption in carbon and glass epoxy composites [76].

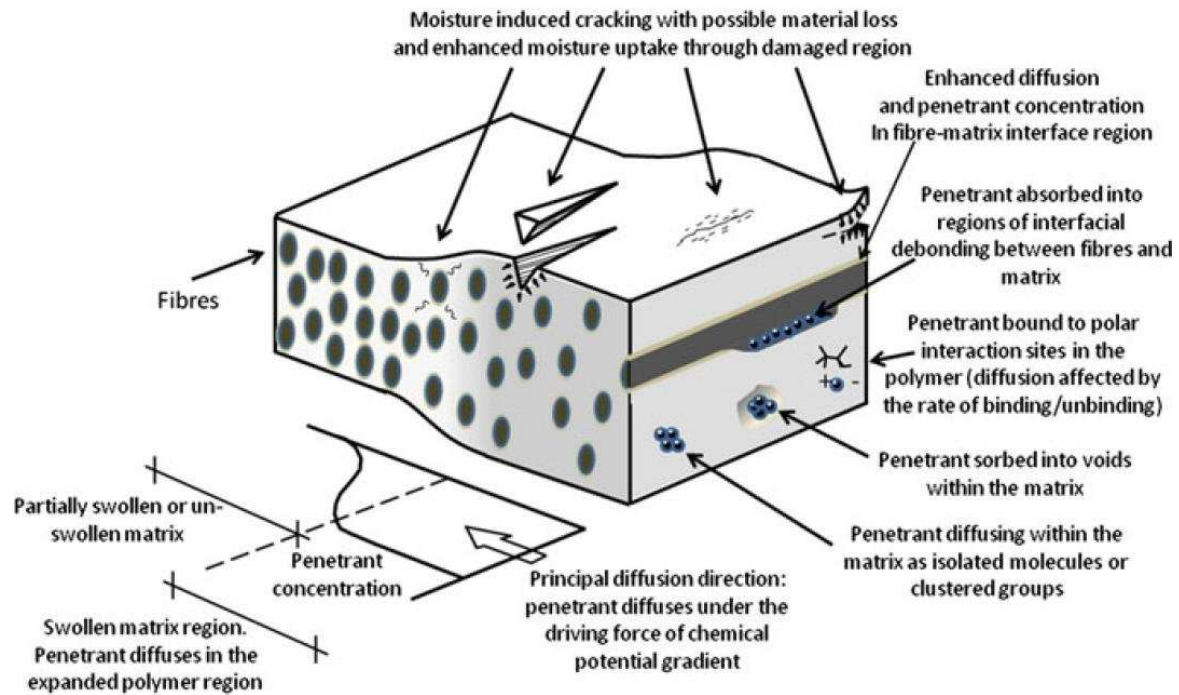


Figure 10: Schematic illustration of possible moisture sorption locations and mechanisms (readapted from [77] by [53]).

The Figure 10 summarizes the different possible degradation mechanisms induced by water in composite materials. A good review of the different interactions between composites and water molecules has been proposed by Bond and Smith [77]. However, irreversible chemical reactions (oxidation) can also occur during sea water immersion, due to reactions with water or oxygen [78],[79]. As presented in Figure 10, the voids can also play a role in the diffusion process. Several studies have concluded that voids are a major factor influencing the final water content in composite materials [80], [81], but the water in voids may not affect mechanical properties significantly.

To sum up, various degradation mechanisms due to sea water ageing, in the matrix or at the interface between fibres and matrix, will affect the final properties of the composite material. Depending on exposure conditions (time, temperature, and mechanical loading) the composite may be subject to depression of T_g during sea water immersion. Mechanical properties can also be degraded. After a long immersion it is possible to observe a drop in the stiffness, for instance the transverse and shear moduli may be reduced. In addition a reduction of composite strengths can also be expected, and properties in fatigue can also be affected. Several good reviews in the literature deal with these aspects [82],[83].

1.3.1 Damage in composites

Sea water ageing is not the only factor which can affect and degrade the composite during its service life. In such complex structures as tidal turbine blades, the material will also be subjected to a range of mechanical loads which can introduce different types of damage. These can be defined as the irreversible changes in the microstructure of the material, in contrast to plasticisation and swelling which are reversible.

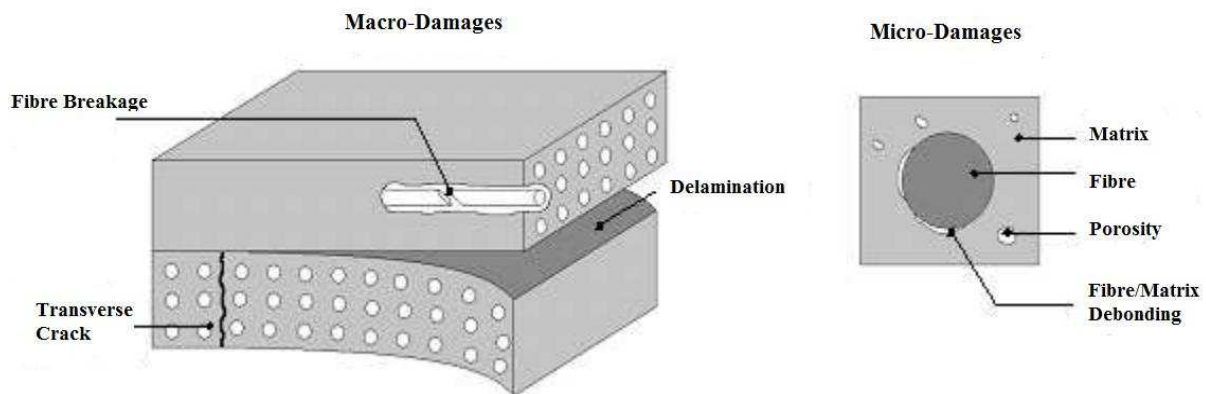


Figure 11: Illustration of the different type of damage in laminated composites [84].

Damage may affect the final strength of the composites. At the micro scale some local failure at the interface between fibre and matrix such as debonding may occur. At the scale of the ply intra-laminar cracks and fibre breakage can appear. Finally at the macro scale delamination, which is an inter-ply debonding, can also appear. These damage phenomena are illustrated in Figure 11 ,[84]. Damage may also develop in composites when they are subjected to fatigue loading, this subject has been treated in [85].

The choice of matrix and fibres, is critical for tidal turbine blades, as these structures will be immersed for two or three decades. Long immersion in water will generate a slow process of degradation which may impact the final strength of these structures and hence change the safety factors. Moreover, it is important to select the manufacturing process (and the curing process) carefully. Parameters such as, fibre content, void content, glass transition and internal stresses are strongly dependent on the manufacturing process.

1.4 Manufacturing process for tidal turbine blades

In the industrial context of composite tidal turbine blades, there are various manufacturing processes. In the first stage of tidal turbine development, blades were produced in small numbers as prototypes but the aim of the tidal industry is to produce tidal turbine in series (small or large) at low cost. There are several manufacturing options.

1.4.1 Blade composition

The other key element in choosing how to manufacture a blade is its composition. Depending on the design, cost, size and technological choices the blade could be composed of different elements such as those presented in the Figure 12, which are produced separately then assembled, or it could be produced in one shot.

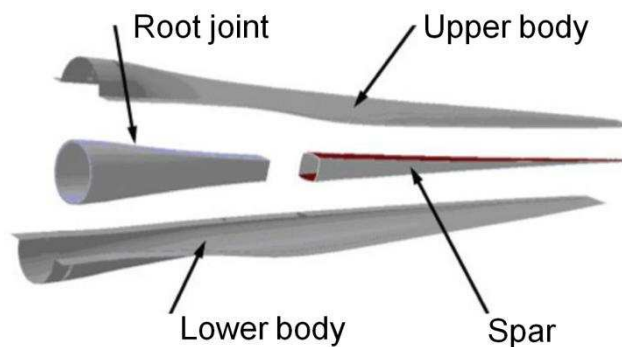


Figure 12: Possible composition of tidal turbine blade

A tidal turbine blade could be manufactured from several parts, for the example above the spar box is manufactured in high performance composites, this part ensures the stiffness of the blade assembly, generally this part is quite thick especially in the root joint. Surrounding this central element the blade body is thinner and ensures the hydrodynamic response of the blade. This type of technical solution requires all these elements to be assembled together with structural adhesive. In order to avoid this assembly, where the adhesive could be a critical point for the durability of the structure, some tidal turbine developers have preferred to produce tidal turbine blades using a one shot process. As a consequence the blade can be manufactured in only one component without a joint.

At present details of manufacturing processes of tidal turbine blades are very rare due to industrial secrecy and competition between the different projects. Nevertheless it is possible to find some examples illustrating the different manufacturing possibilities. For instance the tidal turbine blades of the French company Sabella [86], have been manufactured using different technologies. As presented in Figure 13 below, this type of blade is composed of different elements. The blade bodies (see Figure 13 (a)) have been manufactured using a vacuum infusion process. But the spar box including the root, has been manufacturing using pre-preg composite and an autoclave cure, Figure 13 (b).



Figure 13: Sabella tidal turbine blade during manufacturing, (a) one side of the blade body before vacuum infusion process and (b) final assembly of spar box and blade bodies [86].

In a different approach Airborne Marine developed an RTM (Resin Transfer Moulding) process in order to produce tidal turbine blades for another turbine project [87]. The 4 meter blades presented in Figure 14 below, have been manufactured using a one shot RTM process with embedded insert technology. This concept avoids bolting or adhesive.



Figure 14: Airborne Marine tidal turbine blades for the Tocado turbine, these composites blades have been manufactured using the one shot RTM process [87].

Some details about the major manufacturing processes will be given in the following sections.

1.4.2 Vacuum infusion process

Vacuum infusion is an open mold process. Many composite structures are manufactured with this technique, for instance large structures such as wind turbine blades or boat hulls. One of the mould surfaces is replaced with vacuum bagging or a flexible complimentary mold (silicon part).

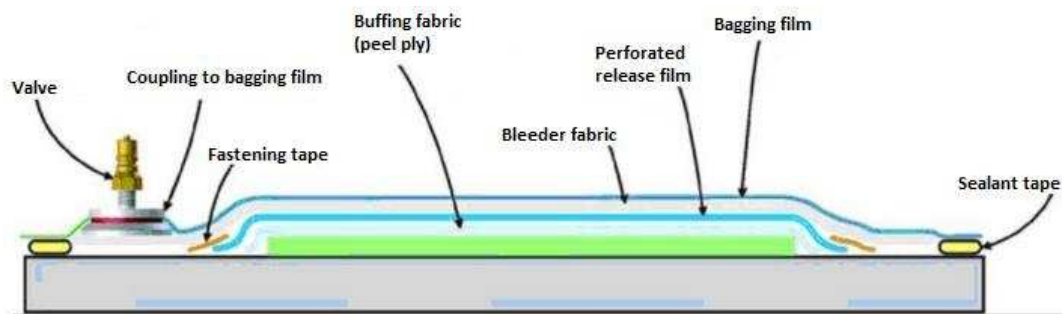


Figure 15: Infusion process [88].

The aim of this method is to diffuse the resin into the reinforcement by capillarity, assisted by the vacuum applied on the dry fabrics. Specific low viscosity resins are used for this application. The flow of resin can be eased by draining layers, breather films are also added to drain the air. The principle vacuum injection method is shown in Figure 15. This process allows a good composite quality and production of large and thick parts for small and medium series.

1.4.3 Resin transfer moulding process

RTM technology allows tidal blades to be manufactured as a single, integrated composite part. Resin Transfer Molding is the process of injecting resin into a closed mould already containing the reinforcement, Figure 16. RTM parts have two finished surfaces, thanks to the two part mold. Reinforcement mat, fabric or UD layers are placed in the mould, which is then closed and clamped. A low-viscosity resin is pumped into the mold helped by the vacuum. Molds for this low-pressure system are usually made using composite material or aluminium. The mold can be temperature regulated in order to facilitate impregnation of the resin in the reinforcement but also to cure the

resin at the end of the process when the mold is filled. This technology is suitable for medium volume production of large components.

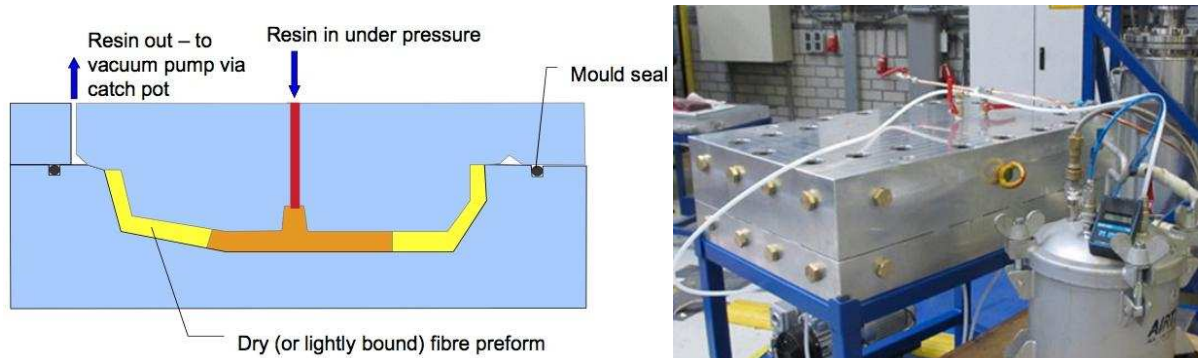


Figure 16: RTM process method (a) [89] and the RTM mold developed by Airborne Marine to produce test plates (b) [90].

Additionally, some RTM processes have been developed for injecting resin at low pressure. These have been developed for better structural performance and faster curing and to improve manufacturing of thick composite structures such as tidal turbine blades. However, these faster processes may induce residual stresses and deformations.

1.4.4 Autoclave pre-preg process

For advanced composites, autoclave processes using pre-impregnated composites are widely used. Autoclave moulding has been the process of choice for the aerospace industry, but also more recently for racing yachts and advanced marine applications. This process uses pre-impregnated uni-directional plies or woven fabrics, which have been partially cured or beta-staged. One disadvantage is that pre-preg has to be kept in a freezer in order to prevent the resin from curing. Multiple prepreg plies are laid down onto a tool surface or a mold with the pre-defined fibre orientations in order to build up the required thickness. Then layers are covered with a release film, breather fabric and a vacuum bag or silicon pressure bag. Figure 17 (a) presents the different components used for the autoclave process. The air is drawn out from the bag to create a vacuum. The mold and part are heated to elevated temperature (100 to 180°C) and pressure is applied (up to 15 bars) to cure the resin in the autoclave, as presented in Figure 17 (b). Regular debulking cycles, close temperature control and sufficient hydrostatic pressure on the part during curing are the basic requirements for achieving high quality parts. The productivity of autoclave moulding is generally quite low since the

manual lay-up, bagging and demoulding cycles consume significant labour and time. Also, the material costs of pre-preg are higher than for the other processes.

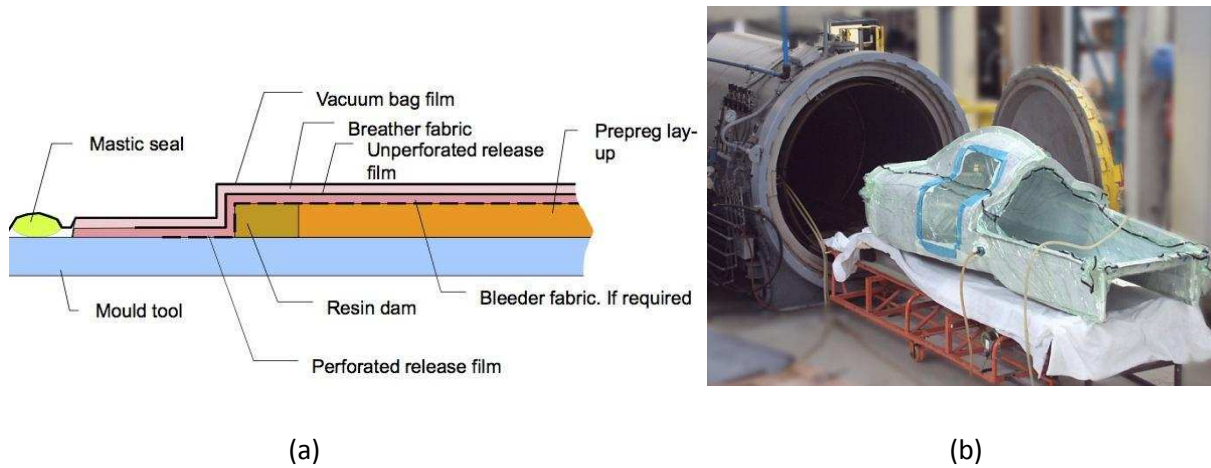


Figure 17: Pre-preg process tooling and components(a) [89] and an example of a part entering the autoclave (b) [91].

2. Aims of the present study

In the first part of this chapter, the principal causes and consequences of sea water ageing on composites materials have been presented. From one material to another the final durability in sea water environment may differ significantly, due to material choice and processing. As a consequence there is a need to understand and evaluate the impact of sea water immersion on composite materials for tidal turbine blades. It is then necessary to predict the changes in material and structural behaviour throughout the service lives of these structures. In the literature few sea water ageing studies have been performed on carbon/epoxy material compared to glass/epoxy. Moreover studies concerning sea water ageing of carbon/epoxy materials for tidal turbine blade are very rare. As a consequence it is difficult to find a data base concerning the evolution of those materials properties during long exposure to sea water. Additionally, few studies have examined the influence of the manufacturing process on sea water ageing phenomena.

The first objective of the present study is therefore to characterize the influence of long term immersion in a marine environment on carbon/epoxy materials intended for tidal turbine blades. To achieve this first objective three different carbon/epoxy composites, which are all good candidates for turbine structures, have been studied. In **Chapter II** the baseline material properties before ageing are presented. This first characterisation is essential, in order to understand composites mechanical behaviour before sea water ageing, and to provide the input data necessary for the development of predictive models in the un-aged state. To age these materials in a reasonable time, it was necessary to develop an accelerating ageing procedure in sea water. In order to attain this goal, sea water ageing has been performed at temperatures above service temperature. A discussion of the pertinence of this accelerated ageing procedure is proposed. Then, to investigate the influence of sea water on the three composites, a characterization procedure has been developed. First, the diffusion of seawater has been studied, these results are necessary to determine ageing times but also provide the input data for diffusion modelling. Then the evolution of the materials' mechanical and physico-chemical properties has been investigated both before immersion and after different sea water ageing periods, **Chapter III**. It has been shown that the water absorption has an influence on only certain composite properties; in order to understand this influence micrographic analysis has been performed.

As damage can initiate, develop and interact with the diffusion process in reinforced composites, the damage phenomenon has been studied before and after different sea water immersions. The initiation and development of damage have been carefully examined.

The second objective is to propose an approach to predict the durability of composites in a marine environment. This is described in **Chapter IV**. To achieve this objective it has first been necessary to develop a model allowing water diffusion profiles to be determined throughout the composite structure. The model is based on composite and resin properties determined in the previous chapters. A progressive multi-scale approach has been used to predict the absorption of water in the composites. This model has been applied to a tidal turbine blade, allowing a first estimation of water concentration after 25 years of immersion in sea water to be made. In parallel, a damage model has been proposed, in order to predict the damage appearance and development in these composite laminates, first dry then subjected to seawater immersion. This model is based on physical properties and helps to understand the effect of sea water ageing on the damage development. Finally a first investigation of the coupling between diffusion and damage has been performed.

The following diagram, Figure 18, provides an overview of the methodology.

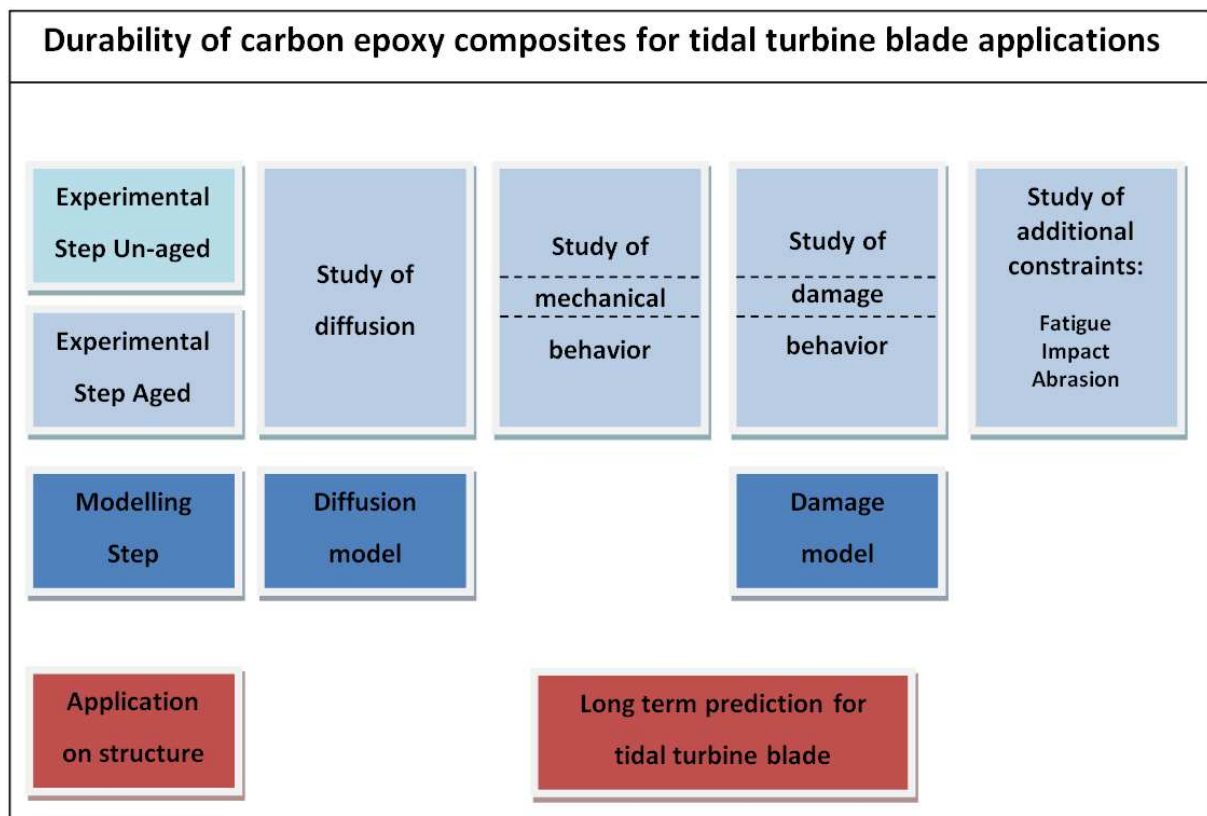


Figure 18: Overview of the study's methodology.

Les objectifs de l'étude

Dans la première partie de ce chapitre, les principales causes et conséquences du vieillissement en eau de mer ont été présentées. D'un matériau à l'autre la durabilité en environnement marin peut changer significativement, à cause du choix de matériau et sa fabrication. Il en découle un besoin de comprendre et d'évaluer l'impact de l'immersion eau de mer sur les composites pour applications pales d'hydroliennes. Il convient également de prédire les changements dans le matériau ainsi que son comportement structural au travers l'exploitation spécifique de ces structures. Dans la littérature peu d'études sur le vieillissement en eau de mer ont été menées sur les matériaux carbone/époxy comparé au verre/époxy. De plus, les études concernant le vieillissement des carbone/époxy pour applications pales d'hydroliennes sont très rares. En conséquence, il est difficile de trouver des données concernant l'évolution des propriétés de ces matériaux durant une longue exposition à l'eau de mer. Egalement, peu d'études comparent l'influence du procédé de fabrication sur les phénomènes de vieillissement en eau de mer.

*Le premier objectif de la présente étude est de caractériser l'influence sur les composites carbone/époxy pour les hydroliennes, de l'immersion au long terme en environnement marin. Pour atteindre ce premier objectif trois différents composites carbone/époxy qui sont tous de bons candidats pour les pales d'hydroliennes, ont été étudiés. Dans le **Chapitre II**, les propriétés de base de ces matériaux sont présentées avant la procédure de vieillissement. Cette première caractérisation est essentielle, dans le but de comprendre le comportement mécanique des composites avant vieillissement en eau de mer. Pour vieillir ces matériaux en un temps raisonnable, il a été nécessaire de développer une procédure de vieillissement accéléré. Une discussion est proposée dans ce chapitre sur la pertinence de ce vieillissement accéléré. Ainsi pour étudier l'influence du vieillissement en eau de mer sur les trois composites, une procédure de caractérisation a été développée. Dans un premier temps, la diffusion de l'eau a été étudiée, ces premiers résultats sont indispensables pour déterminer les temps de vieillissement, mais ils permettent également de fournir des données pour la modélisation de la diffusion. Ensuite l'évolution des propriétés mécaniques et physico-chimiques des matériaux a été examinée avant et après différentes périodes d'immersion en eau de mer, **Chapitre III**. Il a été montré que l'absorption d'eau a une influence seulement sur certaines propriétés des composites. Pour comprendre cette influence des micrographies ont été réalisées.*

Comme l'endommagement peut s'amorcer, se développer et interagir avec le processus de diffusion dans les composites renforcés, le phénomène d'endommagement a été étudié avant et

après différents immersion en eau de mer. L'amorçage et le développement de l'endommagement ont été examinés avec attention.

*Le deuxième objectif est de proposer une approche pour prédire et comprendre la durabilité des composites en environnement marin. Cette approche est décrite dans le **Chapitre IV**. Pour accomplir cet objectif, il a été nécessaire de développer un modèle permettant de déterminer la diffusion d'eau au travers des structures en composites. Le modèle est basé sur les propriétés de la résine et du composite considérés. Une approche progressive multi-échelle a été utilisée pour prédire l'absorption d'eau dans les composites. Ce modèle a été appliqué sur une pale d'hydrolienne, permettant la prédiction de la concentration d'eau après 25 ans d'immersion. En parallèle, un modèle d'endommagement a été proposé, dans le but de prédire l'apparition et le développement de l'endommagement dans les composites stratifiés. Dans un premier temps non vieillis, puis après immersion en eau. Ce modèle est basé sur des propriétés physiques et permet de comprendre les effets du vieillissement en eau de mer sur le développement de l'endommagement. Suite aux développements de ces modèles, de premières investigations sur le couplage entre diffusion et endommagement ont été réalisées.*

La Figure 18 présente une vue d'ensemble de la méthodologie de la thèse.

Chapter II. Materials behaviour in the un-aged state

In this second chapter, three carbon/epoxy materials have been characterized. These are typical of materials used for tidal turbine blade, some of them are already used by the composite industry to produce blades. This characterization consists of studying and comparing the behaviour of the three materials in an un-aged state,(i.e. before ageing), and is divided into three sections:

- A physico-chemical characterization
- A characterization of mechanical properties
- A characterization of the microstructure

In the **Chapter III**, these procedures will be used to follow and characterize the changes in the materials' properties and their behaviour, after accelerated sea water ageing.

In the section on the characterization of the mechanical properties, this study will focus both on in-plane moduli and strengths in composite materials. However a particular attention has been paid to the study of the evolution of the damage as a function of loading. Indeed, in the case of a tidal turbine blade, these structures could be subject to damage due to the action of many loading cases. But water ageing can also initiate a slow process of degradation leading to damage in composites. In order to characterise the damage of composites, a specific test procedure was developed. This is based on the observation of the crack density (i.e. the number of the transverse cracks per unit of length) as a function of loading. These observations have been performed on the different composite materials of the study. The transverse cracking damage mechanism was also studied in order to develop a damage model. This model will be presented and discussed in this chapter. The model identification is based on standardised tests and it will be validated using the inter-fibre tensile cracking tests.

Chapitre II. Comportement des matériaux à l'état non vieillis

Dans ce deuxième chapitre, trois matériaux carbone/époxy ont été choisis pour être étudiés. Ces matériaux sont caractéristiques des matériaux employés dans les pales d'hydroliennes. Certains d'entre eux sont déjà utilisés par l'industrie des composites pour produire des pales d'hydroliennes. Cette caractérisation consiste à étudier et comparer le comportement des trois matériaux à l'état non vieilli (c'est-à-dire avant vieillissement). Cette procédure de caractérisation est divisée en trois sections :

- *Une caractérisation physico-chimique*
- *Une caractérisation des propriétés mécaniques*
- *Une caractérisation de la microstructure*

*Dans le **Chapitre III**, ces procédures seront utilisées pour suivre et caractériser l'évolution des propriétés des matériaux et de leur comportement après vieillissement en eau de mer.*

Dans la seconde section de caractérisation des propriétés mécaniques, cette étude va aussi se focaliser sur les modules et résistance dans le plan des matériaux composites. Cependant une attention particulière sera portée sur l'évolution de l'endommagement en fonction du chargement appliqué. En effet dans le cas des pales d'hydroliennes, ces structures peuvent être sujettes à l'endommagement dû à l'action des nombreux cas de chargement. Mais le vieillissement en eau de mer peut également initier un lent procédé de dégradation conduisant à de l'endommagement dans les composites. Dans le but de caractériser l'endommagement des composites, une procédure d'essais a été développée. Elle est basée sur l'observation de la densité de fissures (c'est-à-dire du nombre de fissures transverses par unité de longueur) en fonction du chargement. Ces observations ont été réalisées sur les différents matériaux composites de l'étude. Le mécanisme d'endommagement lors du développement de fissures transverses a été également étudié dans le but de développer un modèle d'endommagement. Ce modèle sera présenté et détaillé dans ce chapitre. L'identification du modèle est basée sur des essais normalisés et sera validée en utilisant les essais de fissurations transverses en traction.

Chapter II. Materials behaviour in the un-aged state.....	33
1. Materials of the study	37
1.1 Pre-preg material	37
1.2 RTM material	38
1.3 Infused material	39
1.4 RTM/Infusion Resin.....	40
1.5 Choice of materials	41
1.6 Specimens preparation	42
2. Physico-chemical characterization	43
2.1 DSC.....	43
2.2 Density measurement.....	43
3. Mechanical characterization	46
3.1 Elastic properties	46
3.1.1 Tensile test procedure on 0° and 90° laminates	46
3.1.2 Test procedure and calculation on ±45° laminates	49
3.1.3 Four-point bending test procedure and calculation on composites laminates.....	54
3.2 Viscoelastic behaviour	57
3.2.1 Tensile test on composites at different loading rates.....	58
3.2.2 Tension creep test	58
3.3 Interply crack propagation test.....	59
3.3.1 Specimens preparation	59
3.3.2 Acoustic emission (AE)	60
3.3.3 Test procedure	61
3.3.4 Image processing.....	62
3.3.5 Results of inter-ply cracks propagation tests.	63
3.4 Interlaminar fracture toughness	64
3.4.1 Double Cantilever Beam (DCB) test:.....	65
3.4.2 Interlaminar fracture toughness calculations and interpretation.....	68
3.4.3 Modified beam theory (MBT) method:	68
3.4.4 Compliance calibration (CC) method:	69
3.4.5 DCB results for the three unaged materials.	70
3.5 Out-of-plane strengths.....	72
4. Microscope observations.....	76
4.1 Optical microscopy.....	76
4.1.1 Infused composite	76

4.1.2	RTM composite	77
4.1.3	Pre-preg composite	78
4.2	Scanning electron microscopy (SEM)	80
4.2.1	SEM observation on Infused material in the unaged state	82
4.2.2	SEM observation on RTM material in the unaged state.....	83
4.2.3	SEM observation on Pre-preg material in the unaged state	85
5.	Damage Modelling	87
5.1	Model based on physical parameters.	87
5.2	Damage model for the prediction of the crack density	88
5.3	Definition of the threshold of the damage	89
5.4	Definition of the effect of the damage	91
5.5	Definition of the kinetics of the damage development	92
5.6	Identification of the model	95
5.7	Validation on Carbon/Epoxy materials	96
5.8	Summary and conclusion about the damage model	99

1. Materials of the study

In this study three processes and materials have been chosen to produce samples for tests, for characterization before and after sea water ageing. In the following sections, each material will be described in terms of composition, and some details will be given about the manufacturing processes.

1.1 Pre-preg material

The first material that we chose for this study was based on a carbon fibre reinforced epoxy pre-preg. This pre-preg was transformed into a composite using the autoclave process. Pre-preg could be used in blade spars and, due to the high quality of both this material and the process, this material will be a good reference for ageing tests. The different samples and composite plates were produced by FMC Composites in Brest, as presented in Figure 19. For this material, the UD pre-preg layers are composed of HexPly® M21 matrix and UD HexTow® IMA carbon fibres. Pre-preg curing conditions were respected following product data specifications. Full vacuum was applied on the stacked prepreg, then 7 bar gauge for autoclave pressure at 180°C for 120 minutes. This material is of high quality and can be classified as an aeronautical material. It may be expensive for the tidal turbine blade applications, but it will serve as a good reference during this study. In this document, this material will be referred to as *Pre-preg material*.



Figure 19 : A pre-preg part under vacuum going into the FMC autoclave, [91].

1.2 RTM material

The second material choice resulted from a collaboration between Airborne Marine, Ifremer and the LBMS. It was a carbon/epoxy composite made by vacuum assisted resin transfer moulding (VA-RTM), produced by Airborne Marine. This material will be referred to as *RTM material*. It could be used in both blade body and blade spar elements. Airborne has already used the RTM process to manufacture one-shot tidal turbine blades [92] and propeller blades [93] (see Figure 20).



Figure 20 : AMBV (Alkmaar class Mine-hunting vessel) composite propeller and mould engineered by Airborne Marine.

Figure 20 presents a propeller blade manufactured with VA-RTM process technology. In that project, Airborne Marine's focus was on industrialising the VA-RTM process for the cost effective manufacturing of composite propeller blades. This blade design has a full thickness laminate composed of glass and carbon fibres, with UD, 0°, 90° and $\pm 45^\circ$ layup. The blade is composed of 180 plies and the thickness at the root of the blade is 88 mm. The RTM process on a double sided heated metal mould was used because of the complex geometry of the blade. The injection strategy was studied to provide maximum reliability of the process. The selection of the resin is very important due to the very thick blade laminates. Ideally, long pot life, low viscosity, low shrinkage and low exotherm are needed, when selecting the epoxy resin.

The one-shot closed mould (VA) RTM-technology in combination with automated pre-form technology offers an answer to the production of tidal turbine blades in series. In addition, it offers

the possibility to construct tidal blades without adhesive bonding which is very beneficial for the reliability of the composite blades.

To manufacture our samples and composites plates for testing, Airborne Marine used a R&D VA-RTM mould with a technical surface of 600 by 400 mm. This provides composite plates under similar conditions to those of an industrial mould for blade manufacturing.

1.3 Infused material

The third composite material is a carbon/epoxy manufactured by vacuum infusion; this material could be used to manufacture the blade body. This carbon epoxy was manufactured in the LBMS Laboratory, using UD layers of carbon Tenax-E IMS65 and the same epoxy resin as the RTM material. The samples were made on a glass plate using a Teflon anti-adhesive layer, with a vacuum of 0.95 bars for the infusion process. In order to have two smooth sides on the plates, an aluminium perforated plate was set up over the carbon layers. Common vacuum consumables were used: peel ply, resin flow mesh, release film, vacuum bag, etc. Figure 21 shows an example of the vacuum infusion process in the LBMS laboratory. These components are widely used in the nautical industry. Before the infusion process, the air and bubbles of air were extracted from the mixed resin (resin with hardener) using a vacuum chamber at 0.95 bars of vacuum depression. After polymerisation of the resin at room temperature (24 hours), all the plates were cured at 65°C for 16 hours, following resin curing specification datasheets. This material will be referred to as *Infused material*.

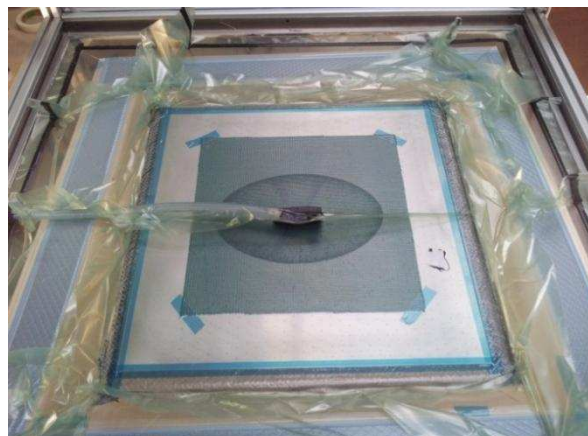


Figure 21 : Infusion process (LBMS laboratory).

1.4 RTM/Infusion resin

The RTM and Infused materials were manufactured using the same resin, so it was interesting to manufacture pure resin plates to complete the material characterisation. With these it will be possible to compare the effect of sea water ageing on pure resin and reinforced resin.

To manufacture this plate of pure resin, a three part mould was machined, as shown in Figure 22. Then using a 2.5 mm spacer it was possible to obtain a thickness of 2.5 mm for the final resin plate. Both parts were treated with a liquid mould release agent. On one side of the mould there is an insert for the injection of the liquid resin, and on the opposite side there is another insert used for the air evacuation.

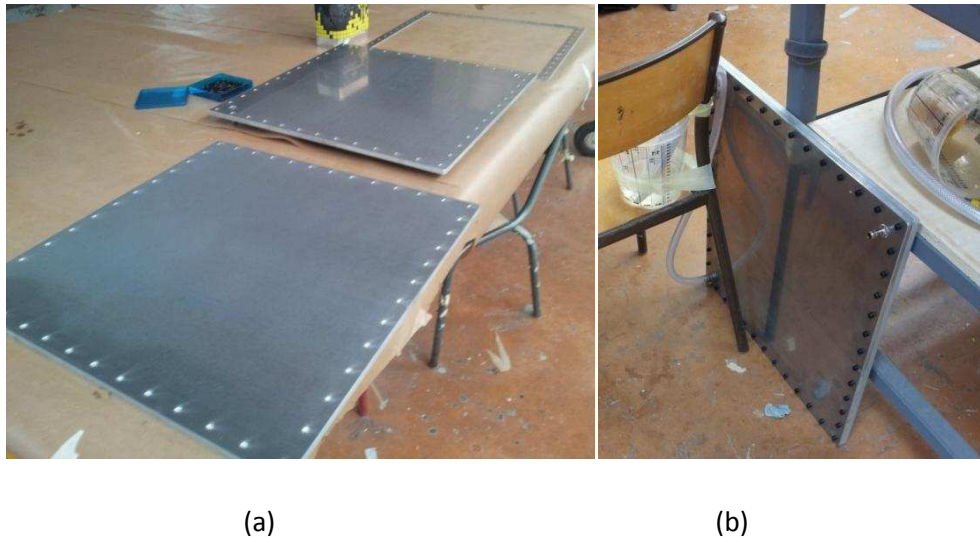


Figure 22 : Three part resin mould (a), gravity moulding process (b).

To mould the resin, only gravity was used to fill the cavity of the mould with the resin mix. Before injecting the resin into the mould, the mixed resin (resin with hardener) was degassed using a vacuum chamber at 0.95 bars of vacuum depression. After polymerisation at room temperature for 24 hours, the resin plate was cured under the same curing conditions and time as the infused material. Then the plate of pure resin was removed from the mould. Figure 23 shows the resin plate after opening the mould cover. The mould was well filled and visual observation indicated no trace of defects or porosity within the resin plate.



Figure 23 : Resin plate after polymerisation and curing.

1.5 Choice of materials

This choice of material here reflects the different current possibilities for manufacturing tidal turbine blades. It also allows the impact of fibre, matrix, and interface on the ageing mechanisms to be studied. The Pre-preg material could be considered as an aeronautical material, but pre-preg material is already used in the Tidal Energy industry [23],[94],[95]. Infused material was historically used for racing sailing boats, but it is used for wind turbine blades and could be used for the Tidal industry. Finally the RTM material developed by Airborne Marine is already employed on different tidal turbine blades in service or in development [96], so this type of material is a strong candidate for marine applications and tidal turbine blades. Some details about the material composition are presented in Table 1, for confidentiality reasons complete details of the commercial grades cannot be provided. For this study, materials were produced with different orientations and thicknesses.

Materials	Process	Resin	Fibre
Infused	Infusion	Infusion/RTM resin	Tenax-E IMS*
RTM	RTM low pressure	Infusion/RTM resin	not available
Pre-preg	Autoclave 7 bar	Hexcel M21	IMA

Table 1: Materials, process, resin and fibre compositions, (*IMS: intermediate modulus).

The different mechanical properties of the constitutive fibres and matrix of the three different composites are presented in Table 2, these values are taken from manufacturers' technical data sheets.

Material	E_{fibre} (GPa)	E_{matrix} (GPa)	σ^r_{fibre} (GPa)	σ^r_{matrix} (MPa)
Infused	290	3.6	6.00	72
RTM	242	3.6	4.137	72
Pre-preg	276	3.3 [2]	5.655	nc
Resin	E_{resin} (GPa)		σ^r_{resin} (MPa)	
	3.6		72	

Table 2: Nominal fibre and matrix tensile properties from technical data sheets.

Technical data about the UD carbon fabric for the RTM and Infused materials are given in Table 3. As these materials were manufactured with the same resin but with different processes and UD carbon fibres, it is important to take into account this composition when considering diffusion of water.

Carbon fibres type	Carbon content	Glass content	Polyester content	Binder resin powder	Areal weight (g/m ²)	Carbon fibre diameter (μm)
Infused	96%	0	4%	0	204	5
RTM	93%	3%	2%	2%	333	7.2

Table 3: Technical data about UD carbon fabric composition.

1.6 Specimen preparation

After obtaining the composite panels (a total of 30 for the study), different preparation steps were necessary before testing them. Specimen preparation is divided in 7 steps, this preparation is detailed in the Appendix section A. The final step is the testing, presented in the next section.

2. Physico-chemical characterization

To ensure as far as possible good quality of each material and to obtain reference values for mechanical properties before ageing, an initial series of quality control tests was performed. To check the T_g of as-received materials, DSC analyses were also performed. Then the density of samples from each composite plate was determined, this allowed the fibre contents of the composites to be estimated.

2.1 DSC

All composite panels were checked using DSC (Differential Scanning Calorimetry) to verify the state of cure before putting the materials to be aged in sea water baths. A TA Instruments Q200 DSC was used with a heating rate of 10 °C/minute. The glass transition temperature (T_g) is also useful to determine the maximum sea water ageing temperature for accelerated conditions.

Table 4 shows the results. It is possible to observe that the Pre-preg material has the highest T_g while the other composites have a T_g around 80°C. As sea water ageing can affect the material glass transition (T_g), additional DSC measurements were also used subsequently to follow the evolution of the T_g during the immersion of composites in sea water. This is necessary to insure as possible that the temperature of ageing remains sufficiently low compared to the T_g.

Materials	Curing process	T _g
Infused	16h@65°C	75°C (1)
RTM	12h@65°C	77°C (2)
Pre-preg	2h@180°C	198°C (3)
Pure resin	16h@65°C	78°C (2)

Table 4: Curing process and glass transition (T_g) temperature resulting for each material. The numbers between brackets are the coefficient of variation (the same notation is used for all tables in the document).

2.2 Density measurement

In order to understand some possible discrepancies between the materials under investigation, it is necessary to determine the fibre volume fraction. A method based on the measurement of the density is used.

To check the density of each type of material, density measurements were performed with a helium pycnometer, using two specimens of approximately $10 \times 30 \times h \text{ mm}^3$ (where h , is the thickness of the material) for each material. A specific procedure was defined, 10 cycles of purge of the chamber with the sample and then 40 cycles of measurement to allow accurate measurement. The Figure 24 illustrates an example of pycnometry density measurements for the Pre-preg and Infused materials.

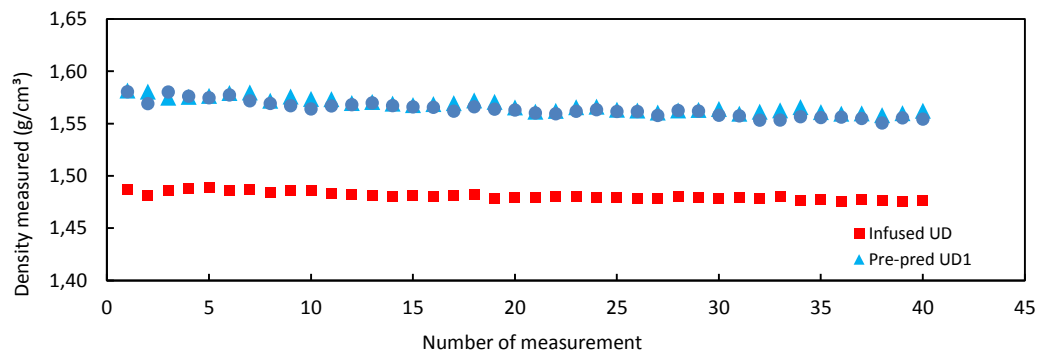


Figure 24 : Example of density measurements for Pre-preg and Infused material.

Materials	Stacking sequence	Density (kg/m^3)	Fibre volume fraction (%)
Infused	8 x 0°	1480(4)	54.6 (0.3)
Infused	16 x 0°	1491(2)	56.4 (0.2)
Infused	[+45,-45,0,90]s	1475 (2)	52.3 (0.2)
RTM	8 x 0°	1475 (1)	50.1 (0.1)
RTM	16 x 0°	1493 (4)	52.8 (0.3)
RTM	[+45,-45,0,90]s	1462 (1)	48.1 (0.2)
RTM	[+45,-45,0,90,90,0,-45,+45]s	1503 (1)	54.2 (0.1)
RTM	[+45/-45/0/90/90/0/-45/+45]4s	1520 (2)	57.1 (0.12)
Pre-preg	8x0°	1571 (3)	58.3 (0.3)
Pre-preg	16 x 0°	1563 (2)	56.7 (0.2)
Pre-preg	[0,0,90,0,0]	1563 (4)	56.7 (0.3)
Pure resin	/	1168 (5)	/

Table 5 : Density measurements and estimated fibre content of studied materials, mean (standard deviation), UD (unidirectional) and QI (quasi-isotropic) and pure resin.

Gas pycnometry is recognized as one of the most reliable techniques for obtaining apparent volume and density. This technique is non-destructive as it uses the gas displacement method to measure volume. Inert gases, such as helium or nitrogen, are used as the displacement medium.

Density calculations using the gas displacement method are much more accurate and reproducible than the traditional Archimedes water displacement method. Density measurements allow fibre content to be estimated if it is assumed that there is no porosity. Table 5, shows the results on the different materials with different orientation and thicknesses.

3. Mechanical characterization

This section presents the different mechanical tests performed. This mechanical characterization will provide a reference before ageing and allow the different materials to be compared. In Chapter III, this procedure will be repeated on aged specimens, making possible a comparison before and after sea water ageing.

3.1 Elastic properties

Quasi static tests were performed on unidirectional (0 and 90°) and multi-axial ($\pm 45^\circ$) specimens in order to determine intrinsic properties of the plies such as elastic constants (moduli, Poisson's ratios) and strengths. These properties were determined in the un-aged state and then after different ageing periods using standardized tests using both simple tensile loading and four-point bending.

3.1.1 Tensile test procedure on 0° and 90° laminates

One of the most common tests to determine properties of composites laminates is the tensile test on unidirectional composite, either in the fiber direction or perpendicular to the fibres. The properties obtained include modulus of elasticity, Poisson's ratio, tensile strength, and ultimate tensile strain.

a) *Tensile test procedure and property determination*

During the tensile test, a specimen of a UD composite is placed into the wedge grips of a mechanical testing machine and loaded slowly in tension. To determine the modulus of elasticity and Poisson's ratio, strains were measured during the test, using extensometers (or digital image correlation for some specimens). Specimens were loaded up to failure, the point at which tensile strength and ultimate tensile strain are determined. According to the ASTM D3039 [97], specimens of quasi-UD 0° and 90° plies were prepared and tested. Table 6 presents the different specimens tested.

Materials	Stacking sequence	h: thickness (mm)	Sample size (mm ²)	Nbr of sample/condition
Infused	8 x 0°	1.7	250 x 25	3
Infused	8 x 90°	1.7	250 x 25	3
RTM	8 x 0°	2.5	250 x 25	3
RTM	16 x 0°	5	250 x 25	3
RTM	8 x 90°	2.5	250 x 25	3
Pre-preg	8 x 0°	2	250 x 15	3
Pre-preg	8 x 90°	2	125 x 15	2
Resin	/	2.5	20 x 150 (B1)	3

Table 6: Average specimen dimensions for tensile tests on the three different materials and the pure resin.

Tensile tests were also performed on the un-aged resin. Specimens of resin were cut using high pressure water jet cut in the same way as for the composite samples. Resin samples were cut according to the standard ISO 527-2 [98], using the 1B specimen dimension ($l_3 = 150\text{mm}$, $b_1 = 10\text{mm}$).

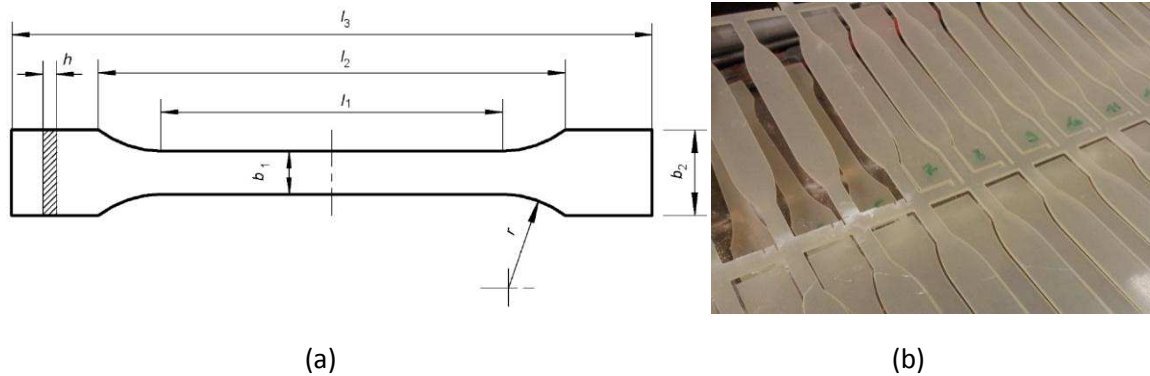


Figure 25: Tensile test resin specimen dimension (a) and the specimens used for the tests (b).

The load was introduced at a speed of 2 mm/min on an Instron electro-mechanical tensile machine. An extensometer was used to determine the strain during the test and ultimate strain, it was placed in the middle of the specimen. The tensile stress at break corresponds to the point of rupture of the resin specimen. The modulus of elasticity is the slope of a secant line between 0.05% and 0.25% strain on the stress-strain plot, as presented on the Figure 26 (a). Then tensile modulus is calculated using Eq.1:

$$E_{resin} = \frac{(\sigma_2 - \sigma_1)}{(\varepsilon_2 - \varepsilon_1)} \quad \text{Eq. 2}$$

Where ε_1 and ε_2 are respectively the strain of 0.0005 and 0.0025, σ_1 and σ_2 are the stresses corresponding to these strains.

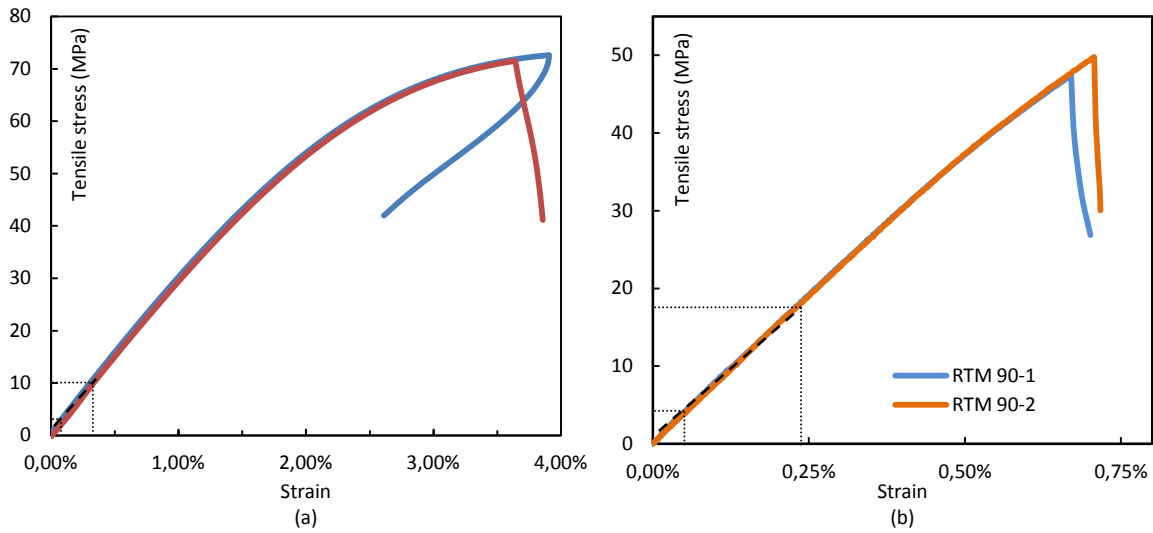


Figure 26: Illustration of tensile modulus determination on the resin (a) and on the composite (b).

b) Tensile test results

All tensile test results are presented in Table 7. The results have been obtained according to the standard ISO 527-5 [9], moduli have been determined with the same procedure as for the neat resin, Figure 26 (b). The tensile stress at break corresponds to the point of rupture of the composite specimen. RTM and Infused materials show similar properties in terms of transverse moduli and strengths. But due to the different carbon fibres and fibre content, the Infused material has a higher longitudinal modulus and strength.

The Pre-preg has a much higher longitudinal modulus, due to the use of intermediate modulus fibres. The matrix is a two-phase polymer with thermoplastic nodules, as will be shown in section 4.

Materials	E_{11} (GPa)	E_{22} (GPa)	X_t (GPa)	Y_t (MPa)
Infused	136.90 (1.79)	7.12 (0.36)	2.21 (0.10)	45.97 (2.42)
RTM	112.98 (3.15)	7.17 (0.01)	1.66 (0.07)	46.21 (1.21)
Pre-preg	170.05(6.19)	8.78 (0)	2.35(0.34)	43.84 (0)
	E_{resin} (GPa)		σ^r_{resin} (MPa)	
Resin	3.00 (0.01)	/	69.6 (2.8)	/

Table 7: Tensile test results on Infused, RTM, Pre-preg material and pure resin.

3.1.2 Test procedure and calculation on $\pm 45^\circ$ laminates

A number of experimental methods have been proposed to determine the in-place shear behavior of composite laminates. The torsion test of thin-walled tubes is considered to be the most accurate method for in-plane shear modulus and shear strength. However, this type of test is very expensive to perform, and requires special specimens [100]. Other shear test methods proposed are: the Iosipescu test [101],[100], the $\pm 45^\circ$ tension test [102],[103],[104] and the off-axis tension test [102],[103],[105]. The present study will only focus on the $\pm 45^\circ$ tension test.

a) *Test procedure*

The in-plane shear behavior was determined using ASTM D3518 [9]. For this test a balanced, symmetric lay-up composed only of $+45^\circ$ and -45° plies was used. For Pre-preg, Infused and RTM materials, $[+45,-45]_{2s}$ samples are described in Table 8.

Materials	Reference	h: thickness (mm)	Sample size (mm ²)	Nbr of samples/condition
Infused	IUT 45F-	1.7	250 x 25	3
RTM	A 45-	2.5	250 x 25	3
Pre-preg	IMA 45-	2	190 x 15	3

Table 8: Average specimen dimension for $\pm 45^\circ$ tensile test on Pre-preg and Infused materials.

This test for evaluation of in-plane shear response was originally proposed by Petit [104] and was later improved by Rosen [107]. Using expressions derived from laminated plate theory, the in-plane shear stress in the material coordinate system is directly calculated from the applied axial load, and the related shear stress is determined from longitudinal and transverse normal strain data.

For all these tests, the tension was introduced at a speed of 2 mm/min. These results are used to create an in-plane shear stress-shear strain curve. Indices 1 and 2 indicate the fiber direction and transverse to the fiber direction in the plane of the ply respectively, as illustrated in Figure 28.

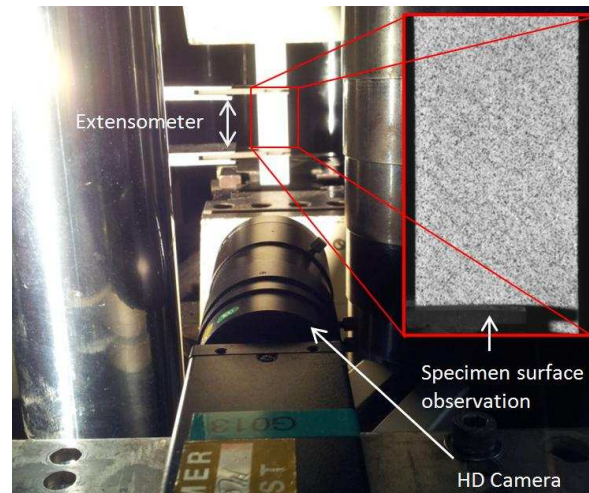


Figure 27: Test procedure for the determination of in plane shear response of composites.

The in-plane shear stress in the material coordinate system is directly calculated from the applied axial load and specimen cross-section. The related shear stress is determined from longitudinal and transverse normal strain data obtained either by strain gauges or extensometers or, in our case, using image correlation (the method for correlation will be detailed in the following section). The image acquisition rate for digital image correlation was 1 Hz. The test procedure is presented in Figure 27, the load is applied in the x direction as presented in Figure 28.

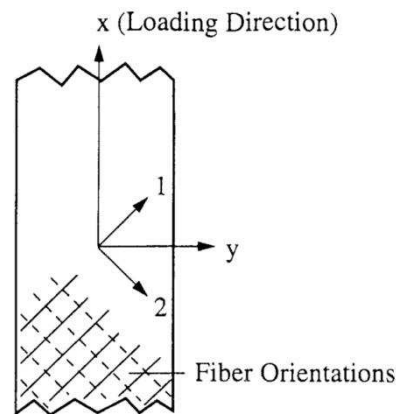


Figure 28: Definition of specimen and material axes according to ASTM D3518[11].

An HD camera was used to measure the strains but an axial extensometer was also used to compare with 2D digital image correlation (DIC) and to validate this method. In our case the extensometer provided the strain only in the loading direction but there is a need to have the strain in both directions. Figure 29 presents a comparison between the two methods, values are very similar up to high strains, when the extensometer starts to slide on the surface of the specimen.

Another way to monitor the strains could be to use strain-gages, but due to the numbers of specimen to test and difficulty in bonding strain gauges to wet, aged specimens, image correlation was more practical and allows strains to be measured over a larger area.

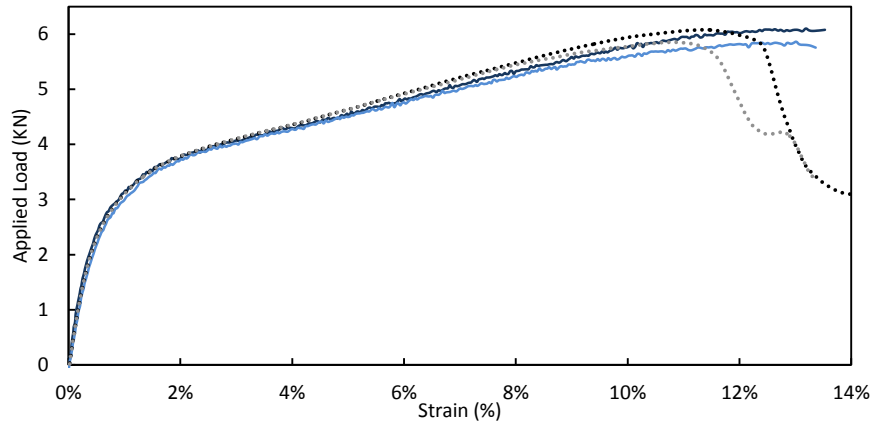


Figure 29: Comparison between normal strains measured by extensometer (dotted lines) and image correlation (continuous lines) during tension test on +/-45° Infused laminates.

To proceed to 2D digital image correlation, Ncorr was used. Ncorr [108], [109] is an open source 2D DIC (Digital Image Correlation) code based on MATLAB, and developed at Georgia Institute of Technology. It is capable of determining displacement and strain fields from the given input speckle images. All procedures to use Ncorr, to prepare specimens for speckle and to determine strains are briefly presented in Appendix 3.

b) Determination of shear properties

To calculate the maximum in-plane shear stress for the $\pm 45^\circ$ laminate Eq.3 is used based on the maximum load during the test. If the shear modulus is to be calculated, the shear stress is determined at each required data point using Eq.4.

$$\tau_{12}^m = \frac{P^m}{2A} \quad \text{Eq. 3}$$

$$\tau_{12i} = \frac{P_i}{2A} \quad \text{Eq. 4}$$

Where τ_{12}^m is the maximum in-plane shear stress in MPa. P^m is the maximum load in Newtons. τ_{12i} is the shear stress at i -th data point in MPa, P_i is the load at i -th data point in Newtons and A is the cross-sectional area.

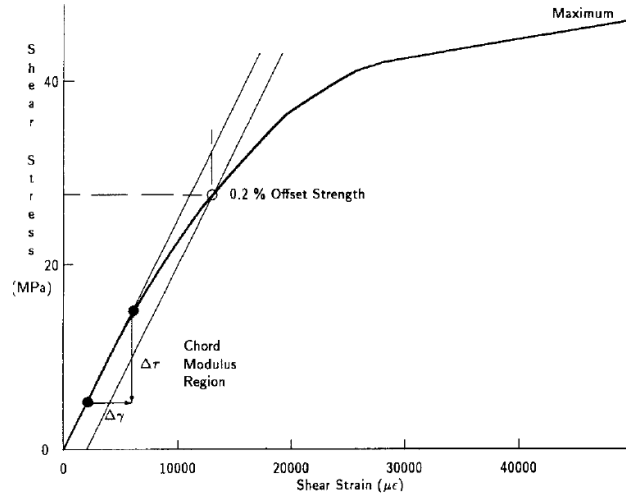


Figure 30: Illustration of shear modulus determination according to ASTM D3518.

To obtain the shear modulus or maximum shear strain, it is possible to determine the shear strain at each required data point using Eq.5. Then the maximum shear strain is determined from Eq.6:

$$\gamma_{12i} = \varepsilon_{xi} - \varepsilon_{yi} \quad \text{Eq. 5}$$

$$\gamma_{12}^m = \gamma_{12} \text{ at maximum stress} \quad \text{Eq. 6}$$

Where γ_{12i} is the shear strain at i -th data point in $\mu\epsilon$. ε_{xi} is the longitudinal normal strain at i -th data point, $\mu\epsilon$ and ε_{yi} the lateral normal strain at i -th data point in $\mu\epsilon$; and γ_{12}^m is the maximum shear strain.

The chord shear modulus of elasticity using Eq.6, is determined over a $4000\mu\epsilon$ shear strain range (± 200), starting with the lower strain point in the range of 1500 to 2500 $\mu\epsilon$, inclusive. A graphical example of chord shear modulus determination is presented in Figure 30.

$$G_{12}^{chord} = \frac{\Delta\tau_{12}}{\Delta\gamma_{12}} \quad \text{Eq. 7}$$

Where G_{12}^{chord} is the shear chord modulus of elasticity in GPa, $\Delta\tau_{12}$ is the difference in applied shear stress between the two shear strain points in MPa and $\Delta\gamma_{12}$ the difference between the two shear strain points (nominally 0.004).

c) *Results*

Each material was tested before ageing. Figure 32 presents the tensile test on $\pm 45^\circ$ specimens for the Pre-preg (red/orange curves), RTM (grey points) and Infused material (blue dotted lines). In general terms, it is possible to decompose this response into two parts. The first part corresponds to the linear response of the material, which is directly linked to the matrix properties. The second part of this response is non linear due to the viscoelastic nature of the matrix and the damage introduced. Reorientation of the fibres may also occur, but this phenomenon has not been observed here. Thus the stress in the section of the specimen continues to rise until failure.

Materials	τ_{12}^m (MPa)	G_{12} (GPa)
Infused	69.9 (1.7)	3.6 (0.02)
RTM	68.7 (5.0)	3.86 (0.3)
Pre-preg	81.0(0.1)	4.44 (0.01)

Table 9: Results of in plane shear strength and modulus for the three materials.

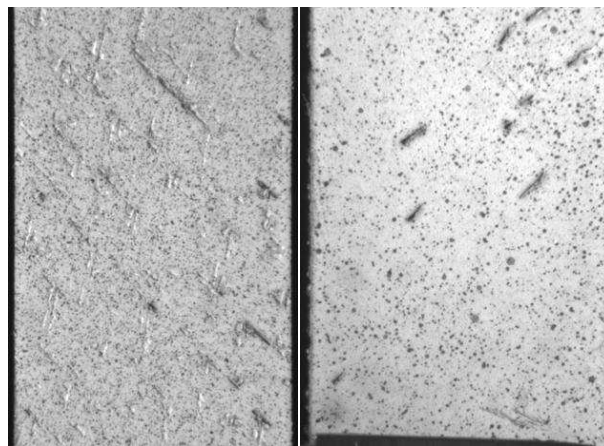


Figure 31: Example of $\pm 45^\circ$ RTM specimens presenting voids on their surface.

According to Table 9, the shear properties of the RTM and the Infused material are very similar. This is not unexpected as they are based on the same resin, but the Infused material has an average strain to failure of 26 % whereas that of the RTM is only 16%. This difference could be explained by the difference of fibre stitching between the two materials but also by the presence of voids at the surface of the RTM materials, which lead to lower strain to failure and more scatter in these results. Figure 31 shows the surface of two RTM specimens with voids. The response of the Pre-preg material is rather higher with low scatter, although modulus values for all three materials are quite similar.

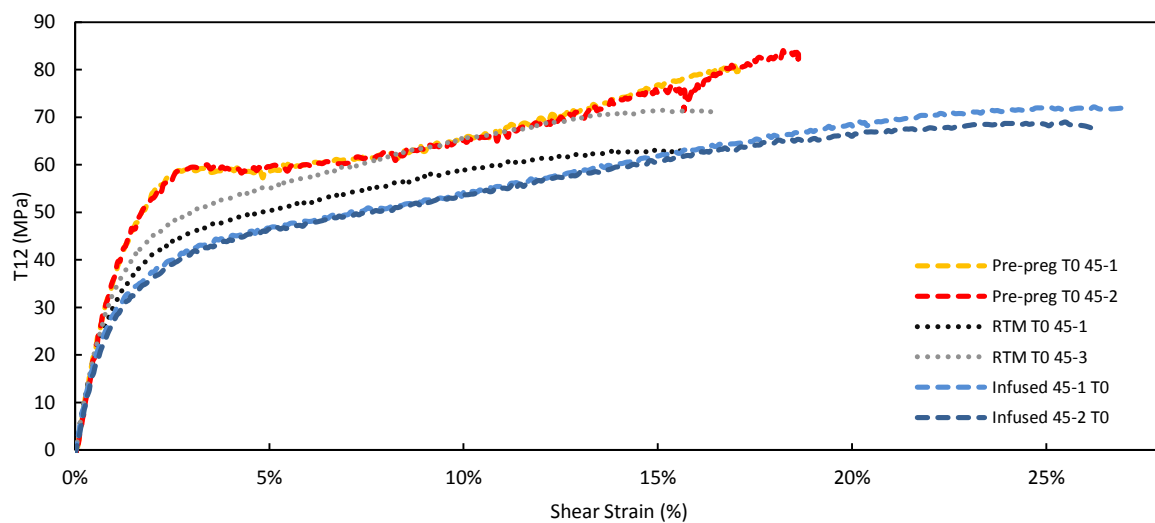


Figure 32: Shear stress response of the three carbon/epoxy materials before ageing.

3.1.3 Four-point bending test

a) *Four-point bending test procedure*

Flexural strength and stiffness are not basic material properties, they are the combined effects of a material's basic tensile, compressive and shear properties. However, this test could be used to study the combined effect of fatigue and sea water ageing. Moreover, it enables failure in the fibre direction to be obtained without using a machine with a high loading capacity. The flexural response of a composite beam is obtained by recording the load applied during the test and the resulting strain. The strain can be measured directly with a strain gauge or it could be obtained by measuring the displacement at the centre of the beam. The bending moment M_f , depends on the geometry of

the specimen and the applied load and can be determined using beam theory. In the case of the four point bending test the load, F , applied by the testing machine is transmitted to the specimen through support rollers. Then the applied load is reacted below the test sample by two additional supports. In view of the symmetry of the configuration, each of the four spans carries a load $F/2$, as shown in Figure 33.

In order to characterize the flexural strength of the carbon/epoxy materials, quasi-isotropic (QI) specimens were tested. Table 10 presents the different samples tested and their dimensions. During this study we were not able to test the infused material in flexure to failure, due to the low thickness of the sample (1.7 mm). RTM and Pre-preg were tested, and in the case of the RTM materials we had the possibility to test different thicknesses (2.5 and 5 mm). For both materials, the load was applied at 2 mm/min with an Instron electromechanical testing machine.

Materials	Stacking sequence	h (mm)	Width: b (mm)	L'(mm)	L(mm)
RTM	[+45,-45,0,90]s	2.5	15	60	80
RTM	[+45,-45,0,90,90,0,-45,+45]s	5	20	100	200
Pre-preg	[+45,-45,0,90]s	2	15	60	80

Table 10: Four point bending test specimens average dimensions and stacking sequences.

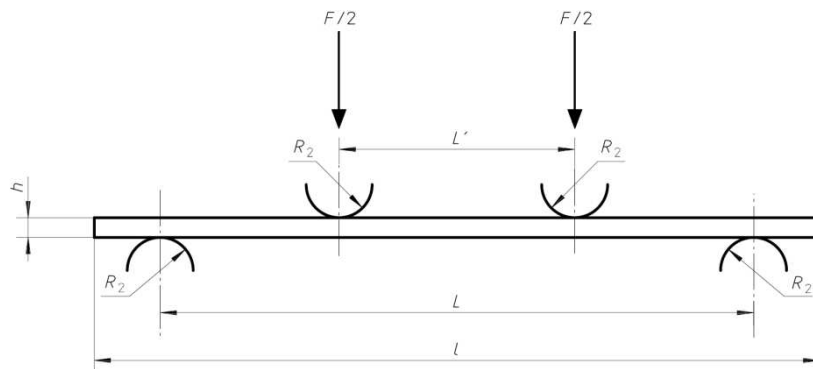


Figure 33: Four point bending test configuration according to ASTM D7264 standard.

b) *Determination of flexural strength and stiffness*

When flexural load is applied to the specimen, the three basic stress states are induced on the beam, tension, compression, shear. The specimen failure occurs when one of these three stresses

reaches its limit. Thus in a four-point bending test, the maximal stress in the middle of the beam is written as in Eq.7:

$$\sigma = \frac{M_f}{\left(\frac{I_{GZ}}{\nu}\right)} \quad \text{Eq. 8}$$

Where M_f is the bending moment, I_{GZ} is the moment of inertia of the beam section and ν is the distance to the neutral axis of the beam. The maximal bending and the moment of inertia can be written as:

$$M_f = \frac{F.L}{8} \quad \text{and} \quad I_{GZ} = \frac{b.h^3}{12} \quad \text{Eq. 9}$$

Thus by substituting Eq.7 and Eq.8 it is possible to obtain the maximal stress:

$$\sigma = \frac{3}{4} \cdot \frac{F.L}{bh^3} \quad \text{Eq. 10}$$

In the case where the loading span is not 1/2 of the support span for the four point bending test setup, the maximal stress (σ_f) is written as presented in Eq.10:

$$\sigma_f = \frac{3}{2} \cdot \frac{F.(L-L')}{bh^3} \quad \text{Eq. 11}$$

Where L' is the length of the inner loading span, as presented on Figure 33.

c) *Four-point bending test results*

Table 11 presents the four-point bending test results on the different materials. RTM material has been tested in different thicknesses and a significant difference is noted between the two results. This difference could be explained by the fact that the fibre content is higher in the QI 5 mm (54%) than in the QI 2.5 mm (48%). Additional samples of QI 2.5 mm have also been tested. These samples were cut in two other plates, and quite large differences were observed for mean flexural strength, -10% to +8%. These results will be used for flexural fatigue tests, but to follow aging specimens will all be taken from the same plate.

Materials	σ_f (MPa)	Failure mode
RTM QI 2.5 mm	466.9 (20.57)	C
RTM QI 5 mm	559.7(56.2)	C
Pre-preg QI 2 mm	474.8(34.8)	C

** C: failure in compression mode (including interlaminar shear)*

Table 11: Flexural strength and stiffness for RTM and Pre-preg materials.

3.2 Viscoelastic behaviour

In composite materials the fibres carry the majority of the load, but the matrix plays an important role, as it transfers loads between the fibres and between each ply of the laminates. This matrix is also a binder to prevent fibre buckling. Because the matrix has viscoelastic behaviour [110], [111], composite laminates will exhibit some time dependence [112].

It has been previously shown in Chapter I that during wet ageing some changes will occur in mechanical properties, such as failure strength, fracture toughness, fatigue life. But the viscoelastic creep behaviour of composites is particularly sensitive to hygrothermal degradation [113],[114], [115]. The influence of the water ageing on the viscoelastic characteristics has been well documented by Chateauminois et al. [116] among others. The water acts as a plasticiser in the epoxy resin network and the molecular mobility of the smallest units of the network significantly increases in water.

The aim of this section is to have a first indication of the viscoelastic behaviour of the different carbon/epoxy composites, and then to evaluate the effect of sea water ageing on this behaviour. Dimensional stability under stress is essential in many applications so creep can be a significant problem. Tidal turbine blades can be subject to creep loading and loaded at different rates. Additionally it is possible to use viscoelastic and creep behaviour properties to model the long term behaviour of composites, as presented by Dillard in [117].

First, to establish the time dependence of composite properties, tensile tests were performed on $\pm 45^\circ$ laminates with different loading rates. Then, in order to characterize the creep behaviour, tension creep tests were performed. For this characterization only infused material was tested, using a $\pm 45^\circ$ stacking sequence, $[+45,-45]_{2s}$ on specimens with dimensions of (250 x 25mm²); these tests were repeated after ageing, in order to reveal the impact of sea water ageing on the non linear behaviour of this composite.

3.2.1 In-plane shear test on composites at different loading rates

The test procedure was based on the same method as presented in the section 3.1.2 (p.49). Three loading rates were studied, 0.2, 2 and 20 mm/min.

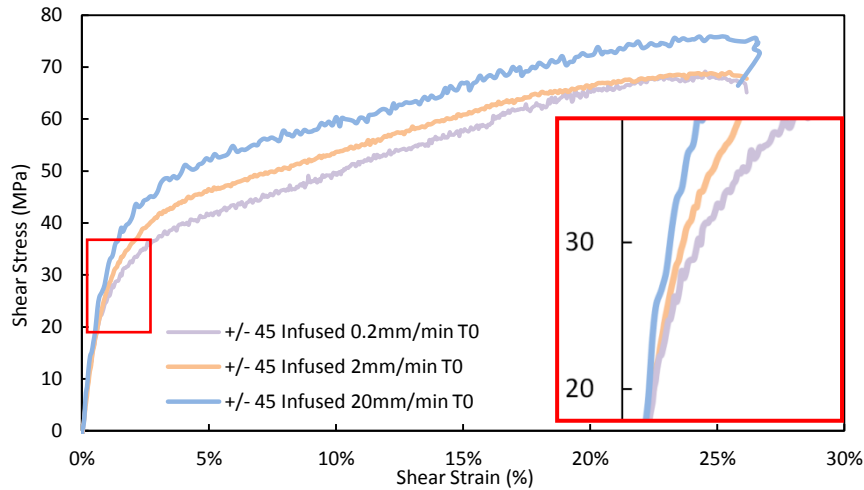


Figure 34: Response of $\pm 45^\circ$ Infused composites at three different loading rates.

The results for the infused materials are presented in Figure 34. This figure represents the evolution of shear stress as a function of the shear strain for the three loading cases. A higher loading rate induces a higher shear yield stress. These results show the classical time dependence of this composite and the viscoelastic behavior of its epoxy resin. These initial results indicate that it will be necessary to account for viscoelastic effects in modeling long term behavior of matrix dominated properties.

3.2.2 In-plane shear creep test

Tension creep tests have also been used to study the non linear behaviour of infused composites under in-plane shear loading, using a $\pm 45^\circ$ stacking sequence. Three load levels were applied, 1200 N (14 MPa) for 1000 seconds, then 3600 N (42 MPa) for 4000 seconds and 4800 N (56 MPa) during for 1000 seconds, as presented on Figure 35 (b). For each step the load was applied at 42.5N/s. Longitudinal and transverse strains on the specimen surface were analysed using the DIC, as presented previously. The increase in the strains as a function of the time during the applied load steps, is presented in Figure 35 (a).

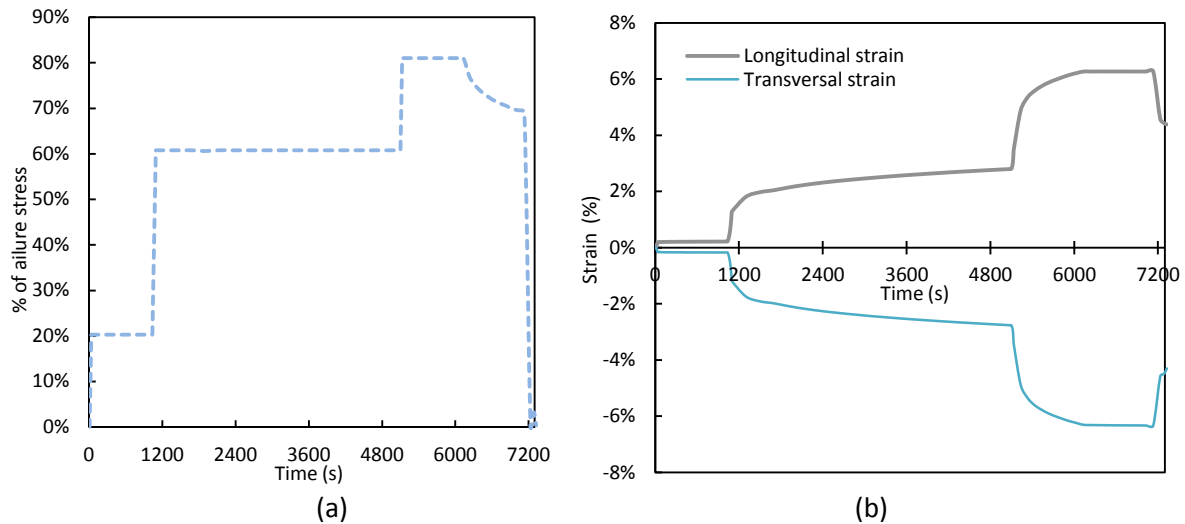


Figure 35: Creep behaviour of Infused materials, a) Loading sequence, b) creep strains/

During the second creep load period, at 61% of the failure stress, the strain in the un-aged specimen increases from 1.3 to 2.8% in one hour. In chapter III, the results from the same test performed after sea water ageing will be presented, in order to have a first indication of the effects of sea water ageing on the non linear behaviour of this composite.

3.3 Transverse crack kinetics test

3.3.1 Specimens preparation

An important parameter in material selection for tidal turbine blades is the resistance to damage initiation and propagation. Both intra- and inter-laminar crack propagation have been examined before and after aging. The interlaminar tests will be described in section 3.4, here intralaminar tensile cracking will be presented using tensile loading on different stacking sequences of 0 and 90° layers [118]. Samples of the Infused and Pre-preg composites with a $[0_2, 90_2]_s$ stacking sequence were prepared and tested on an electro-mechanical testing machine. Table 12 presents the details of specimen dimensions, stacking sequence, and specimen numbers. All specimen edges were polished before testing to improve observation, and to remove crack initiators after water jet cutting. The polishing process involved different papers with 240, 500, 800 and 1200 grit sizes.

Materials	Reference	Stacking sequence	Specimen size (mm ²)	Number of specimens/condition
Infused	IUT F1	[0,90] _{4s}	250 x 25	3
Infused	IUT F2	[0 ₂ ,90 ₂] _s	250 x 25	3
Pre-preg	IMAM21 F1	[0 ₂ ,90 ₂] _s	250 x 15	3
Pre-preg	IMAM21 F2	[0 ₂ ,90 _{1/2}] _s	250 x 15	3

Table 12 : Specimen information for intralaminar tensile cracking tests.

3.3.2 Acoustic emission (AE)

Damage development was followed by recording acoustic emissions. The acoustic activity within a material and especially its variation as a function of applied loading, is often analysed to detect micro-crack initiation. The AE is defined as a phenomena where a transient elastic wave is created, caused by damage within the studied material. The energy dissipation which results in damage (initiation and development) can be analyzed. Various authors have attempted to relate acoustic emission characteristics (energy, amplitude) to damage mechanisms, [119],[120],[121]. The origins of damage characterization using AE can be traced back to 1971 with the work of Mehan and Mullin [122]. Summarized by Gutkin [123], early approaches simply tried to classify damage based on a single AE parameter, such as the study by Valentin et al.[124]

Mehan and Mullin [122] analyzed different failure mechanisms in composites and isolated three basic failure mechanisms by optical means. These mechanisms, which were caused by tensile loading of epoxy specimens containing only a few fibres, were:

- Fibre Fracture
- Matrix Cracking
- Interfacial Debonding

In the present study, to follow the crack kinetics corresponding to interfacial debonding and mesoscopic crack in 90° plies, MISTRAS Micro II equipment was used with two NANO 30 sensors. An acoustic coupling gel was used to ensure uniform contact and improve transmission of the wave through the sensor area. In this study, we focused on acoustic sources characterized by an amplitude level between 55-60 db. This choice of amplitude was obtained based on published work and after comparing optical observation and amplitudes of events. Mechraoui presented some ranges of amplitude corresponding to different mechanisms of damage identified in organic matrix composites [125]. Figure 36 presents a comparison between different published classification models [125].

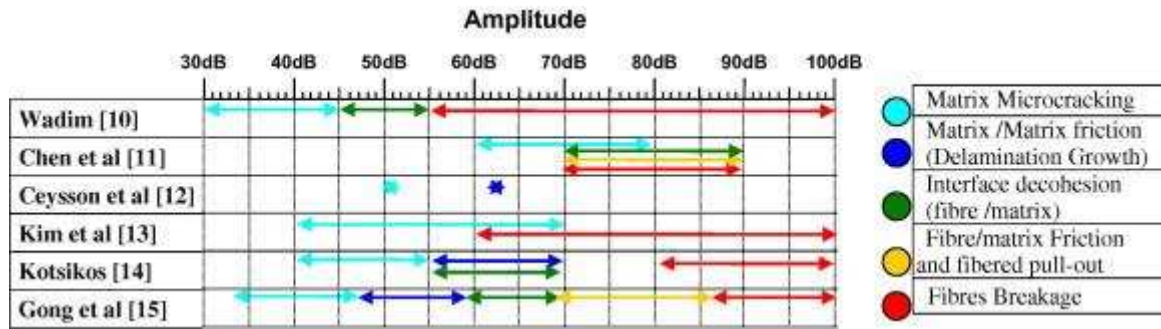


Figure 36 : Amplitude distribution according to the damage mechanisms in composite materials [126].

The AE sensors were monitored with this threshold, one sensor at each end of the specimen in order to localize emissions and remove parasite recordings. This threshold corresponds to the fibre/matrix interface cracking. The location of the AE sensors is shown in Figure 37. The load signal was also recorded.

3.3.3 Test procedure

All samples were tested at 1mm/min on an electro-mechanical testing machine. One edge of the specimens was painted white to improve observation of the cracks. Then, monitoring of the crack development was performed using two high definition cameras, Figure 37. The image acquisition frequency was 1 Hz.



Figure 37 : Test set-up to measure intralaminar tensile cracking.

3.3.4 Image processing

To achieve automatic image processing and crack counting, a program was developed with Matlab™ software. First, the program trimmed the edge of each image to keep only the specimen image, and the angle of each image was corrected. Then images of the two cameras were assembled to obtain the complete surface of the specimen. In a second step the program processed the images to highlight the cracks, with a filter based on a Gaussian function convolution. Figure 38 shows an example of the image treatment, the thickness of the specimen is approximately 1.7 mm.

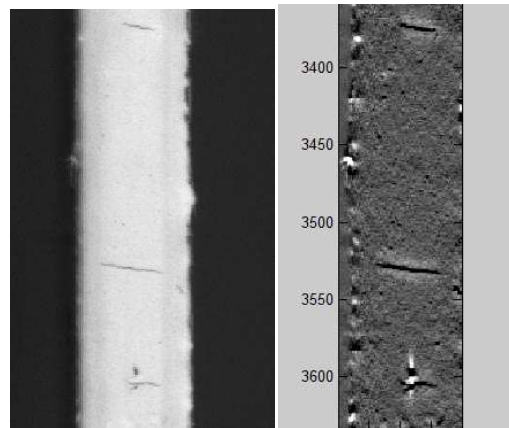


Figure 38 : Visualization of cracks before (left) and after (right) Matlab™ processing on a $[0_2,90_2]_s$ sample.

At this stage the cracks were then counted automatically by differentiating levels of grey on a vertical line defined in the programme (based on 90° plies location). In the case of $[0,90]_{4s}$ specimens, it is possible to count cracks along three different vertical lines, one the 90° plies at the center (C) of the specimen and two others on both exterior sides (L and R) of the specimen. Figure 39 illustrates the crack counting and the different positions.

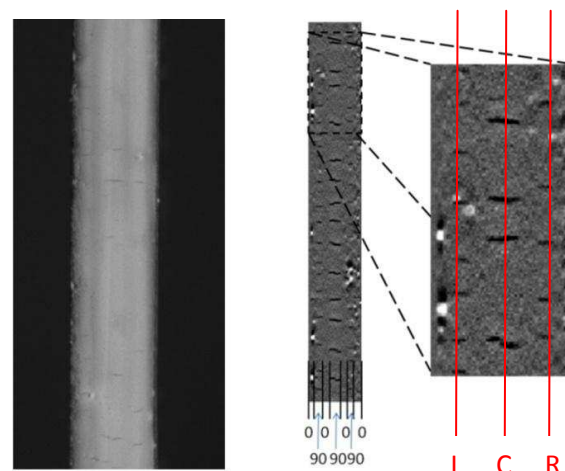


Figure 39 : Visualization of cracks before (left) and after (right) Matlab™ processing on a $[0,90]_{4s}$ sample putting in exergue possible location of cracks.

A comparison between automatic and manual counting is presented in Figure 40. Comparing these two methods on $[0_2,90_2]_s$ and $[0_2,90_{1/2}]_s$ specimens, it is possible to see that the crack development is very similar for both methods. The threshold of damage is at the same applied stress. The automatic method provides a good average number of cracks but for low stresses below the threshold (0 to 400 MPa), the Matlab script counts some cracks due to noise. In the case of $[0,90]_{45}$, the exterior crack counting (L and R lines on Figure 39) is not accurate with the automatic method due to their position close to edges. On the edge of the specimen, in some cases, 90° plies are not clearly visible. This could be due to polishing of specimen edges, the paint on the edge of the specimen or, at high loads, 0° fibre breakage. Nevertheless this procedure provides reliable results for the central 90° zone.

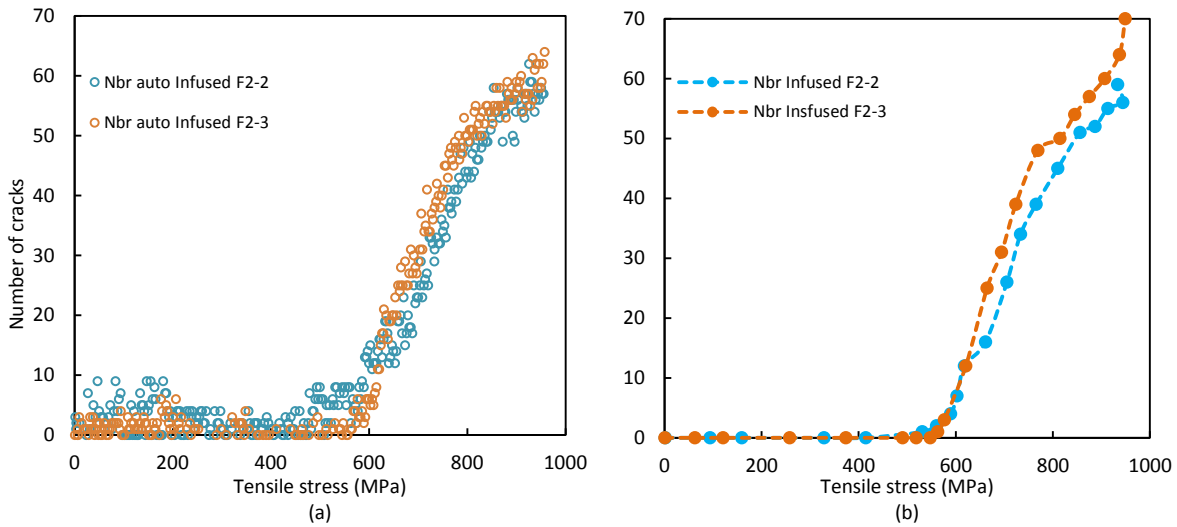


Figure 40: Comparison between automatic counting (a) and manual (b) methods on $[0_2,90_2]_s$.

3.3.5 Results of intralaminar tensile cracking tests.

Tests have been performed on Pre-preg and Infused materials with difference stacking sequences. Figure 41 presents the different tests on these materials in the un-aged state. On Figure 41 (a) Pre-preg $[0_2,90_2]_s$ (blue triangles) and $[0_2,90_{1/2}]_s$ (red squares) results are shown. On Figure 41 (b) Infused $[0,90]_{45}$ (blue and purple circles) and $[0_2,90_2]_s$ (grey squares) results are given. For the Infused $[0,90]_{45}$ materials, there is a single 90° ply on the left and right edge (purple circle) but double 90° plies in the centre position (blue circles) of the specimens. These figures show the normalized crack density ($\bar{\rho}$) which is the number of cracks (N) multiplied by the thickness of the 90° plies (h_{90}) and divided by the observation length (L_{obs}) according to Eq.12:

$$\bar{\rho} = \frac{N \times h_{90}}{L_{obs}} \quad \text{Eq. 12}$$

A first inspection of these figures reveals a significant effect of the thickness of the 90° plies on the damage threshold. For the Pre-preg material on F1 specimens ($[0_2, 90_2]_s$), initiation of damage starts at 250 MPa but for the F2 specimens ($[0_2, 90_{1/2}]_s$), first cracks appear at 350-400 MPa. In a similar way for the F1 Infused specimens which includes two different thicknesses of 90° plies, the damage threshold depends on the thickness of 90° plies. It has been shown [126] that strength in the transverse and shear directions depends on ply thickness. Thinner plies have higher strengths than thicker ones.

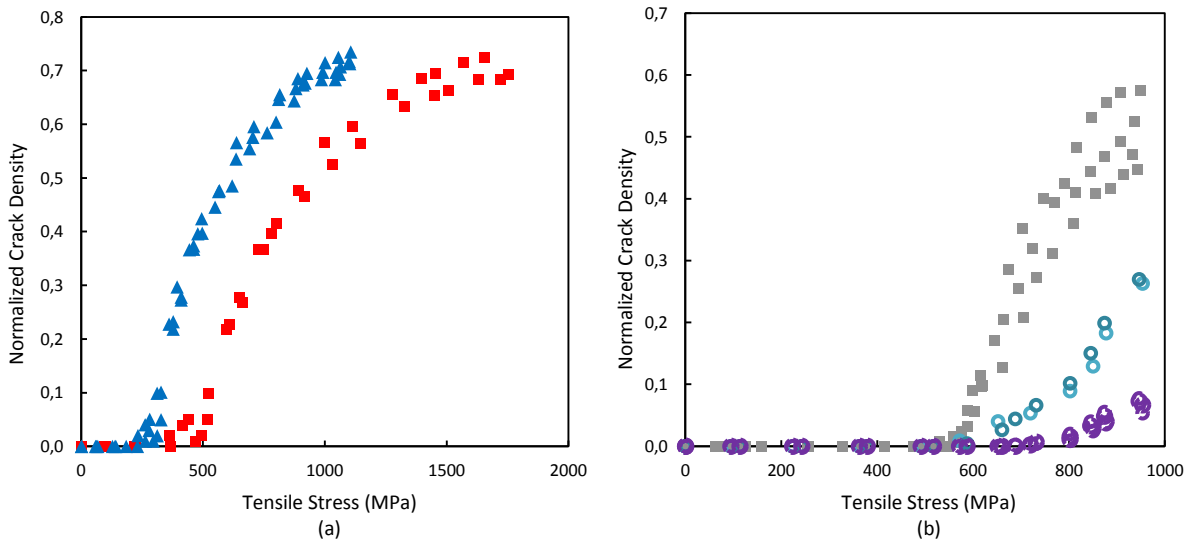


Figure 41: Evolution of normalized crack density as a function of applied stress for Pre-preg (a) and Infused (b) materials. Pre-preg $[0_2, 90_2]_s$: blue triangles, Pre-preg $[0_2, 90_{1/2}]_s$: red squares, Infused $[0_2, 90_2]_s$: grey squares, Infused $[0_90, 0_90]_s$: blue circles for centre 90° and purple circles for single 90° plies on specimen sides.

3.4 Interlaminar fracture toughness

Interlaminar fracture or delamination is one of the most frequent failure modes of laminated composites [127],[128],[129],[130]. Its occurrence greatly reduces the stiffness and thus may limit the life of a tidal turbine structure, leading to failure during service [127]. Interlaminar stresses become significant and affect the overall performance where geometrical and material discontinuities exist. Delaminations and their growth can be characterized by strain energy release rate (G) and the manner in which the load is applied. A delamination may be loaded in Mode I

(tensile), Mode II (in-plane shear), Mode III (out-of-plane shear), or a combination of these Modes (mixed mode), see Figure 42. The critical strain energy release rates (G_c) at which the delamination begins to extend vary significantly depending on the mode of loading [131]. Characterization of delamination resistance has thus been the subject of the development of various test methods. The most common test methods DCB (Double Cantilever Beam) and ENF (End Notched Flexure) use beam specimens with artificial delaminations. The ASTM D 5528 standard [132] and ISO 15024 [133] recommend the use of Double Cantilever Beam (DCB) specimens to measure the Mode I fracture toughness G_{IC} of fibre reinforced polymer composites. The End Notch Flexure (ENF) test for pure Mode II fracture toughness G_{IIc} common among researchers is yet to be approved by ASTM. ASTM D6671 [134] recommends the use of a Mixed-Mode bending (MMB) test that can measure fracture toughness over a wide range of combinations of Mode I and Mode II loading.

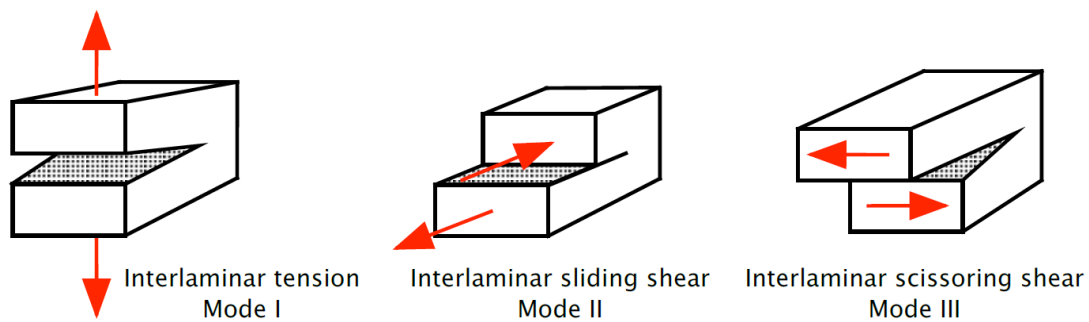


Figure 42 : Fracture test loading modes

Mechanical properties of carbon fibres/epoxy laminates are typically significantly affected by moisture absorption [see Chapter I]. The inter-laminar fracture toughness is dependent on different laminate properties such as matrix toughness and the strength of the fibre/matrix interfacial bond. The effects of moisture on the inter-laminar fracture toughness have rarely been investigated in the literature [75], [135]. Moisture effects on mode I properties and the resulting changes in the critical energy release rates were evaluated in the present study, using DCB tests before and after immersion.

3.4.1 Double Cantilever Beam (DCB) test:

The experimental protocol is described in [136] following the ISO 15024 standard. This allows the interlaminar fracture toughness to be defined as a function of crack length, the R curve. This curve may be affected by the presence of fiber bridging between the two arms of the DCB specimen,

leading to a rise in the toughness value with the crack length. For this reason the value of toughness G_{IC} is often taken as the value characterizing the initiation phase of the crack, both from the insert film and from a short delamination introduced during initial loading to extend a few millimeters from the film insert (pre-crack).

Materials	a: initial delamination length	b: specimen width	L: specimen length	h: specimen thickness
Infused UD	50	25	150	3.1(0.1)
RTM UD	50	25	150	5.1(0.2)
Pre-preg UD	30	25	150	3.1(0.1)

All dimensions are in millimeters.

Table 13: DCB specimen average dimensions for the three materials.

This initial delamination is artificial, introduced using a non-adhesive insert film. In our case all specimens were manufactured using a PTFE film of 20 μm . This film, slightly thicker than the standard recommendation ($<15 \mu\text{m}$) is added in the laminate mid-plane (i.e. $[0_8, \text{Insert}, 0_8]$) during manufacture. The slightly thicker film is not critical as specimens were pre-cracked in mode I. Specimen specifications are presented in Table 13. The initial crack length for the Prepreg is rather short, requiring a load block correction, but propagation values can be determined once the crack has extended. Marine aluminum block tabs were used to transmit the load, they were fixed at the extremity of the specimen, as shown in Figure 43 (20x20x10mm³). The loading is applied in the thickness direction, (P : applied load). Aluminum blocks were fixed using Araldite 420AB, adhesive which was cured as described in the previous section on Specimen preparation.

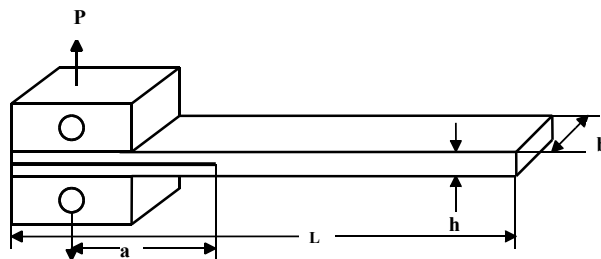


Figure 43: Double Cantilever Beam Specimen.

To identify the composite toughness during this test, the displacement between the two arms of the specimen is measured together with the crack length and the applied force. A tensile load is introduced via the end blocks with an Instron electro-mechanical testing machine, to open the initial

crack and to promote delamination along the mid-beam inter-laminar layer at a quasi-static cross-head displacement of 1 mm/min.

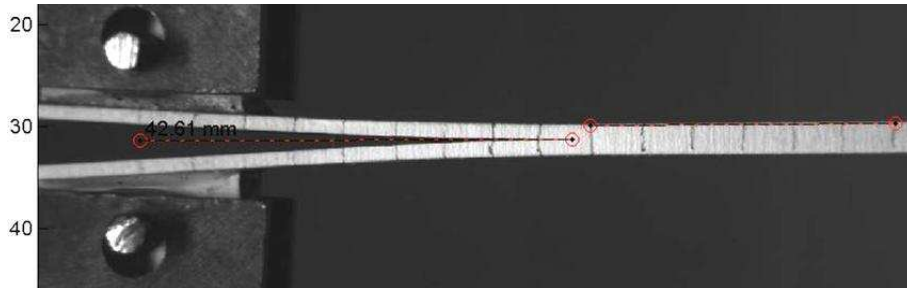


Figure 44: Delamination length measurement using Measure Tool.

Delamination length was determined using an HD camera and then images as shown on Figure 44 were processed using Matlab Measure Tool to measure crack length,. The test procedure is illustrated in Figure 45, an LED light source was used to provide good lighting conditions. The data analysis is either based on beam theory (with corrections for load-blocks and large displacements) or on experimental compliance calibration [137].

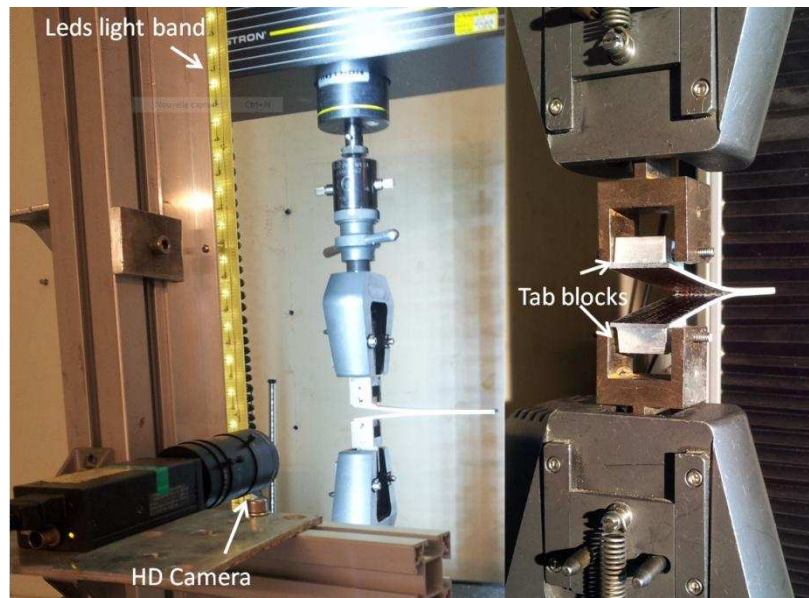


Figure 45: DCB test set-up.

3.4.2 Interlaminar fracture toughness calculations and interpretation

Different values can be used to define the moment of delamination initiation, as presented on Figure 46. The first method consists of the determination of the first non-linearity (NL) on the curve load/displacement. The second method is based on the definition of the displacement for which the crack propagation was experimentally observed (VIS). The last method consists of detecting an increase of 5% of the compliance or the maximal load (MAX/5%).

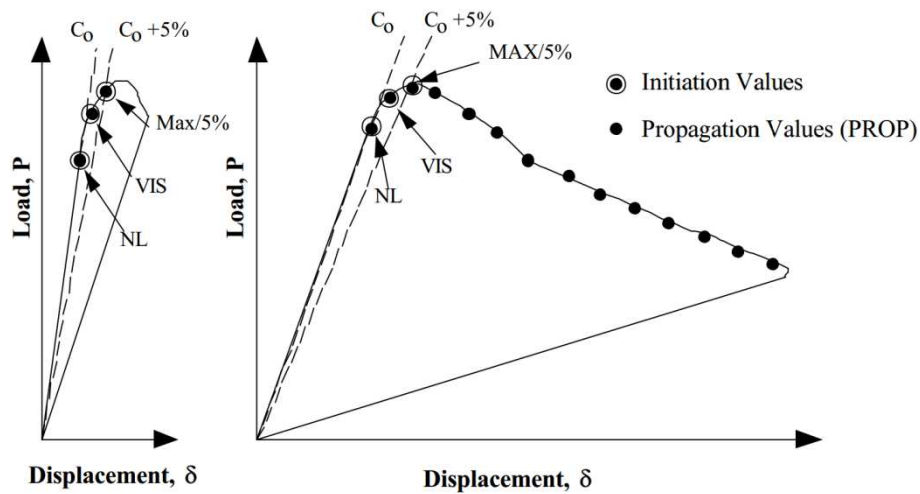


Figure 46: Load displacement trace from DCB test [133].

The ISO standard proposes three methods of G_{Ic} calculation. These methods consisted of (i) a modified beam theory (MBT), a (ii) compliance calibration, and a modified compliance calibration (MCC, not presented here). None of the three methods is clearly superior to the others, and the inclusion of the three is the result of a compromise between European, American and Japanese standards, but the MBT is a more conservative method.

3.4.3 Modified beam theory (MBT) method:

The beam theory expression for the strain energy release rate of a perfectly built-in double cantilever beam is presented in the following equation (Eq.13):

$$G_I = \frac{3P\delta}{2ba} \quad \text{Eq. 13}$$

Where P is the applied load, δ is the load point displacement, b is the specimen width and a the delamination length.

In practice, equation (Eq.13) will overestimate G_I because the beam is not perfectly built-in (i.e., rotation may occur at the delamination front). The modified equation (Eq.14) corrects for this rotation by treating the DCB as if it contained a slightly longer delamination, $a + |\Delta|$ where Δ may be determined experimentally by generating a least squares plot of the cube root of compliance, $C^{1/3}$ as a function of delamination length, Figure 47.

$$G_I = \frac{3P\delta}{2b(a + |\Delta|)} \quad \text{Eq. 14}$$

3.4.4 Compliance calibration (CC) method:

An alternative approach is to plot the logarithm of the compliance C , ($C = \delta_i/P_i$) versus the logarithm of a , the delamination length using the visually observed delamination (VIS, Figure 46) onset values and all the propagation values, as presented on Figure 47.

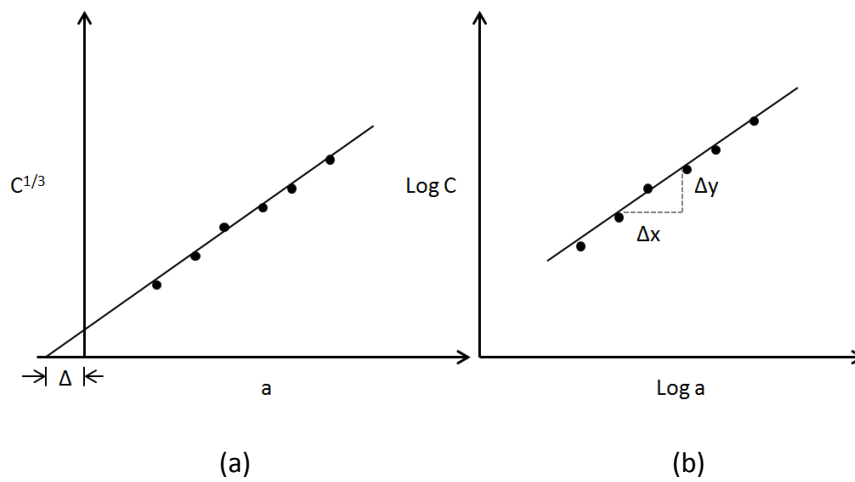


Figure 47 : Modified Beam Theory (a) and Compliance calibration (b) for DCB test.

A straight line is drawn through the data that results in the best least-squares fit. The exponent n from the slope of this line is calculated according to $n = \Delta y / \Delta x$ where Δy and Δx are increment values of y and x respectively, Figure 47. The Mode I interlaminar fracture toughness is determined using this slope n as follows (Eq.15):

$$G_I = \frac{nP\delta}{2ba} \quad \text{Eq. 15}$$

3.4.5 DCB results for the three unaged materials.

A unique procedure has been applied to test all specimens. During the first pre-test from the insert film, some perturbation and instability (Figure 49) occurred during initiation of the delamination and the development of the process zone, Figure 48.

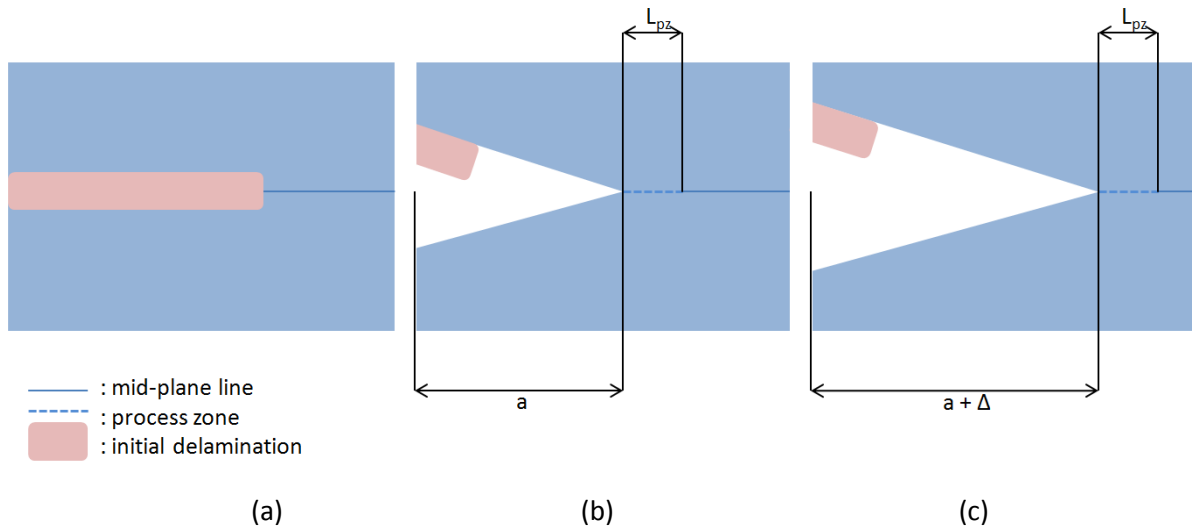


Figure 48: DCB initial and artificial delamination (a), pre-delamination and process zone initiation (b), growing of the delamination (c).

In Figure 49, the load-displacement plots for pre-cracking from the insert and then crack propagation from the pre-crack are presented for two specimens of the pre-preg material. The pre-cracking is shown by a dotted line and then the normal crack propagation by a continuous line. Given the variability in tests from the insert films for the following and future ageing tests, all specimens have been pre-cracked, to develop the crack by 5 mm (± 2 mm), Figure 48 (c). This procedure allows more stable crack propagation and avoids the instability at the initiation of the process zone.

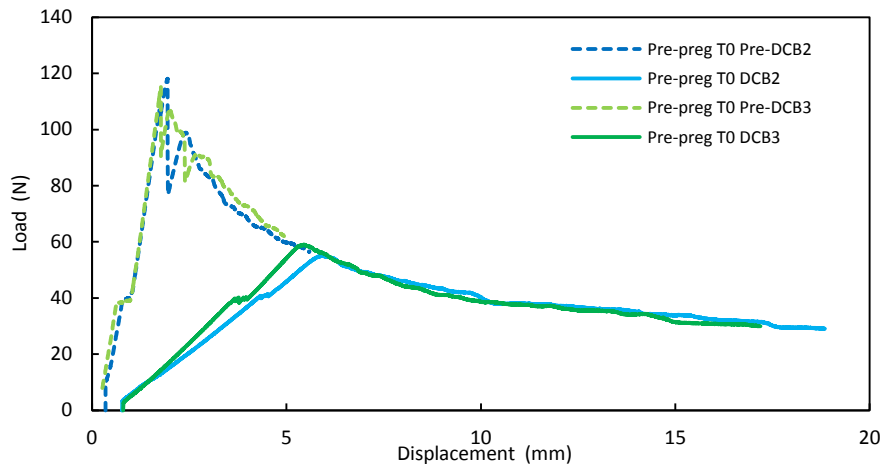


Figure 49: Pre-crack and crack propagation on pre-preg material.

The three materials have a different response during crack propagation. Pre-preg material is manufactured only with carbon/epoxy UD layers, and without stitching. On the other hand the RTM and Infused materials are composed of carbon UD layers stitched with glass or (and) polyester fibres. In this case the stitching can affect the crack propagation, and affect the amount of fibre bridging. This is a real material effect, which will be observed in the composite structure, but it complicates the material comparison.

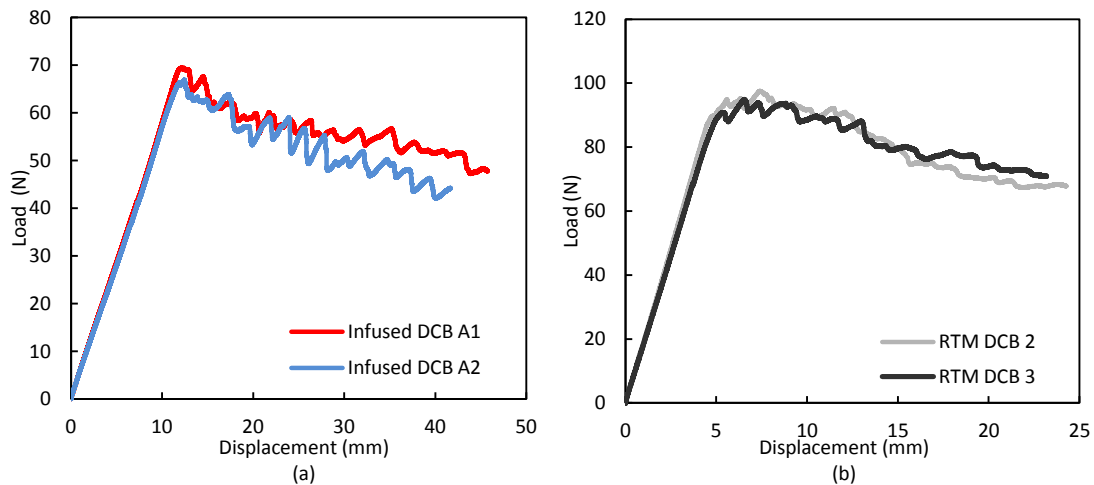


Figure 50: Examples of DCB test on Infused (a) and RTM (b) materials.

Figure 51, illustrates the differences in mode I crack propagation for the three materials. It also shows the presence of fibre bridging due to stitching, during the crack propagation in the case of Infused and RTM materials. For the Pre-preg carbon/epoxy, only slight carbon fibre bridging occurs.

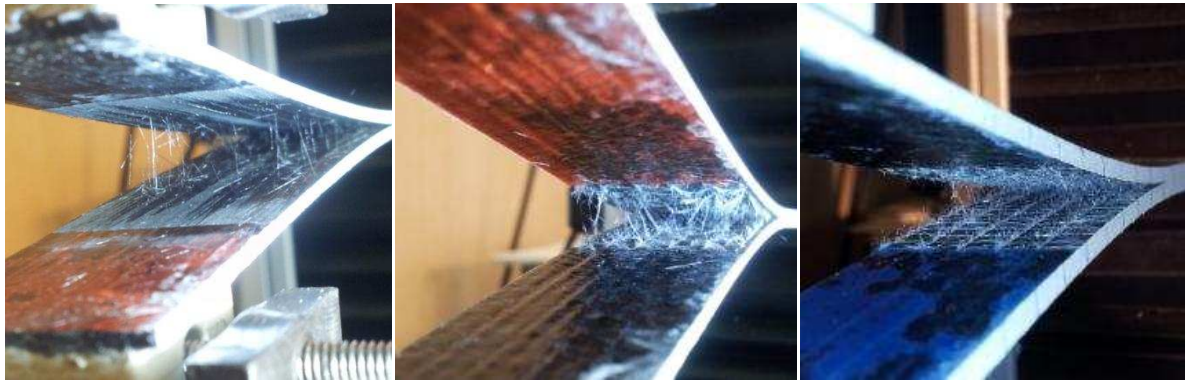


Figure 51: Crack propagation in mode I into Pre-preg, Infused and RTM materials (left to right).

Values of G_{Ic} during propagation for each material are presented in Table 14. These results were obtained using the CC method. It is interesting to note the difference between the infused and RTM materials which have the same matrix resin.

Materials	$G_I(\text{J/m}^2)$
Infused UD	576 (30)
RTM UD	422 (20)
Pre-preg UD	368 (15)

Table 14 : DCB results of re-initiation using CC method.

3.5 Out-of-plane strengths

Finally, the mechanical test matrix was completed by the ISO 14130 [34] test method for the determination of the apparent inter-laminar shear strength (ILSS) by the short-beam method. ILSS tests are often used for monitoring quality and are suitable for the comparison of materials. These tests provide information about the quality of the resin/fibre bond. The procedure supplies only apparent shear properties, as peak stresses occur near to the loading point. In most cases due to the complexity of the stress state and the variety of failure modes that can appear in this type of specimen, it is not possible to relate the short-beam strength to any material property.

However, ILSS failure in composites, are normally dominated by resin and fibre/matrix interface properties.

a) *ILSS test procedure*

The inter-laminar shear strength in the un-aged state has been studied for different material orientations and thicknesses. As this test was used for monitoring the quality of composite materials, an (arbitrary experience-based) acceptance criterion was defined as 45 MPa for the UD materials. It has been shown that ageing has an influence on ILSS strength [139] and in the degradation of fibre/matrix interphase region [140]. Thus this test will provide a reference before ageing and then allow changes to during ageing to be followed.

For these tests, specimens were all taken from composites plates using water jet cutting. The load was applied at 1 mm/minute with an Instron electromechanical testing machine. Figure 52, presents the ILSS test configuration according to the ISO 14130 standard. For these tests the three carbon/epoxy materials were tested with different thicknesses and stacking sequences (unidirectional and quasi-isotropic laminates).

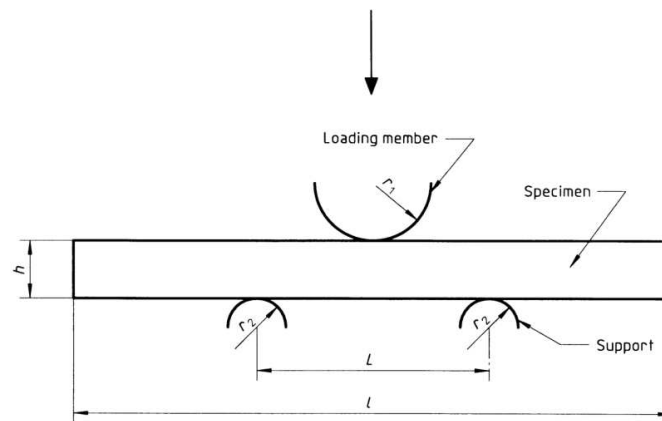


Figure 52 : ILSS loading configuration.

b) *ILSS property calculation*

The apparent inter-laminar shear strength τ_M , expressed in MPa, is calculated using the following equation:

$$\tau_M = \frac{3}{4} \times \frac{F_M}{bh} \quad \text{Eq. 16}$$

Where: F_M is the failure or maximum load in Newtons, b is the width of the test specimen in millimetres and h is the thickness of the test specimen in millimetres.

c) ILSS results

ILSS results are presented in Table 15. For all samples the failure mechanism was a single or multiple inter-laminar shear failure Figure 54 presents three examples of ILSS failure in the composites samples for RTM QI 5 mm, Pre-preg UD and Infused UD. It has been shown that ILSS test allows to determine some out-of-plane properties,[141]. For instance the UD specimens permit to determine the S_{13}^c strength and the quasi-isotropic (QI) specimens allow to determine the S_{23}^c strength [141] (since the failure occurs in the 90° plies), as illustrated in Figure 53.

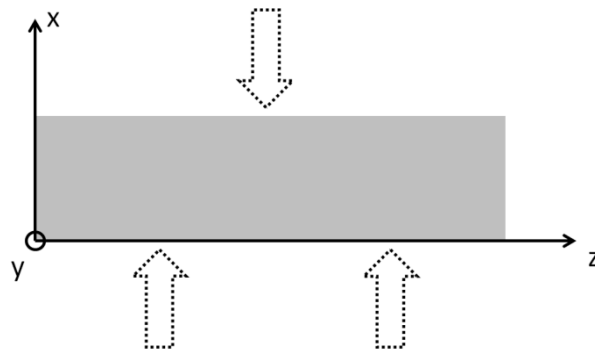


Figure 53: Out-of-plane compression mechanism in unidirectional composite. Shear ILSS test leads to τ_{13} if 0° plies are oriented in (y,z) plan or leads to τ_{23} if 90° are oriented in (y,z) plan.

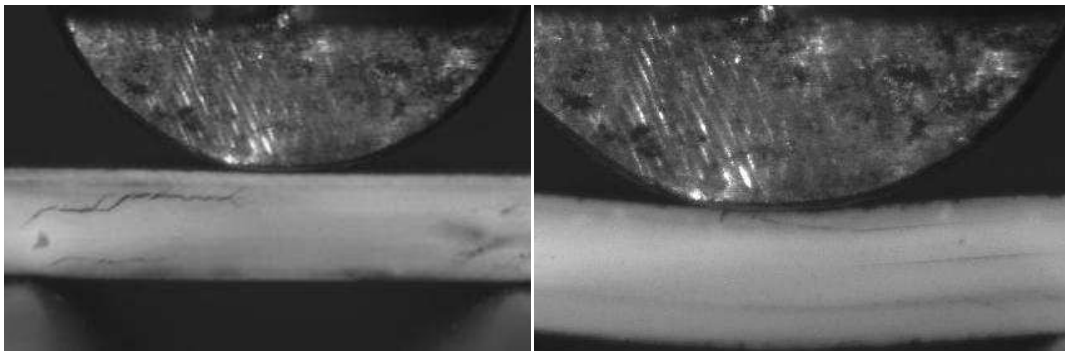


Figure 54: Illustration of inter-laminar shear failure in composites samples.

All results are presented in Table 15. All specimens show values above the acceptance criterion of 45 MPa. For the RTM material, it should be noted that the S_{23}^c remains constant as a function of the thickness while a low decrease is observed for S_{13}^c (around 13%). This difference is not observed on other materials (for instance manufactured using pre-preg plies in autoclave see [141]) and should be investigated in further works to study the influence of the thickness on the out-of-plane properties as a function of manufacturing process.

Materials	h (mm)	b (mm)	l (mm)	ILSS : τ_M (MPa)
Infused UD	1.7	10	20	55.9 (0.2)*
RTM UD	2.5	10	20	67.5 (0.9)*
RTM UD	5	10	25	59.1(1.6)*
RTM QI	2.5	10	20	48.3 (2.8)**
RTM QI	5	10	25	49.82 (3.9)**
RTM QI	10	10	50	49.79 (0.9)**
Pre-preg UD	2	10	20	108.4 (11)*
Pre-preg QI	2	10	20	60.7 (6.6)**

Table 15: Inter-laminar shear strength (ILSS) values, S_{13}^{c*} , S_{23}^{c**} , and specimen dimensions for the three materials.

4. Microscopy observations

In order to visually examine the state and quality of the different composites of the study, two observation methods were used, first an optical microscope coupled with a camera and then a Scanning electron microscope.

4.1 Optical microscopy

Optical microscopy provides a first visual approach of the microstructure of the three composite materials of the study. The specimens were cut from UD samples in the direction perpendicular to the fibres, and specimens were polished. A first comparison between the three materials is presented in Figure 55 then these will be discussed in more detail.



Figure 55: Optical microscope observation of UD samples, left to right, Infused, RTM and Pre-preg materials (dimension A is approximately 1.5 mm, for all three materials).

4.1.1 Infused composite

Observations of the Infused material are presented in Figure 56. It is possible to see the presence of the polyester stitching yarns, which are located between each bundle of carbon fibres, (see red circle in Figure 56). Concerning the presence of voids, very few were located (blue dotted line circle) and their average size was around 20 μ m.

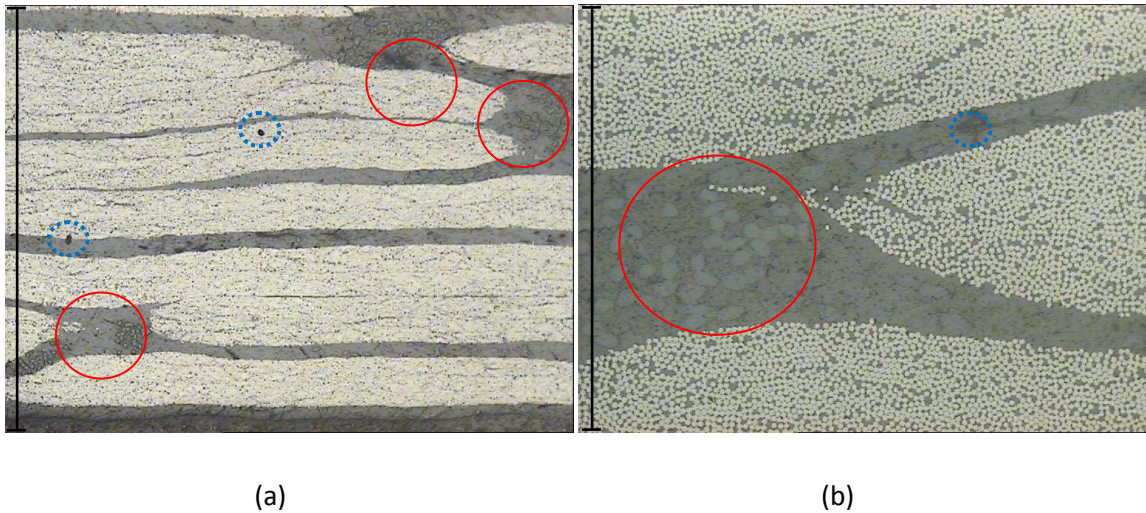


Figure 56: Microscope optical observation of Infused UD (scale bars: (a) 1.5 mm, (b) 0.38 mm).

4.1.2 RTM composite

For the RTM materials some optical observations are presented in Figure 57 and Figure 58. If we compare these to the Infused composite images (at the same observation scale), this RTM carbon/epoxy shows thicker carbon plies, due to their higher areal weight. In Figure 57 it is possible to see the glass fibre stitching (red circles), in the same direction as the carbon fibres. Other stitching fibres are visible in Figure 57 (b) and Figure 58 (green ellipses). These fibres are oriented at $+45^\circ$ or -45° compared to the carbon fibres. These fibres (green ellipse) are polyester.

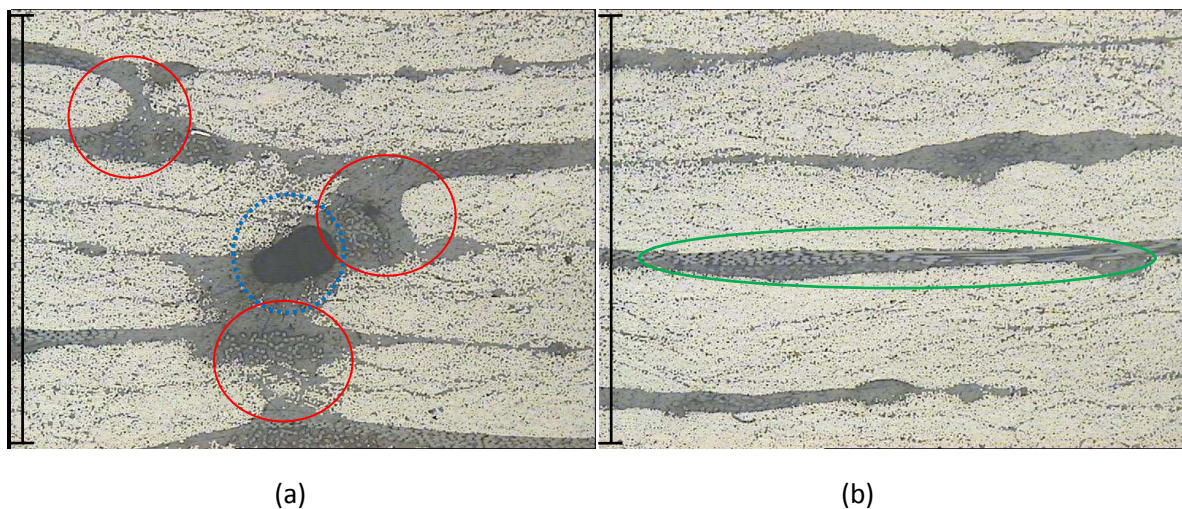


Figure 57: Microscope optical observation of RTM UD (average scales: (a) and (b) 1.5mm).

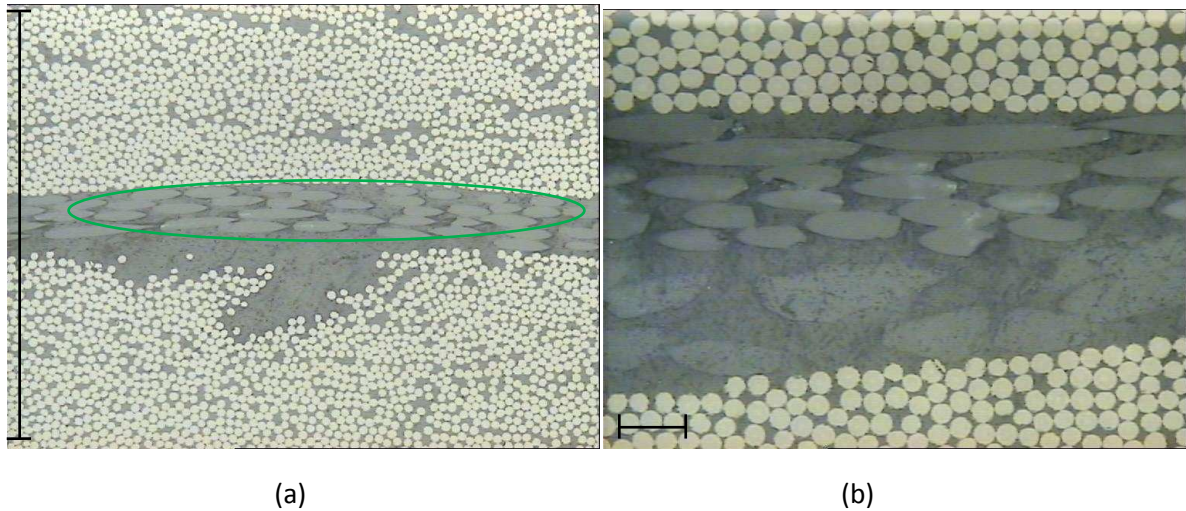


Figure 58: Microscope optical observation of RTM UD (average scales: (a) 0.38mm (b) 20 μ m).

4.1.3 Pre-preg composite

The final observations concern the Pre-preg material, shown in Figure 59. For this material, there are no voids (at these scales of observation). However, these observations reveal the presence of thermoplastic nodules at the interface between each ply. The size of these nodules is quite large, around 20 μ m in diameter. Due to the thermoplastic nature of these nodules, they could play a role during the ageing of this composite. After some investigation and according to the resin patent [142], the nature of the nodules has been identified as polyamide 6.6, with an approximate weight content of 13% in the resin. Polyamide 6.6 is well known to have a strong affinity with water and can absorb between 6 and 10% by weight.

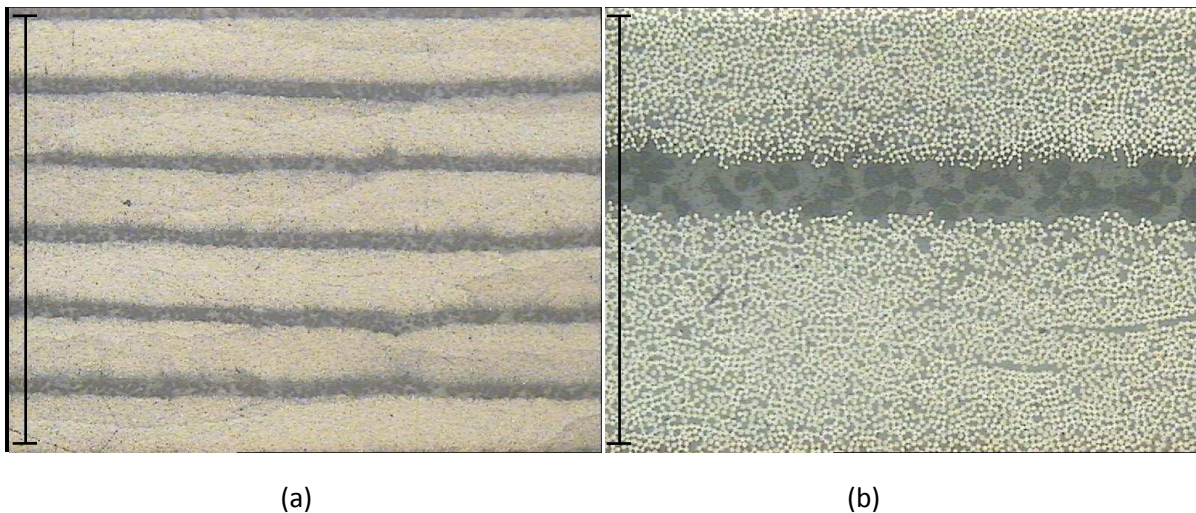


Figure 59: Microscope optical observation of Pre-preg UD (average scales: (a) 1.5 mm, (b) 0.38 mm).

These observations have also allowed the local fibre contents in the ply to be determined with ImageJ software (these values will be used in Chapter IV). The average local fibre rates were estimated using surface ratio measurements, as illustrated in Figure 60 on the UD RTM 2.5 mm material. Based on a series of three measurements per sample, the local fibre contents have been estimated and are compared to the global ones in Table 16.

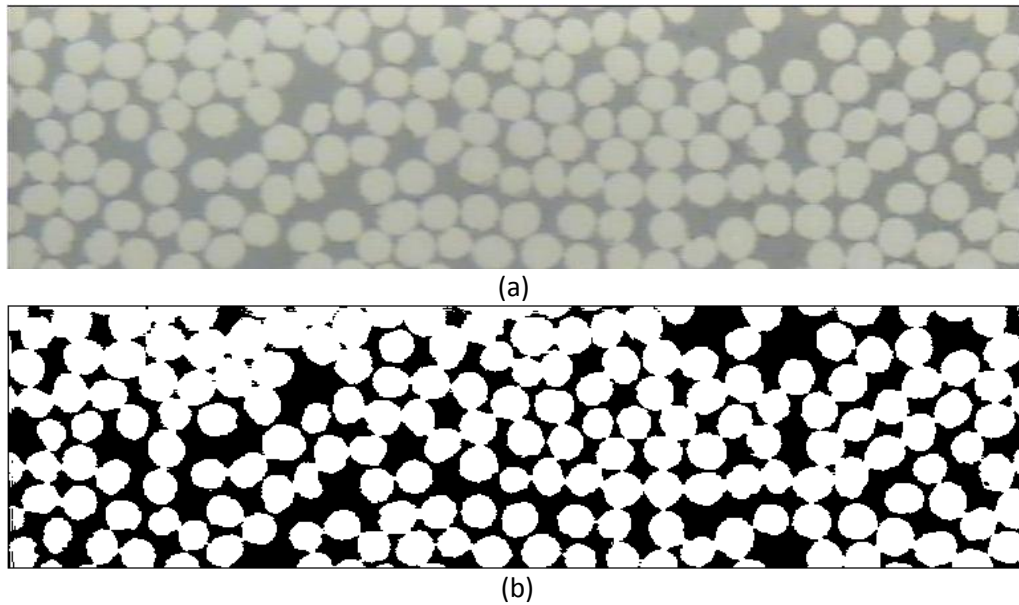


Figure 60: Example of optical microscope observation (a) and ImageJ treatment (b) for UD 2.5 mm RTM material (perpendicular to fibres, fibre diameter is approximately $5\mu\text{m}$).

Materials	Intraply fibre content (%)	Global fibre content (%)
Infused UD	66.4 (0.4)	54.6 (0.3)
RTM UD	65.0 (1.5)	50.1 (0.1)
Pre-preg UD	59.2 (0.6)	58.3 (0.4)

Table 16: Comparison between local (in the ply) and global fibre volume fractions of the UD materials. Global fibre contents have been determined by pycnometry measurements.

The optical observations performed on these three materials, provide information on the internal composite structure. They reveal the complexity of these materials, which include glass fibres, polyester fibres, and thermoplastic nodules. These observations will provide the reference for the observations after ageing.

4.2 Scanning electron microscopy (SEM)

Scanning electron microscopy (SEM), can provide more detailed information on the matrix, fibres and fibre/matrix interfaces. All those components can be observed before and after ageing. This technique can help to understand the failure mechanisms, [143],[144],[145].

SEM observations have been performed on the composite materials of the study, both of the surfaces and fracture surfaces after mechanical tests. In the following sections some published examples of SEM observations and comparison between dry and aged materials will be presented first in order to illustrate how water affects fracture surfaces. Then, some SEM observations of each composite will be presented briefly.

The aim of this section is to show some results obtained in the literature on similar materials on un-aged composites and then after sea water ageing. These observations will help to understand the observations made in the present study.

In the first example, changes to the fracture surfaces of mode II ENF specimens before and after water ageing are shown [139]. These observations give some indication of the mechanisms which contribute to changes in G_{IIC} during accelerated ageing. More cusps and more bare fibres are visible on the aged specimen (a glass/epoxy material aged 5 months at 50°C surfaces), as presented in Figure 61. This indicates that immersion leads to a reduction in matrix plasticity and a degradation of the fibre-matrix interface in this case. They correspond to a drop in G_{IIC} values of 30%.

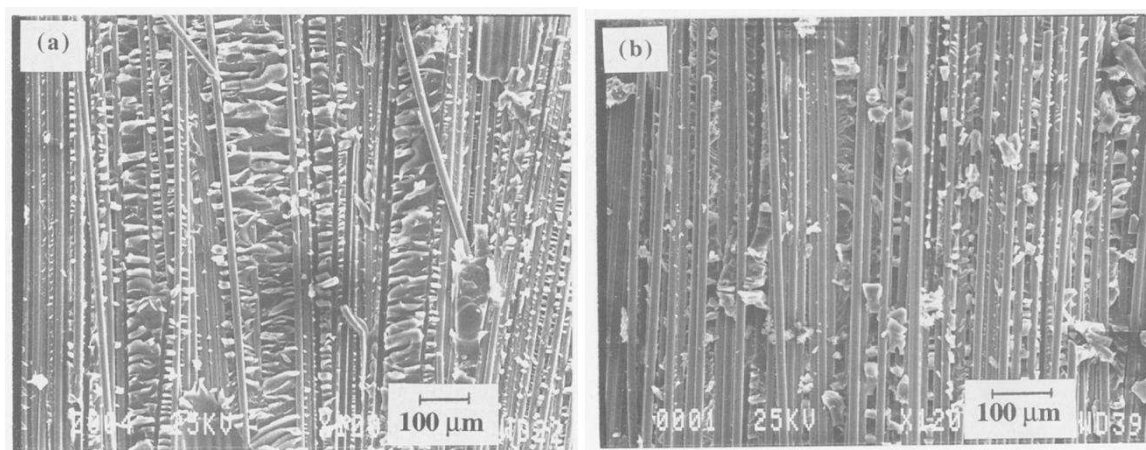


Figure 61: Fracture surfaces of a crack initiation region for mode II ENF glass/epoxy specimens, (a) dry specimen, (b) specimen immersed in distilled water at 50°C for 5 months, [139].

In a second example, the composite shear strength degradation after ageing in seawater was directly linked to the matrix degradation and plasticization. In this carbon/epoxy composite it was proposed that shear strength is governed by the matrix rather than by the interface. Further support for this was obtained from the fracture surfaces as shown in Figure 61. The fracture appears to involve mostly matrix as opposed to occurring directly at the interface, even after aging [146].

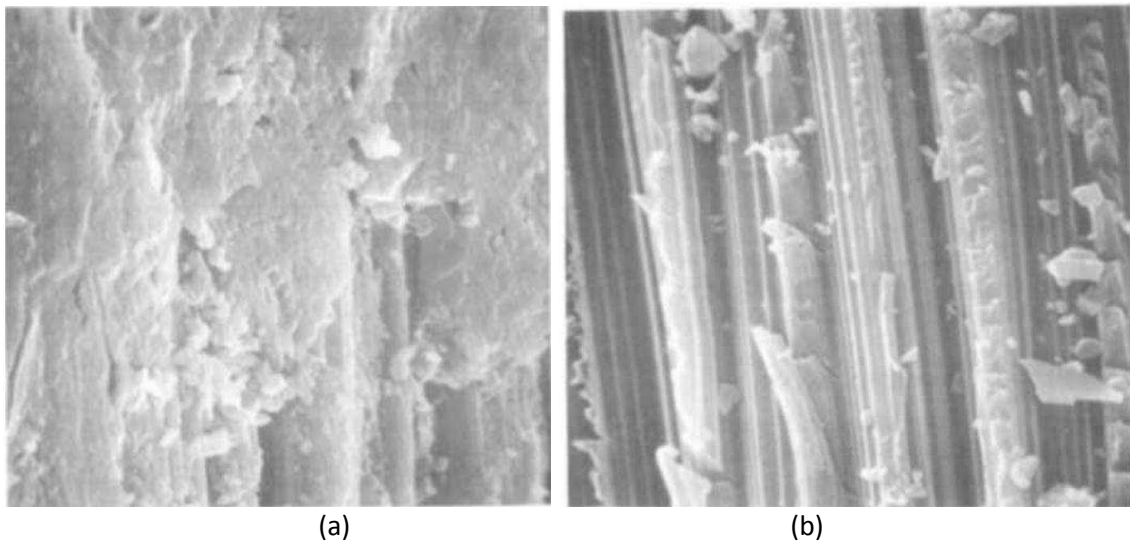


Figure 62: Interlaminar shear fracture surface of carbon/epoxy material dry (a) and exposed to sea water for 11 years (b), [146].

In the last example some observations on different carbon/epoxy materials exposed to sea water are presented. One of these materials showed cracks at the surface of the specimens, the SEM observation, presented in Figure 63, allowed the appearance of cracks in composite materials exposed to water to be visualized [147].

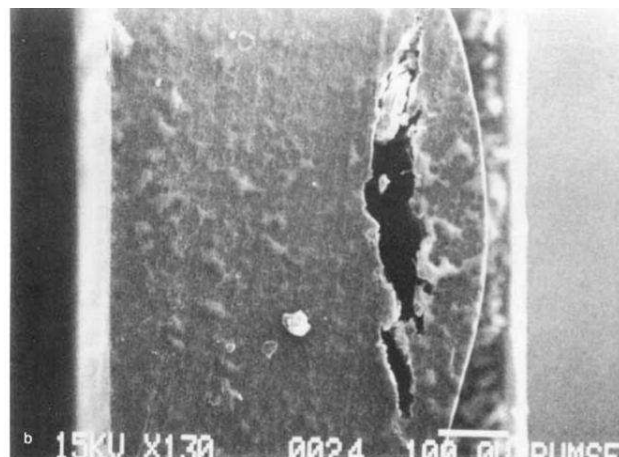


Figure 63: Crack at a carbon/epoxy composite surface after 15 days exposure to water at 90°C, [147] .

4.2.1 SEM observation on Infused material in the unaged state

SEM observations presented in the following figures were obtained after tensile tests, on quasi-UD composites oriented at 0° and 90°. Figure 64 presents the fracture surface on Infused laminates composed of 8 plies oriented at 90°. On Figure 64 (a) it is possible to observe the surface of the specimen after the failure, at the top of this picture the polyester fibres of the stitching are visible (green oval). These polyester fibres are oriented in the load direction and could affect the transverse strength. In the second plane of this figure (a), the carbon fibres appear, they seem to be well adhered to the matrix.

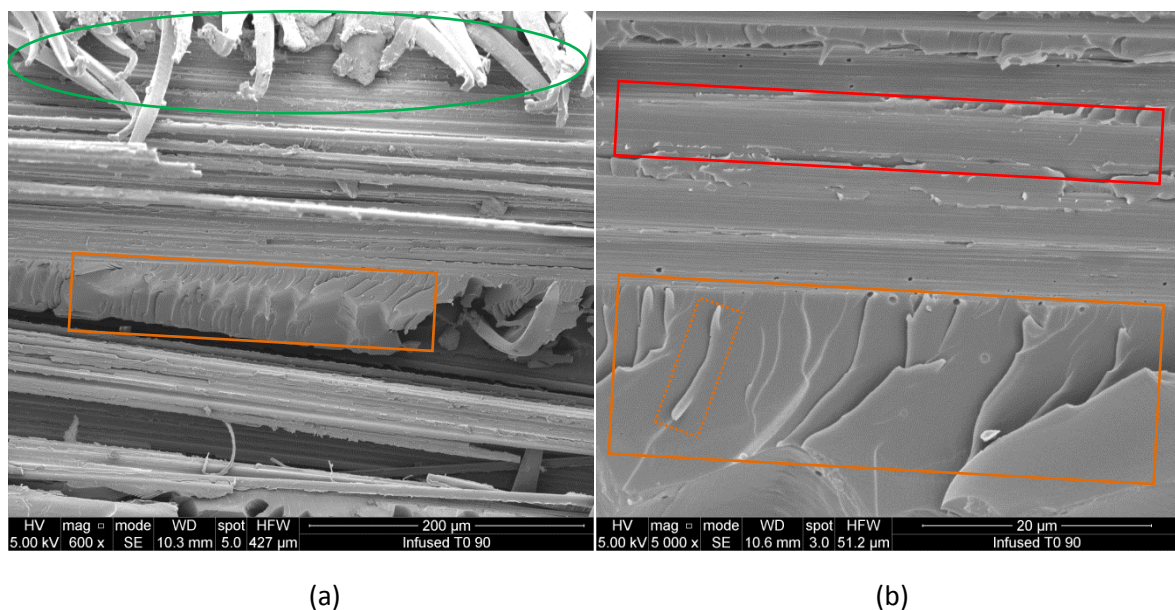


Figure 64: SEM observation on tensile fracture surface on UD Infused laminates in transverse direction, before ageing.

Figure 64 (b) is focused on the fracture surface of the resin in tension. On the top of this figure it is possible to observe the fibres furrows (red rectangle) left by the fibres after debonding. Then on the bottom of the figure it is possible to see a planar separation in the matrix (orange rectangle). In this region is possible to observe brittle cracks on the resin (orange rectangle in dotted line).

Figure 65 presents a fracture surface of the Infused material after a quasi UD tensile test oriented at 0°. After tensile failure the carbon fibres still seem to be well bonded to the matrix, Figure 65 (b), there is little fibre pull-out but interface cracks are visible on the left hand side. It is possible to observe the interface between two plies of carbon, in Figure 65 (a). This region is still bonded to each carbon layer. In this rich region of resin it is possible to observe the presence of fibres sticking (green oval).

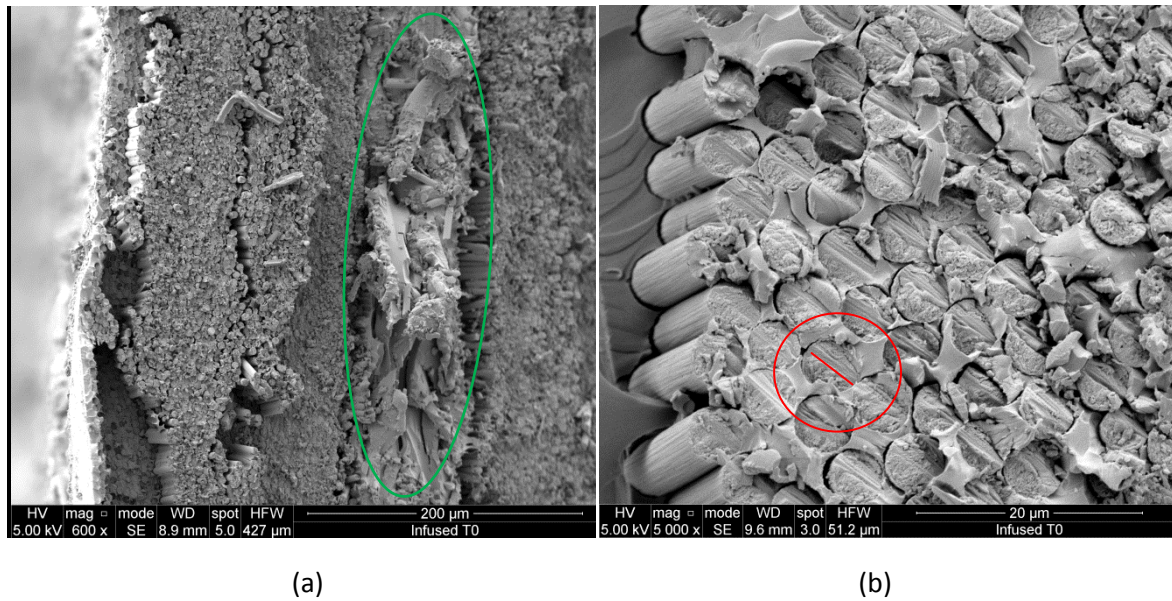


Figure 65: SEM observation on tensile fracture surface on UD Infused laminates loaded in the fibre direction, before ageing.

4.2.2 SEM observation on RTM material in the un-aged state

Same observations have been made on the RTM material after tensile test on UD specimens oriented at 0° and 90° , both composed of 8 layers of carbon. Figure 66 presents a fracture surface of an RTM specimen after a longitudinal tensile test. It is possible to observe the presence of cavities (blue dotted circles) at the surface of the specimen in Figure 66 (a), these porosities are quite numerous compared to Infused and Pre-preg samples. A zoom between two composites layers is presented in the Figure 66 (b), in these layers fibres and matrix are well bonded together. In this image, it is also possible to see a resin-rich region, where fracture occurs. The fracture surface in this region seems to be brittle.

Another observation presented in Figure 67, shows a region close to the surface of the specimen, Figure 67 (a). On Figure 67 (b), a focus on the fibres is presented, showing a good interfacial adhesion between fibres and matrix after a tensile test.

Other observations have been made after transverse tension tests on this material. Figure 68 presents fracture surface after those tests. As presented in Figure 68 (a), in the matrix region between carbon plies, fibres (green oval) are oriented in the tensile direction. In this matrix region (red rectangle) fracture seems to be brittle.

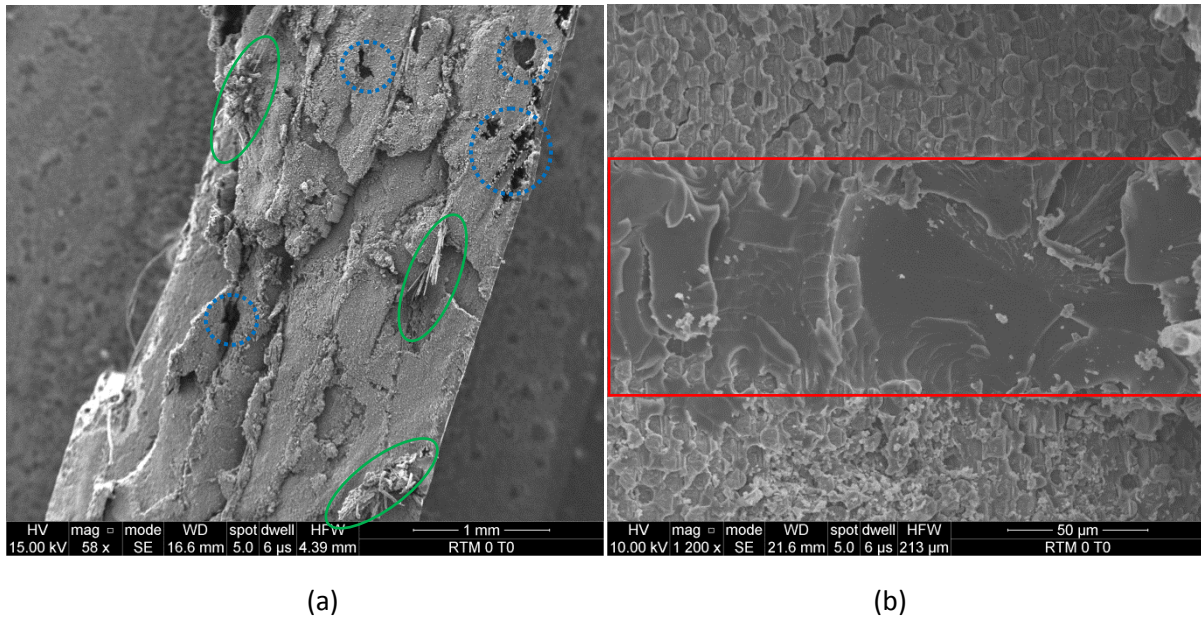


Figure 66: SEM observation on tensile fracture surface on UD RTM laminates loaded in the fibre direction, before ageing. Global surface of the specimen (a), focus between two plies of the laminate (b).

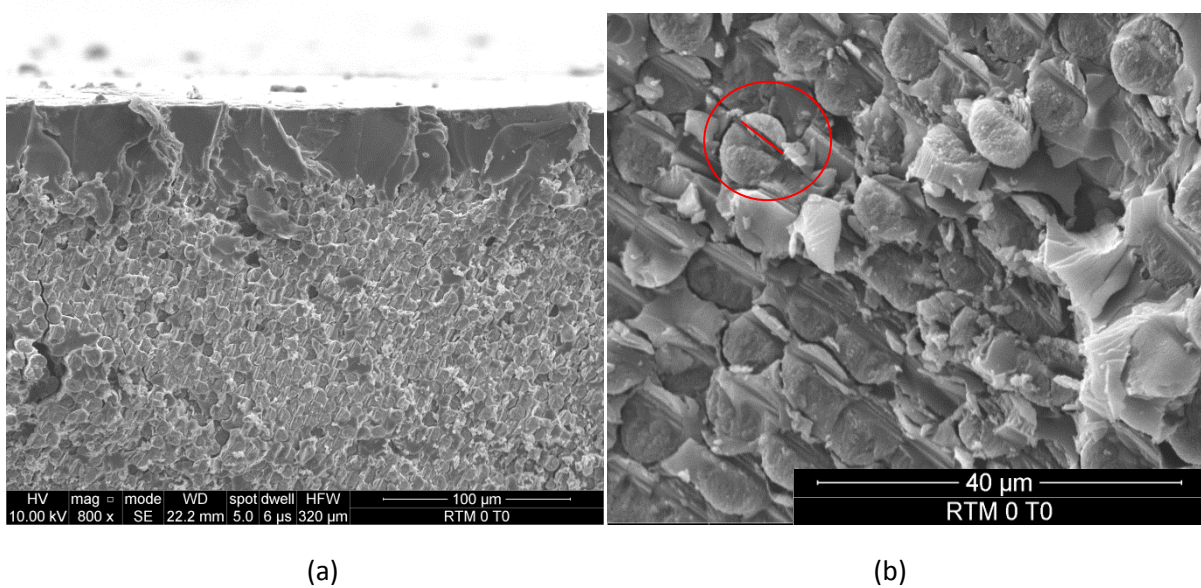


Figure 67: SEM observation on tensile fracture surface on UD RTM laminates loaded in the fibre direction, before ageing. Region on specimen surface (a), focus on fibres (b).

On Figure 68 (b), an observation close to the surface region is presented. In this region, it is possible to see large porosities. These probably initiate failure in the matrix in this region of the specimen.

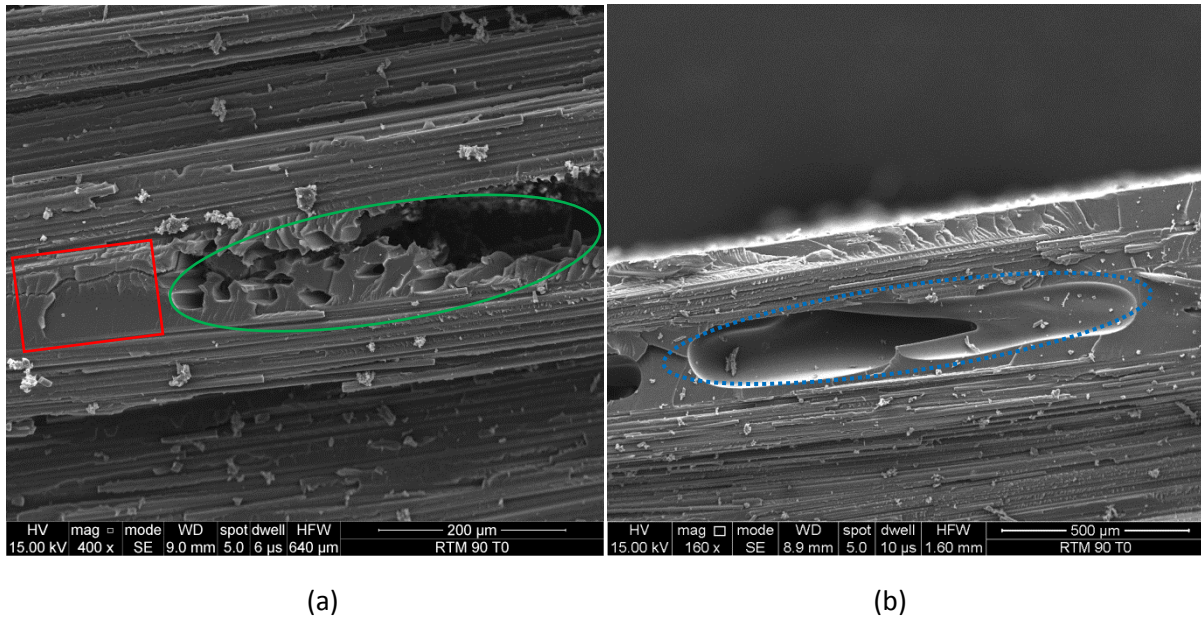


Figure 68: SEM observations on tensile fracture surface on UD RTM laminates tested in the transverse direction, before ageing.

4.2.3 SEM observation on Pre-preg material in the unaged state

For Pre-preg material, only observations on transverse tensile specimen are presented. Figure 69 presents the observations on this specimen before ageing.

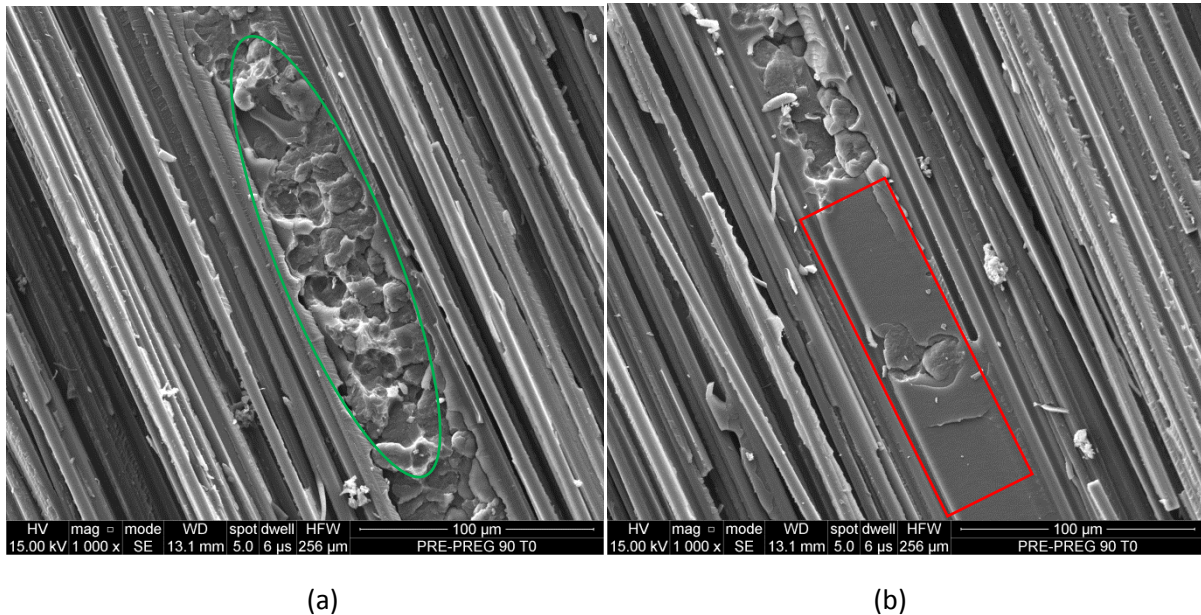


Figure 69: SEM observation on tensile fracture surface of UD Pre-preg laminates in transverse direction, before ageing.

Figure 69 (a) shows a fracture focused on a region between two plies of carbon layers. In this region (green oval) the nodules are visible and seem to play a role in the fracture mechanism. As presented in Figure 69 (b), brittle failure occurs in the resin in this region (red rectangle).

In addition there appears to be a strong bond between matrix and fibres. As presented in Figure 70, the fracture occurs in the resin leaving a skin of matrix over the composite fibres.

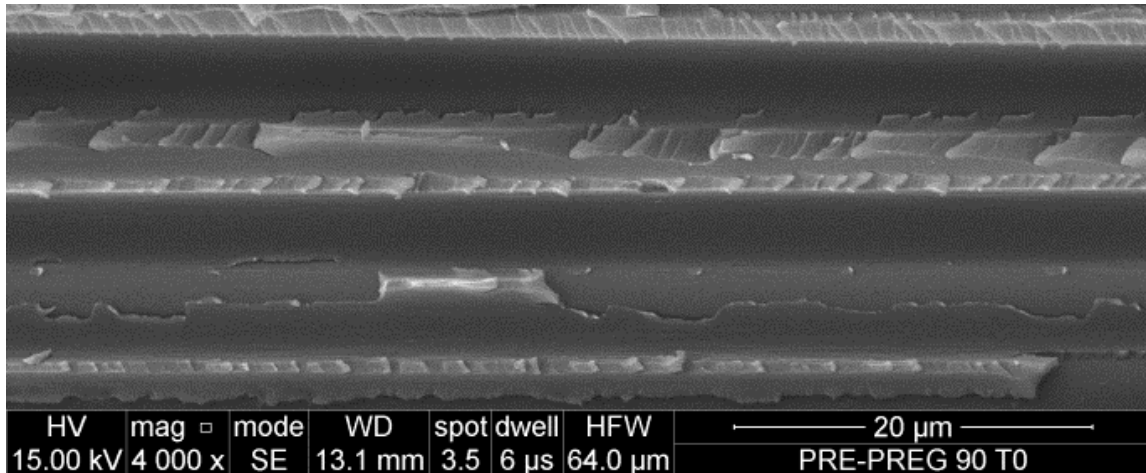


Figure 70: SEM observation on tensile fracture surface on UD Pre-preg laminates in transverse direction, before ageing. Focus on interface region between matrix and fibres.

In the next Chapter, these observations will be compared to fracture surfaces observed after ageing.

5. Damage Modelling

In this section, a damage model taking into account the crack development in composite materials will be presented. Then methods to identify and validate the model during the accelerated ageing will be presented.

The aim of using this model in this study is to develop a better understanding of damage initiation and propagation in these composites laminates. Additionally this model was developed to take into account the sea water ageing effects on damage appearance and kinetics, in order to account for these effects in a prediction of the long term behaviour of composite tidal turbine blades in a marine environment. Damage can also create new pathways for water diffusion, and as a consequence may also influence the long term diffusion of water. In this chapter the model will be applied to predict damage for un-aged materials, but in the following chapter it will be used to predict damage after sea water ageing.

5.1 Model based on physical parameters.

Transverse cracking (intra-laminar) is the principal damage mechanism of UD laminated composites loaded off-axis. A transverse crack in a multiaxial laminate is always followed by a delamination at the interface between the plies. This micro-delamination (inter-laminar crack) may have a major influence on the saturation of transverse cracks [148] and on the other hand the out of plane composite strength [141]

The damage model applied here has been developed by Carrere et al in [149] in order to represent this phenomenon. In that work the model was developed and validated using physical parameters from literature and physical parameters determined in the present study on the different composite materials. Here, the main components of this model will be presented and then the predictions of the model will be compared to the damage test results presented in section 3.3.5 .

This model must be able to be implemented in a Finite Element code, in order to use it to predict damage in large structures such as tidal turbine blades. Many models exist in the literature to predict damage in laminate composites, a good review is proposed in [150]. The purpose here is not to develop a new model but to build on the knowledge developed in the World Wide Failure Exercise [150], [151], [152].

This damage model is based on three main elements:

(I) The definition of the damage threshold (taking into account the effect of the ply thickness [126] and the multi-axial stress state [118]),

(II) The equations allowing the kinetic of the crack density to be described (based on a Finite Fracture Mechanics approach [153]),

(III) The definition of the effect of the damage (based in this study on a multi-scale numerical approach proposed in a previous study [154], [155]).

These three main elements necessitate the identification of the elastic properties of the ply, the identification of the strength and the identification of the toughness. These parameters can be easily determined using standardized tests, such as those presented previously. These basic parameters have an important physical meaning and their evolution as a function of the ageing will be described in the next Chapter.

5.2 Damage model for the prediction of the crack density

As explained previously, this section will focus on the description of transverse cracking. In order to develop a damage model, the first step consists of the definition of the damage mechanisms. It has been previously demonstrated that when a transverse crack is created a micro-delamination appears at the matrix crack tip, located in the interface between the cracked ply and the adjacent one [156],[157],[148], so the effect of transverse cracks and micro-delaminations must be included in the model.

Two damage variables are thus considered to represent these two damage mechanisms:

- The normalised crack density noted $\bar{\rho}$, this is the number of cracks multiplied by the thickness of the considerate plies and divided by the observation length and;
- The micro-delamination rate noted $\bar{\mu}$, this is the delaminated area normalized by the interface surface.

Finally, the constitutive law can be written as given in Eq. 17:

$$\underline{\underline{\sigma}} = \underline{\underline{\tilde{C}}} : (\underline{\underline{\varepsilon}} - \underline{\underline{\varepsilon}}^{th}) \quad \text{Eq. 17}$$

Where $\underline{\sigma}$, $\underline{\varepsilon}$, $\underline{\varepsilon}^{th}$ are respectively the stress, the total strain and the thermal strain expressed in the material coordinate system. $\underline{\tilde{C}}$ is the damaged elastic stiffness.

The three elements of the model, the threshold, the effect of the damage, and the kinetics of the damage development, are presented in the following discussion.

5.3 Definition of the threshold of the damage

The damage threshold is described by a failure criterion, based here on Hashin's hypotheses [158]. This criterion makes a distinction between two modes of failure: the fibre mode and the inter-fibre mode. For each failure mode, a distinction is made between failures in tension and in compression, due to their different mechanisms. In this study we will focus on the inter-fibre mode of failure. The failure criterion is written as presented in Eq.18:

	Tension	Compression
Fibre	$f_1^+ = \left(\frac{\langle \sigma_{11} \rangle_+}{X_t} \right)^2$	$f_1^- = \left(\frac{\langle \sigma_{11} \rangle_-}{X_c} \right)^2$
Interfibre	$f_2^+ = \left(\frac{\langle \sigma_{22} \rangle_+}{Y_t^{is}} \right)^2 + \left(\frac{\langle \sigma_{12} \rangle}{S_c^{is}(1-p\sigma_{22})} \right)^2$	$f_2^- = \left(\frac{\langle \sigma_{22} \rangle_-}{Y_c} \right)^2 + \left(\frac{\langle \sigma_{12} \rangle}{S_c^{is}(1-p\sigma_{22})} \right)^2$

$$\text{Where: } \begin{cases} \langle X \rangle_+ = X \text{ si } X > 0 \\ \langle X \rangle_+ = 0 \text{ si } X < 0 \end{cases} \text{ and } \begin{cases} \langle X \rangle_- = 0 \text{ si } X > 0 \\ \langle X \rangle_- = X \text{ si } X < 0 \end{cases} \quad \text{Eq. 18}$$

The parameters X_t , X_c , Y_t^{is} , S_c^{is} and Y_c are respectively the fibre tensile and compressive strengths, the in-situ transverse tensile and in-plane shear strength and the compressive strength. The parameter p is a shape factor (see [118]). It has been shown that transverse and shear strengths depend on the thickness of the ply [126]. This is why the notion of the in-situ strengths was introduced. The in-situ strengths are defined based on the work of Camanho and al. [126]. The in-situ

strengths are a function of the thickness of the ply t and depend on the elastic properties of the ply. The transverse in-situ tensile strength is given by Eq.19:

$$Y_t^{is} = \max(Y_t^{thick}, Y_t^{thin}) \quad \text{Eq. 19}$$

Where Y_t is the transverse strength measured on a $[90]_n$ laminate, Y_t^{thin} and Y_t^{thick} are given in Eq.20:

$$Y_t^{thin} = \sqrt{\frac{8G_I^{c,ply}}{\pi t_{ply} \Lambda_{22}^0}} \quad \text{and} \quad Y_t^{thick} = 1.12\sqrt{2Y_t} \quad \text{Eq. 20}$$

And $G_I^{c,ply}$ is the mode I toughness of the ply. The identification procedure of the toughness of the ply will be explained in the following section 5.5. The thickness of the ply is noted t_{ply} . The variable Λ_{22}^0 is given by Eq.21:

$$\Lambda_{22}^0 = 2 \left(\frac{1}{E_{22}} - \frac{\nu_{12}^2}{E_{11}} \right) \quad \text{Eq. 21}$$

Where E_{22} and E_{11} are the modulus values in the longitudinal and transverse directions, ν_{12} is the Poisson's ratio. The in-situ shear strength is presented in the following equation, Eq.22:

$$S_c^{is} = \min(S_c, S_c^{thin}) \quad \text{Eq. 22}$$

Where S_c is the shear strength measured on a $[\pm 45]_s$ laminate using the method presented in the previous section (3.1.2). Thus, S_c^{thin} is given by Eq.23:

$$S_c^{is} = \sqrt{\frac{8G_{12}G_{II}^{c,ply}}{\pi t_{ply} \Lambda_{22}^0}} \quad \text{Eq. 23}$$

And $G_{II}^{c,ply}$ is the mode II toughness of the ply. Figure 71 represents the evolution of the transverse *in-situ* tensile strength as a function of the thickness of the ply, (t_{ply}), with $G_I^{c,ply} = 0.2 \text{ N/mm}$, $E_{11} = 136000 \text{ MPa}$, $E_{22} = 7120 \text{ MPa}$ and $\nu_{12} = 0.32$.

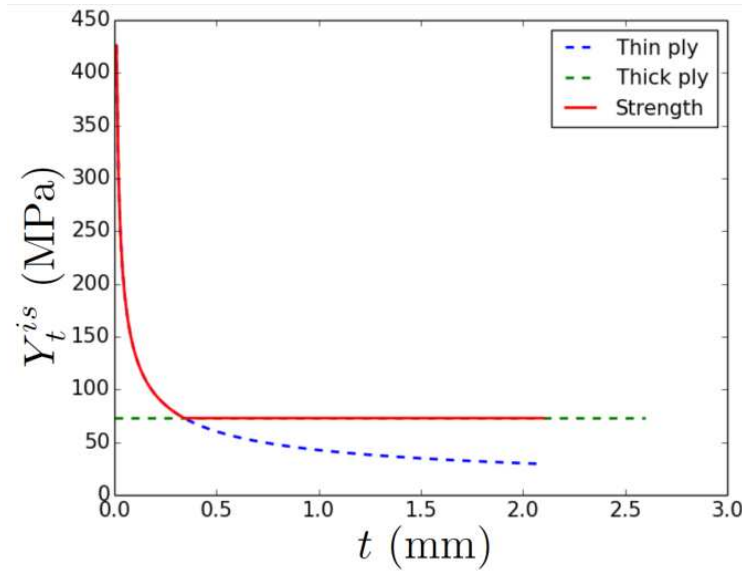


Figure 71: Evolution of the in-situ strength as a function of the thickness.

Using this first development, a stress criterion was established to define the threshold of damage in carbon/epoxy composites. This criterion takes into account the thickness of the ply. Criterion parameters can be easily determined with simple standardised tests.

5.4 Definition of the effect of the damage

In order to define the effect of the damage on the elastic properties of the ply, a numerical homogenization procedure presented in previous work has been used [154],[155]. It allows the homogenized elastic properties to be determined for several coupled $(\bar{\rho}, \bar{\mu})$. Assuming that the loss of stiffness of the laminate is the only reason for the loss of stiffness of the 90° ply, an equivalent stiffness of the damaged ply is identified. More details are given in [155]. Based on this approach, it has been shown that the variation of the compliance tensor can be written as presented in Eq.24:

$$\Delta \underline{\underline{S}}(\bar{\rho}, \bar{\mu}) = \bar{\rho} \underline{\underline{H}}^a + \frac{\bar{\mu}}{1 - \bar{\mu}} \underline{\underline{H}}^b + \bar{\rho}^2 \underline{\underline{H}}^c + \bar{\rho} \frac{\bar{\mu}}{1 - \bar{\mu}} \underline{\underline{H}}^d + \frac{\bar{\mu}}{1 - \bar{\rho} \bar{\mu}} \underline{\underline{H}}^e \quad \text{Eq. 24}$$

The fourth order tensors $\underline{\underline{H}}^a$ to $\underline{\underline{H}}^e$ are named effect tensors. It has been shown that the components of these tensors are only a function of the initial elastic properties of the ply and of the nature of the fibres (i.e. carbon or glass). The non-null components of the effect tensors are given in [149], for carbon/epoxy materials.

5.5 Definition of the kinetics of the damage development

The creation of a new crack requires specific conditions; it is possible in two cases:

- If the inter-fibre criterion is fulfilled for the first time, a first crack could be created,
- If the ply is already damaged, a new crack could be created.

The criterion used to describe the evolution of the number of cracks as a function of the loading is based on a Finite Fracture approach. This indicates that the change of the potential energy ΔW between two steps of loading is compared to the toughness of the ply of the ply ($G_I^{c,ply}$ that is defined in this section). ΔW is the energetic variation between two states, the state at time time t with a number of cracks equal to N and a state at time $t + \Delta t$ with a number of cracks $N + \Delta N$ [153]. ΔW is written as presented in Eq.25.

$$\Delta W = G^{c,ply} \Delta N S_f^{2+} \quad \text{Eq. 25}$$

Where S_f^{2+} is the surface of a single crack, as presented in Figure 72. This surface is equal to $t_{ply} \times w$ (where w is the width of the laminate). Following the work of Hashin [153], the energy change could be written as:

$$\Delta W = \frac{1}{2} \int_V [\underline{\underline{\sigma}}(t + \Delta t) : \underline{\underline{\tilde{S}}}(t + \Delta t) : \underline{\underline{\sigma}}(t + \Delta t) - \underline{\underline{\sigma}}(t) : \underline{\underline{\tilde{S}}}(t) : \underline{\underline{\sigma}}(t)] dV \quad \text{Eq. 26}$$

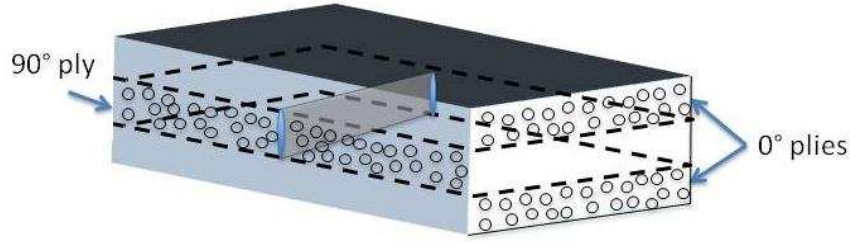


Figure 72: Representation of the surface S_f^{2+} corresponding to a single crack.

In Eq.25, $\underline{\tilde{S}}$ is the damaged compliance tensor. It can be calculated using the results presented in section 5.4. Using the St Venant principle it is supposed that the reaction of a crack mainly affects the energy of this ply. Moreover, it is assumed that once a crack is created, this crack creation takes place over the whole thickness and width of the ply. By homogenizing the behavior in the length of the ply L , we are able to write the following equation, Eq.27:

$$\Delta W = \frac{1}{2} t_{ply} w L [\underline{\sigma}(t + \Delta t) : \underline{\tilde{S}}(t + \Delta t) : \underline{\sigma}(t + \Delta t) - \underline{\sigma}(t) : \underline{\tilde{S}}(t) : \underline{\sigma}(t)] \quad \text{Eq. 27}$$

The number of cracks in Eq.24 is replaced by the normalized crack density $\bar{\rho} = \frac{N}{L} t_{ply}$ which leads to this equation, Eq.28:

$$[\underline{\sigma}(t + \Delta t) : \underline{\tilde{S}}(t + \Delta t) : \underline{\sigma}(t + \Delta t) - \underline{\sigma}(t) : \underline{\tilde{S}}(t) : \underline{\sigma}(t)] = G^{c,ply} \frac{\bar{\rho}}{t_{ply}} \quad \text{Eq. 28}$$

Solving Eq.27 at each loading step allows the evolution of the damage to be calculated. It should be noted that only the components of the stress which can induce transverse cracks (σ_{22} and σ_{12}) are taken into account in Eq.28.

The last point concerns the definition of the toughness of the ply involved in Eq.28. The procedure to define the total toughness of the ply $G^{c,ply}$ is presented in [149]. The toughness of the ply is a function of the mode mixity. The mode mixity is defined using the strain which can induce

transverse cracks (i.e. ε_{22} and ε_{12}), following the same hypothesis as for a cohesive zone model [159]. Then it is possible to define the energy released in the ply in mode I G_I^{ply} and in mode II G_{II}^{ply} as a function of total toughness of the ply $G^{c,ply}$. A linear criterion for the mode mixity is used. Finally it is possible to define the total toughness of the ply $G^{c,ply}$ as presented in Eq.29:

$$G^{c,ply} = \left[\left(\frac{\cos(\theta)}{G_I^{c,ply}} \right) + \left(\frac{\sin(\theta)}{G_{II}^{c,ply}} \right) \right]^{-1} \quad \text{Eq. 29}$$

The evolution of the micro-delamination ratio $\bar{\mu}$ [154] is explicitly calculated as a function of $\bar{\rho}$ by:

$$\bar{\mu} = a_h \bar{\rho}^2 + h b_h \bar{\rho} \quad \text{Eq. 30}$$

Where a_h and b_h are material parameters that can be found in [154] for an carbon/epoxy.

In order to apply the model, it is necessary to determine the toughness of the ply, $G_I^{c,ply}$. In some cases, the material toughness of the ply could be different from the toughness measured at the interface between the plies using the standardized fracture tests, such as DCB [133] or MMB [134]. As a consequence the kinetics of damage will be over-estimated if those values are used. Thus it is necessary to identify this toughness with another method. One possibility consists of using the threshold of the damage measured on a cross-ply laminate with a thin 90° ply. The appearance of this first crack can be easily detected with Acoustic Emission or by visual observation. Then, using the classical laminate theory, it is possible to determine the transverse stress in the 90° ply (σ_{22}^{in}). This stress is equal to the in-situ strength Y_t . Using this stress in Eq.20, it is possible to obtain the following expression for $G_I^{c,ply}$ in Eq.31:

$$G_I^{c,ply} = \frac{1}{8} (\sigma_{22}^{in})^2 \pi \cdot t_{ply} \Lambda_{22}^0 \quad \text{Eq. 31}$$

Finally, the toughness $G_I^{c,ply}$ determined in Eq.31 is used in Eq.28, in order to determine the kinetics of the damage development.

5.6 Identification of the model

Figure 73 summarises the different steps and conditions to complete in order to determine the evolution of the crack density of a ply in a laminate as a function of applied load. To create a crack, it is necessary to have a ply already damaged or which has reached the inter-fibre failure criterion. If these conditions are not met, this procedure is then incremented to a higher loading step until the creation of a crack. After crack initiation and also during propagation, their effects are taken into account in calculation of the resulting damaged elastic stiffness.

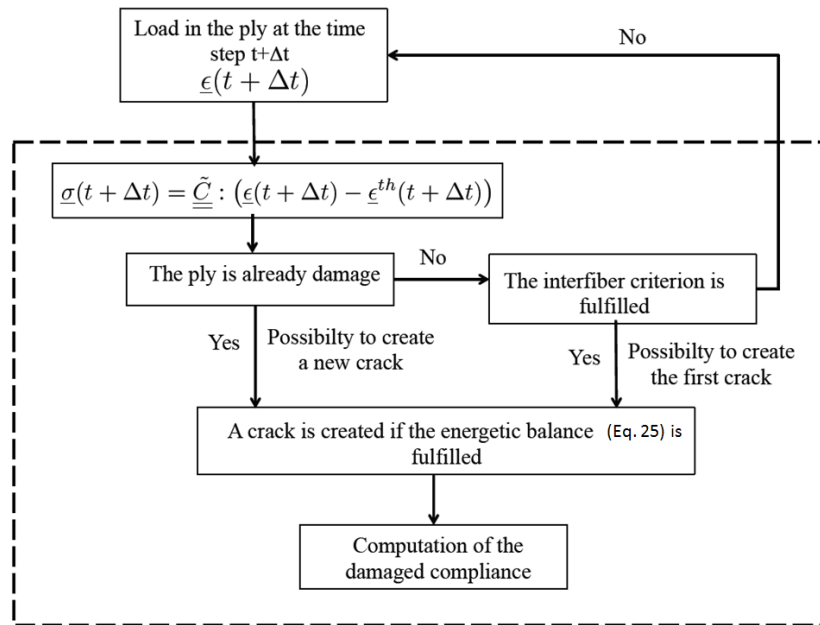


Figure 73: Flowchart presenting the different processes in the model allowing the crack density to be predicted as a function of the loading.

In summary, the identification of this model requires the following tests:

- Tensile (and compressive) tests on the UD ply, in order to identify the elastic properties and strength in the longitudinal and the transverse directions, described in section 3.1;
- Tensile tests on a $\pm 45^\circ$ laminate in order to identify the in-plane shear modulus and strength, according to the test procedure presented in section 3.1.2;

- And finally one test on a cross-ply laminate $[0,90_{1/2}]_s$ to identify the toughness of the ply, using the determination of the threshold of damage, Eq.31.

This model has been validated using data on materials from the literature, in [149] on carbon/epoxy and glass/epoxy. In the next section, the validation will be extended using the materials of the study and the experimental results previously determined in this chapter. It is important to note that the thermal residual stresses can have a strong influence on the prediction of the first transverse crack. These residual stresses are difficult to model, this is the reason why, for sake of simplicity, the stress free temperature T_0 is assumed to be reduced by 50% as proposed by some authors in the literature [118].

5.7 Validation on Carbon/Epoxy materials

Two carbon/epoxy materials have been investigated. These materials are the Pre-preg and Infused materials, previously characterized in this study. Their properties are given in Table 17.

Materials	E_{11} (GPa)	E_{22} (GPa)	ν_{12} *	X_t (GPa)	Y_t (MPa)	G_I^c (N.mm ⁻¹)
Infused	136	6.8	0.4	2.2	45	0.57
Pre-preg	170	8.7	0.3	2.35	43	0.36

*not measured, chosen equal to common literature values for this kind of material

Table 17: Materials physical properties determined previously and used in the model

For the Pre-preg material, two cross-ply laminated are investigated: a $[0_2,90_{1/2}]_s$ and a $[0_2,90_2]_s$. For the Infused composite two cross-ply laminates $[0,90,0,90]_s$ and $[0_2,90_2]_s$ have been modelled.

The Pre-preg toughness has been identified using Eq.35, with $\sigma_{22}^{in} = 65$ MPa. This stress is attained in the 90° ply for an applied load corresponding to the threshold of the damage in a $[0_2,90_{1/2}]_s$ lay-up, as presented in section 3.3.5.

As shown in Figure 74, the toughness of the Pre-preg identified previously, allows the threshold of the damage to be described correctly for the thin 90° ply laminate ($[0_2,90_{1/2}]_s$ represented in red on this figure). However, the crack density is slightly underestimated. This difference could be due to an overestimation of the micro-delamination (eq. 30). Moreover the experimental determination of the crack density for such thin plies is difficult. However, the

evolution of the threshold of the damage as a function of the thickness of the 90° ply is quite well predicted.

In another case presented in Figure 74 as the blue curve, the threshold was defined by the stress criterion (see Eq.19). The model provides a good estimation of the initiation of the damage. The evolution of the crack density as a function of the applied load on the $[0_2, 90_2]_s$ lay-up is quite well predicted. This allows the identification of the toughness of the ply using the threshold of the damage in a laminate with a thin 90° ply to be checked.

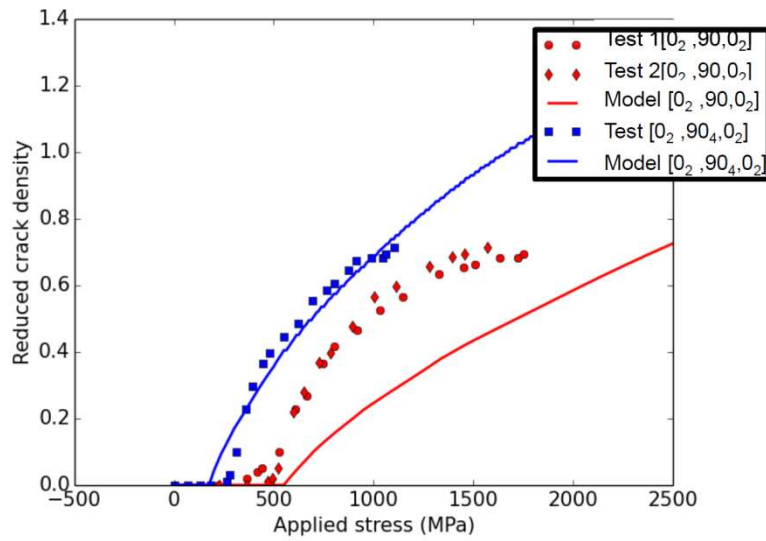


Figure 74: Evolution of crack density in 90° ply as a function of the loading for two Pre-preg laminates $[0_2, 90_{1/2}]_s$ and $[0_2, 90_2]_s$.

For the Infused material, $G_I^{c,ply}$ value has been identified equal to $0.2 \text{ N}\cdot\text{mm}^{-1}$ following the procedure given in section 5.3 on a $[0, 90, 0, 90]_s$ Infused laminate (see Figure 75). This value is lower than the toughness of the interface identified using the DCB tests. In this experimental section 3.4.5, it has been highlighted that fibre stitching and carbon fibre bridging tend to increase the interfacial toughness during propagation. This is why $G_I^{c,ply}$ is lower than experimental value, and this allows a better description of the kinetics of damage

It is worth mentioning, that the toughness of the ply identified using the threshold of the damage on a laminate with a thin 90° ply, provides correct results concerning the evolution of the crack density for both the thin ply and the ply with double thickness, as presented in Figure 75 for the $[0, 90, 0, 90]_s$ Infused cross-ply laminate .

The Figure 76 presents a comparison between model and experimental results on $[0_2,90_2]_s$ Infused cross-ply laminates. In this case the model described the initiation of damage in a correct manner. This threshold is slightly overestimated, but the kinetics of damage development are well predicted by the model.

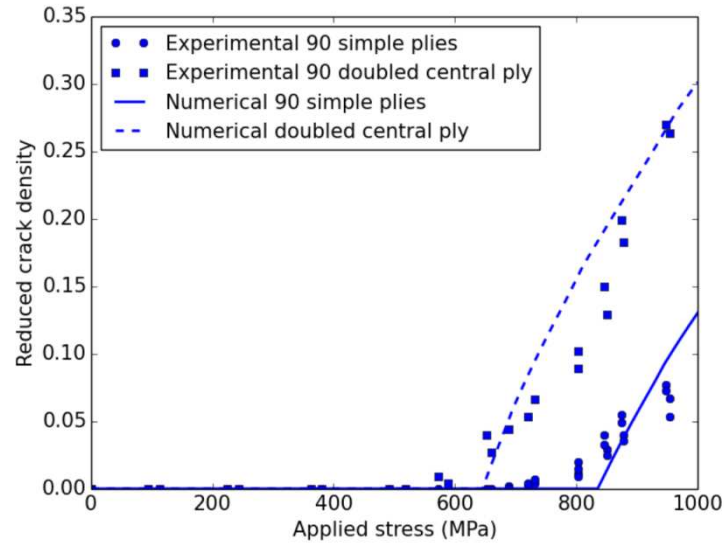


Figure 75: Evolution of the crack density in the 90° ply as a function of the loading for a $[0,90,0,90]_s$ Infused laminate. The threshold of damage in the double central ply is used to identify the toughness of the ply. The experimental results correspond to two tests.

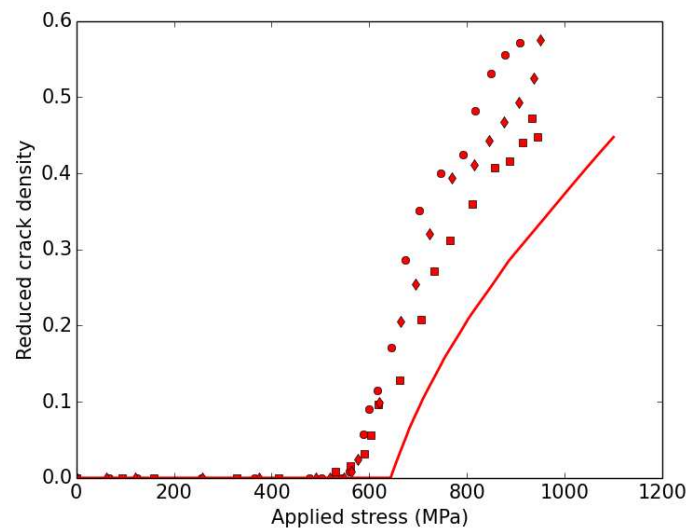


Figure 76: Evolution of the crack density in the 90° plies as a function of the loading for a $[0_2,90_2]_s$ Infused laminate. Comparison between model (line) and experimental results (points)

5.8 Summary and conclusion on the damage model

The previous sections have presented key points of a model to predict the evolution of the crack density as a function of the applied load. A damage model based on simple physical parameters has been proposed and model predictions have been compared to results for different composite materials. The threshold of the damage is described by a failure criterion which takes into account the effect of the ply thickness. The kinetics of the damage are modeled by a Finite Fracture Mechanics approach using composite toughness. Finally, the effect of the damage on the elastic properties is identified thanks to multi-scale finite element calculations. Only a few standard tests are needed to identify the parameters of the model (moduli, strengths and the toughness of the ply).

For this study in the un-aged state, experiments have been performed on two carbon/epoxy materials representative of a composite material used in tidal blades. For these materials, a good agreement was found between the model prediction and experimental results. Both threshold and kinetics are quite well estimated by the model. In the following chapter, a new set of model parameters will be identified after sea water ageing. These will then be used in the model and predictions will be compared test results on aged to $0^\circ/90^\circ$ specimens.

Dans cette étude à l'état non vieilli, des expérimentations ont été réalisées sur deux matériaux représentatifs des matériaux utilisés dans les pales d'hydroliennes. Pour ces matériaux un bon accord a été trouvé entre les résultats expérimentaux et les prédictions du modèle. Le seuil et la cinétique sont tous deux bien estimés grâce au modèle. Dans les chapitres suivants les paramètres du modèle seront identifiés après vieillissement en milieu marin, ils seront ainsi comparés à ceux déterminés expérimentalement après vieillissement.

Chapter III. Effects of sea water ageing on composite materials

Tidal turbines and their components, will be directly in contact with sea water throughout their service life. Results in Chapter I have shown that ageing phenomena can reduce composite mechanical properties, and as a consequence reduce the lifetime of such structures. It is necessary to understand how sea water will diffuse into and act on carbon/epoxy materials in order to predict the lifetime of composite marine energy structures.

In Chapter II, the behaviour of three possible materials for tidal turbine blade applications has been studied in the un-aged state, in order to have references before sea water ageing. In this chapter, various investigations will be performed to characterize how sea water affects carbon/epoxy materials.

The first part of this chapter will focus on the mechanisms of water diffusion in such polymeric materials. The composites of the study are manufactured using carbon fibres and epoxy, and it has been recognized that carbon fibres are not sensitive to the water. Epoxy resin on the contrary has some affinity with water molecules. Different models describe how these molecules diffuse in polymers, and they will be presented here.

Then a procedure to accelerate the sea water ageing process will be presented for each material. Because the water ageing phenomenon is a thermally activated process it may be possible to use an Arrhenius law to predict long term kinetics, but this needs to be verified.

The last point of this study concerns the characterization of the effects of sea water ageing on these materials. First, the kinetics of sea water diffusion will be studied for each material. These diffusion results will indicate when the composites are saturated with water. Then the effects of the marine environment will be characterized using the same standardized tests as those presented in Chapter II. This procedure has been repeated at different ageing times in order to characterize changes in properties. Finally the impact of sea water on the materials of the study will be discussed and compared in terms of both diffusion and mechanical behaviour.

Chapitre III. Effets du vieillissement en eau de mer sur les matériaux composites

Les hydroliennes et leurs composants, par exemple les pales en composites, sont directement en contact avec l'eau de mer au cours de leur durée de vie. Les phénomènes de vieillissement peuvent réduire les propriétés mécaniques des composites et en conséquence réduire la durée de vie de ces structures. Les matériaux composites sont perméables et l'eau de mer diffuse à travers ces matériaux. Il est nécessaire de comprendre comment l'eau de mer va diffuser et interagir dans les matériaux carbone/époxy dans le but de prédire la durée de vie des structures récupératrices d'énergies marines en composites.

Dans le précédent Chapitre II, le comportement de trois possibles matériaux pour des applications pales d'hydroliennes a été étudié à l'état non vieilli dans le but d'avoir des références avant le vieillissement en eau de mer. Dans le chapitre suivant, de nombreuses investigations seront menées pour caractériser comment l'eau de mer affecte les matériaux carbone/époxy.

La première partie de ce chapitre va se focaliser sur les mécanismes de diffusion d'eau dans ce type de matériaux polymères. Les composites de l'étude sont fabriqués en utilisant des fibres de carbone et une résine époxy. Il a été reconnu que les fibres de carbone sont insensibles à l'eau. Au contraire la résine époxy a des affinités avec les molécules d'eau. Différents modèles décrivent comment ces molécules d'eau diffusent dans les polymères, ces modèles seront présentés ici.

Le dernier point concerne la caractérisation des effets du vieillissement en eau de mer sur ces matériaux. Premièrement la cinétique de diffusion d'eau dans chaque matériau sera étudiée. Ces résultats de diffusion vont indiquer quand les composites sont saturés en eau. Ensuite les effets de l'environnement marin seront caractérisés en utilisant la même procédure normalisée, comme présentée dans le Chapitre II. Cette procédure a été répétée à différent temps de vieillissement dans le but de caractériser les changements de propriétés. Finalement l'impact de l'eau de mer, sur les matériaux de l'étude sera discutée et comparée pour chaque comportement mécanique et de diffusion.

Table of contents

Chapter III. Effects of sea water ageing on composite materials	101
1. Ageing in a marine environment: phenomena and mechanisms	105
1.1 The processes of water diffusion	105
1.1.1 Water diffusion mechanism	105
1.1.2 Sea water	106
1.2 The diffusion models	107
1.2.1 The Fickian approach	107
1.2.2 The Langmuir approach	110
1.3 Diffusion in composite materials	112
1.3.1 A first approach for diffusion in composites	113
1.3.2 Non Fickian diffusion in composites	115
1.4 Measurement of water concentration in polymers and composites	115
1.5 Temperature dependence of the diffusion process	116
2. Accelerated sea water ageing	117
2.1 Necessity to accelerate ageing	117
2.2 Procedure and conditions used to accelerate ageing	117
3. Characterisation of sea water ageing	120
3.1 Characterisation of the water diffusion into Pre-preg, RTM and Infused materials	120
3.1.1 Sea water diffusion neat epoxy resin	121
3.1.2 Sea water diffusion in three composite materials	123
3.1.3 Effect of material orientation on the diffusion process	127
3.1.4 Effect of composite thickness on the diffusion of seawater	129
3.2 Physico-chemical characterization	130
3.2.1 Change in Tg during ageing	130
3.3 Effect on elastic properties	131
3.3.1 Tensile properties of neat resin (40°C and 60°C)	131
3.3.2 Tensile properties of 0° and 90° laminates	133
3.3.3 Effect of sea water ageing on in-plane shear behaviour	136
3.4 Influence of aging on non linear properties	136
3.4.1 Tensile tests at different loading rates	136
3.4.2 Creep behaviour	137
3.5 Effect of sea water ageing on damage propagation	138
3.6 Effect on interlaminar fracture toughness	140
3.7 Effect on out of plane stress	142

3.8	Additional investigation on ageing	143
4.	Microscopy observation of ageing effects	145
4.1	Composite surface exposed to sea water	145
4.1.1	Infused material	145
4.1.2	Pre-preg material	147
4.1.3	RTM material	147
4.2	Fracture surface after longitudinal tensile tests.	148
4.2.1	Infused material	148
4.2.2	RTM material	150
4.3	Fracture surface after transverse tensile tests.	152
4.3.1	Infused transverse	152
4.3.2	RTM transverse	153
4.3.3	Pre-preg transverse	154
4.4	Interlaminar fracture surface after DCB test	156
4.4.1	Infused material	156
4.4.2	RTM material	158
4.4.3	Pre-preg	160
5.	Influence of manufacturing process	164
5.1	Influence of manufacturing process on the kinetic of diffusion	164
5.2	Effect of manufacturing process on properties after water ageing	167
5.2.1	Tensile longitudinal and transverse strength	167
5.2.2	Shear strengths and modulus	168
5.2.3	ILSS shear strength for UD and QI materials	169
5.3	A first conclusion about sea water ageing in composites for tidal turbine	171

1. Ageing in a marine environment: phenomena and mechanisms

The sea water ageing phenomena result from the diffusion of water inside composite materials, inducing chemical and physical changes. In general, these changes are not beneficial for the state of health of this kind of material, because mechanical properties are affected and are often reduced. Water diffusion in composites is a complex phenomenon involving specific mechanisms which depend on the resin chemistry, the fibre/matrix interface and the manufacturing parameters.

1.1 The processes of water diffusion

Metals, glasses, certain ceramic materials are impermeable, but this is not the case for polymer materials, which are permeable to water. Water diffuses into these polymers, and in particular the epoxy resins of the present study [160]. Diffusion is the process by which matter is transported from one part of a system to another as a result of random molecular motions; this is the definition of the diffusion process proposed by Crank in 1956 [161] and 1975 [162]. In the case of the marine environment the matter transported will be water molecules.

1.1.1 Water diffusion mechanism

Diffusion or sorption is a molecular process, water molecules move through polymer materials, from a region of higher concentration to another one with a lower concentration.

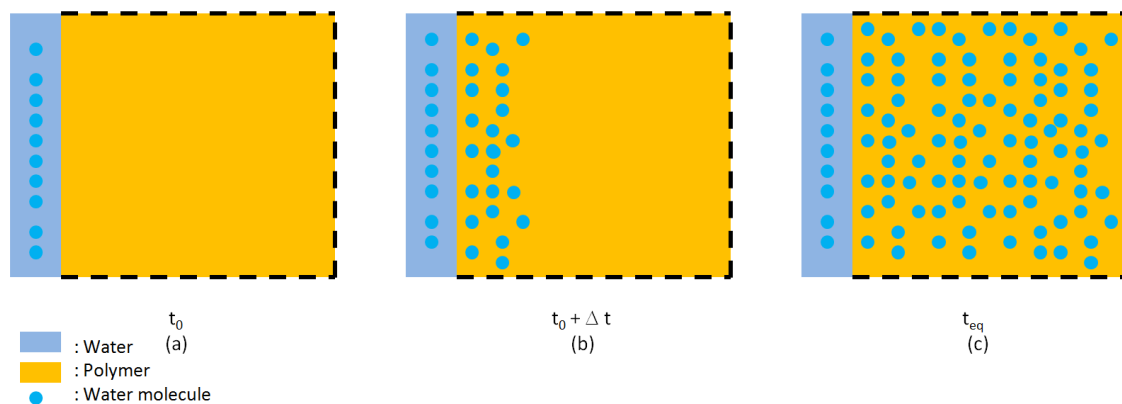


Figure 77: Representation of water diffusion through polymer material as a function of time.

Figure 77 represents the process of diffusion into polymer materials at different diffusion times. Thus, when a polymer specimen is immersed in water, Figure 77 (a), the specimen surface absorbs the water immediately and tends to reach a steady-state. During subsequent immersion time, the water penetrates deeper into the sample (Figure 77 (b)) until an equilibrium of water inside the specimen is reached, as presented in Figure 77 (c).

The speed of this transport of water molecules through the polymer material is characterized by D , the diffusion coefficient, usually expressed in $\text{m}^2.\text{s}^{-1}$. This movement of water molecules is described by the diffusion laws and is reversible (desorption).

1.1.2 Sea water

The nature of the water can influence the ageing mechanisms due to chemical interactions. Tidal turbines are used in a liquid environment (sea water) and the water content at equilibrium is linked with the chemical potential of water. As a consequence the saturation level decreases when the concentration of the dissolved matter in water increases, for instance, salt and other minerals. For example, the dissolved matter concentration is higher in sea water than river water, as presented in Figure 78.

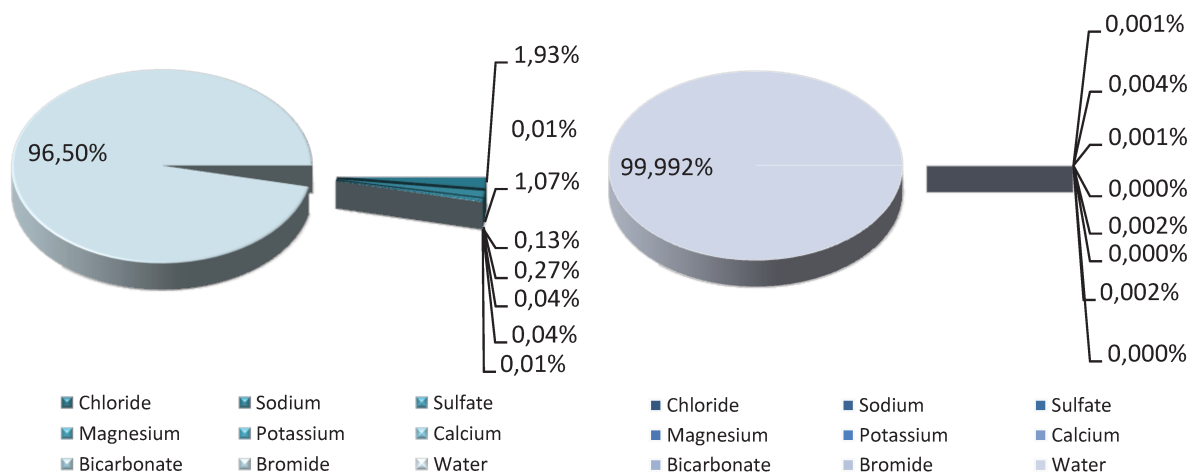


Figure 78: Diagram presenting the difference of constituent concentration in sea water and river water.

In an ocean environment most materials immersed will also be subject to biological aggression, called bio-fouling. This involves the adhesion of marine micro-organisms and animals onto the material surface. In addition to its effects on hydrodynamic behaviour this fouling can induce damage development by modifying the surface of the material. This aspect will not be studied here but is an important aspect of tidal turbine design, as it implies the use of anti-fouling paints and regular maintenance.

1.2 The diffusion models

Water molecules will diffuse into polymer by activated jumps in the direction of the gradient concentration. There are basically four main diffusion processes in polymer materials, as presented in [48]:

- Fickian diffusion,
- Langmuir's diffusion,
- Case II diffusion [163] (due to polymer relaxation or devitrification),
- And the coupled reaction diffusion (due to chemical water-polymer reaction, hydrolysis).

For all these phenomena the kinetics of water diffusion in polymer can be studied by mass uptake using gravimetric analysis (this measurement method will be presented in section 1.4). In this section only the first and second processes of diffusion will be detailed.

Fick's first and second laws [164] provide the basic equations used to model diffusion through polymer materials (Crank and Park, 1975 [165]). To describe absorption in epoxy resins, Fick's laws are frequently used [166],[167],[168] but in some cases, water sorption presents anomalies or additional complexity [169],[170]. An alternative diffusion model attributable to Langmuir is then frequently invoked.

1.2.1 The Fickian approach

Heat transfer by conduction and water diffusion present some similarities, both processes resulting from random molecular motion, thus there is an obvious analogy between the two phenomena. This analogy was recognized by Fick (1855), [164], who was the first to apply the

mathematical equation of heat conduction proposed by Fourier (1822), [171], in order to develop the equations of diffusion which bear his name.

d) *First law of diffusion*

Fick's first law of diffusion in isotropic materials is based on the hypothesis that the flux of substance in the direction x , through unit area of a section is proportional to the concentration gradient measured normal to the section:

$$F = -D \frac{\partial C}{\partial x} \quad \text{Eq. 32}$$

Where F is the flux of substance diffusing across a unit area par unit of time, C is the concentration of the diffusing substance, x is the space coordinate measured normal to the considered section and D is the diffusion coefficient which is proportional to the squared velocity of diffusion substance particles. This coefficient is dependent on different parameters such as, temperature, pressure, material structure, and the nature of the diffusing substance, [172].

e) *Second law of diffusion*

Fick's second law corresponds to the conservation balance of matter during the diffusion of a substance in an element of volume. This second law describes the non-steady state. Thus for the case of diffusion in one dimension, it can be written as presented in Eq.33 below:

$$\frac{\partial C}{\partial t} = D \frac{\partial^2 C}{\partial x^2} \quad \text{Eq. 33}$$

Where t is the time in seconds and D is the diffusion coefficient in $\text{m}^2.\text{s}^{-1}$. Nevertheless, in the case of liquids which interact with high polymers, the diffusion coefficient is generally a function of the diffusing substance concentration. In this case Fick's second law can be written as:

$$\frac{\partial C}{\partial t} = \frac{\partial}{\partial x} \left(D \frac{\partial C}{\partial x} \right) \quad \text{Eq. 34}$$

A simpler approach presented by Crank in [162], presents a mathematical solution for a semi-infinite plate, in which is dissolved a diffusing substance (i.e. water). In this case, it is assumed that the substance extends to infinity on one side of the boundary interface and that the plate extends to infinity on the other side. In a plane sample the diffusion behaviour will be the same as in a semi-infinite sample (while neglecting the edge effects), until the liquid reaches the centre of the sample. The spatial (in the x-direction) and temporal evolutions of the liquid concentration below the surface are given by the following equation, Eq.35:

$$\frac{C_t - C_0}{C_1 - C_0} = 1 - \frac{4}{\pi} \sum_{n=0}^{\infty} \frac{(-1)^n}{(2n+1)} \exp\left(-D \frac{(2n+1)^2}{e^2} \pi^2 t\right) \cos\left(\frac{(2n+1)\pi \cdot x}{e}\right) \quad \text{Eq. 35}$$

Where C_0 and C_t are the concentrations of liquid in the sample at the initial time, when $t=0$ (usually $C_0=0$), and at equilibrium. C_1 represents the uniform concentration of the liquid at the sample surfaces. D is the diffusion coefficient, x is the distance from the mid plane of the sample, t is the time of immersion in the fluid and e the thickness of the sample.

Considering that M_t is the total mass of water absorbed by the considered material at a time t and M_{∞} is the mass of water at saturation (when diffusion reaches an equilibrium state). It is possible to write Eq.36:

$$\frac{M_t}{M_{\infty}} = 1 - \frac{8}{\pi^2} \left[\sum_{n=0}^{\infty} \frac{1}{(2n+1)^2} \exp\left(-\frac{(2n+1)^2}{e^2} D \pi^2 t\right) \right] \quad \text{Eq. 36}$$

The coefficient D can thus be determined (Eq.37) from the slope of the relative mass uptake, M_t/M_{∞} as a function of square root of time divided by thickness, \sqrt{t}/e , (where $dy = M_t/M_{\infty}$):

$$D = \frac{\pi}{16} \left(\frac{dy}{d\sqrt{t}/e} \right)^2 \quad \text{Eq. 37}$$

Usually D is determined at the beginning of the linear part of the curve (between 0 and 0.5 of M_t/M_∞). Figure 79 represents the typical Fickian kinetics of diffusion obtained for a polymer, the water absorption is initially proportional to the square root of time and reaches a plateau value which represents the mass at saturation.

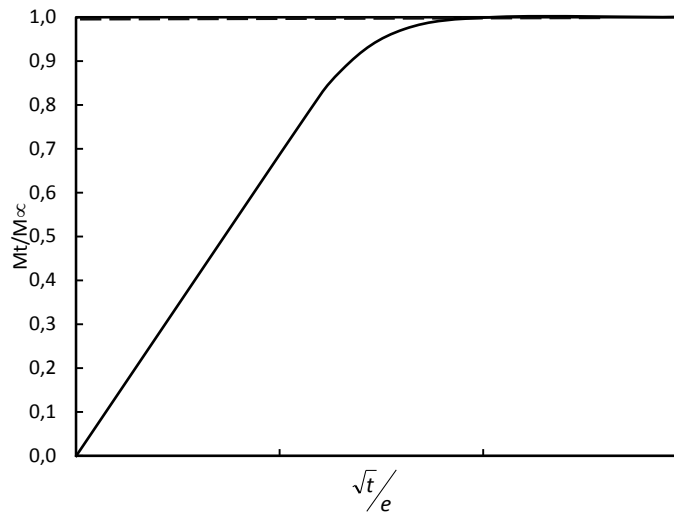


Figure 79: Kinetics of diffusion according to Fick's law.

The fact that the mass uptake rises proportionally with the root time is often considered as proof that the considered diffusion process shows Fickian behaviour, but in many cases this is a first approximation. The independence from the sample thickness should also be checked.

1.2.2 The Langmuir approach

The Fickian approach cannot be applied in all cases. For some composites, the diffusion process seems to be Fickian at low mass uptake but then presents an inflexion or a slow and continuous mass uptake in place of an equilibrium [173], [174]. The Langmuir diffusion model has been discussed in many articles. For instance Carter and Kibler have developed in 1978 a Langmuir-type model, [170], which describes a certain case of anomalous moisture absorption in polymers and composites. It can be explained quantitatively by assuming that absorbed moisture is divided in two phases, a mobile and a bonded phase. The model considers a system with n molecules of mobile water and N molecules of bonded water.

At a given time, there are $\gamma \cdot n$ trapped molecules among the n mobile molecules and $\beta \cdot N$ mobile molecules among the N trapped molecules, it is then possible to write:

$$\begin{cases} D \frac{\partial^2 n}{\partial z^2} = \frac{\partial n}{\partial t} + \frac{\partial N}{\partial t} \\ \frac{\partial N}{\partial t} = \gamma \cdot n - \beta \cdot N \end{cases} \quad \text{Eq. 38}$$

At saturation, $\gamma \cdot n = \beta \cdot N$, then using Fick's equation and the concept of "trapping-untrapping", [170], we obtain the simplified solution in Eq.39, if 2γ and 2β are very small compared to k :

$$\frac{M_t}{M_\infty} = \frac{\beta}{\gamma + \beta} e^{-\gamma t} \left[1 - \frac{8}{\pi^2} \sum_{p=1}^{\infty} \frac{e^{-kp^2 t}}{p^2} \right] + \frac{\beta}{\gamma + \beta} (e^{-\beta t} - e^{-\gamma t}) + (1 - e^{-\beta t}) \quad \text{Eq. 39}$$

- For the initial part of the absorption, for short ageing times, Eq.39 becomes approximately:

$$\frac{M_t}{M_\infty} = \frac{4}{\pi^{3/2}} \left(\frac{\beta}{\beta + \gamma} \cdot M_\infty \right) \sqrt{kt} \quad \text{for } (kt \leq 0.7) \quad \text{Eq. 40}$$

- For the final part of the absorption, for long ageing times, Eq.39 becomes approximately:

$$M_t = M_\infty \left(1 - \frac{\gamma}{\beta + \gamma} \cdot e^{-\beta t} \right) \quad \text{for } (kt \geq 1) \quad \text{Eq. 41}$$

$$\text{With } k = \frac{\pi^2 D}{e^2} \quad \text{Eq. 42}$$

It is worth mentioning that for $\gamma = 0$ and $\beta = 1$, one obtains the Fickian solution. The kinetics of diffusion expected by the Langmuir model are shown in Figure 80.

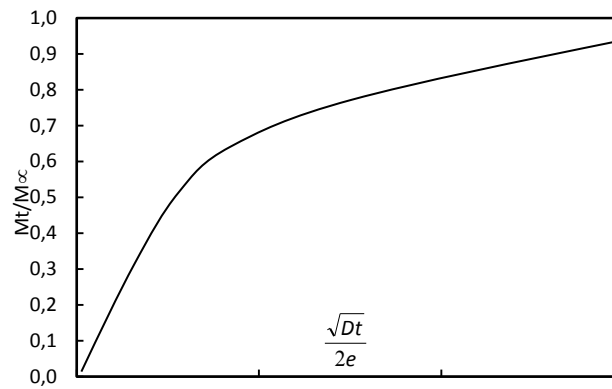


Figure 80: Kinetics of diffusion expected from the Langmuir model.

1.3 Diffusion in composite materials

In the specific case of composite materials, diffusion and the determination of diffusion coefficient(s) are more complex due to their heterogeneous nature. Moreover for carbon/epoxy composites, it is widely considered in the literature that the carbon fibres are impermeable to water. Thereby, if we consider an UD layer of composite, in the transverse direction, the impermeable carbon fibres introduce a complex tortuosity to the water diffusion pathway. Figure 81 illustrates this aspect of water diffusion in neat resin (a) (homogeneous) compared to composite (b). As a consequence diffusion behaviour in composite materials will be different to diffusion in pure polymers and the diffusion coefficient(s) for composites will be determined by the heterogeneous and anisotropic nature of this type of material.

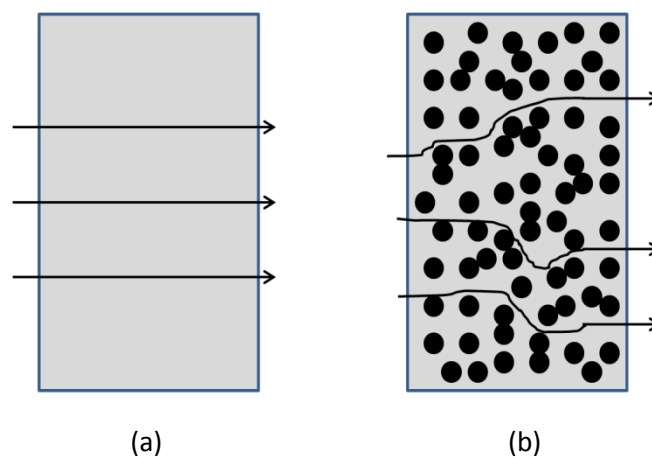


Figure 81: Schematic representation of diffusion through (a) homogeneous material (e.g. epoxy resin) and (b) heterogeneous material (e.g. composite carbon/epoxy).

Barrer, in 1968 [175] proposed a summary of the first research on this subject. More progress followed, with the advances in mechanics of heterogeneous materials and homogenization methods. In 1976, Shen and Springer [176], characterized and determined the diffusion coefficients in composite materials, using the analogy between heat transfer and water diffusion. This was based on previous work of Springer and Tsai, where the authors proposed equations to define thermal conductivities of unidirectional materials [177].

1.3.1 A first approach for diffusion in composites

According to the work of Shen and Springer cited above, it is possible to define diffusion parameters for unidirectional composites. First of all the diffusivity D_x is the water diffusion coefficient for a material composite in the direction normal to the surface, which can be numerically determined. For composite materials reinforced by fibres the coefficient of diffusion D_x can be determined using four parameters:

- The Diffusion coefficient of the resin D_r ,
- The Diffusion coefficient of the fibres D_f ,
- The volume fraction of fibres V_f ,
- The angle of fibres α .

The relationship between these parameters can be established thanks to the similarity between heat conduction and water diffusion. Thus the concentrations of temperature (Eq.43) and water (Eq.44) are described in the following equations of respectively Fourier and Fick:

$$\rho C \frac{\partial T}{\partial t} = K_x \frac{\partial^2 T}{\partial x^2} \quad \text{Eq. 43}$$

$$\frac{\partial C}{\partial t} = D_x \frac{\partial^2 C}{\partial x^2} \quad \text{Eq. 44}$$

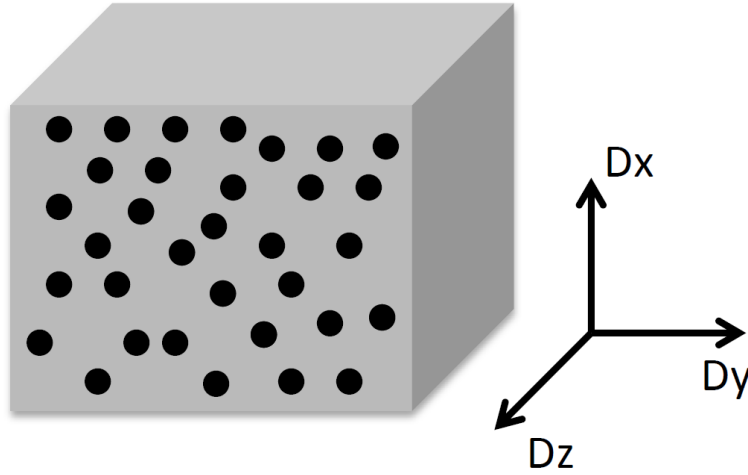


Figure 82: Illustration of diffusion in composites representing the diffusion in normal and fibres directions for an UD composite.

Some approximations for thermal conductivities, parallel (K_{11}) and normal (K_{22}) to fibre directions were given in [177], (for composite material where $V_f < 0.785$). The parameters $K_x / \rho C$ and D_x are measurements of the “speed” at which the temperature and water concentration spread into the material. In most cases, and specifically for carbon fibres, the diffusion coefficient for the composite is much lower than for the resin. Thus the expressions of thermal conductivities K_{11} and K_{22} presented in [177], can be simplified and allow the expressions for D_{11} and D_{22} , the water diffusion coefficients in parallel and normal directions to the fibres to be obtained, as presented in Figure 82 :

$$D_{11} = (1 - V_f) D_r \quad \text{Eq. 45}$$

$$D_{22} = (1 - 2\sqrt{V_f / \pi}) D_r \quad \text{Eq. 46}$$

D_x is linked to D_{11} and D_{22} by Eq.16 (fibres must be parallel to the surface, $\alpha = 90^\circ$, $\beta = 90^\circ$ and $\gamma = 0^\circ$, see Appendix 3). In this case $D_x = D_y = D_{22}$ and $D_z = D_{11}$:

$$D_x = D_{11} \cos^2 \alpha + D_{22} \sin^2 \alpha \quad \text{Eq. 47}$$

$$D_y = D_{11} \cos^2 \beta + D_{22} \sin^2 \beta \quad \text{Eq. 48}$$

$$D_z = D_{11} \cos^2 \gamma + D_{22} \sin^2 \gamma \quad \text{Eq. 49}$$

This approach is not the unique one, in the literature there are many expressions allowing diffusion coefficient to be determined normal to the surface in composites, [178],[179],[180],[181],[182]. A good review of homogenised transverse diffusion coefficient models for composites is presented by Dana et al. in [183].

1.3.2 Non Fickian diffusion in composites

In composite materials, there are other possible complications for diffusion, linked to the eventual diffusion in the interfacial region between matrix and fibres. Also, damage can occur in composites (at the interface or in the resin) during sea water ageing, alternatively pre-existing damage, due to the manufacturing process, can affect water diffusion. The effects leading to anomalies in composites diffusion have progressively been incorporated into the diffusion models, as presented in [184], [51], [185]. A particular type of abnormal diffusion in composites was investigated by Derrien and Gilormini in [186]. Their work concerns the effect of matrix swelling in composite materials. During ageing the matrix is swollen, this deformation is restrained by the fibres, which are not deformable. So a stress state develops in the resin, this phenomenon induces a change in the water solubility and diffusivity. As a consequence the diffusion behavior can have the appearance of a Langmuir diffusion process while no specific free water/polymer interaction sites exist.

1.4 **Measurement of water concentration in polymers and composites**

In the previous sections the notion of mass uptake was introduced. When polymer or composite materials are exposed to water, the mass of the considered material will increase. In order to measure and follow the evolution of water entry in these materials, there is a large variety of experimental approaches, but the simplest and certainly the most popular is gravimetric analysis.

Before exposure to water, samples are weighed in order to obtain the mass, w_0 , in the “dry state”. Throughout exposure to water samples are then regularly weighed, and the mass, $w_{(t)}$, at “wet state” is measured at each time t . Thus the weight change at a t time is m_t , and can be expressed as presented in Eq.50:

$$m_t = \frac{w_t - w_0}{w_0} \quad \text{Eq. 50}$$

Other methods exist, depending of the range of the water concentration to be observed, such as proton NMR, chemical titration, dielectric spectroscopy, and Infrared spectroscopy. In this study gravimetric analysis using a precision balance will be used.

1.5 Temperature dependence of the diffusion process

For polymer and composite materials, the diffusion phenomena are thermo-activated, as a consequence the diffusion coefficient of both materials is dependent on the temperature of ageing. Thus the diffusion coefficient is linked to temperature and often, but not always, follows an Arrhenius law:

$$D = D_0 \cdot \exp\left(\frac{-E_a}{RT}\right) \quad \text{Eq. 51}$$

Where D_0 is a temperature dependent factor, E_a is the activation energy for water diffusion in the considered material, R is the gas constant and T is the absolute temperature. This dependence on temperature is a key factor for accelerated ageing.

2. Accelerated sea water ageing

2.1 Necessity to accelerate ageing

Tidal turbines will evolve in a marine environment, and the expected service life of these structures is 20-25 years according to their manufacturers. Their composite blades will be exposed to water throughout this period. In order to design and optimise these structures, their long term behaviour must be known. It is clear that it is impossible to wait 25 years and see what happens, so the ageing phenomena must be accelerated to obtain information in an experimentally acceptable time, typically a few months.

The aim of accelerated sea water ageing tests is to accelerate the mechanisms occurring in a normal marine environment and decrease the time required to degrade the material. For sea water ageing, the principal mechanism introducing degradation into the material is the diffusion of water. As presented previously the diffusion phenomenon in polymers and composites is thermally activated, so the key parameter will be the temperature. The accelerating environment must be chosen carefully in order not to induce degradation mechanisms which will not appear during service life. For instance, for polymer materials such as thermoset epoxy resins there are reactions of depolymerisation, oxidation and other reactions occur at faster rates as the temperature of a composite gets closer to the T_g of the thermoset matrix. For these reasons, it is widely recommended that the temperatures used for accelerated ageing be at least 10 to 15 °C below the T_g of the considered materials. In order to study the long term behaviour of the materials of this study, an accelerated ageing procedure will be used.

2.2 Procedure and conditions used to accelerate ageing

As presented in the previous Chapter II, three different composite materials have been tested. These materials are of different natures, in terms of manufacturing process, type of carbon fibres and resin. Thus they have to be aged under specific conditions.

To reproduce and accelerate sea water ageing, the Ifremer laboratory proposes different ageing tanks with natural seawater. This water is directly pumped from the bay of Brest to the different tanks presented in Figure 83.



Figure 83: Ifremer sea water ageing tanks with natural and renewed sea water from the bay of Brest.

For this study the tanks at 25, 40, 60 and 80°C will be used to characterize the diffusion of water into the studied materials. But to accelerate the ageing process, the RTM and the Infused materials will be aged at 60°C, allowing these materials to be aged 15°C below their T_g . For the Pre-preg materials as the T_g is about 205°C it is possible to age at higher temperature, so this material was aged at 80°C. For the neat epoxy resin, specimens were aged at 40 and 60°C. Table 18 summarises the different T_g 's and the temperature chosen to age each material.

Material	T_g	Ageing Temperature
Infused	75°C (1.4)	60°C
RTM	77°C (2.0)	60°C
Pre-preg	205°C (1.7)	80°C
Pure resin	78°C (1.6)	40 and 60°C

Table 18: Comparison between T_g and temperature for accelerated ageing for the materials of the study.

This diffusion study will also indicate the time required to reach the equilibrium state, corresponding to the maximum level of water uptake in the material. This characteristic time will be the starting point for the mechanical tests and other analyses. This time will be referenced as " T_1 ", which will depend on the nature of the material and the thickness of the samples. T_0 is the reference for non-aged materials, T_2 and T_3 will be additional longer times for mechanical tests beyond T_1 . In most cases T_2 and T_3 are defined as: $T_2 = T_1 + 1$ month and $T_3 = T_1 + 2$ months. Thus the materials will be tested at three different ageing times as presented in Figure 84.

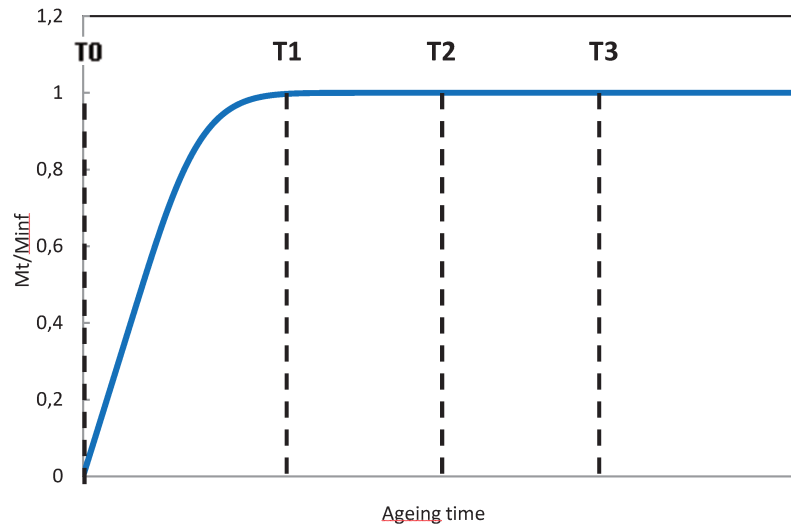


Figure 84: Accelerated test characteristic times for testing superposed on a Fickian diffusion law, T_0 , T_1 , T_2 and T_3 .

Times and temperatures having been defined, a last possible ageing test parameter is the pressure. As tidal turbines will be in service at an average depth of 40 meters, depending on the size of the turbine and on the location of the site of electricity production, the pressure of the water on the blade will be approximately between 2 and 4 bars.

Various previous studies have examined the influence of pressure on water diffusion and in most cases effects are very small at such low pressures [187],[188],[189].

3. Characterisation of sea water ageing

In this section the effect of sea water ageing on the materials of the study will be discussed. The objectives of this section are multiple. First, the objective is to characterize and understand how the sea water diffuses into the different materials under different conditions (time, temperature, material thickness and material orientation). This first part will allow the time to age materials to a saturation state (equilibrium or quasi equilibrium of water content in the materials) to be determined. In a second part the different materials will be tested at different ageing times (T_1, T_2, T_3), following the characterization procedures presented in Chapter II. The objective of this characterization procedure is to understand how properties depend on ageing, and to compare materials in order to establish some conclusion on the influence of the manufacturing process on long term performance in seawater. It will also provide data for modelling.

3.1 Characterisation of the water diffusion into Pre-preg, RTM and Infused materials

In this section the diffusion kinetics of sea water for neat resin and the three types of composite materials will be presented. Sea water ageing was performed on each material at different temperatures. Specimens of each material with different thicknesses and material orientations were cut from composite plates by high pressure water jet in the following dimensions, (3 specimens per condition of $50 \times 50 \times \text{thickness mm}^3$). Then those samples were measured and weighed and finally distributed in four circulating natural sea water tanks at different temperatures: 25, 40, 60 and 80°C. Temperature was continuously monitored and controlled to $\pm 1.5^\circ\text{C}$. Based on regular weight measurements made during ageing the water uptake was determined as a percentage of the initial specimen weights (see Eq.50).

First, results from an investigation on the neat epoxy resin will be presented (the epoxy resin used to manufacture the RTM and Infused materials). Then diffusion data for the three composite materials will be presented. Finally the effect of the composite thickness and the fibre orientation on the diffusion process will be discussed.

3.1.1 Sea water diffusion neat epoxy resin

Samples of pure resin were immersed at 25, 40, 60 and 80°C for more than 11 months. The evolution the mass of water inside the different samples of neat resin is plotted as a function of the square root of time in Figure 85. The variability of the water uptake measure is very low, as presented in Appendix 5.

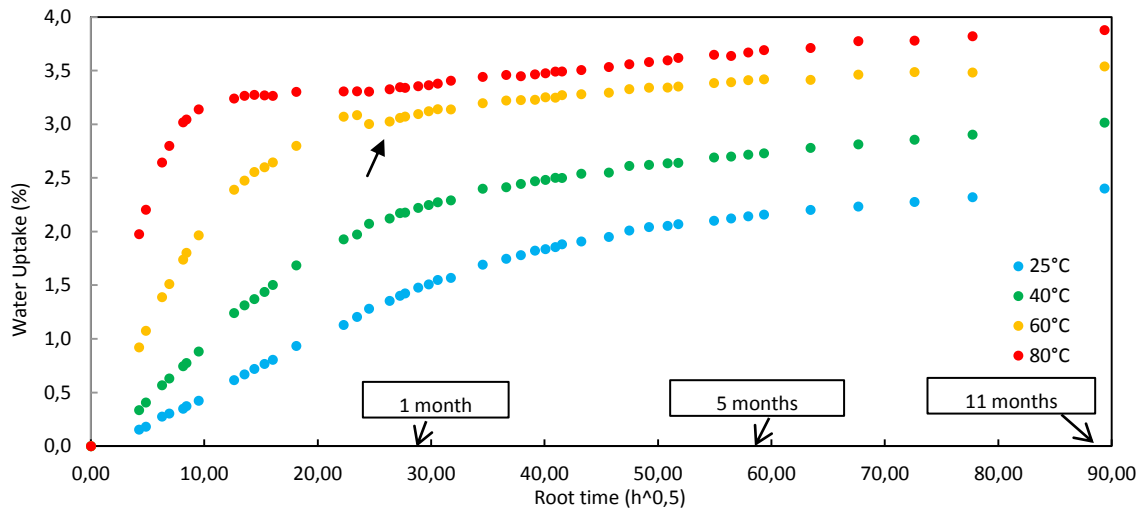


Figure 85: Plots of mean measured weight gains for pure epoxy resin.

Ageing at 80°C ($T_g + 2^\circ\text{C}$) is too high for the pure resin. As a consequence different phenomena can affect the sorption of water and result in a non Fickian diffusion process. A first plateau is followed by a gradual increase in weight. For lower temperatures such as 60°C, the diffusion process may be taken as Fickian to a first approximation. After the linear part of the sorption curve, water uptake reaches a quasi-equilibrium around 800 hours with an average weight gain around 3.0%. However after this quasi plateau, the weight is still increasing slowly.

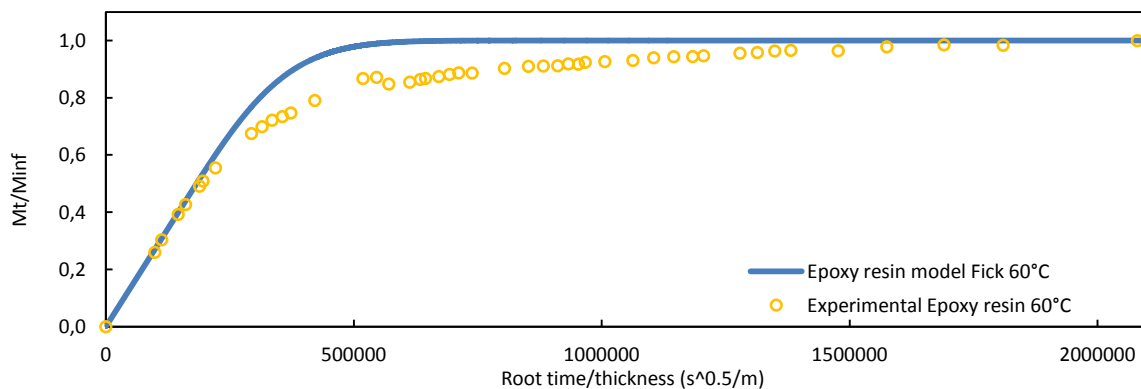


Figure 86: Plots of mean measured weight gains versus the associated Fickian law for an ageing temperature of 60°C.

After a long exposure of 8000 hours the rate of water reaches an average level of 3.5%. The sorption curve at 60°C is compared to a Fickian behaviour in Figure 86. It should be noted that during these measurements a technical problem occurred in the tank at 60°C. As presented in Figure 85 with the arrow, there was a drop in water temperature during two days and this could affect the transition between the linear part of the sorption and the plateau. However, as presented in Figure 86, the diffusion process at 60°C for the pure resin could not be closely fitted to a Fickian law, especially in the long term exposure part of the curve.

At 40°C the sorption process is slower than 60°C but seems to present the same anomaly of diffusion. After the linear part of the sorption, the rate of water in the resin reaches a level of 2.6% after 2200 hours, but this level rises slowly to 3.1% after 8000 hours. In Figure 87, the diffusion process of the resin epoxy resin at 40°C is compared with the Fickian law. As presented previously at 60°C, for short diffusion times the resin presents a Fickian shape. But for long term immersion an anomalous diffusion is recorded.

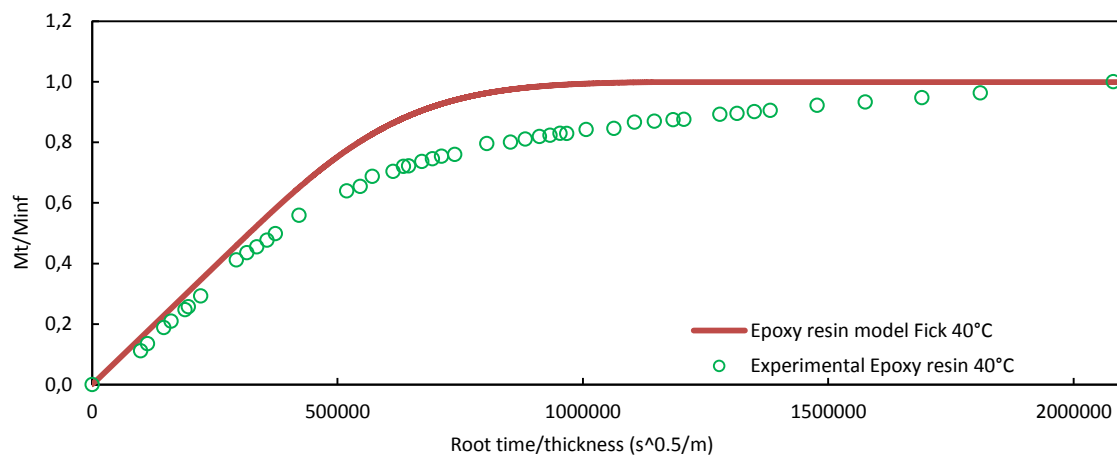


Figure 87: Plots of mean measured weight gains versus the associated Fickian law for an ageing temperature of 40°C.

At 25°C the diffusion process seems to reach a plateau, but to conclude on the diffusion process at this temperature, more measurements (more time) are needed.

As a first conclusion on the diffusion process of seawater in the resin, it is important to note that for the different temperatures of ageing, the water uptakes did not reach the same maximum content. This indicates that different mechanisms occur, the temperature dependence may indicate an effect of swelling. Additionally for the different ageing temperatures, after a quasi equilibrium and for long term exposure, absorption of water is still slowly rising to higher concentration of water (+0.5%). This non Fickian behavior could be due to plasticization of the matrix. A drop of the T_g below the temperature of ageing will induce more mobility in the polymer network, leading to an increase

water diffusion. Due to swelling and / or plasticization of the resin micro-cracks may appear and slowly affect the diffusion [173],[190]. Oxidation can also appear, this mechanism is directly linked to the environment of ageing, specifically linked to the temperature. Oxidation of the resin during sorption leads to non-Fickian processes. An oxidized resin has a higher sorptive affinity towards water [169]. As shown in Figure 88, depending on the ageing temperature, some color changes can be noted on the surface of resin specimens. The resin becomes darker, particularly at 80 and 60°C, suggesting oxidation of the material surface.



Figure 88: Epoxy resin samples used for weight measurement at 80, 60, 40 and 25°C (left to right) suggesting oxidation of the resin.

3.1.2 Sea water diffusion in three composite materials

a) *Infused material*

The first composite presented is the Infused material. Three specimens were immersed and measured for each condition of temperature (60, 40 and 25°C). These specimens were cut into UD plates with an average thickness of 1.7 mm. Specimens were immersed for 15 months. The weight gain measurements are presented in Figure 89. A stable weight gain is noted after 900 hours in sea water at 60°C. Scatter is not represented because measurements showed very low variability as presented in Appendix 6. For this ageing condition the material reaches a maximum weight gain of 0.8%. The diffusion kinetics of this material could be fitted to a Fickian law at 60°C, as presented in Figure 90, but it is worth mentioning that the last measurements after 6 500 hours, seem to show that water content is slowly rising for long immersion times. More measurements are needed to draw conclusions on this phenomenon but it is analogous to the resin results.

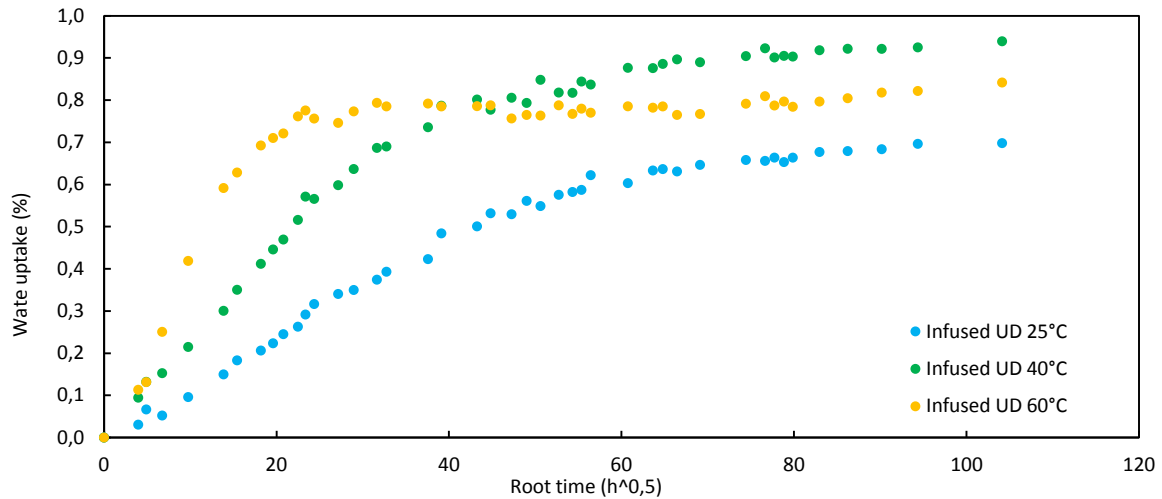


Figure 89: Plot of mean measured weight gains for the UD Infused material immersed in sea water at different temperatures.

At 40°C, the concentration of water seems to reach a plateau after 3600 hours of immersion, but the weight gain is clearly higher than that at 60°C. The average weight gain at equilibrium is about 0.9%.

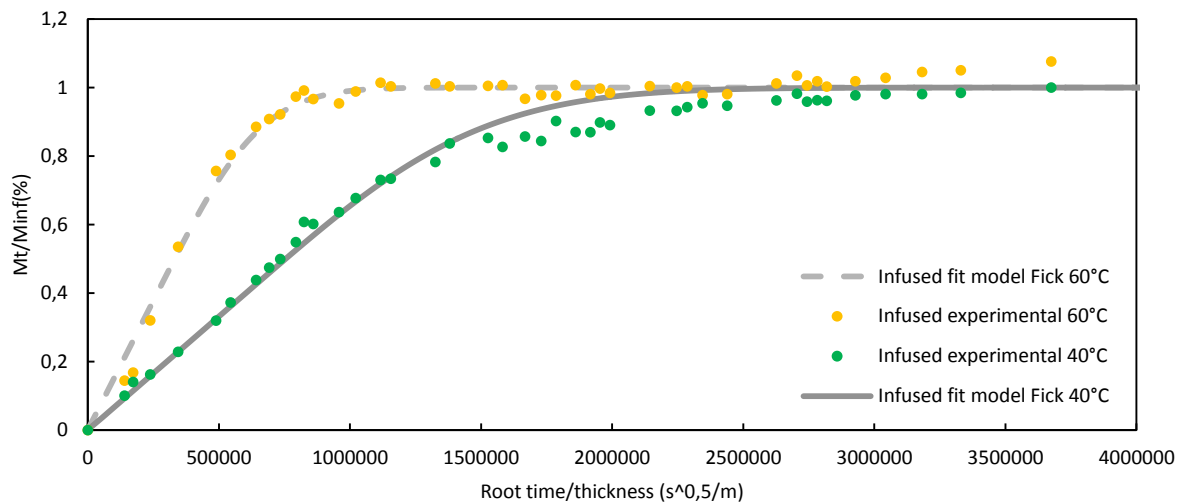


Figure 90: Comparison between experimental diffusion results and the Fickian law of diffusion at 40 and 60°C for the Infused material.

These phenomena could be related to the plasticisation of the material during the immersion at 60°C, where the T_g decreases below the 60°C, but this would lead to an increase in water content. A possible explanation for this difference is that the material was not completely cured before ageing. In Appendix 8, DSC results are presented showing two heating cycles. There is a gap of approximately 7°C between the two glass transitions. This suggests that during ageing at 60°C the

material undergoes post curing, as a consequence its affinity towards water decreases. Despite this phenomenon, the diffusion kinetics at 40°C can be fitted to a Fickian law as presented in Figure 90. Concerning the last temperature of 25°C, the diffusion curve is starting to reach an equilibrium state, but it is too early to conclude even after 10000 hours.

b) *RTM material*

The second composite presented is the RTM material. Three specimens were immersed and measured for each condition of temperature (80, 60, 40 and 25°C). These specimens were cut in UD plates with an average thickness of 2.8 mm. Other specimens of 5mm UD and 2.9 mm quasi-isotropic RTM material have also been immersed and measured. The measurements on these latter specimens will be presented in the following sections 3.1.3 and 3.1.4. Figure 91 presents the curves of sea water diffusion for the different temperatures.

At 80 and 60°C the water diffusion process reaches an equilibrium state after about 900 and 2400 hours respectively. These diffusion kinetics can be fitted to a Fickian law as shown in Figure 92. However, as presented for the pure resin and the Infused material, after long immersion of 5600 hours in sea water at 60°C the weight is slowly rising (from 1.34 to 1.41%). For the other lower temperatures (40 and 25°C), more time is needed to conclude on the stabilisation of the diffusion to an equilibrium state.

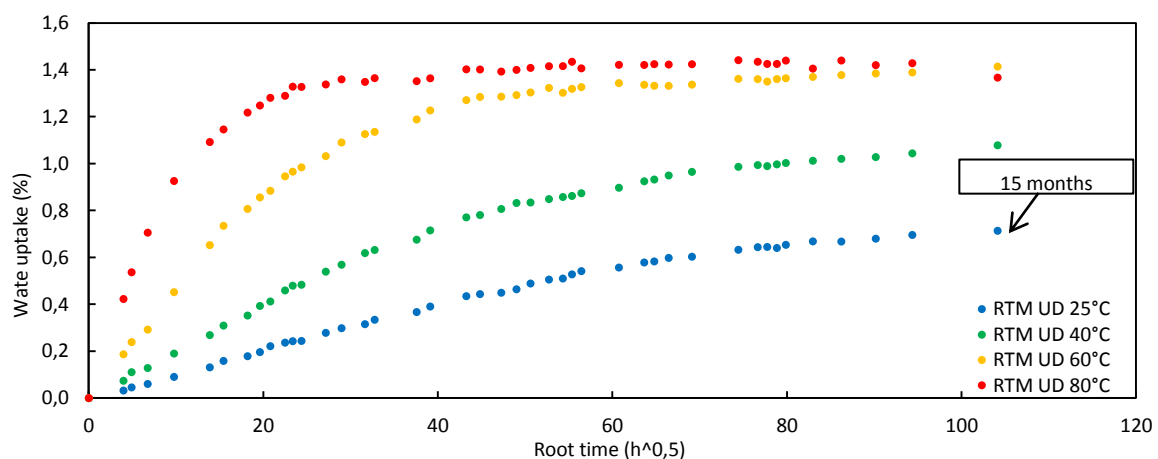


Figure 91: Plot of mean measured weight gains for the UD RTM material immersed in sea water at different temperatures.

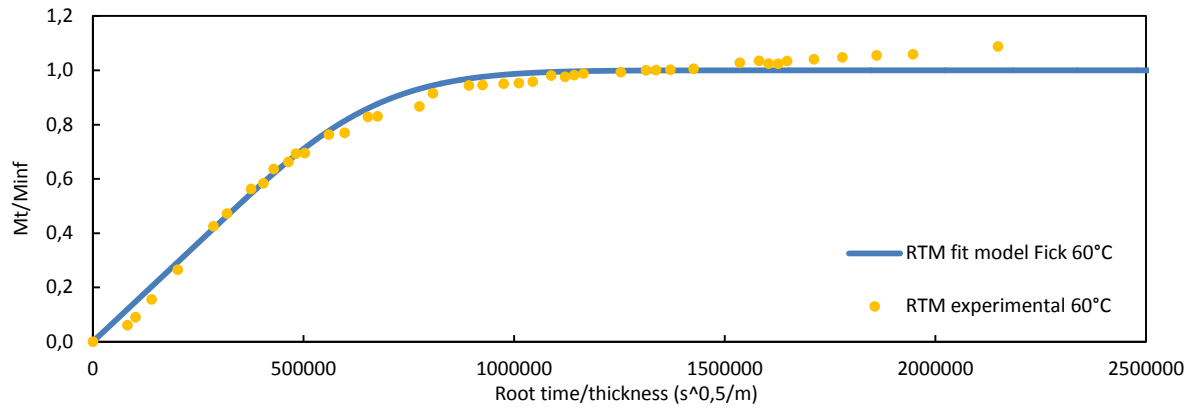


Figure 92: Comparison between experimental diffusion results and Fickian law of diffusion at 60°C for the RTM material.

c) Pre-preg material

The third material presented is the Pre-preg, this material is considered as a reference in this study. For the characterisation of the water diffusion into this material different UD specimens were used, with different thicknesses, 1.3, 2.06 and 3.12 mm. First, the diffusion of the 1.3 mm thick material will be discussed. Then in section 3.1.4., the thicker sample behaviour will be compared.

The Pre-preg material shows a high T_g compared to other materials (205°C). Thus for this composite the diffusion at 80°C will be discussed. The specimens have been immersed for more than 7000 hours, as shown in Figure 93. In this case the diffusion processes reach approximately the same weight gain, 0.9% ($\pm 0.05\%$) at all temperatures.

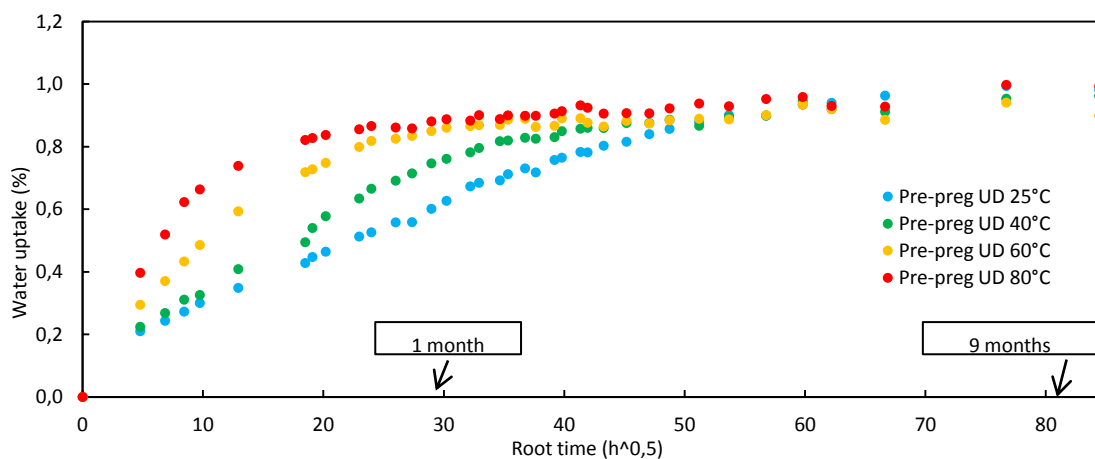


Figure 93: Plot of mean measured weight gains for the UD Pre-preg material immersed in sea water at different temperatures.

For these specimens at 80°C a time of 850 hours is needed to attain the equilibrium of the diffusion process. These diffusion kinetics are compared to a Fickian model in Figure 94. Here the diffusion process is Fickian to a first approximation.

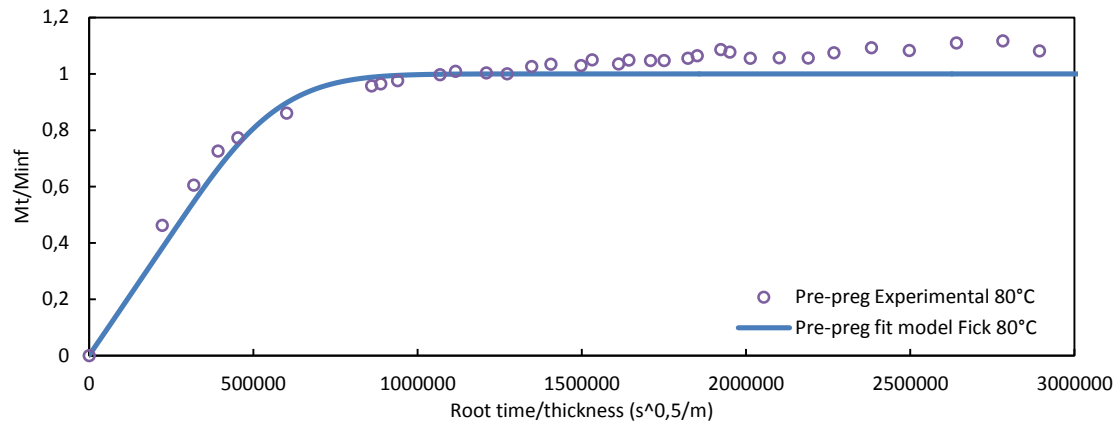


Figure 94: Comparison between experimental diffusion results and Fickian law of diffusion at 80°C for the Pre-preg material.

3.1.3 Effect of material orientation on the diffusion process

In the composition of a tidal turbine blade, different orientations of layers are possible. So it is important to understand the influence of the material orientation on the diffusion process. Two cases will be presented.

In the first case, specimens of UD Infused materials (1.7mm) were used. These specimens have been cut in the same plate of UD, but only one type of specimen is a square of 50 x 50 mm². The others are rectangular of 100 x 25 mm², but one was cut with the long axis in the fibre direction and for the other it was perpendicular to the fibre direction, as presented in Figure 95. All specimens have the same thickness and the same surface, thus only the geometry and orientation of the fibres are different.



Figure 95: UD Infused specimens with different geometries and orientations.

The specimens have been immersed in sea water at 60°C for more than 1000 hours. They were regularly weighed. The measurements are presented in Figure 96. There are no significant differences between the different specimens. The kinetics of diffusion remain the same, independent of the orientation of the material. Specimens reach an equilibrium state of water at the same time with a very similar weight gain.

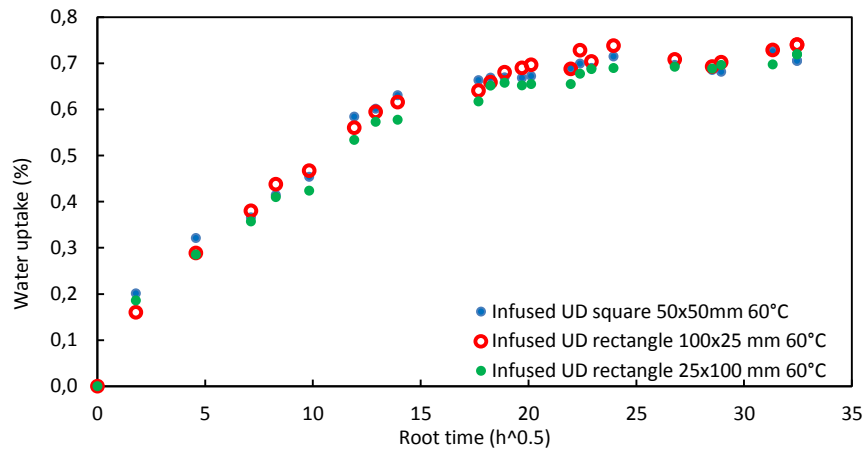


Figure 96: Comparison of diffusion process at 60°C, between UD Infused material with different orientations and geometries.

Another investigation was performed on the RTM material. Unidirectional and quasi-isotropic stacking sequences were compared. For this comparison square samples of each type of orientation were used (50 x 50mm²). They were immersed in the sea water tank at 60°C for more than 10000 hours. The results are presented in Figure 97. According to Figure 97, the previous conclusion is confirmed. The kinetics of water diffusion are independent of the material orientation.

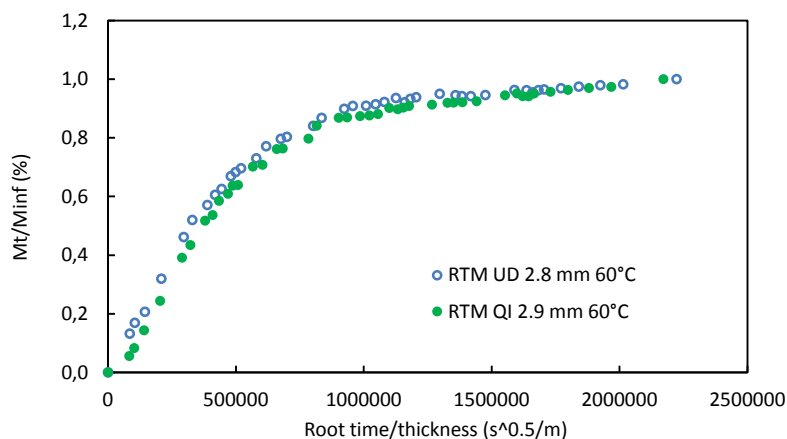


Figure 97: Comparison of diffusion process between RTM UD and QI samples, immersed in sea water at 60°C.

3.1.4 Effect of composite thickness on the diffusion of seawater

Composite tidal turbine blades are very thick, especially in the root area, in order to resist the very high current loads. Thickness can also vary along the blade profile, so it is important to characterise the influence of the composite thickness on the diffusion process, to check that results can be applied to thicker blade materials. In order to characterize this effect, gravimetric measurements were made on Pre-preg and RTM specimens of different thicknesses.

UD Pre-preg specimens of three thicknesses (1.3, 2.06 and 3.12mm) were immersed at 80°C. Figure 98 compares the diffusion curves for the different specimens. The kinetics of diffusion are not affected by the thickness of the samples. It seems that the diffusion process is independent of the thickness in this range.

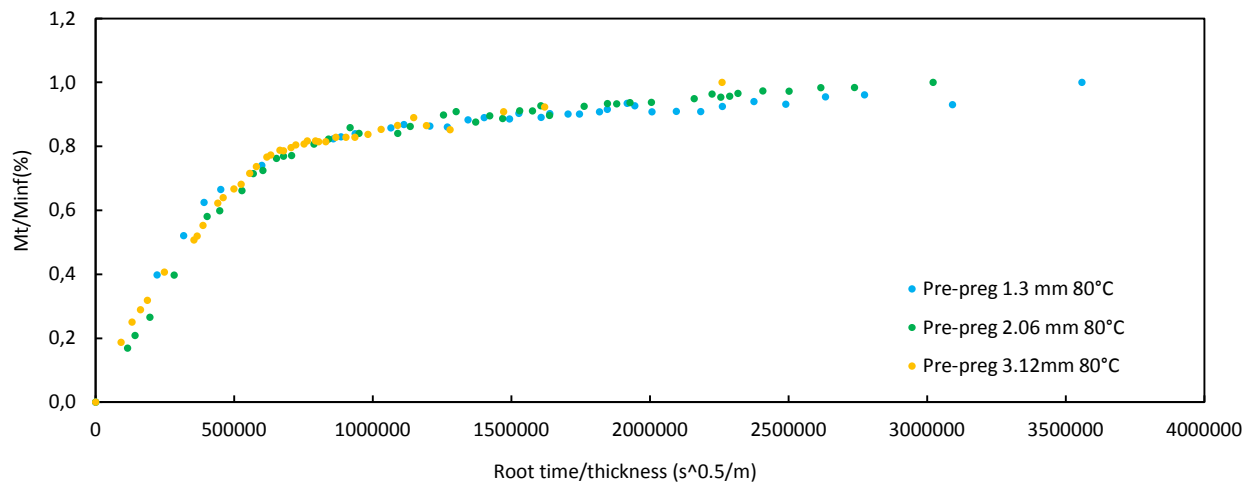


Figure 98: Influence of sample thickness. Comparison of mean measured weight gains for Pre-preg UD 1.3, 2.06 and 3.12 mm 80°C.

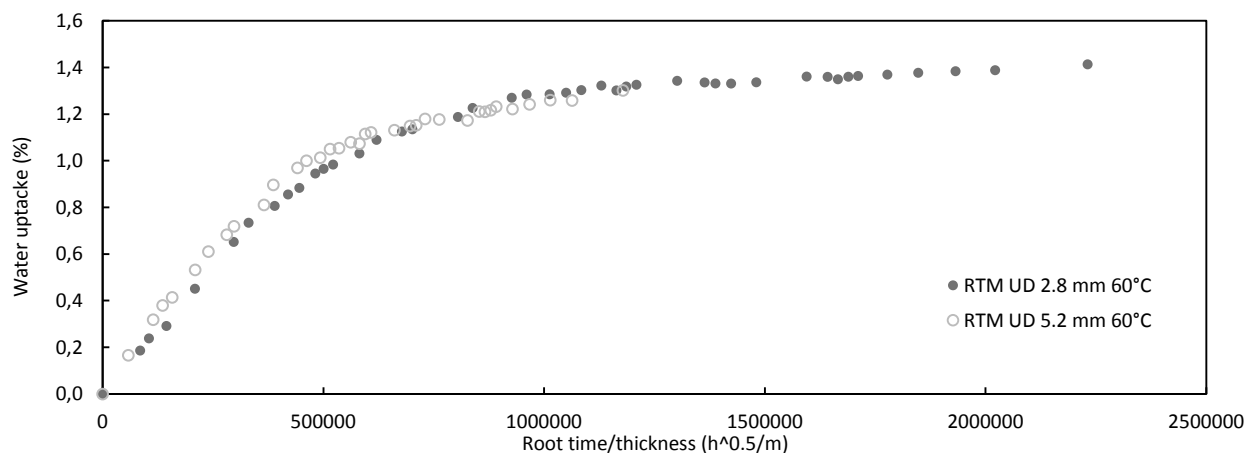


Figure 99: Influence of sample thickness. Comparison of mean measured weight gains for RTM UD 2.5mm and UD 5mm at 60°C.

In Figure 99, a comparison between samples of 2.8 mm and 5.2 mm thickness is presented for the RTM materials during immersion at 60°C. As presented previously, the water diffusion is not influenced by the thickness of the materials.

In summary, three carbon/epoxy materials manufactured with different processes have been immersed for more than 15 months. This allows the kinetics of diffusion to be studied. Additionally the pure resin used to manufacture RTM and Infused materials was also characterised. To extend this study, different thicknesses and orientations of material were immersed in order to examine the influence of these parameters on the diffusion process. In section 5.1 more comparisons are presented between different composites of the study and the Table 22 will summarise the different diffusion coefficients obtained for these materials. Thus it has been highlighted that for the epoxy resin, other mechanisms (oxidation) occur at the “higher” temperatures 40 and 60°C. The quasi Fickian behaviour of the resin is subjected to some anomalous diffusion for long immersion. The kinetics of diffusion are independent of thickness and composite orientation. However, the ageing temperature influences the maximum water content (for RTM and Infused materials). As a consequence ageing at 60°C can be more severe than ageing at 40°C. To clarify this last point some further investigation on the pure resin will be presented below, in order to compare the influence of sea water ageing at 40°C and 60°C on the resin modulus and tensile strengths.

3.2 Physico-chemical characterization

3.2.1 Change in Tg during ageing

Matrix plasticization can occur during sea water ageing of composite materials. In order to follow this phenomenon Tg measurements were made on the three materials during the ageing process. These were performed on samples taken from the specimens used for mechanical test (UD ILSS specimens). Some difficulties were encountered in measuring the Tg on the aged RTM composite due to the high water content. The glass transition and water vaporisation phenomena were superposed (Appendix 10), making it difficult to determine the Tg for all ageing times. In the case of Infused composites it was possible to characterise Tg depression with ageing time as presented in Figure 100, (Figures in Appendix 7 and Appendix 9 present the DSC measurements at T0 and T3). Tg measurements were also performed on Pre-preg material during ageing but the Tg was not significantly affected as shown in Appendix 12.

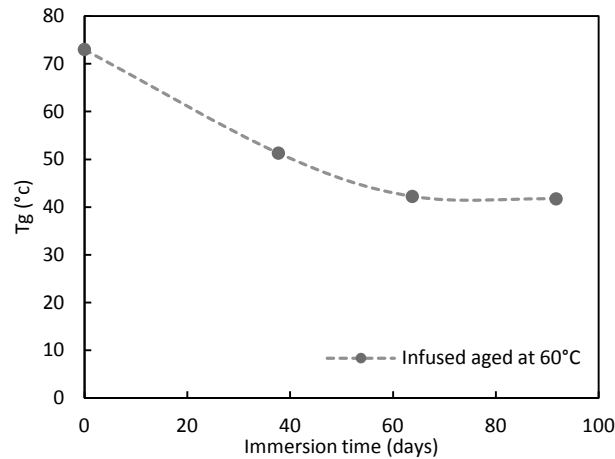


Figure 100: Evolution of glass transition for Infused materials during sea water ageing at 60°C.

Figure 100 clearly shows the drop in T_g and explains why the diffusion behaviour is not simple. Samples aged at 60°C are initially above T_g but as aging proceeds they go from the glassy to the rubbery state.

3.3 Effect on elastic properties

A procedure to characterise elastic properties was presented in the previous chapter, this procedure will be repeated at different ageing times in order to follow the evolution of those properties during ageing. Tensile results for the epoxy resin will be described first, then the results for the different composites will be presented.

3.3.1 Tensile properties of neat resin (40°C and 60°C)

The evolution on tensile properties of the resin has been characterised after sea water ageing at 40 and 60°C.

In Figure 101 the modulus and tensile strength are plotted as a function of the immersion time in sea water at 40°C. During accelerated ageing at 40°C, some changes in resin properties occur. Due to plasticization both tensile strength and modulus are reduced, a drop of 18% and 16% of strength

and modulus is observed. The evolution of these properties seems to reach a plateau after 20 days, however the epoxy resin is fully saturated in water after 90 days at 40°C.

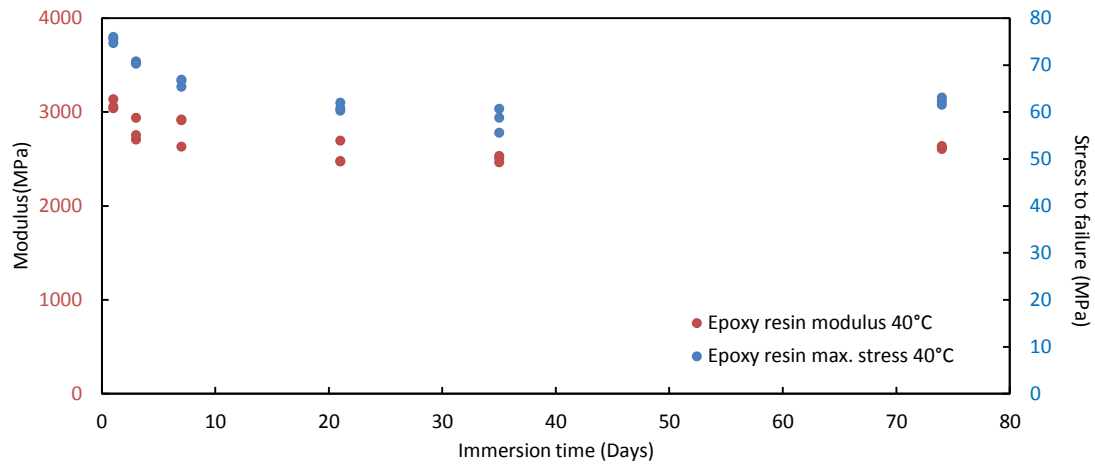


Figure 101: Evolution of epoxy resin tensile properties during sea water ageing at 40°C (strength and modulus).

As composite materials were aged at 60°C (RTM and Infused), tensile tests on unreinforced resin have also been conducted after 60°C immersion. Figure 102 presents the tensile test results during immersion at 60°C. A weakening of both strength and modulus are observed, but those property changes occur more quickly after ageing at 60°C. The drop of properties is also more important compared to the ageing at 40°C. A reduction of 50% of tensile strength and 30% of the modulus are observed after 148 hours (approximately 6 days).

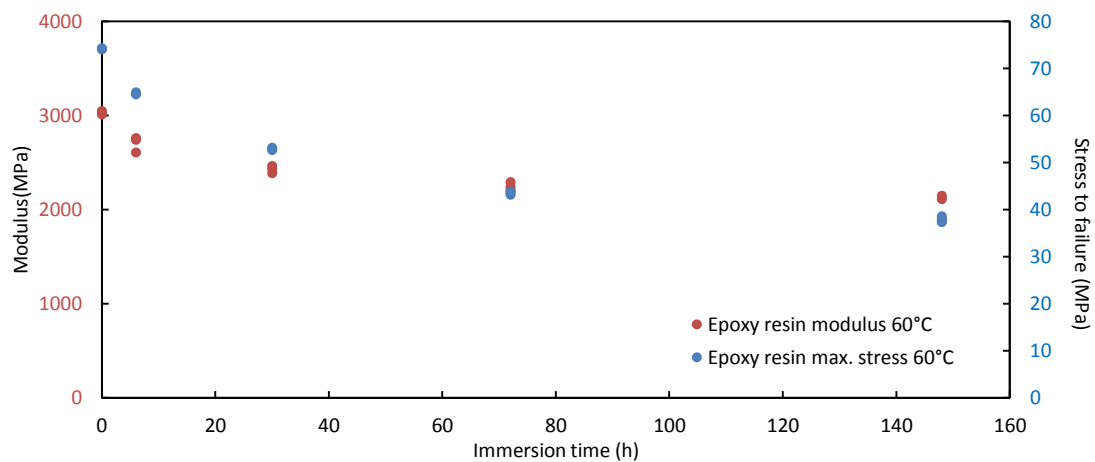


Figure 102: Evolution of epoxy resin tensile properties during sea water ageing at 60°C (strength and modulus).

To conclude on the effect of sea water ageing on matrix resin tensile properties it is possible to observe a reduction of tensile strength and modulus for both ageing conditions. But it appears that ageing at 60°C induces more changes in properties than at 40°C. This difference could be explained by the fact that at 60°C the amount of water in the epoxy resin is higher, as presented in Appendix 14. Specimens aged at 40°C reach a maximum weight gain of 2.7% as shown in Appendix 13, against 4.9% at 60°C. At 60°C the Tg depression is faster than at 40°C, which permits diffusion of more water inside the epoxy resin. However, if we plot and compare the evolution of modulus as a function of weight gain at 40 and 60°C, the points and curves are similar as presented in Figure 103 (a), whereas the same comparison with tensile strengths does not match, as presented in Figure 103 (b). This may be due to an embrittlement of the sample surface at 60°C due to oxidation, which results in crack initiation and premature failure. The reversibility of the ageing process will be discussed in Section 3.8.

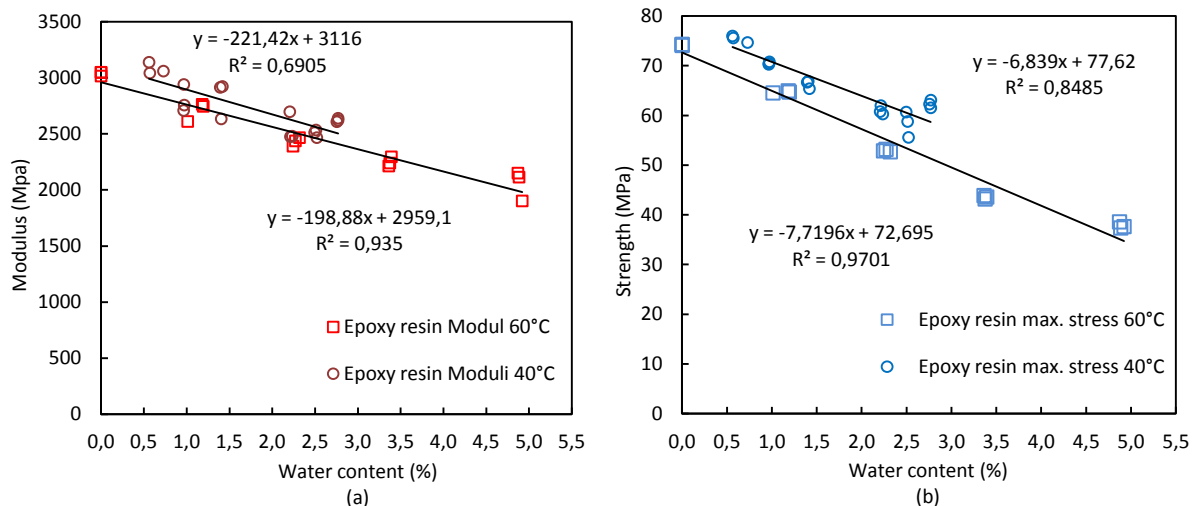


Figure 103: Comparison of the effect of sea water ageing temperature (40 and 60°C) on epoxy resin modulus (a) and strength (b).

3.3.2 Tensile properties of 0° and 90° laminates

For the three composite materials, a characterization of the mechanical properties was performed with tensile tests on specimens cut from UD panels at 90° and 0° after saturation. Only the UD RTM specimens cut at 90° were characterised up to and at saturation (in this case T1 is not saturation time). Three samples were tested in the wet state at 20°C for each condition and material. No significant effects on moduli have been observed, as presented in Figure 104. Scatter bars are not represented because they are very small, between 1 and 4 %.

Figure 105 shows that water uptake has a particularly large effect on both composite strengths, first due to matrix plasticization as indicated by the previous tests on the pure resin, which increases failure strain, followed by reductions due to fibre/matrix interface changes or micro crack appearance in the 90° plies. It is possible to observe drops of transverse strengths of 53%, 34% and 33% for Infused, RTM and Pre-preg respectively after T3. For the longitudinal strengths drops of 28%, 35% and 30% are noted for Infused, RTM and Pre-preg respectively, for the same ageing period (saturation time plus two months).

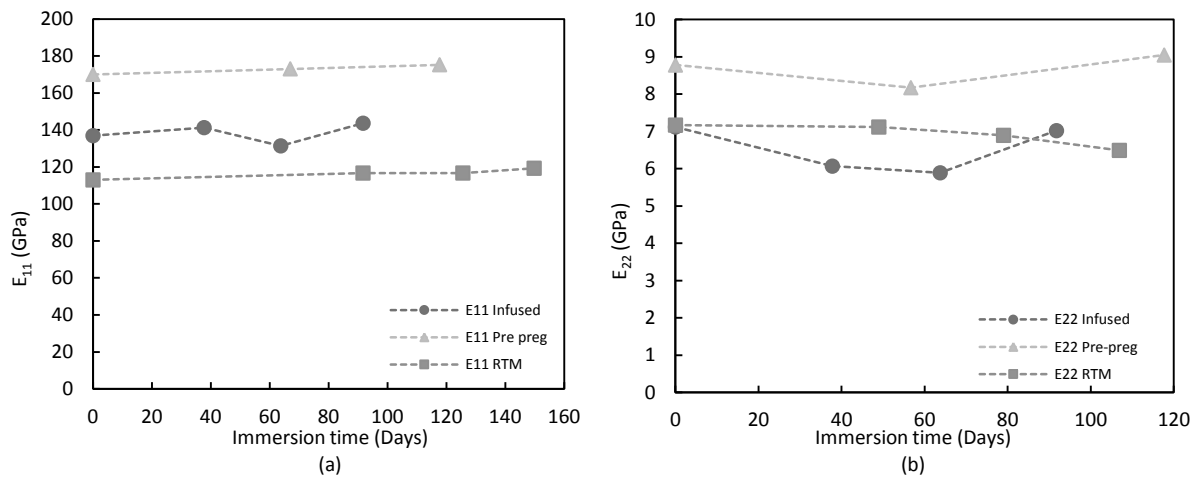


Figure 104: Plots of the evolution of mean longitudinal (E_{11}) (a) and transverse (E_{22}) (b) moduli for the three materials during accelerated sea water ageing.

For strengths, coefficients of variation are between 4 and 13 % for all three materials with no significant difference between them, Figure 105.

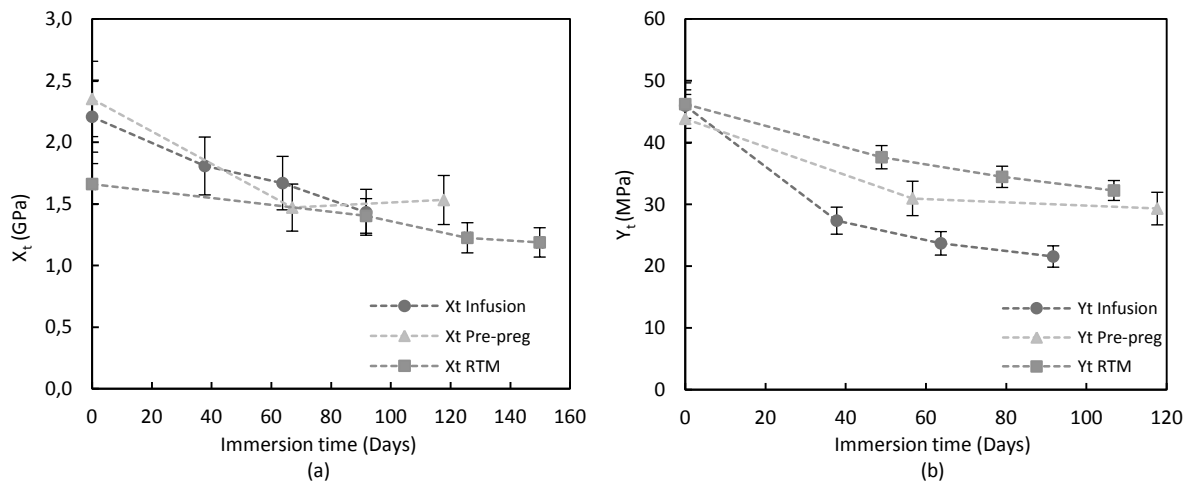


Figure 105: Plots of the evolution of mean longitudinal (X_t) (a) and transverse (Y_t) (b) tensile strengths for the three materials during accelerated sea water ageing. Scatter bars show standard deviations.

The stability of the moduli can be explained by the fact that carbon fibres are not affected by sea water ageing and composite moduli are mainly governed by fibre modulus. But the weakening of composite strengths is directly linked to the reduction of matrix (and fibres/matrix interface) properties. The drop of longitudinal strength is surprising and presumably results from the fact that the weakened matrix cannot transfer load between the fibres as effectively as in the dry state. The drop in transverse tensile strength is explained by the drop in the matrix tensile strength, as presented in section 3.3.1. The weakening of the interface also plays a role in strength degradation, some investigations have been conducted in section 3.7, where interfacial strength decreases due to water ingress. At the ply scale, matrix swelling induces compressive stress σ^c on the fibre. We can express σ^c as presented in Eq.52, where C is the stiffness of the ply, ε is the total strain, ε^{th} is the thermal strain induced by the process and ε^{hydro} is the hydric strain induced by the presence or not of water in the material. After sea water ageing ε^{hydro} will increase, as a result compressive stress induced by the resin on the fibre will be reduced, thus interface strength will decrease.

$$\sigma^c = C : (\varepsilon - \varepsilon^{th} - \varepsilon^{hydro}) \text{ Eq. 52}$$

A comparison has been made between an estimation of tensile moduli degradation based on a classical law of mixtures using both infused carbon fibre and resin mechanical properties. The methods and data are presented in Appendix 16 and Appendix 17. The theoretical estimate corresponds to the effect of ageing on the Infused composite moduli after saturation, as presented in Table 19. As in this estimation only the matrix strength is changing during ageing, this suggests that if there is any fibre/matrix interfacial decohesion it is not affecting modulus values.

Infused UD Properties	Theoretical loss between T0 and T1	Experimental loss measured between T0 and T1
E ₁₁	0.2%	-3.1%
E ₂₂	17.9%	14.7%

Table 19: Comparison between an estimation of tensile properties degradation based classical mixture law and the experimental measurement after saturation time (for the Infused UD). The composite mixture law is based on infused matrix and fibres properties at T0 and T1.

3.3.3 Effect of sea water ageing on in-plane shear behaviour

Tensile tests on $\pm 45^\circ$ laminates of Pre-preg and Infused have been performed during the sea water ageing in order to determine the effect on in-plane shear response. The results are presented in Figure 106. Shear strengths for both materials show large reductions, about 24% for Infused and 30% for the Pre-preg material after respectively 117 days of immersion at 60°C and 92 days of immersion at 80°C . This phenomenon is illustrated in Appendix 18 and Appendix 19. For the Infused materials the reduction of this strength (16% after saturation) is lower than the reduction of matrix strength (28% after saturation).

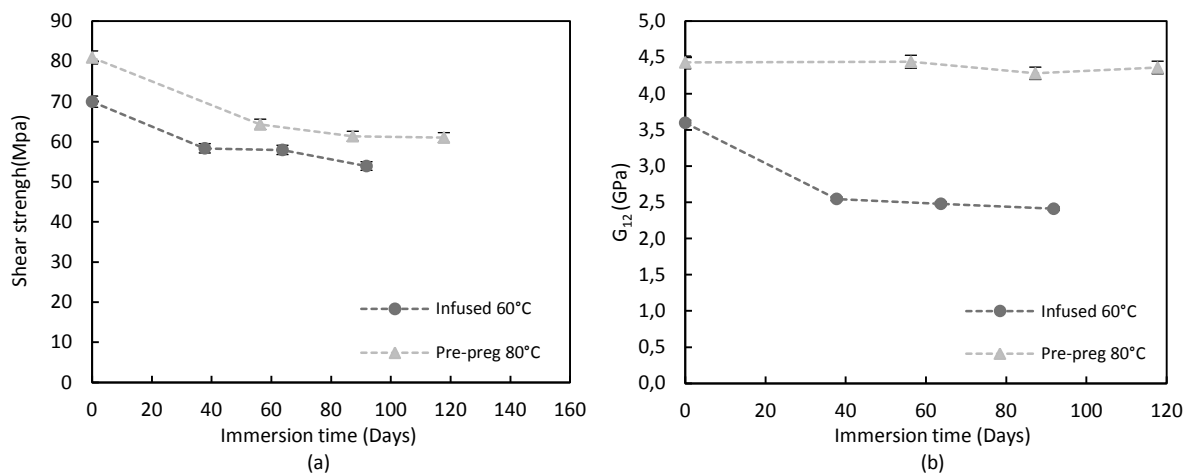


Figure 106: Plots of the change in mean tensile shear strength (a) and tensile shear modulus (b) for the Infused and Pre-preg materials during accelerated sea water ageing. Scatter bars show standard deviations.

Concerning the changes in the shear moduli during sea water ageing, the materials are not following the same behaviour, as presented in Figure 106 (b). Infused shear modulus is subject to a drop of 33% after T3 while for the Pre-preg the modulus remains constant. This shows the importance of the matrix selection for long term immersion.

3.4 Influence of ageing on viscoelastic properties

3.4.1 Tensile tests at different loading rates

In Chapter II the influence of the loading rate on the shear response of Infused $\pm 45^\circ$ laminates was studied. It was shown that these composites exhibit a viscoelastic behavior due to the epoxy

resin. Those tests at 0.2, 2 and 20mm/min loading rates have been repeated on sea water aged Infused specimens. For all loading rates a drop of the modulus and a shift of the non linear part were observed, as presented in Figure 107. After sea water ageing the Infused material still shows viscoelastic behaviour. Appendix 20 presents a comparison before and after sea water ageing.

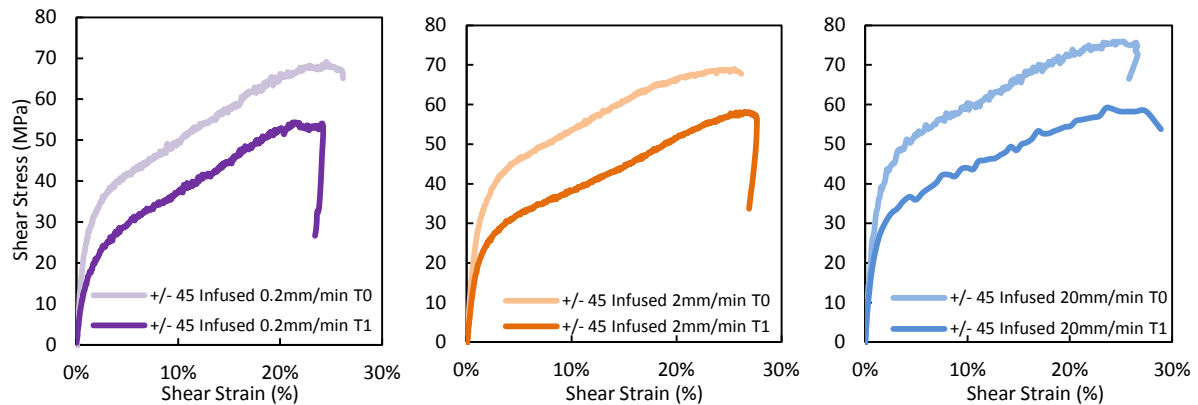


Figure 107: Response of $\pm 45^\circ$ Infused composites at three different loading rates 0.2, 2 and 20mm/min (left to right) before ageing (T0) and after ageing (T1).

3.4.2 Creep behaviour

In Chapter II the creep behaviour of the un-aged Infused material was presented. In this section creep behaviour before and after ageing will be discussed. The Infused $\pm 45^\circ$ specimen was aged for 37 days in sea water at 60°C (T1), allowing the sample to be saturated in water, then the same creep loading sequence was applied.

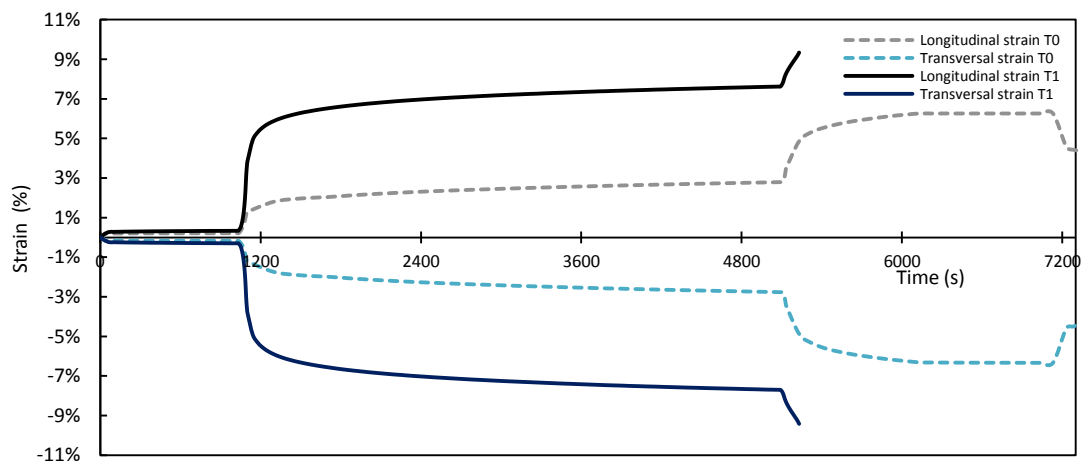


Figure 108: Creep response of Infused material before(dotted line) and after sea water ageing (continuous line).

In Figure 108, a comparison is presented for two states of ageing (T0 and T1). A significant change in creep response for aged samples appears after the second load increment of 3600 N. For the same applied load, aged specimen strains are higher than for un-aged specimens. It has been previously shown that carbon fibres are insensitive to creep [191]. Thus it is reasonable to conclude that the change in creep behaviour is a consequence of the shear viscoelastic modulus reduction observed on composites and resin (due to plasticisation of the matrix). At the beginning of the third loading step of 4800N (56.2MPa), failure occurs in the aged specimen, whereas the un-aged specimen completed the last loading step. As shear strength decreases during ageing, as shown in Figure 106, the specimen fails.

3.5 Effect of sea water ageing on damage propagation

In this section the intra-laminar crack propagation behaviour will be investigated for different sea water ageing times and results will be compared to those obtained before ageing. The specimen details are presented in Chapter II (see section 3.3). Only Infused F1 $[0,90,0,90]_s$, F2 $[0_2,90_2]_s$ and Pre-preg F1 $[0_2,90_2]_s$ results will be presented here.

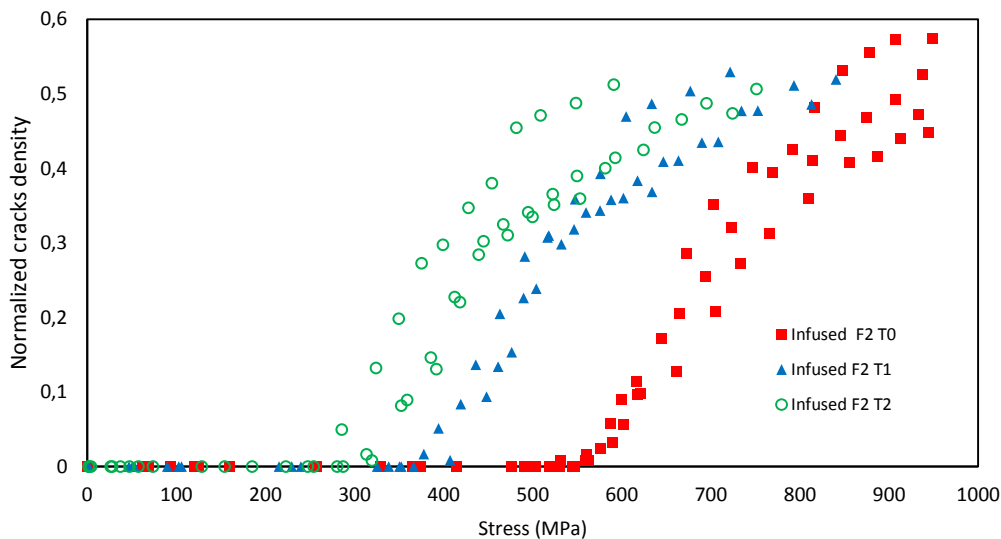


Figure 109: Evolution of normalized crack density for infused composite $[0_2,90_2]_s$ before ageing (red square), at saturation (blue triangle) and at saturation time plus one month (green circle) (3 specimens per condition).

Results for normalized crack density as a function of the applied stress are presented for Infused $[0_2,90_2]_s$ laminates for different immersion times (T0, T1 and T2), in Figure 109. There is a horizontal shift of the different curves. For the aged materials damage initiation occurs at lower

stresses. This can be explained by the fact that for the 90° plies, their strengths are reduced due to the drop of composite transverse strength observed after sea water ageing, previously presented in section 3.3.2. But it is interesting that the kinetics of damage propagation remain constant after sea water ageing.

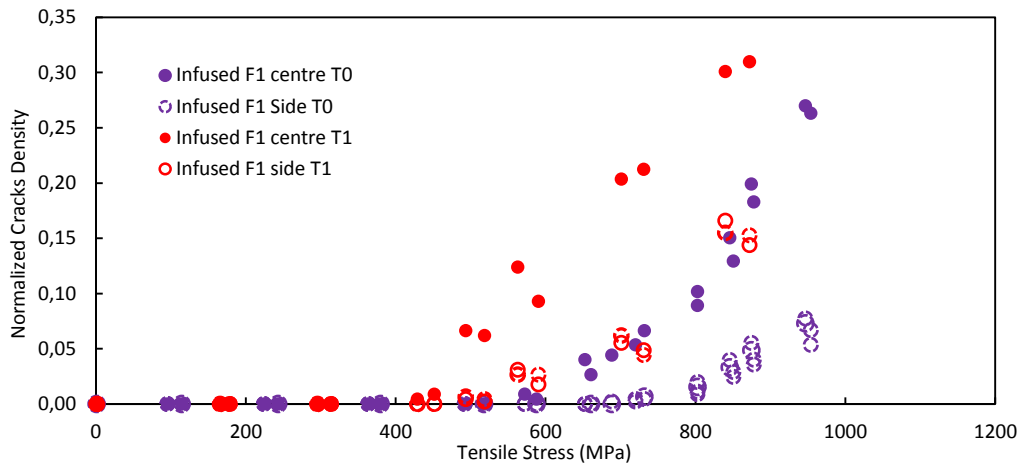


Figure 110: Evolution of normalized crack density for infused composite [0,90,0,90]_s before ageing (purple round for the doubled 90° plies and purple dotted circles for the single 90° plies), at saturation (red round for the doubled 90° plies and red dotted circles for the single 90° plies), 3 specimens per condition.

Figure 110 shows the results obtained at T0 and T1 for Infused laminates [0,90,0,90]_s. Once again a shift is observed on the damage propagation curves. The initiation of damage after sea water ageing appears at a lower tensile stress level for both 90° plies (in the centre of the specimen where the 90° plies are doubled and in each single ply on both sides). But the kinetics of damage still remain the same before and after saturation.

Some tests have been also performed on Pre-preg [0₂,90₂]_s materials at T0, T1 and T2. No significant changes in the kinetics of damage development have been observed for un-aged or aged specimens of this material, as presented in Figure 111.

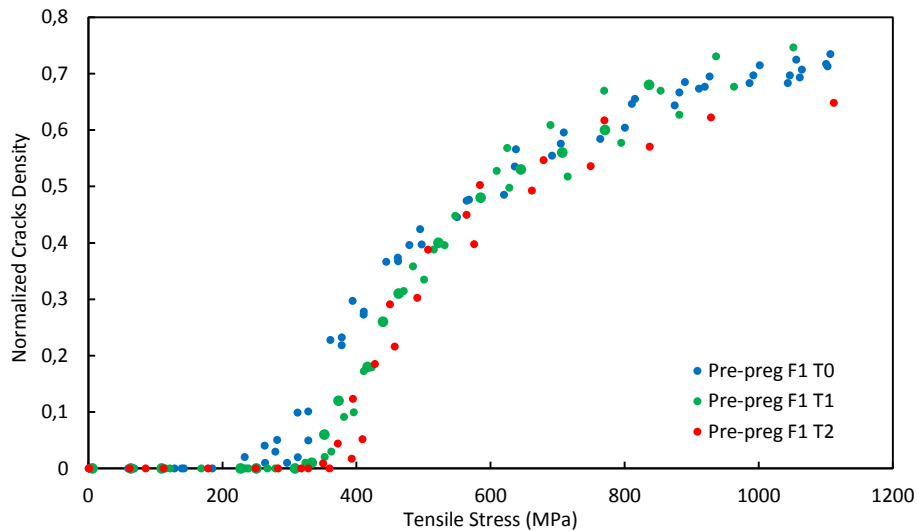


Figure 111: Evolution of normalized crack density as a function of applied stress for Pre-preg $[0_2,90_2]_s$, before (blue points) and after ageing (green points T1, red points T2).

Contrary to the results presented previously on Infused materials, the initiation of damage in Pre-preg composite occurs at a higher stress level after ageing (230-260 MPa for un-aged material and 330-390 MPa after sea water ageing). One possible explanation for this might be that before sea water ageing the 90° plies present in the $[0_2,90_2]_s$ Pre-preg laminate are subject to residual stresses induced during the manufacturing process. So to start to induce damage in these plies at T0 it is necessary to apply a certain stress level of A MPa. Then during the sea water ageing water ingress in the Pre-preg and specifically in the thermoplastic nodules present at the interface, the residual hygrothermal stresses may be relaxed. Then it would be necessary to apply a higher stress level $A+\Delta A$ MPa to initiate damage in these 90° plies, [46].

3.6 Effect on interlaminar fracture toughness

The evolution of composite materials toughness has been investigated using DCB tests during ageing. DCB tests were performed on un-aged material, then after three ageing times. The effect of water ageing on the toughness is quite limited, as shown in Figure 112. However, as previously mentioned during characterisation of the un-aged material, the results concerning the toughness of the ply could be artificially increased due to high fibre bridging caused by both stitching and out of plane carbon fibres. It has been shown in the literature that in case of fibre bridging, crack propagation demands additional energy to pull out and debond the bridged fibres, [192]. Indeed, multiple cracking phenomena have been observed after sea water ageing, (see Appendix 22), and

such multiple cracks result in higher values of toughness, [193]. In order to avoid this effect the ISO standard proposed using initiation values either from the insert or from a short pre-crack to characterize delamination, as these provide conservative fracture energies. When these initiation values were calculated for the Infused composite an important drop in fracture energy was observed between T0 and T1 T2 T3, Figure 113.

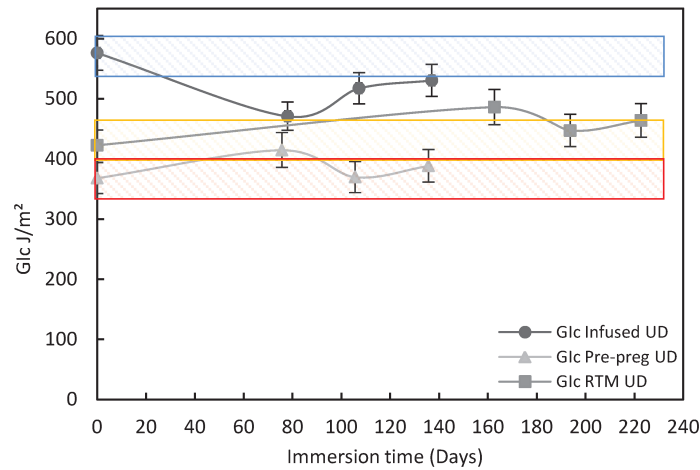


Figure 112: Evolution of critical strain energy release rate G_c in carbon/epoxy Pre-preg, Infused and RTM materials during sea water ageing.

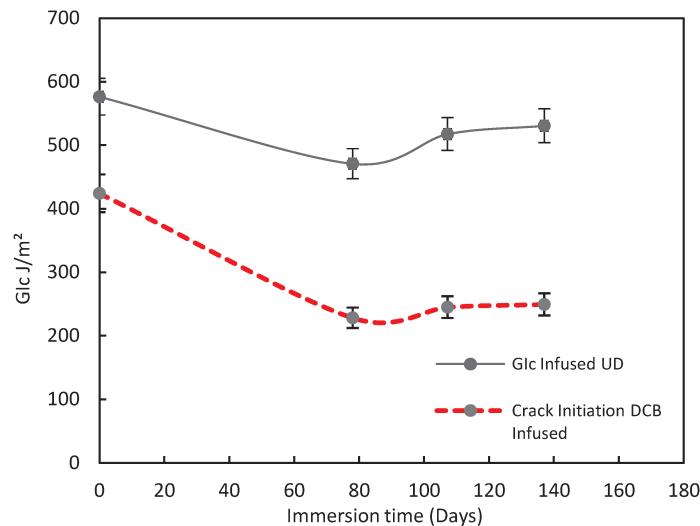


Figure 113: Initiation fracture energies from film insert, Infused composite during sea water ageing.

This example of mode I fracture shows that even using a normalized test, different appreciations of ageing effects can be obtained. The initiation G_c values are consistent with the drop observed in transverse tensile strength after saturation, whereas the presence of fibre bridging,

which will be found in a structure with UD reinforcement, can slow crack growth and improve damage tolerance.

3.7 Effect of ageing on out of plane strength

The changes in the interlaminar shear strength during ageing have been followed for different material orientations and thicknesses.

According to Figure 114, the decrease in interlaminar shear stress in both cases is quite important, about 20-30% for UD (a) and 16-27% for QI (b) materials. The study performed on unreinforced resin showed a large drop in tensile strength (50%) after saturation so this may dominate. However, as will be shown later by fractography, the fibre/matrix bonding is also weakened.

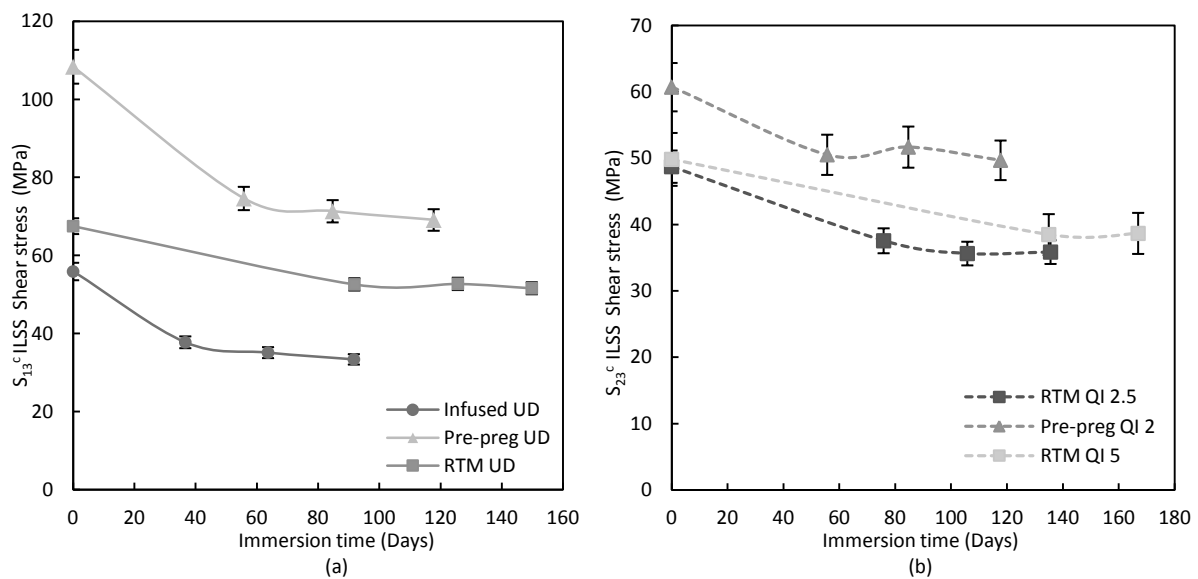


Figure 114: Changes in mean ILSS shear stress strength during sea water ageing for three different UD (a) and QI (b) materials. Scatter bars show standard deviations.

It is worth mentioning that S_{13}^c and S_{23}^c are quasi independent on the thickness, as presented for the RTM QI 2.5 and 5 mm, see Figure 114. Small differences could be explained by the differences of porosity of fibre content. Additionally it is important to note that the reduction in S_{23}^c correlates with the degradation of the transverse tensile strength, because for the QI sequence the 90° plies fail first in shear.

3.8 Additional investigation on ageing

Some further investigations were performed in order to highlight some facts concerning sea water ageing and accelerated ageing. The first point concerns the reversibility of accelerated sea water ageing. To understand this reversibility some specimens of resin and composite were aged and then dried under the same conditions of time and temperature. Finally the dried specimens were tested and results were compared to those from wet specimens.

Table 20 presents the results obtained under both conditions for four point bending tests on Airborne QI 5.2 mm material. As previously shown, flexural strength decreased after ageing. For specimens aged and then dried, the initial un-aged flexural strength was obtained, suggesting that the ageing process is reversible.

RTM QI 5.2 mm	T0	T1 136 days	T1 Dried 60°C
Flexural modulus (MPa)	556.6(56.1)	413.7(41.6)	549.4(51.9)

Table 20: Illustration on reversibility of the ageing process, presented on RTM QI 5 mm flexural strength (T0: un-aged, T1: saturated in water, T1 dried: saturated in water and then dried).

In Figure 115, a comparison is presented between aged and aged and dried (60°C) epoxy resin specimens. Reversibility of the ageing process is shown for resin tensile modulus and strength.

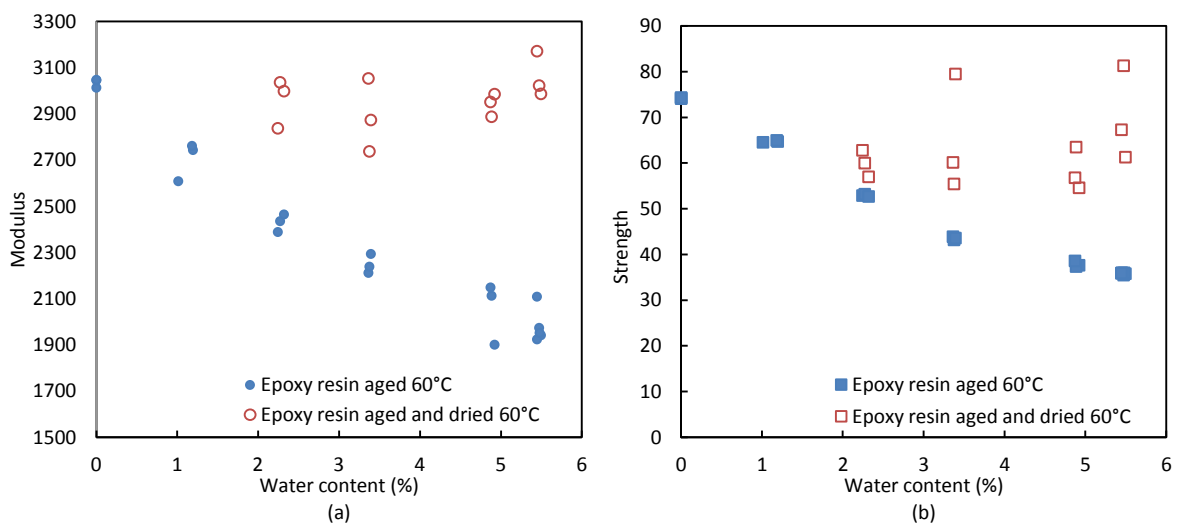


Figure 115: Illustration on reversibility of ageing process for tensile modulus (a) and tensile strength (b) of the epoxy resin aged (blue) and aged and dried (red) at 60°C.

According to Figure 115 (a) and (b), it is shown that the ageing process is quite reversible for the tensile modulus while for the strength the ageing process is not completely reversible. This phenomenon suggests that additional ageing mechanisms occur during immersion of the resin in the water at 60°C. Oxidation can explain this additional degradation of strength, oxidation may create surface cracks on epoxy samples.

Additionally the question of the temperature effect on the ageing process was studied. The effects of accelerated sea water ageing at 60°C were compared to those from dry ageing in an oven at 60°C. This should indicate whether the property changes are due to temperature or to water. This comparison is presented in Table 21. This table presents the results obtained after transverse tensile tests on RTM 2.8 UD. Both modulus and strength are presented in un-aged, wet ageing and dry ageing conditions. After thermal ageing, the modulus increases slightly, this may be due to surface oxidation. But transverse strength remains constant after thermal ageing, whereas a significant drop appears after sea water ageing.

RTM UD 90° 2.8mm	T0	T1 SW 60°C 48 days	T1 Oven 60°C 48 days
E22 (GPa)	7.17(0.01)	7.24(0.15)	8.10 (0.32)
Yt(MPa)	46.21(1.21)	37.72(1.17)	45.34(3.96)

Table 21: Comparison between effects of sea water ageing and thermal ageing on RTM UD 2.8 mm after transverse tensile test, (SW: sea water).

As a conclusion on the reversibility of sea water ageing process and the effect of temperature on the evolution of the properties, it seems that the process of sea water ageing is largely reversible at 60°C for the composite studied. With the comparison between accelerated water ageing and thermal ageing, it is reasonable to conclude that for this composite material the temperature doesn't induce other significant mechanisms of degradation, suggesting that water ingress is the only cause of the changes of properties. However for epoxy resin it has been highlighted that sea water ageing phenomena is not the only degradation process leading to strength reduction. Oxidation of the epoxy resin may appear during the ageing process at 60°C, inducing additional degradation.

4. Microscopy observation of ageing effects

In the previous sections, results from experimental investigations were presented for three materials. It has been highlighted that all composites are affected by the sea water ageing process, which leads to strength reduction. In Chapter II some fracture surfaces of un-aged materials were presented. In the following sections, SEM observations will be presented before and after exposure to sea water, in order to have a better understanding of the mechanisms responsible for early failure after sea water ageing.

4.1 Composite surface exposed to sea water

The first observations presented in this section are on UD specimens of each material oriented at 0°. Some cross sections of each specimen have been directly exposed to sea water at 60°C during 6 months. Specimens were mounted in a casting epoxy resin. All specimens have been polished. The following figures present some observations after this immersion period.

4.1.1 Infused material

The Figure 116 presents the surface state of the infused specimen after sea water immersion, observations were made on the edge of the specimen. The orange dotted line shows the separation between the casting resin and the edge of the specimen. In Figure 116 (a) and (b), is possible to observe matrix swelling on the edge of the specimen (blue dotted rectangles). In matrix rich regions of the whole specimen, especially between the plies, swelling was also observed (see Figure 117 (b)). In Figure 116 (b), a focus on the edge of the specimen is presented. In this resin-rich region of matrix (blue dotted rectangle), the swelling of the matrix is significant. This phenomenon leads to an interfacial decohesion between resin and fibres.

Figure 117 (a) presents a zoom on the polyester stitching fibres located between two plies of carbon. Some debonding between these fibres and the resin is also visible (green oval). These decohesions could create new pathways for water diffusion. In Figure 117 (b) the whole thickness of the specimen is presented.

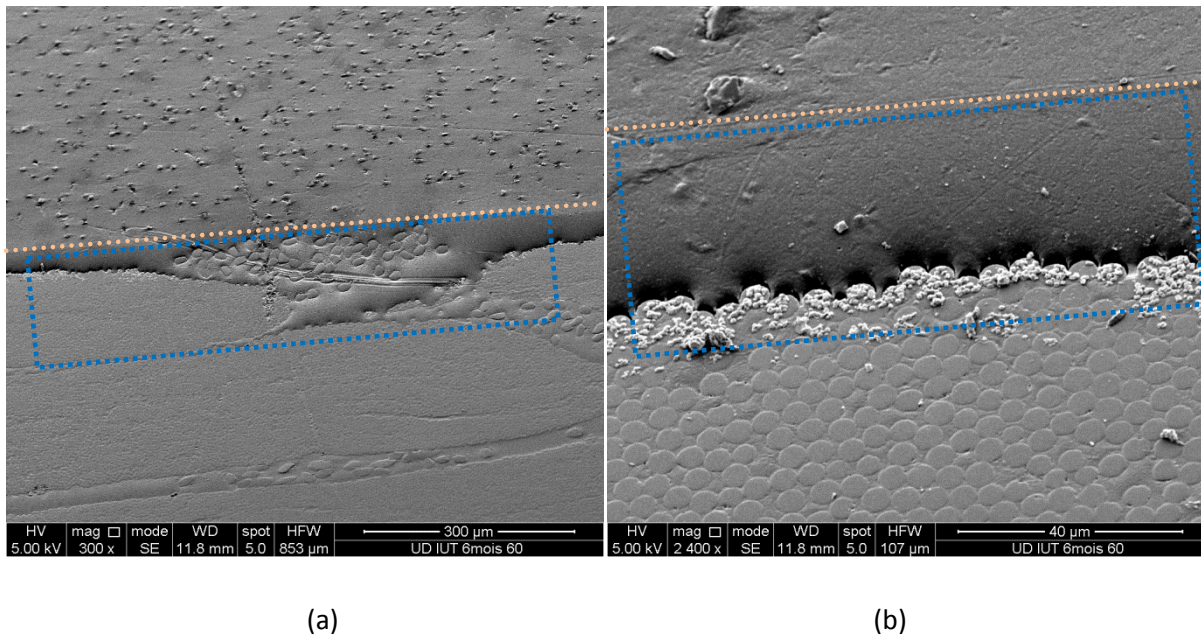


Figure 116: SEM observation of Infused UD cross section immersed during 6 months. (edge region).

As noted previously, in numerous locations of the specimen (blue dotted rectangles) it is possible to observe matrix swelling. In the view in Figure 117 (b), it is also possible to observe an intra-ply crack (red rectangle). This crack may be the consequence of matrix swelling, though internal stresses could also be responsible.

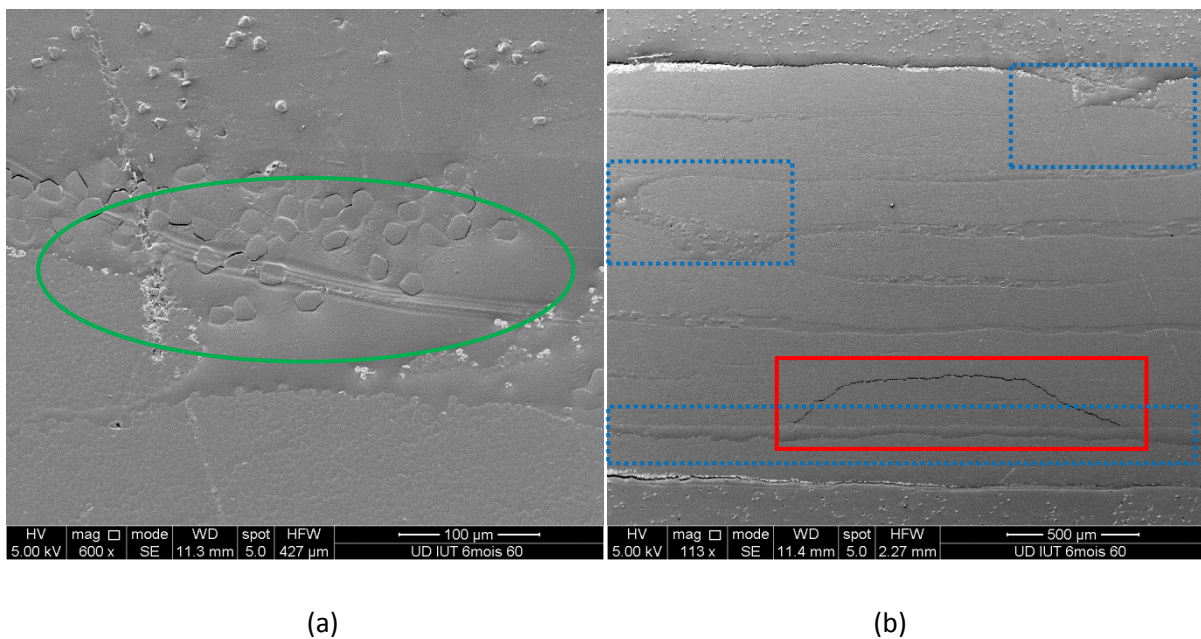


Figure 117: SEM observation of Infused UD cross section immersed during 6 months, (a) presents a region between two plies where stitching fibres are located, (b) presents the whole thickness of the specimen and highlights a crack.

4.1.2 Pre-preg material

Some observations have also been made on the Pre-preg material. Swelling has not been observed in this specimen. However, as shown in Figure 118 (a) and (b), debonding occurs at the interface between matrix and fibres between each ply (blue dotted rectangles). Concerning the impact of sea water on the thermoplastic present at this interface it is quite difficult to conclude. In Figure 118 (a) and (b) (green circles) the nodules seem not to be affected by ageing, but a few nodules do show some decohesion (see Figure 118 (b)).

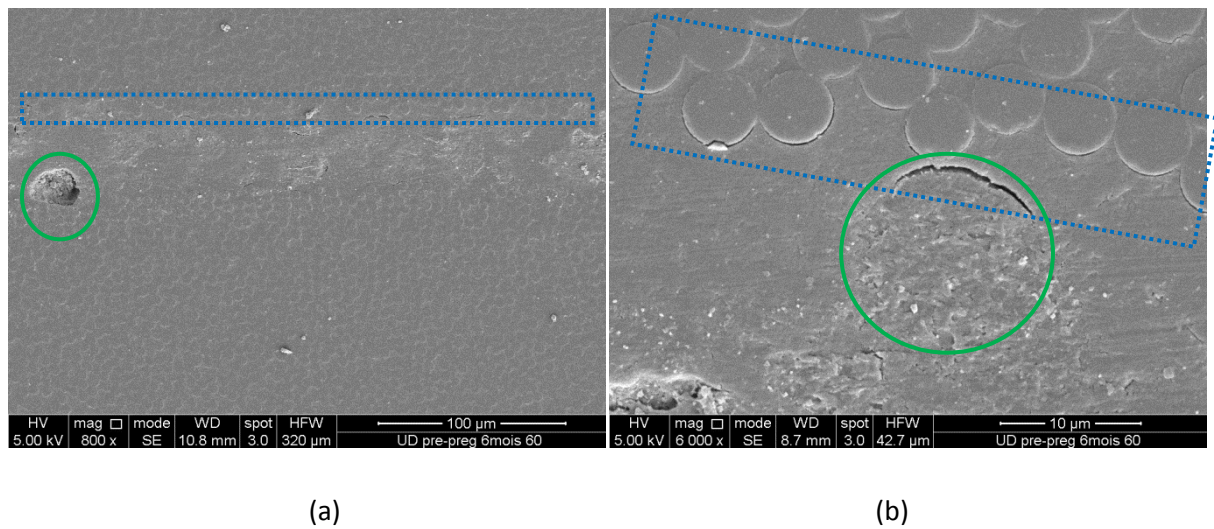


Figure 118: SEM observation of Pre-preg UD cross section immersed during 6 months, (a) presents a region between two plies where are located nodules, (b) presents a focus in interply region.

4.1.3 RTM material

The final material observed here is the RTM composite. As seen for the Infused material, swelling occurs in the matrix region in the RTM material.

Figure 119 (a) shows a region between two plies of carbon. In this region it is possible to observe some tunnels in the resin (green circle). These tunnels are the imprints of fibre stitching which has been degraded during sea water ageing. Figure 119 (b) focuses on these tunnels. As observed previously in other materials, RTM composites are also subject to decohesion between resin and matrix at the interface between each ply (blue dotted rectangle).

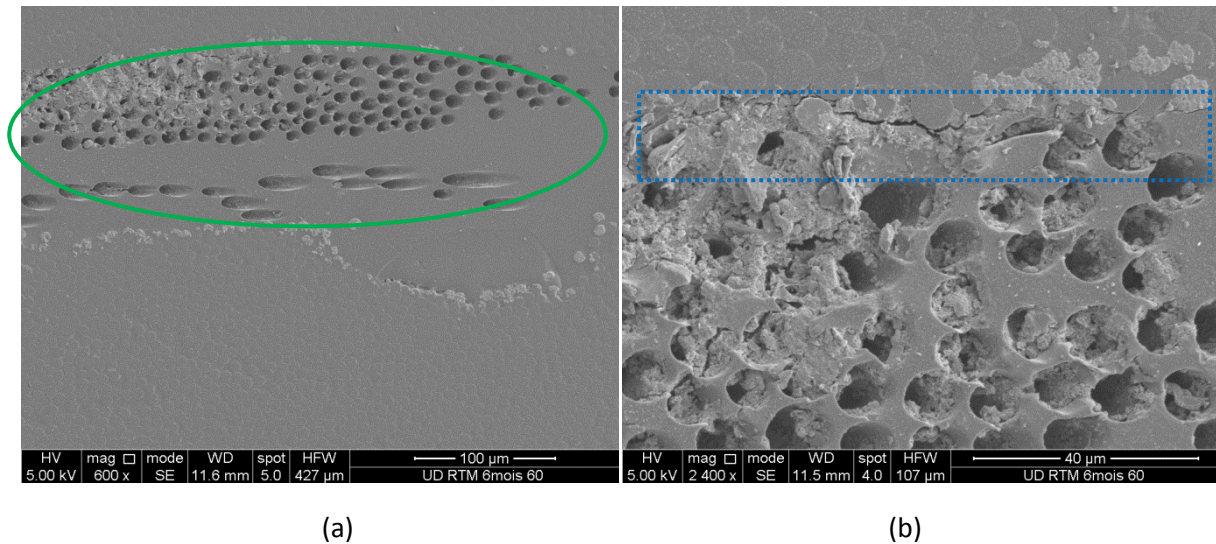


Figure 119: SEM observation of RTM UD cross section immersed during 6 months, (a) presents a region between two plies, (b) presents a focus on an interply region and stitching fibres.

These images underline the complexity of these materials. In all materials some changes have been observed after ageing. The main changes occur in interply regions at the interfaces between matrix and fibres. RTM and Infused materials are subject to swelling in resin-rich regions. These observations have been performed on non loaded samples, in the next section some fracture surfaces from mechanical test specimens will be presented and compared for different ageing states.

4.2 Fracture surface after longitudinal tensile tests.

Fracture surfaces presented in this section have been obtained after tensile tests (in the longitudinal and transverse directions to fibres). Fracture surfaces of the specimens used for the mechanical tests, presented in section 3.3 , were observed using SEM. They have been compared to the specimens tested at T0. Only specimens aged to T3 are presented here (saturation time + 2 months).

4.2.1 Infused material

The SEM observations allow the fracture surfaces at T0 and T3 to be compared for the Infused material. In this case the samples were loaded in the fibre direction. Figure 120 presents the fracture surfaces after T0 (a/c) and T3 (b/d). In the Figure 120 (a) and (b) the fracture surface was observed at an angle. Notable differences are presented here, before ageing Figure 120 (a) and (c), the fibres are

still well bonded to the matrix. Failure of fibres seems to appear in the same plane as the matrix. But after sea water ageing fibre pull out appears (orange arrows), and fibres and matrix are no longer well bonded (orange S marks), as presented in Figure 120 (b) and (d). Indeed, as soon as the matrix does not play its role to transfer the load, it leads to a drastic loss of strength, [194], [195]. The efficiency of the matrix load transfer can thus be reconsidered. These phenomena corroborate with the early failure of these specimens after sea water ageing, presented previously in the mechanical testing section. Figure 121 (a) shows the edge of the specimen. This observation could be compared to Figure 120 (c), which was also taken close to the edge of the specimen. In both resin rich regions of these specimens, the matrix presents the same fracture surface (red rectangles). This could be explained by the fact that in tension the interface fails first (especially after ageing), as a consequence the matrix does not show any difference in terms of deformation. But as presented in the previous figures of aged composites, significant fibre splitting phenomena occur after sea water ageing (blue dotted rectangles).

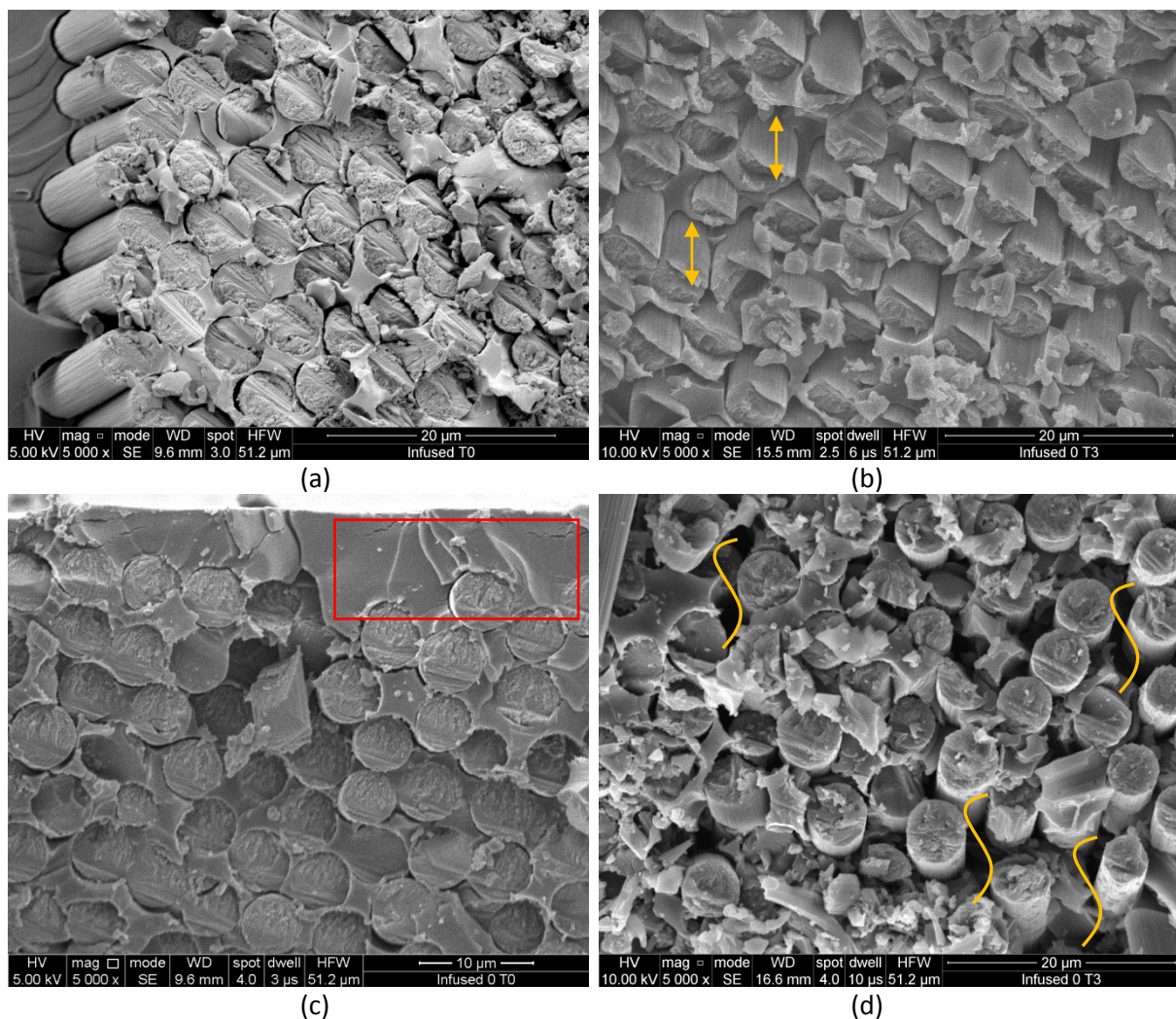


Figure 120: SEM observation of Infused UD fracture surface after longitudinal tensile test, (a), (c) for un-aged material, (b), (d) for specimen aged T3.

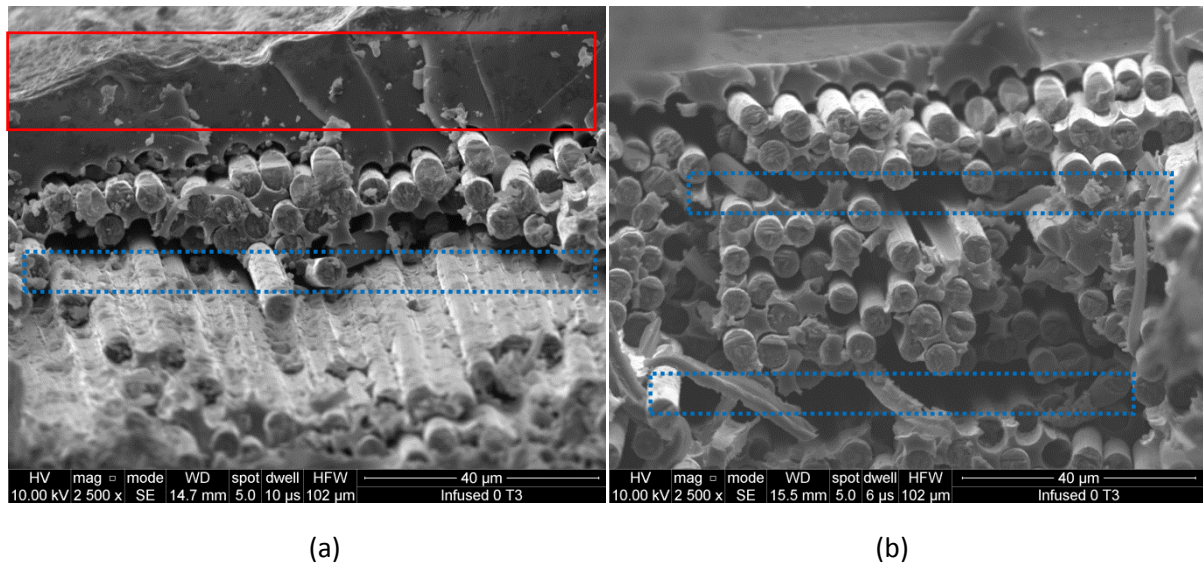
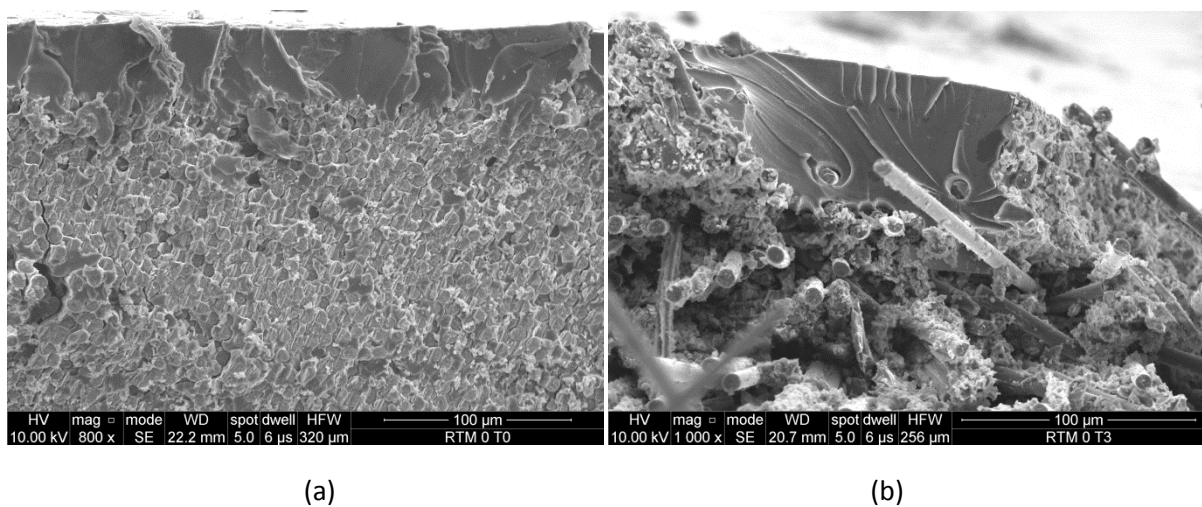


Figure 121: SEM observation of Infused UD fracture surface after longitudinal tensile test T3, (a) edge specimen region, (b) interply region.

4.2.2 RTM material

The same observations have been made on the RTM material. Figure 122 presents the fracture surfaces for both ageing conditions in different regions of the specimens. Figure 122 (a) and (b) allow fracture surface at T0 and T3 of ageing to be compared. In those regions close to the edge of the specimen, fracture surfaces show extensive fibre pull out after sea water ageing. As presented for the Infused material, RTM fibre/matrix bonding is clearly weakened. Figure 122 (c) and (d) are focused on the interply region. After sea water ageing in this region, fibre breakage and fibre pull-out phenomena appear clearly.



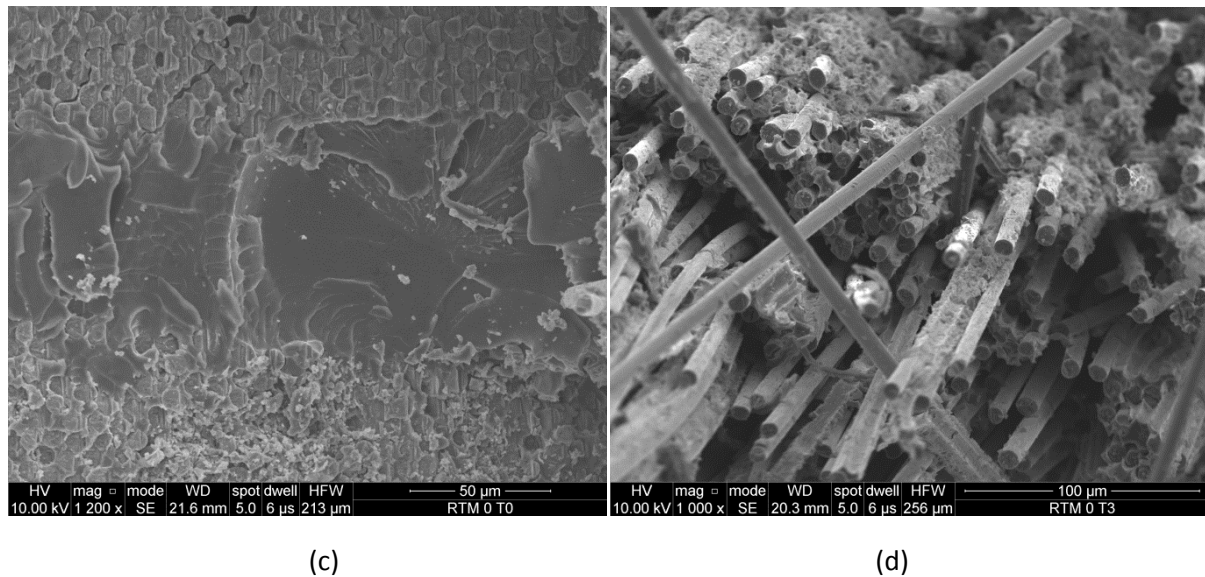


Figure 122: SEM observation of RTM UD fracture surface after longitudinal tension test, (a) T0 and (b) T3 compare edge observations, (c) and (d) compare interply regions.

In Figure 123 (a) and (b) a focus on the fibre fracture surfaces is presented. It is possible to observe changes. Before ageing, Figure 123 (a), it is possible to distinguish a chop mark on the fracture surface of the carbon fibres. These chop marks are not present after ageing, suggesting that cracks leading to failure propagate in the un-aged specimen. The direction of failure is indicated in Figure 123 (a) (orange arrow).

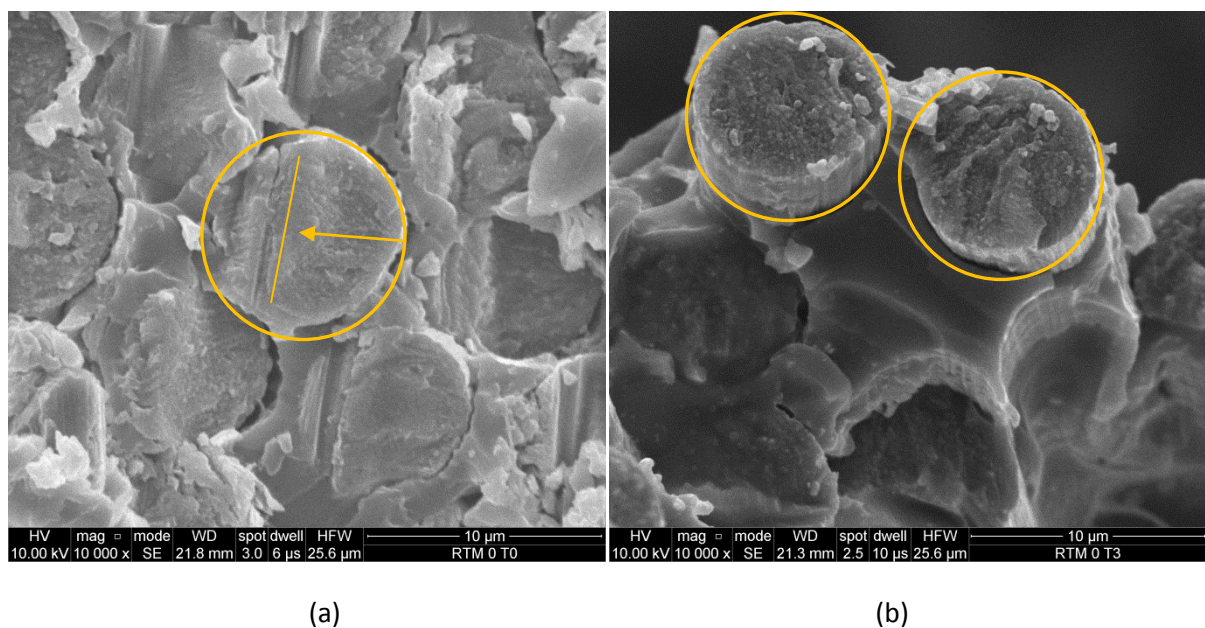


Figure 123: SEM observation of RTM UD fracture surface after longitudinal tension test, (a) T0 and (b) T3 are focused on the fibres fracture surfaces.

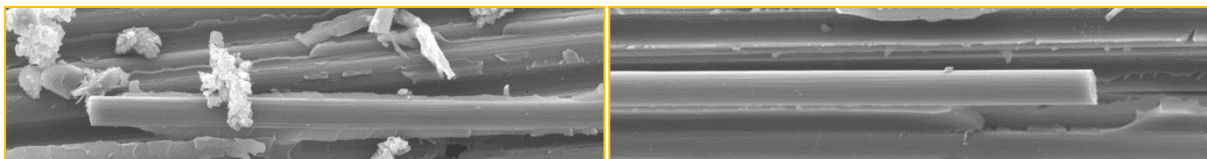
For un-aged specimens, fibre failure leads to a local overloading. The final failure is thus due a propagation in a plane of a crack. For the aged specimen, the degraded matrix leads to overloading of the other fibres in a larger domain than in a sound material, so that the probability to break another “weakest link” is increased. The failure load decreases and fibre pull-out appears, as presented on the Figure 123 (b).

4.3 Fracture surfaces after transverse tensile tests.

The different observations presented in this section have been obtained using SEM. Observations have been made after tensile tests perpendicular to fibres. Some comparisons between fracture surfaces will be presented on the three materials, before and after sea water ageing (To and T3).

4.3.1 Infused transverse

Figure 124 presents fracture surfaces after transverse tensile test on the infused material. These observations were made in intra-ply regions. Figure 124 (a) and (b) (orange dotted rectangle) present a focus on a single fibre. Before ageing the fibres are still well bonded to the matrix (c). Some fibres are detached from the matrix, but for those fibres it is possible to distinguish pieces of resin still attached along the fibre, suggesting that the interface is good (a). Then after sea water ageing, there is less adhesion between fibres and matrix. The interface between fibres and matrix seems to be weakened, as presented in Figure 124 (b), where the fibres are clean. In Figure 124 (d) matrix ribbons are visible, which are not present before ageing (c) (red rectangles), suggesting a more ductile matrix failure after ageing.



(a)

(b)

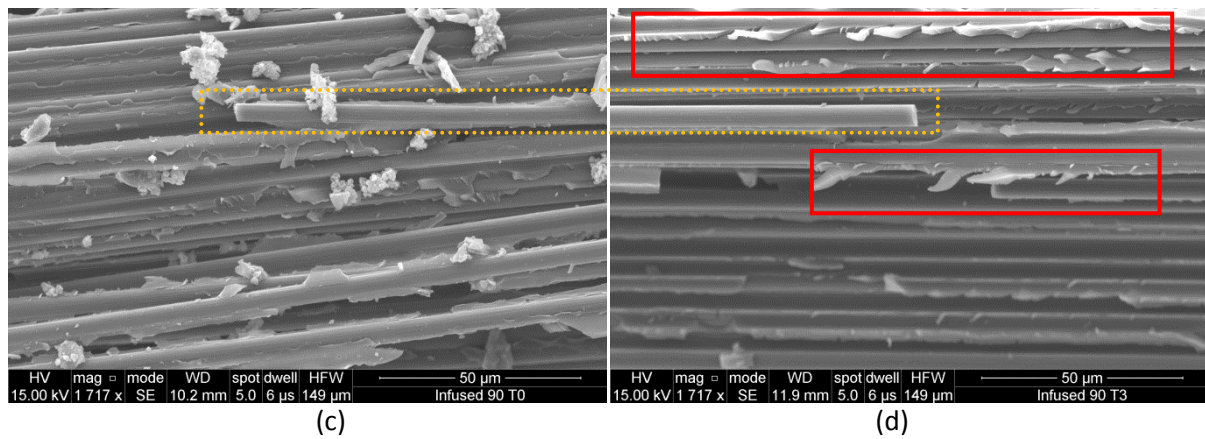


Figure 124: SEM observations of Infused UD after transverse tensile test, observations are focused on intra-ply region. (a) before ageing T0, and (b) after ageing T3. (c) and (d) present a focus on carbon fibres.

4.3.2 RTM transverse

The same type of observations were made on the RTM material before and after ageing. Changes in fracture surfaces after ageing are quite similar, as presented in Figure 125 (c) and (d). More debonded carbon fibres appear after sea water ageing.

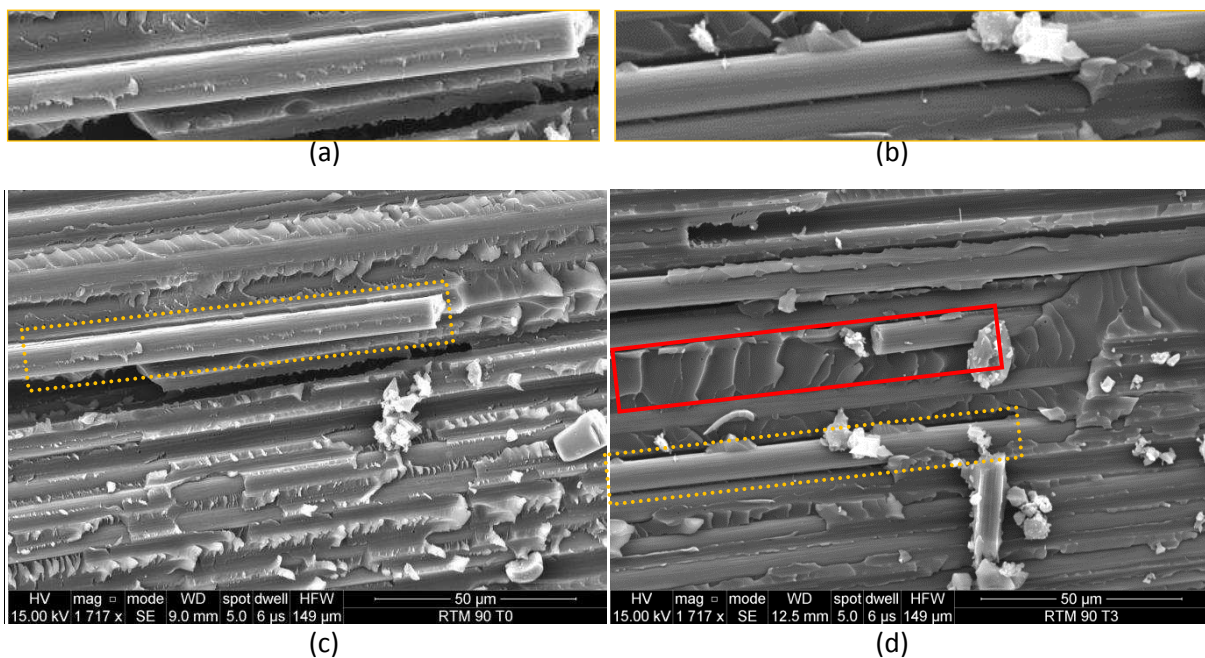


Figure 125: SEM observations of RTM UD after transverse tensile test, observations are focused in intraply region. (a) before ageing T0, and (b) after ageing T3. (c) and (d) present a focus on carbon fibres

The fracture surfaces of the resin present between the carbon fibres are composed of numerous small cusps. After ageing it appears that fewer cusps are present (red rectangle).

Figure 126 (a) and (b) present observations in the interply regions of the material. In this resin rich region (red rectangle), it is possible to observe some changes. As presented previously, before ageing the failure of the resin is quite brittle. At T0, some cusps are present but after sea water ageing more regular features are visible in the matrix (different shape), indicating more ductility in the resin.

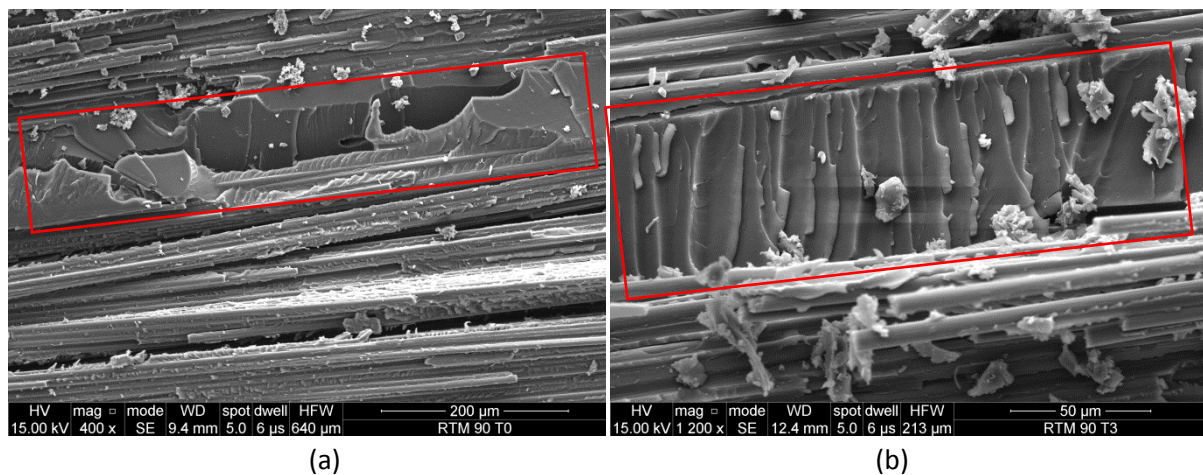


Figure 126: SEM observation of RTM UD after transverse tensile test, (a) presents a region between two plies at T0, (b) presents a focus in interply after sea water ageing T3.

4.3.3 Pre-preg transverse

Some observations have been made on Pre-preg composites after transverse tensile tests for both conditions of ageing. Figure 127 (a) and (b) presents observations on the edge of the specimens before and after ageing.

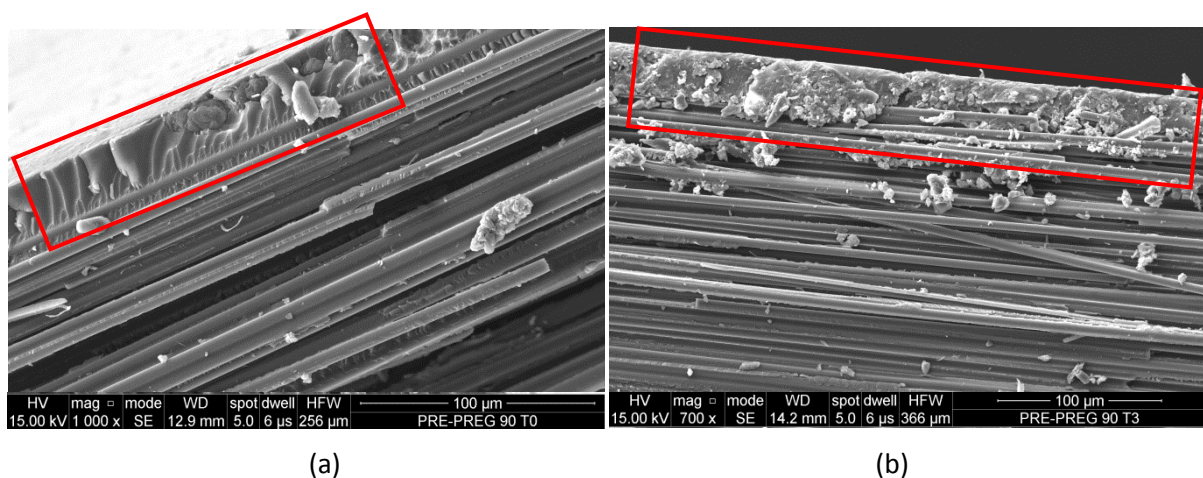


Figure 127: SEM observations of Pre-preg UD after transverse tensile test, observations are focused in edge region before (a) and after sea water ageing (b).

Figure 128 (a) and (b) present observations in the middle of the specimen section. It is possible to distinguish interply matrix with the thermoplastic nodules. After sea water ageing (b) the fracture surface in this matrix rich region is not as planar as before ageing (a). This difference could be due to matrix or matrix/nodules weakening after long exposure to sea water.

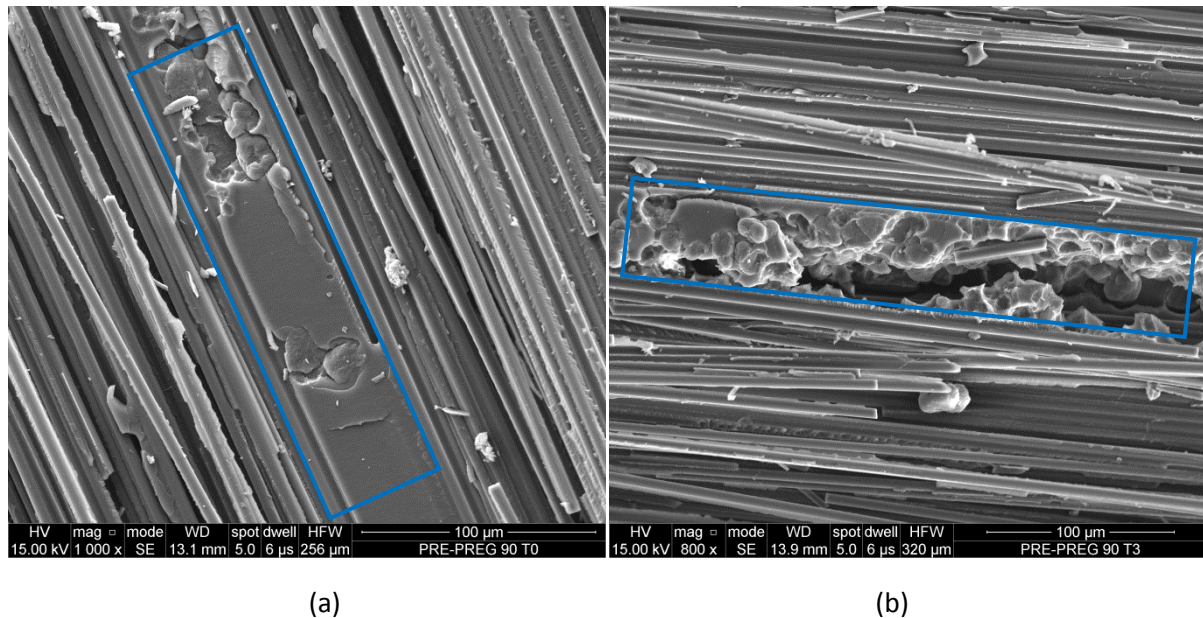


Figure 128: SEM observations of Pre-preg UD after transverse tensile test, observations are focused on interply regions, before (a) and after sea water ageing (b).

Figure 129 (a) and (b) shows details of the fracture surface located in a transverse ply of carbon. Before sea water ageing most of the carbon fibres are still well bonded to the matrix. After ageing, the fracture surface presents more fibre/matrix separation and more fibres are visible.

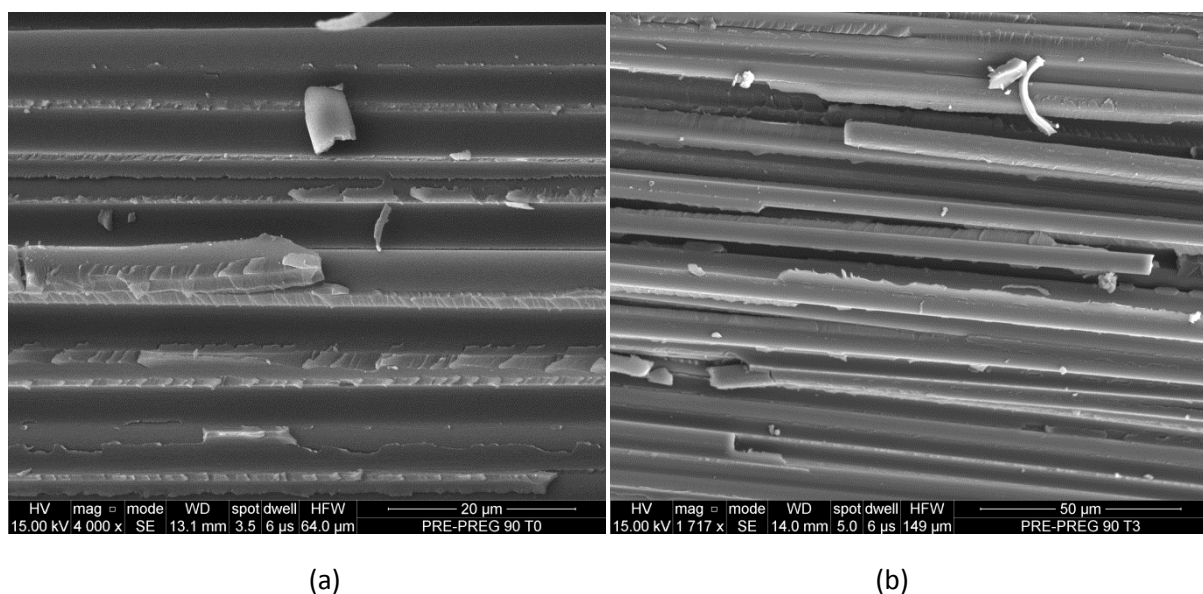


Figure 129: SEM observations of Pre-preg UD after transverse tensile test, observations are focused in intraply region, before (a) and after sea water ageing (b).

4.4 Interlaminar fracture surface after DCB test

The result that toughness G_{Ic} seems to remain constant during ageing when other properties such as in-plane strengths decrease, is quite surprising. It was therefore important to observe fracture surfaces after interlaminar fracture tests. In this section some comparisons will be presented before and after ageing. These SEM observations are focused in a range of 10 mm after initiation of the crack.

4.4.1 Infused material

The Figure 130 presents an overall view of Infused DCB fracture surfaces, before and after ageing. At this observation scale, it is possible to distinguish differences in crack propagation. In Figure 130 (a), the crack was propagating in the interply region, in the matrix. Then after sea water ageing, more carbon fibres are visible at the surface (seen Figure 130 (b)), suggesting that changes occur in the matrix and at the interface between fibres and matrix.

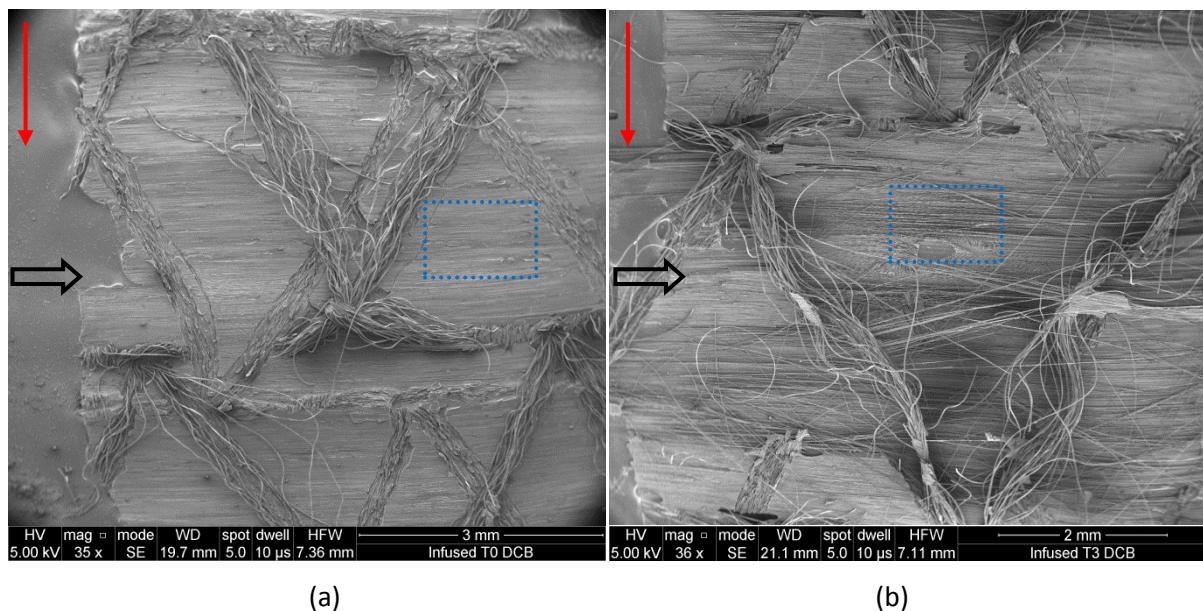


Figure 130: SEM observation of Infused material after crack propagation using DCB test, observations present a large view on the specimen fracture surface, arrows show the direction of the propagation. (a) T0, (b) T3.

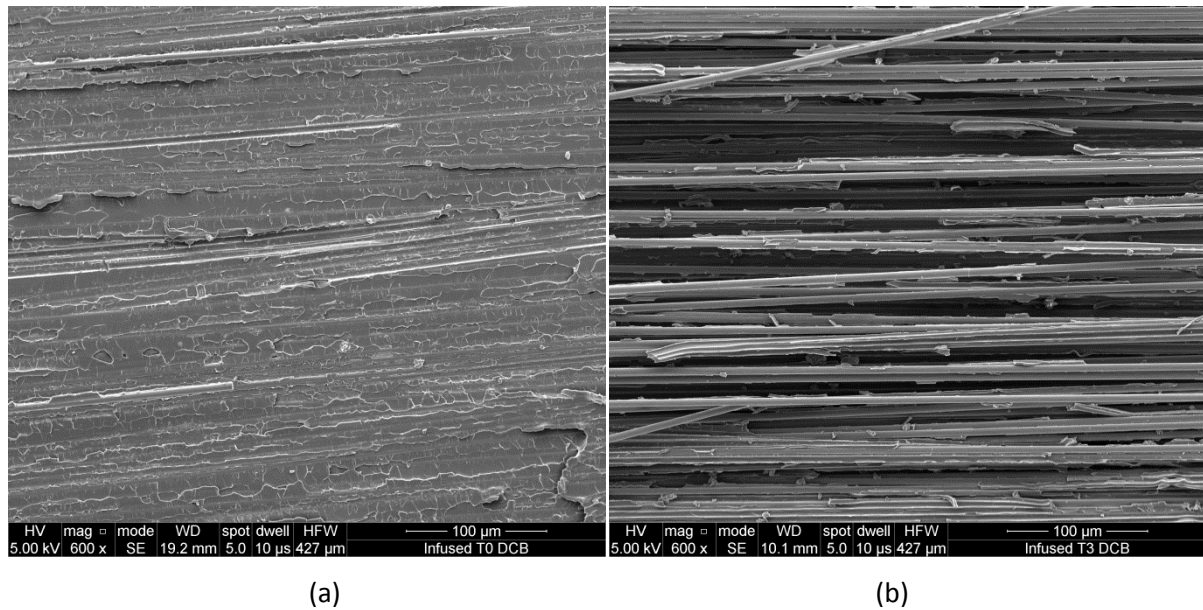


Figure 131: SEM observation of Infused material after crack propagation using DCB test, observations present a detail on the specimen fracture surface, (a) T0, (b) T3.

The Figure 131 (a) and (b) present more details for the two conditions of ageing (T0 and T3). It is clearly visible that before ageing, the crack propagates in the interply region. After sea water ageing the crack propagates within the carbon ply, suggesting that fibre/matrix adhesion has been strongly affected.

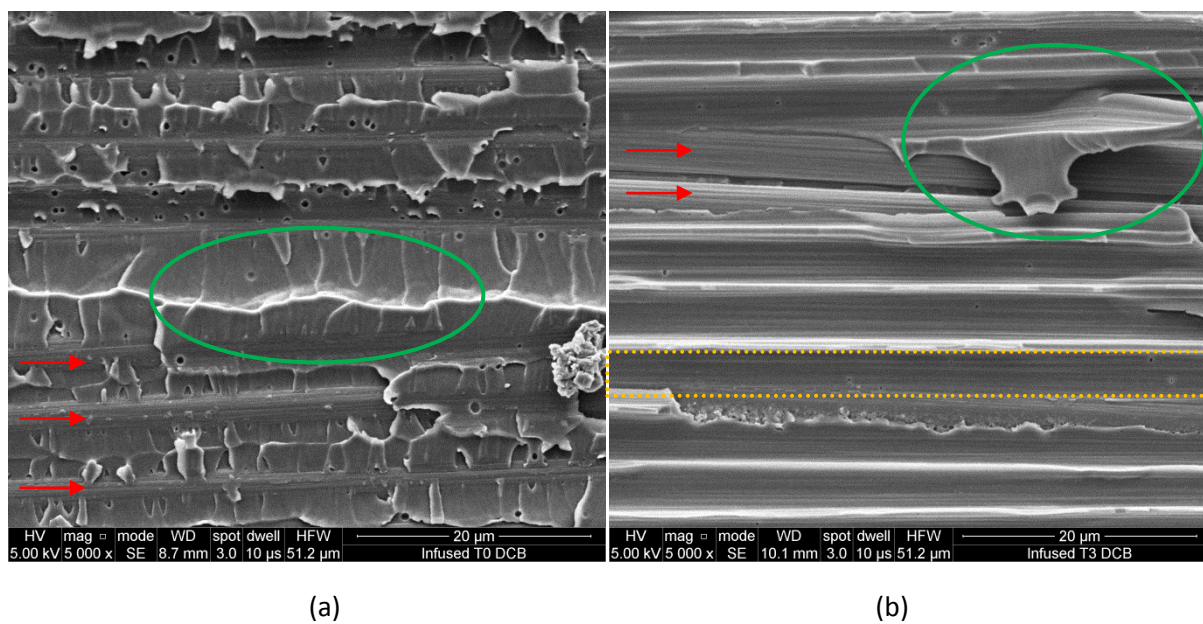


Figure 132: SEM observation of Infused material after crack propagation using DCB test, observations focus on carbon fibres ((a) T0 and (b) after saturation time plus 2 months).

Figure 132 (a) and (b) focuses on the carbon fibres. These observations were made in the same location as presented in Figure 131. Before ageing (a), it is possible to observe fibres strongly bonded to the matrix (the red arrows show some semi-apparent fibres). At T0 some ribs were created in the matrix between the carbon fibres (green oval). After sea water ageing adhesion was affected, as a consequence more fibre imprints are visible (orange dotted rectangle). After sea water ageing it is also possible to observe the formation of a ribbon of matrix between carbon fibres, suggesting that after ageing the matrix is more ductile.

4.4.2 RTM material

The same observations were made for the RTM materials. Figure 133 (a) and (b) presents an overview of specimens after DCB tests. In this case changes are not as clear as those presented for Infused material. Some differences could be noted (blue dotted squares), it seems that before ageing the crack was propagating in the matrix and after ageing cracks are still propagating in the matrix but carbon fibres are more apparent. Some detailed observations in these zones will be presented in the following figures.

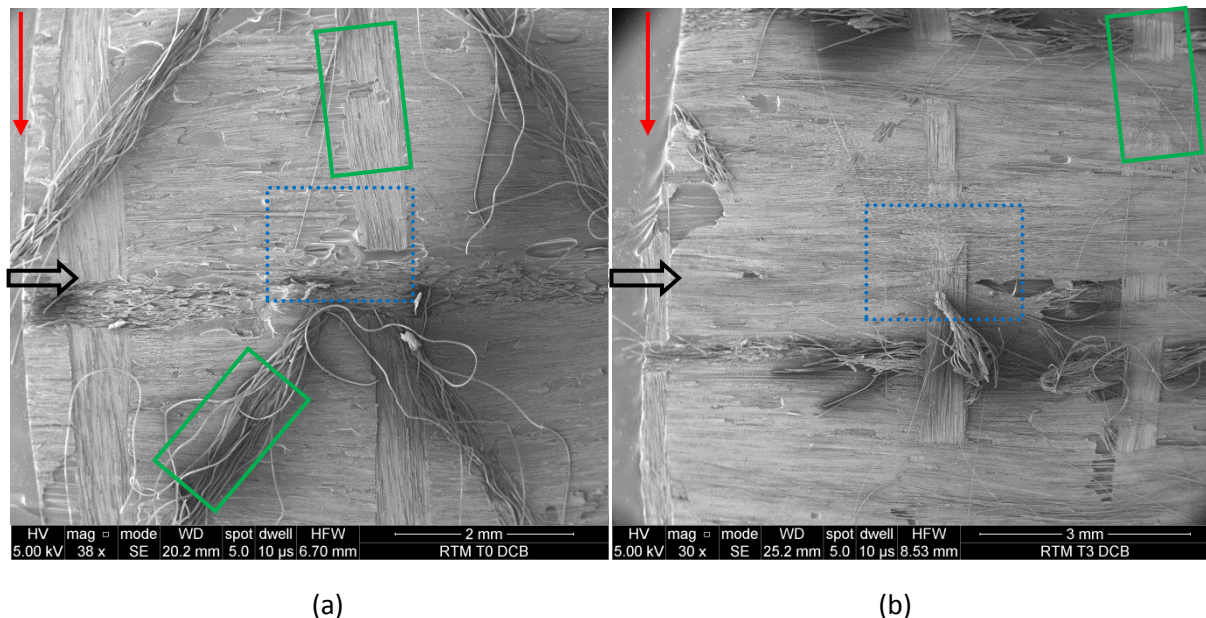


Figure 133: SEM observation of RTM material after crack propagation using DCB test, observations present a large view on the specimen fracture surface, arrows show the direction of the propagation.

At T0 polyester stitching is visible (V), and imprints of transverse glass fibres can be noted, see (green rectangles). At T3 the polyester stitching is no longer visible.

Figure 134 (a) and (b) presents details of the region presented in the previous figures. At this observation scale differences are more evident. As presented for the Infused material, after sea water ageing (b), crack seems to propagate within the carbon ply, and more carbon fibres are detached.

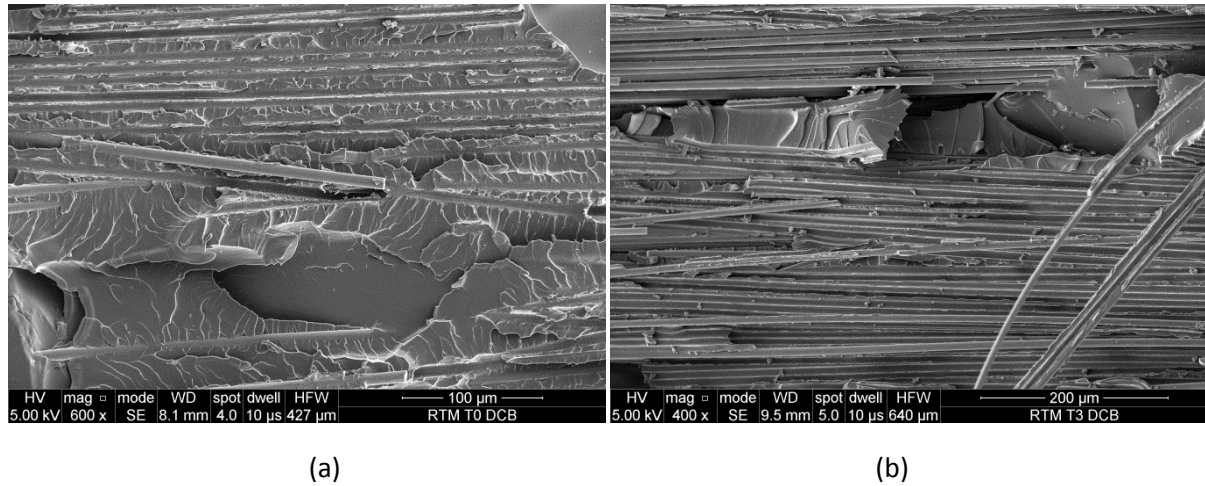


Figure 134: SEM observation of RTM material after crack propagation using DCB test, (a) T0 and (b) T3.

As shown in Figure 135 (a), before ageing, the same characteristic ribs appear in the matrix on RTM material (orange dotted rectangle, peel fracture). After sea water immersion, the fracture surfaces change, fibre imprints are visible, some fibres are visible but the surrounding matrix is detached (red rectangles). Moreover cusps initiations appear along fibres at after ageing.

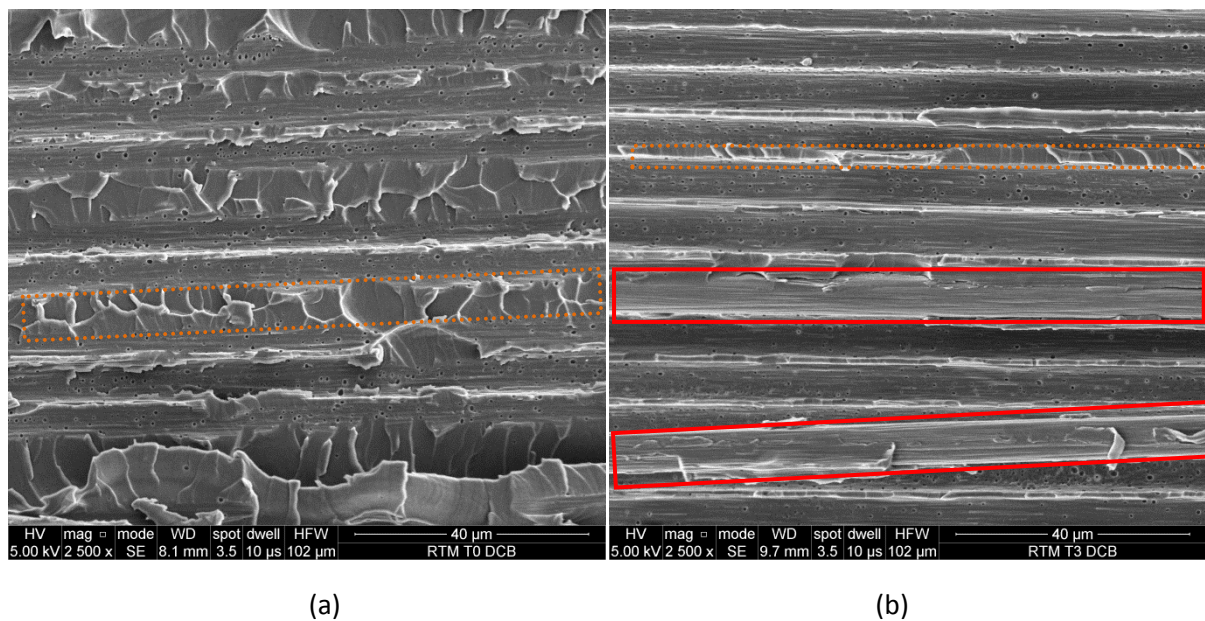


Figure 135: SEM observation of RTM material after crack propagation using DCB test, observations present a large view on the specimen fracture surface, arrows show the direction of the propagation. (a) T0, (b) T3.

4.4.3 Pre-preg

Finally, observations were made on the Pre-preg material, before and after sea water ageing. In Figure 136 (a) and (b) it is possible to observe that the crack propagates in the ply before sea water ageing. Then at T3, crack propagates between the plies, in the matrix rich (and nodules region).

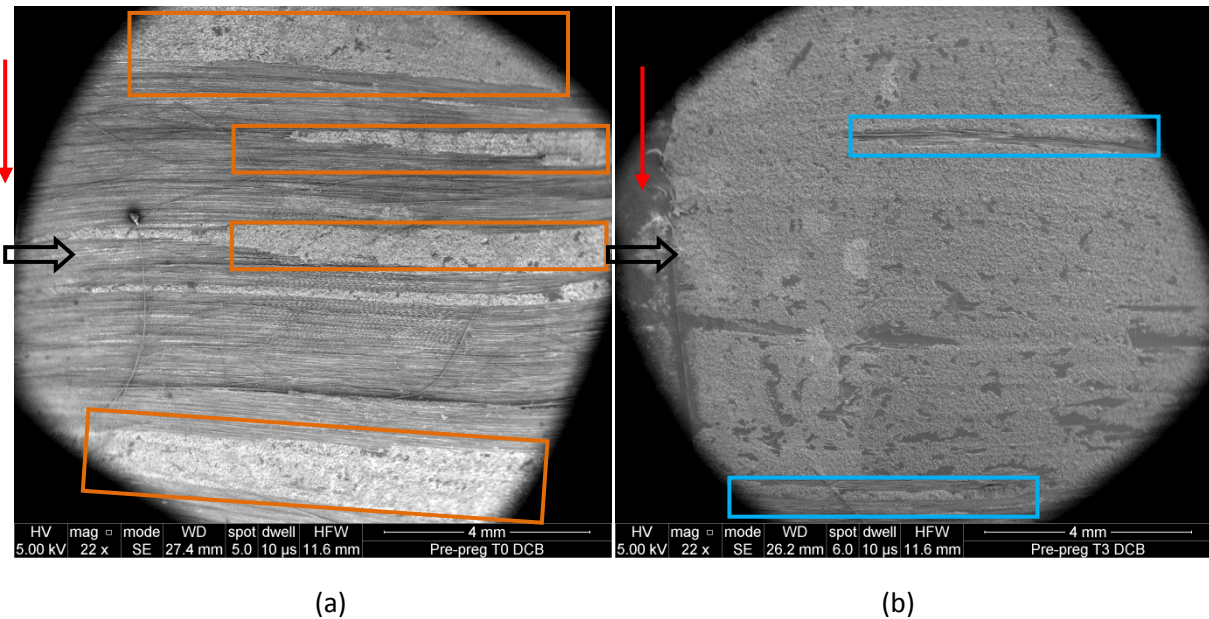


Figure 136: SEM observation of Pre-preg after crack propagation during DCB test, (a) T0, (b) T3.

A first hypothesis could be formulated. After ageing in water the nodules, which improve toughness in the dry state, weaken the interply toughness, which induces changes in the fracture surfaces. But the nodules may not be the only cause, a change in adhesion between matrix and nodules may also occur due to nodule swelling.

Figure 137 (a) and (b) allow the propagation of the crack before and after sea water ageing to be compared, in order to observe the propagation in interply and intraply region for both conditions of ageing. Before water absorption (a) fibres and matrix are well bonded. Then after ageing it seems that the interface between fibres and matrix has been weakened, and after sea water ageing most of the crack propagation occurs in the interply region.

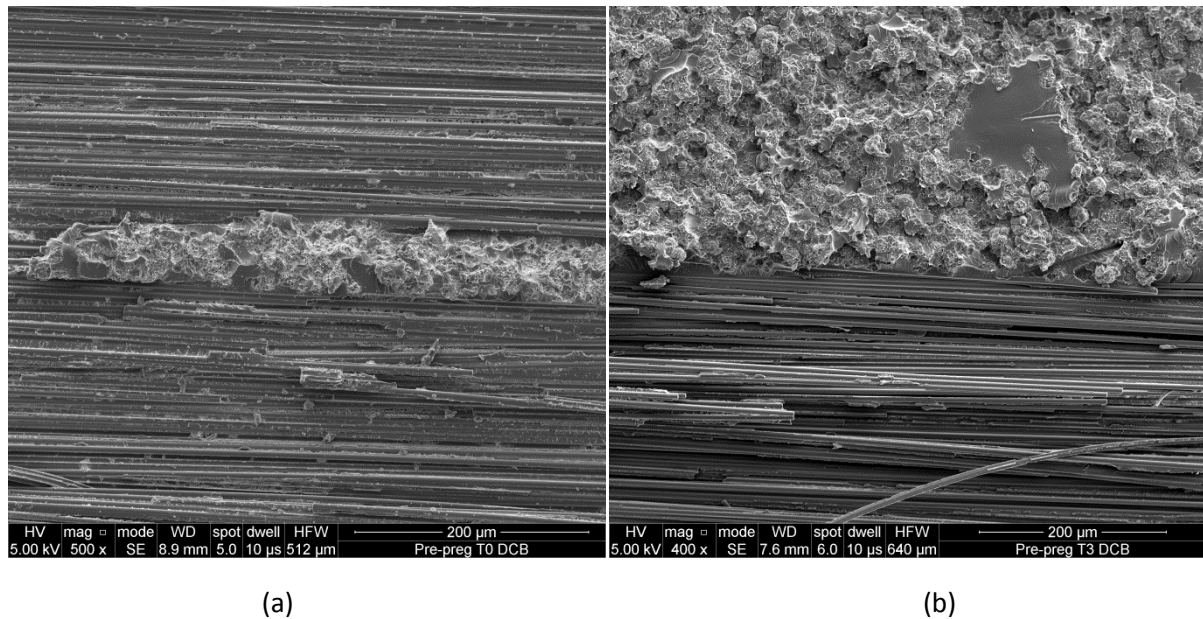


Figure 137: SEM observation of Pre-preg after crack propagation during DCB test, (a) T0, (b) T3.

Figure 138 shows the prepreg intraply region, where some fibres are detached and leave imprints. Before ageing, at the interface region between fibres and matrix some brittle failures appear. Then after ageing in water, it is possible to observe more deformation of the matrix, see Figure 138 (b). Failure of the matrix seems to be more ductile after ageing.

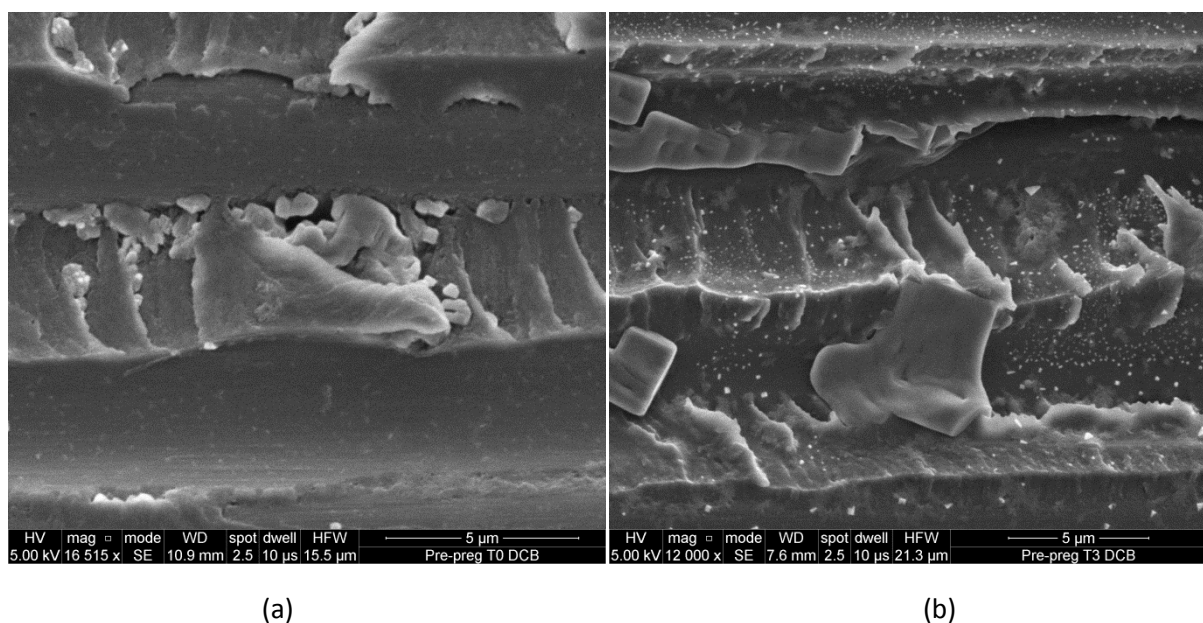


Figure 138: SEM observation of Pre-preg after crack propagation during DCB test. Observations are focused on fibre imprints, (a) T0, (b) T3.

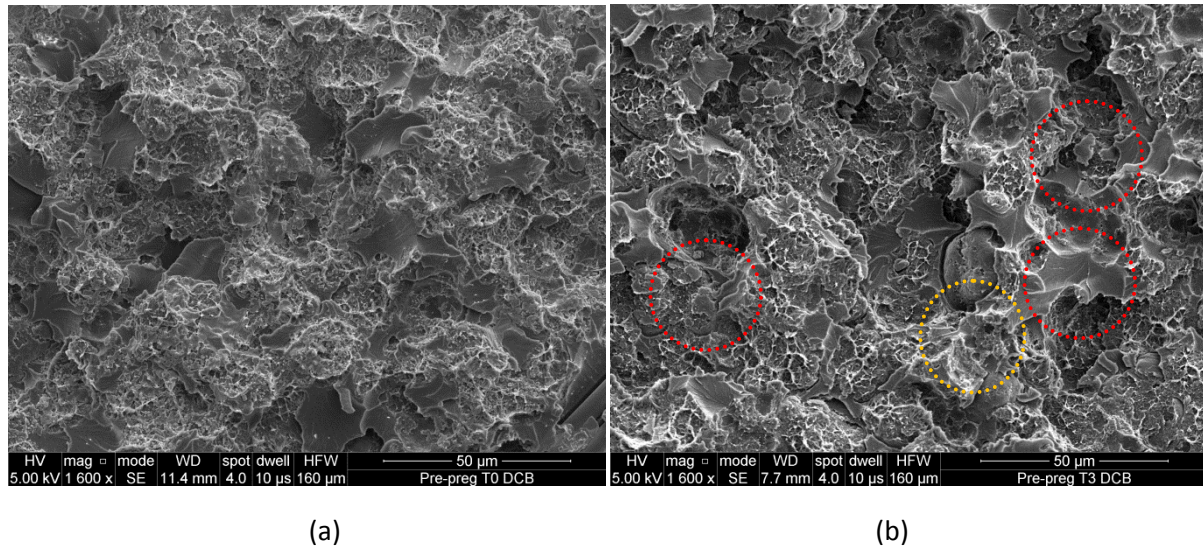


Figure 139: SEM observations of Pre-preg after crack propagation during DCB test, observations are focused on interply crack propagation, (a) T0, (b) T3.

Figure 139 (a) presents a detail of the interply region. Before ageing in this matrix rich region, thermoplastic nodules were well blended into the resin, suggesting a good adhesion between those two phases. After sea water ageing, the interfaces between matrix and nodules seem to be weakened. Debonding appears as presented in Figure 139 (b) (orange circle). Additionally it is possible to observe that some nodules are detached during crack propagation (red dotted circles). A focus on nodules before and after ageing is presented in the figures in Appendix 23 and Appendix 24.

These observations suggest that ageing in seawater affects toughness, but the G_{Ic} versus crack length plots do not show a significant change with ageing. One possibility is that there is indeed a change in toughness but the test analysis does not reflect it. This could occur if the propagation mechanism changes from single to multiple crack advance. The analysis assumption that energy goes into the creation of only two crack surfaces is thus no longer valid, as it was suggested previously in section 3.6. Additionally another hypothesis could be formulated in order to explain the apparent stability of G_{Ic} during sea water ageing. As shown in Figure 140, before sea water ageing crack propagates in the matrix, then after sea water ageing fibre/matrix interface is weakened. As a consequence fibres are less bonded to the matrix, so when cracks encounter fibres they propagate at the interface between fibre and matrix. This may explain why more fibres are visible on fracture surfaces after sea water ageing. However this new phenomenon does not require more energy because of the weakening of the interface, as a consequence the energy to propagate the crack is not modified.

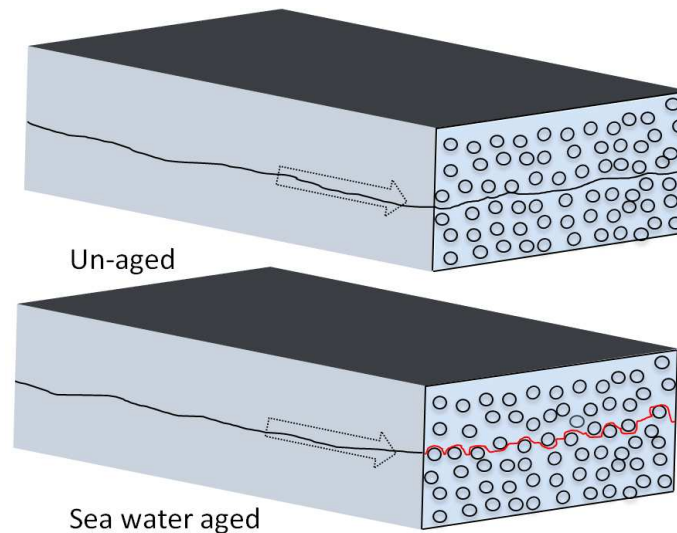


Figure 140: Illustration of crack propagation phenomena (mode I) in un-aged and aged states.

These observations on fracture surfaces before and after ageing, reveal some notable changes in the three materials of the study. Sea water induces modifications in fracture behaviour. It was highlighted that both matrix and fibre/matrix interface were weakened during immersion in water. As a consequence failure in the matrix is more ductile after immersion. The interface is clearly affected, causing more fibre pull out, and splitting during tension tests. Infused and RTM materials present similar fracture surfaces after ageing, specifically in the matrix. In the case of the Pre-preg, both matrix and interface are affected by ageing, but thermoplastic nodules are also degraded, inducing changes in the matrix between each ply. All those changes correspond to the property reductions observed in the mechanical testing section.

Tout au long de ces observations sur les faciès de rupture avant et après vieillissement, des changements notables ont été observés dans les trois matériaux de l'étude. L'agression de l'eau de mer induit des modifications dans le comportement à la rupture des matériaux. Il a été mis en évidence que la matrice et l'interface/fibre matrice ont été affaiblis après immersion en eau de mer. En conséquence la rupture dans la résine est plus ductile après immersion. L'interface est clairement endommagée, induisant plus de déchaussement et de glissement de fibres durant les essais en traction. L'Infusé et le RTM présentent des faciès de ruptures similaires après vieillissement, surtout dans la résine. Dans le cas du Pre-preg, la matrice et l'interface sont affectés par le vieillissement. Mais les nodules de thermoplastiques sont aussi dégradés, induisant des changes dans la matrice entre chaque pli. Tous ces changements sont en corrélation avec la réduction des propriétés observées durant la partie sur les essais mécaniques.

5. Influence of manufacturing process

Throughout this chapter sea water effects on the three composite materials were characterised. Changes in mechanical and physico-chemical properties were observed. The manufacturing process may clearly have an influence on the degradation of the material properties and on the time to degrade them. The comparison between materials of the study is not easy to perform, because they are not composed of the same constituents. Thus it is difficult to extract the real influence of the process because too many parameters play a role. For instance, the nature of the epoxy resin, fibre content, stitching and its nature, porosity levels, presence of fillers (nodules, epoxy powder), curing. To characterise the direct influence of the process on the ageing process and its consequences, it would be necessary to use the same components to manufacture composite samples. So in this section only a partial comparison between materials will be made, treating them each as a complete system which could be used in a tidal turbine blade. First, the sea water diffusion characteristics of each composite will be compared. Then, the changes in normalised mechanical properties during sea water ageing will be compared, in order to rank them in terms of resistance to sea water ageing.

5.1 Influence of manufacturing process on the kinetic of diffusion

The diffusion processes were presented previously for the different materials of the study. In order to compare the influence of the manufacturing process, the water uptake during immersion at 60°C is presented in Figure 141 for three UD composites manufactured using infusion, pre-preg autoclave and RTM processes. The RTM picks up significantly more water at equilibrium (~1.4% for RTM, ~0.8 for Infused and ~0.9 for Pre-preg).

A reasonable comparison can be made between RTM and Infused materials, because they were manufactured with the same resin. These two materials do not have exactly the same volume fraction of fibres (50% for RTM and 54% for Infused) but this difference is not sufficient to explain the large difference in weight gain.

However, the RTM material has a higher amount of porosity, which may explain these differences. Also, if we compare samples of QI and UD laminates both manufactured with the same RTM process, Figure 142, the UD ($V_f = 50\%$), has a higher weight gain than the QI ($V_f = 48\%$). The UD material has 0.84% ($\pm 0.12\%$) porosity and QI has 0.38% ($\pm 0.17\%$) porosity. Thus the porosity level

induced by the RTM process seems to have an important influence on the water content in these composite materials, as shown previously elsewhere [80],[81].

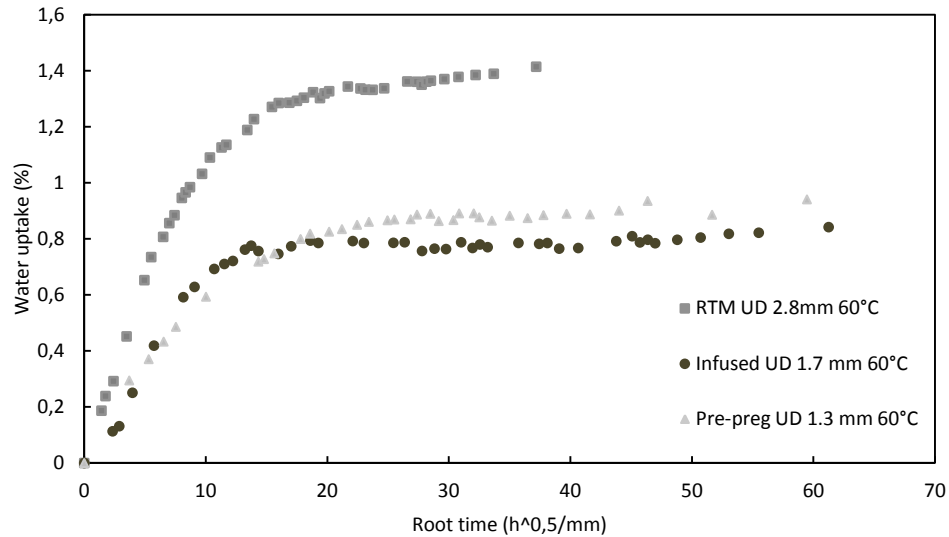


Figure 141: Weight gain as a function of the square root of time normalised by the thickness for the three types of materials used in this study.

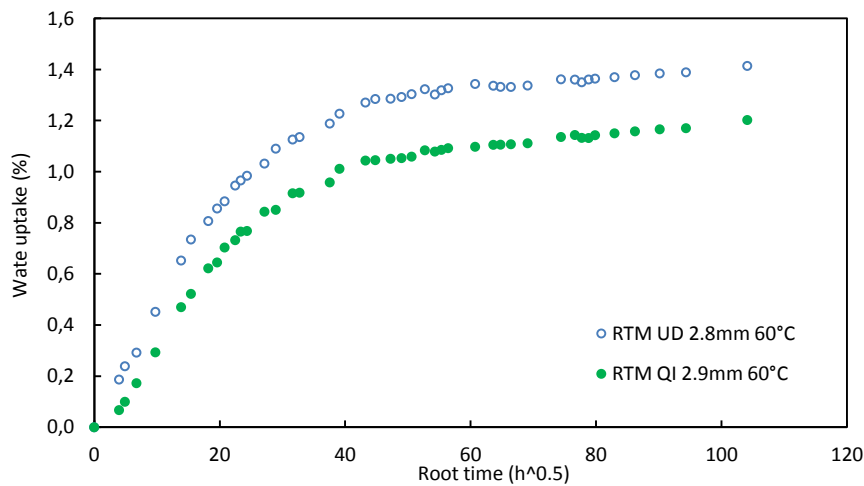


Figure 142: Comparison of weight gains for RTM UD and QI samples, immersed in sea water at 60°C. The water content is plotted as a function of the square root of time.

The Infused and Pre-preg materials show similar diffusion curves in spite of the different natures of their epoxy resin and the presence of thermoplastic nodules in the Pre-preg materials, which have high affinity with water (6-10% of maximum water uptake). Indeed these polyamide nodules occupy 13% of the matrix volume. It is interesting to observe that when these diffusion curves are normalized with respect to maximum water content, Figure 143, there is a good

superposition. The saturation plateau is attained after the same average normalised time. Only small differences between the materials appear after long immersion in seawater.

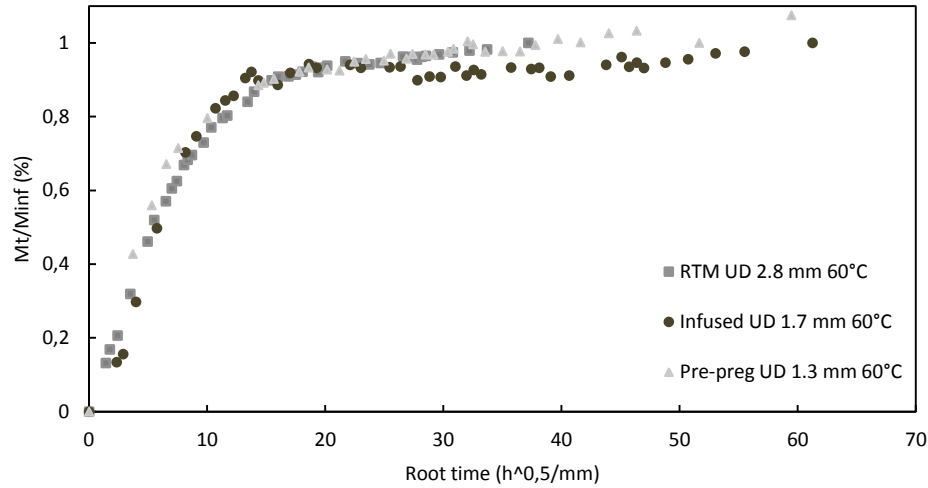


Figure 143: Evolution of the water content normalised by the maximum content of water as a function of the square root time normalised by the thickness for the three types of materials used in this study.

Based on these results presented on the previous diffusion curves and in the Table 22, it is not unreasonable to conclude that manufacturing process does not have a strong effect on the diffusion for these materials, at least on a global scale, but the manufacturing process may affect the influence of this water on the material behaviour. The diffusion results obtained are in the typical range for carbon epoxy materials, as presented in various other studies [36], [182],[196].

Ageing temperature	Materials experimental diffusion coefficient D_{exp} ($E-14 \text{ m}^2.s^{-1}$)					
	Epoxy resin 2.55 mm	Infused UD 1.7mm	RTM UD 2.8 mm	RTM QI 2.9 mm	RTM UD 5.2 mm	Pre-preg 1.29 mm
25°C	16.3	5.6	8.8*	8.4*	**	4.28
40°C	32.2	9.5	14.8*	14.6*	**	11.2
60°C	135	48.8	52.9	49.5	65.6	32.6
80°C	**	**	257.9	213.7	**	73.1

* For these temperatures or thicknesses material is not clearly saturated.

** These conditions have been not experimentally investigated.

Table 22: Sea water diffusion coefficients determined experimentally for the different materials of the study. These coefficients have not been corrected with an edge coefficient of correction.

5.2 Effect of manufacturing process on properties after water ageing

As previously noted, it is difficult to identify the influence of the manufacturing process on the long term behaviour in a marine environment. In order to compare the resistance of the materials to ageing, the changes in mechanical properties have been normalised by the properties before ageing, in particular tensile strengths, shear strength and modulus, and Interlaminar shear strength on UD and QI materials.

5.2.1 Tensile longitudinal and transverse strength

The following figures compare the changes in longitudinal (Figure 144) and transverse (Figure 145) strengths during sea water ageing.

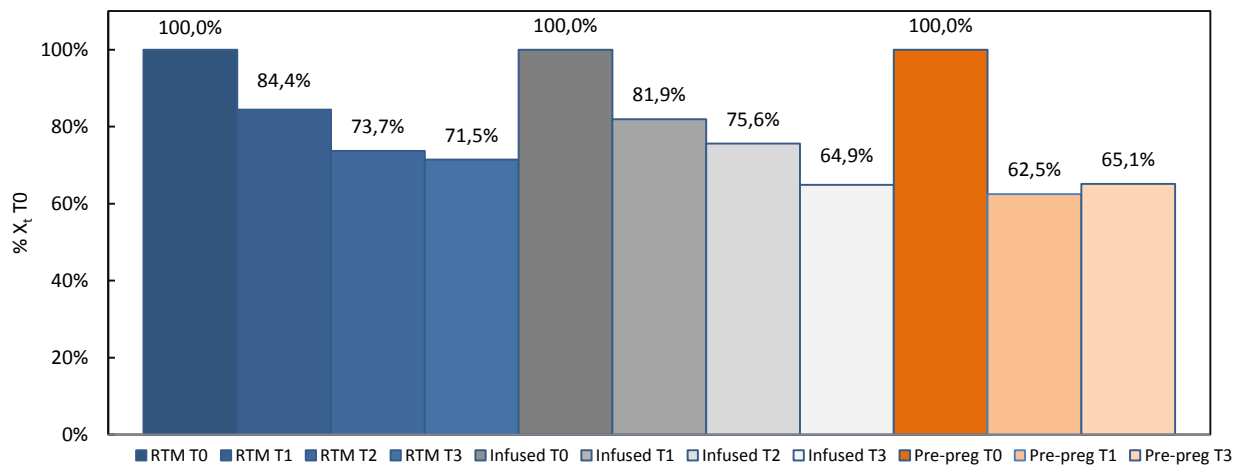
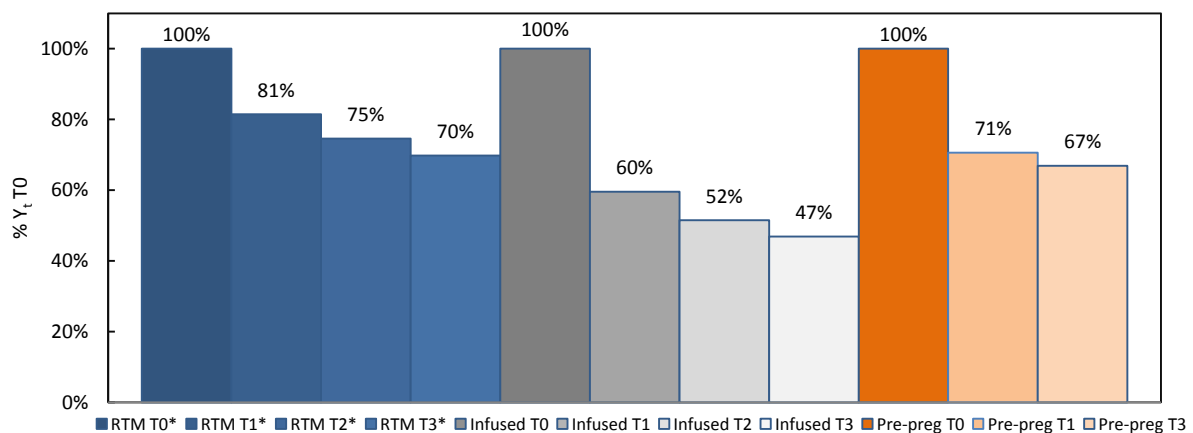


Figure 144: Evolution of normalised longitudinal tensile strength X_L , during sea water ageing for the three materials.



*In this case RTM material was tested between un-aged state and saturation time T1 does not correspond to the saturation. T1=49 days, T2=79 days T3=106 days. Time to saturate this material is approximately 90 days.

Figure 145: Evolution of normalised transverse strength Y_T , during sea water ageing for the three materials.

Concerning the evolution of the longitudinal strength during sea water ageing, all three materials are subject to similar mean drops of around 30%. These results may appear quite surprising, there is a common idea that longitudinal strength is dominated by fibres and as carbon fibres are not sensitive to water the strength should not be either. However, the stress transfer between fibres is controlled by the matrix and fibre/matrix interfaces and these are sensitive to water, even when the composite is based on prepreg and cured at high temperature in an autoclave.

It is also important to underline that while large drops in properties are noted at saturation the properties of RTM and Infused materials continue to change (T2, T3). This suggests that it is not sufficient simply to take saturated property values for long term strength predictions.

After saturation, RTM and Pre-preg material are subject to approximately the same transverse strength reduction, again around 30%, while the infused material seems to be more affected by sea water ageing in this case.

5.2.2 Shear strengths and modulus

In-plane shear strengths and modulus have been characterized on Infused and Pre-preg materials. As presented in Figure 146 tensile shear strength loss for both materials is quite similar, around 25%. For shear modulus, this property remains constant for the Pre-preg while the Infused shear modulus drops by 30%.

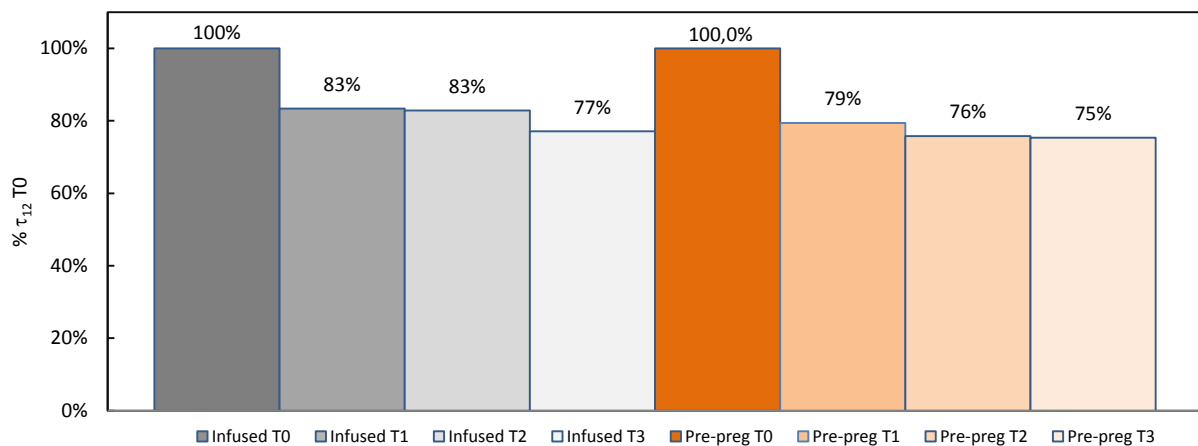


Figure 146: Evolution of normalised in-plane shear strength τ_{12} , during sea water ageing for Infused and Pre-preg materials.

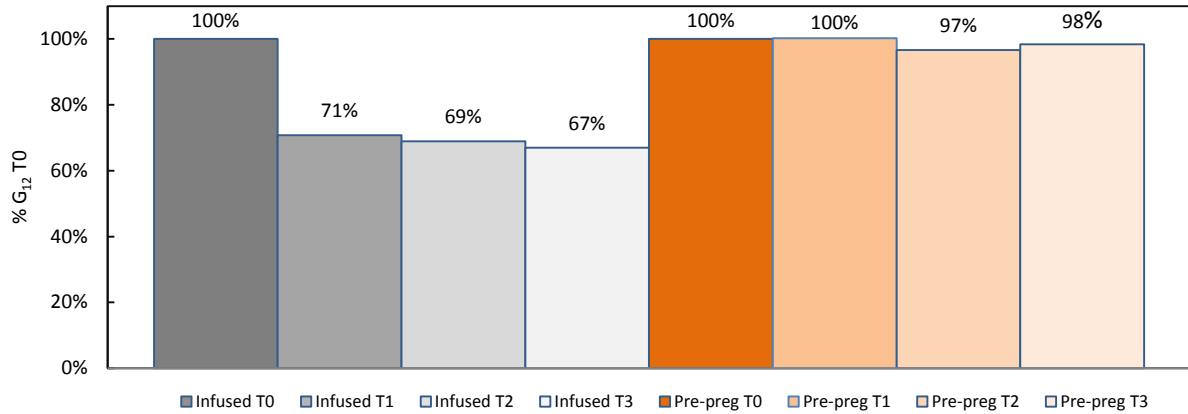


Figure 147: Evolution of normalised tensile shear modulus G_{12} , during sea water ageing times for Infused and Pre-preg materials.

5.2.3 ILSS shear strength for UD and QI materials

The normalized ILSS strength was studied for each material during sea water ageing. Figure 148 compares these changes for UD materials and Figure 149 for QI RTM and Pre-preg.

In the UD case the RTM material presents the lowest reduction of this properties during sea water ageing. It is possible that stitching influences ILSS strength, Infused and RTM do not use the same stitching patterns (density, diameter, type of fibres), while the Pre-preg has no stitching. A good review of the effect of stitching on composite mechanical properties has been presented by Mouritz et al. in [197]. This shows that stitching is not inert, particularly with respect to out-of-plane loading.

For the ILSS strength of QI laminates, the same reduction occurs as presented for the UD RTM, Figure 149. But for the Pre-preg QI, the drop of the ILSS strength seems to be less important. It is difficult to explain this difference between UD and QI Pre-preg. The Pre-preg material is made up three different phases, differences in interlaminar zone geometry and nodule distributions are possible.

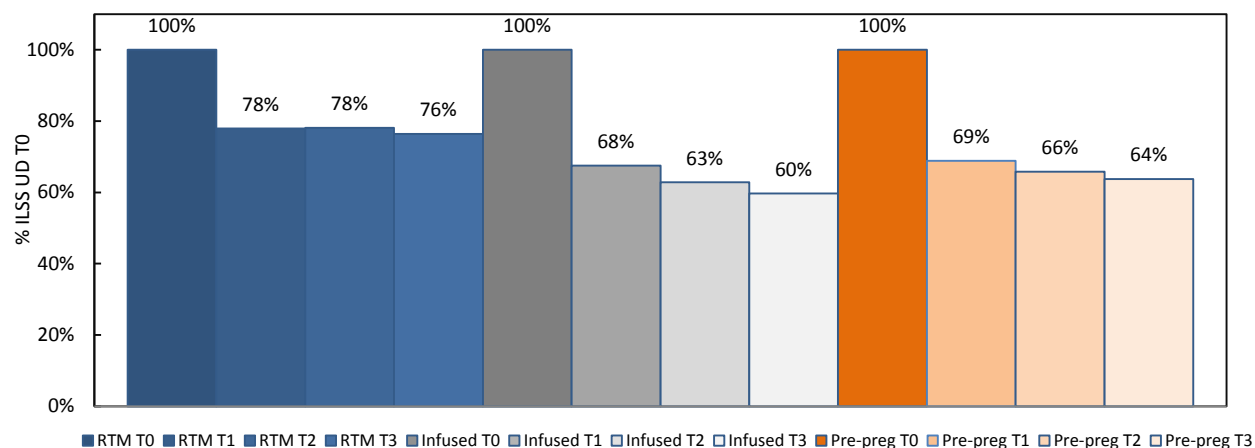


Figure 148: Evolution of normalised ILSS strength, during sea water ageing times for the three UD materials.

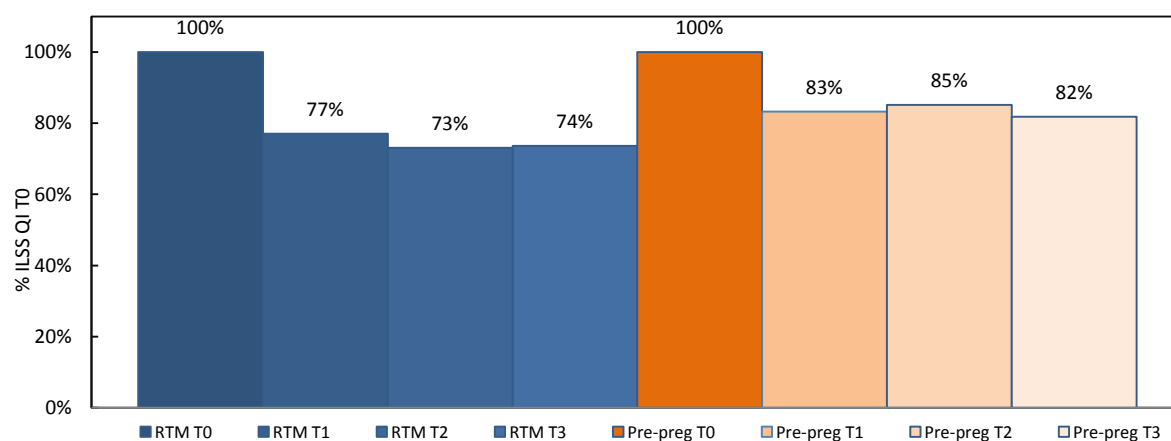


Figure 149: Evolution of normalised ILSS strength, during sea water ageing times for the RTM and Pre-preg QI materials.

5.3 A first conclusion on sea water ageing in composites for tidal turbine

Throughout this chapter three candidate materials for tidal turbine blade applications have been studied. The water diffusion behaviour has been studied for different stacking sequences and at different water temperatures. It has been shown that thickness and orientation do not influence kinetics of diffusion significantly. This result is important regarding the final application of the blade as it allows coupon data to be used in modelling the structure. However, time and temperature are key factors in the ageing process. Accelerated ageing by raising water temperature has been applied taking into account the T_g of each material, in order to age specimens for mechanical characterization.

While properties in the fibre direction are hardly affected when samples are saturated with sea water there is a strong influence on longitudinal strength which must be accounted for in tidal turbine blade design. Moreover transverse composite strength was also affected by water ingress. Off-axis properties are all affected, though this is less surprising given the resin property dependence on water. Damage initiation is also a function of ageing, which causes a shift of the threshold of damage to lower loads. Considering that the carbon fibres are not affected by the sea water, it seems reasonable to conclude that most of the property degradation observed is related to the loss of matrix properties, with some weakening of the fibre/matrix interface at longer times.

However, the present study has also revealed the limits of the accelerated ageing method based on increasing water temperature. For the Pre-preg composite this approach is valid, and allows long term properties to be estimated. For the two composites based on the lower T_g resin this approach is questionable, as excessively high temperature (60°C) introduces unrepresentative ageing mechanisms such as oxidation. While extrapolation of mechanical test data to longer times may then be conservative, these data cannot be used to make quantitative predictions of property changes for lower temperatures. To be more representative of Infused and RTM composites sea water ageing, the acceleration of ageing procedure must be revised. As a consequence it is necessary to age these materials at 40°C (or less). However at this temperature the accelerating factor is much lower. Reducing ageing temperature to 40°C, requires 4 times longer to reach saturation. For instance to aged the 2.8mm UD RTM material at 60°C it requires 100 days, but at 40°C it will require 400 days. This time difference is not negligible for Industrial R&D studies. In order to reduce this time the sample thickness could be reduced, if materials parameters such as fibre content and porosity remain the same. Figure 150 shows the influence of specimen thickness on ageing time. This figure

illustrates the difference of time to saturate the composite in water as a function of thickness. Another option is to reduce temperature and thickness.

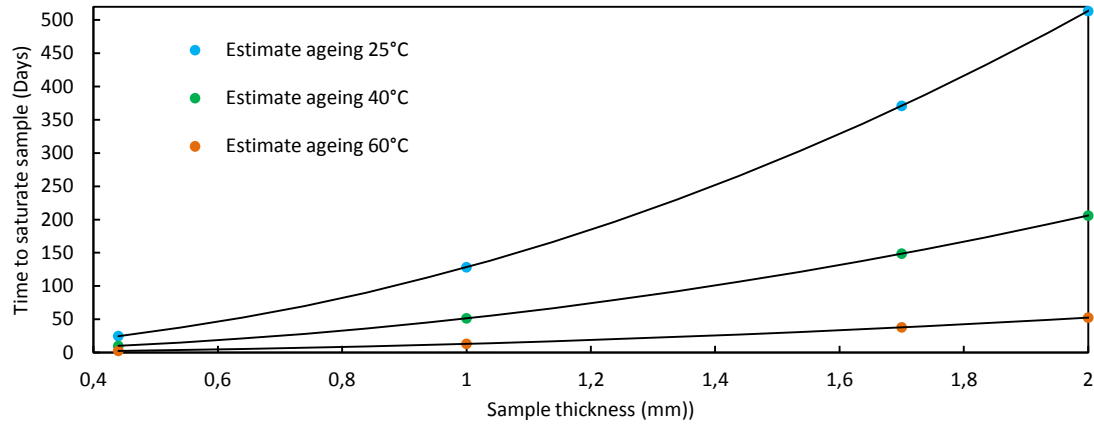


Figure 150: Time needed to saturate composites sample in water as a function of ageing temperature and thickness.

Additionally others factors could be considered to accelerate ageing, for instance the loading, but this requires a very detailed knowledge of coupling effects.

In order to predict the water entry in composites at different temperature and then predict the evolution of material mechanical possible it seems important to be able to model the anisotropic diffusion in composite laminates. As a consequence the next chapter will investigate this modelling.

Une première conclusion à propos du vieillissement en eau de mer des composites pour hydroliennes

Au cours de ce chapitre trois matériaux candidats pour les applications pales d'hydroliennes ont été étudiées. Les processus de diffusion de ces trois matériaux carbone/époxy ont été étudiés pour différentes séquences d'empilement de matériaux et à différentes températures d'eau. Il a été montré pour tous les matériaux que l'épaisseur et l'orientation n'influencent pas la cinétique de diffusion. Ce premier élément est important vis-à-vis de l'application finale. Cependant le temps et la température sont des facteurs clés du processus de vieillissement. Les conditions de vieillissement accéléré ont été choisies en prenant le compte la T_g de chaque matériau considéré. Ainsi la procédure de vieillissement en eau de mer a été utilisée pour vieillir différents échantillons pour le plan d'essais de caractérisation.

En suivant cette procédure de vieillissement accéléré, des dégradations ont été observées et mesurées dans les différents matériaux de l'étude. Pendant que les propriétés dans la direction des fibres sont durement affectées quand les spécimens sont saturés en eau de mer il y a une influence importante sur la résistance longitudinale qui doit être prise en compte pour la conception de pales d'hydroliennes. De plus la résistance transverse des composites a été également affectée par la prise en eau. Les propriétés hors axe sont toutes affectées bien que cela soit moins surprenant étant donné la dépendance à l'eau des propriétés de la résine. La propagation de l'endommagement est aussi une fonction du vieillissement, l'eau de mer induit un décalage du seuil d'endommagement vers des chargements plus faibles. En considérant que les fibres de carbone ne sont pas affectées par le vieillissement en eau de mer, il semble raisonnable de conclure que la plupart des dégradations observées sont principalement dues aux pertes de propriétés de la matrice et à l'affaiblissement de l'interface fibre/matrice.

Toutefois la présente étude a permis d'identifier les limites de la méthode de vieillissement accéléré basée sur l'augmentation de la température de l'eau. Pour le composite Pre-preg cette approche est valide et permet d'estimer ses propriétés au long terme. Pour les deux composites fabriqués avec une résine dont la T_g est plus basse, cette approche est questionnable, car une température excessivement importante (60°C) induit des mécanismes de vieillissement non représentatifs tel que l'oxydation. Alors que l'extrapolation de données d'essais mécaniques pour des durées plus longues peut être conservatrice, ces données ne peuvent être utilisées pour faire des prédictions quantitatives des changements de propriétés. Pour être plus représentative pour le vieillissement en eau de mer du RTM et de l'Infusé, l'accélération du vieillissement doit être révisée.

En conséquence il est nécessaire de vieillir ces matériaux à 40°C (ou moins). Cependant à cette température le facteur temps n'est plus le même. En réduisant la température à 40°C, le temps pour atteindre le plateau de saturation est multiplié par 4. Par exemple pour vieillir l'UD RTM à 60°C, 100 jours sont nécessaires, mais à 40°C 400 jours seront requis. Cette différence de temps n'est pas négligeable pour des études industrielles de recherche et développement. Dans le but de réduire ce temps, l'épaisseur des matériaux peut être réduite, si les paramètres tels que le taux de fibres et le taux de porosités restent les mêmes. De plus d'autres facteurs peuvent être considérés pour accélérer le vieillissement, par exemple le chargement. La Figure 150 présente l'influence de l'épaisseur sur le temps de vieillissement. Cette figure illustre également les différences en termes de temps pour saturer le composite eau, en fonction de l'épaisseur et de la température. Une autre option pour réduire le temps vieillissement consisterait à réduire l'épaisseur des éprouvettes.

Dans le but de prédire l'entrée d'eau dans les composites à différentes températures et ainsi prédire l'évolution possible des propriétés mécaniques dans ces composites, il semble important d'être capable de modéliser la diffusion anisotrope dans les matériaux composites. En conséquence le chapitre suivant va investiguer ces modélisations.

Chapter IV. **Multi-physics modelling of diffusion/damage**

In the preceding Chapter, the long term behaviour of different carbon/epoxy composites has been studied using accelerated ageing tests. A significant reduction in composite strengths has been observed after saturation of the material in seawater. For longer immersions only small further changes in these properties occur. No significant changes have been observed for moduli nor for composite propagation toughness. Changes in properties are initially due to matrix plasticisation, which increases, followed by reductions due to fibre/matrix interface changes. It is therefore important to follow the water ingress into composite materials, in order to develop predictive models of property changes through the laminate as a function of diffusion kinetics.

In this chapter a first approach to modelling water diffusion in these composites has been developed. The aim of the model is to be simple but to account for the anisotropic nature of these materials. Then the model has been applied to a tidal turbine blade structure in order to predict long water diffusion under more realistic environmental conditions. In the second part of this chapter the damage model presented in Chapter II has been used in order to predict the propagation of damage in aged carbon/epoxy laminates. This modelling is based on the properties determined after sea water ageing on those materials described in Chapter III. As damage in composite materials involves the development of cracks within certain plies, it is necessary to take into account the effect of damage on the diffusion process. The crack development can create preferential pathways for water diffusion. As a consequence the diffusion model previously developed has been used to make a first estimate of diffusion in damaged composites. Some preliminary coupled test results are also described.

Chapitre IV. Modélisations multi-physiques de la diffusion et de l'endommagement

Dans la partie précédente, le comportement au long terme de différents composites carbone/époxy a été étudié, en utilisant des essais de vieillissement accéléré. Une réduction significative des résistances des composites a été observée, après saturation en eau de mer. Pour des temps d'immersion plus long, peu de nouveaux changements de propriétés apparaissent. Peu de changement ont été constatés tant sur les modules que sur la ténacité des composites. Ces changements de propriétés sont initialement dus à la plastification de la matrice, qui augmente les déformations à la rupture, suivies par des baisses dues aux changements à l'interface fibre/matrice. Il est donc important de suivre la reprise en eau dans les matériaux composites, dans le but de développer des modèles prédictifs des changements de propriétés au travers des stratifiés en fonction de leur cinétique de diffusion.

Le sujet de ce chapitre, est de caractériser et modéliser les effets de la diffusion d'eau de mer sur les composites carbone/époxy pour applications pales d'hydroliennes. Le vieillissement en eau de mer affecte les composites, dû à la diffusion d'eau dans leurs structures. Cette prise en eau est principalement responsable des mécanismes conduisant à la dégradation des propriétés des composites. En conséquence dans ce chapitre une première approche de modélisation de la diffusion d'eau dans les composites a été développée. Le principe de ce modèle est d'être simple, mais aussi de prendre en compte la nature anisotrope de ces matériaux. Ensuite le modèle a été appliqué sur une structure de pale d'hydrolienne, dans le but de prédire la diffusion d'eau au long terme dans des conditions environnementales plus réalistes. Dans la deuxième partie de ce chapitre, le modèle d'endommagement présenté dans le Chapitre II, a été utilisé dans le but de prédire la propagation de l'endommagement dans les stratifiés carbone/époxy vieillis. Cette modélisation fut possible grâce aux propriétés déterminées après le vieillissement en eau de mer de ces matériaux. Comme l'endommagement induit dans les composites le développement de fissures dans certains plis, il est nécessaire de prendre en compte l'effet de l'endommagement sur le processus de diffusion. Le développement de fissures peut créer des chemins préférentiels pour la diffusion de l'eau. En conséquence le modèle de diffusion précédemment développé a été utilisé pour réaliser de premières estimations de la diffusion dans un composite endommagé.

Table of contents

Chapter IV. Multi-physics modelling of diffusion/damage	176
1. Water diffusion modelling in composites	179
1.1 Model presentation	179
1.2 Identification of model parameters	182
1.3 Sensitivity study of the model.....	185
1.3.1 Influence of mesh size on diffusion model.....	186
1.3.2 Influence of fibres content on diffusion model.....	187
1.4 Validation and optimisation of the model	188
1.4.1 A first comparison between FE calculation and experimental results	188
1.4.2 Investigation of fibre arrangement	189
1.4.3 Modelling diffusion on Infused and RTM materials at different temperature.....	193
1.4.4 Prediction of sea water diffusion on Infused material for lower temperature	195
1.5 Application to a tidal turbine blade	197
2. Modelling of damage after sea water ageing.....	201
2.1 Model key elements after sea water ageing.....	201
2.2 Comparison between modelling and experimental results	202
3. Modelling of damage/diffusion coupling.....	204
3.1 Modelling of damage/diffusion coupling.....	204
3.2 First experimental approach on damage/diffusion coupling.....	207
3.2.1 Experimental procedure.....	207
3.2.2 First results and additional investigations.....	209

1. Water diffusion modelling in composites

In the previous chapter sea water diffusion and its effects in composites and in an unreinforced epoxy resin were investigated. It has been shown that diffusion is a complex process and that water ingress can result in reduction of material properties, particularly strengths. However, the studied epoxy resin water diffusion process was certainly affected by other mechanisms such as oxidation, leading to an anomalous diffusion process. RTM, Infused and the epoxy resin diffusion have shown an important dependence on temperature. Nevertheless, sea water diffusion processes for all three composites were close to a Fickian diffusion form, until reaching their saturation plateau. In the following chapter we will consider diffusion in these materials to be purely Fickian to a first approximation. For the epoxy resin the water diffusion phenomenon will also be assimilated to a Fickian diffusion (more details about this choice will be given in the following sections).

However, these experimental water uptake measurements reflect global diffusion properties. To account for the anisotropic nature of composite materials, a diffusion model based on a finite element analysis using Abaqus™ was developed, in order to determine diffusion coefficients in the three material directions. The objectives of this model are to be simple to use and to be applicable to large structures such as tidal turbine blades. The diffusion model has been compared with the experimental diffusion on composites in the transverse direction to fibres. Thanks to the model it is possible to predict diffusion of water along the fibres. Finally, first investigations have been performed to predict the effect of composite damage on the diffusion process. The prediction of the rate of water entry in composites is essential in order to be able to estimate changes in material properties [198].

1.1 Model presentation

Many diffusion models have been developed in the past and, as presented in section 1.3 of Chapter III, the first models of water diffusion drew their inspiration from heat transfer laws [176],[199]. Numerical models have been developed previously in order to estimate composite material diffusivity parameters in parallel and perpendicular directions to fibres [200],[201],[202]. A three-dimensional solution was proposed in order to predict diffusion in composites using a numerical approach based on Fickian law [203]. More recently some work was done in order to develop diffusion models using commercial finite element (FE) software [204]. In the last few years,

various FE diffusion models were implemented using Abaqus™ software, in order to develop three-dimensional water modelling in composites and polymers,[205],[206].

It has been previously shown by Shen and Springer [176], that it is possible to define diffusion parameters for unidirectional composites. The diffusivity D_x is the water diffusion coefficient for a composite material in the direction normal to the surface. For composite materials reinforced by fibres the coefficients of diffusion D_x , D_y and D_z can be determined using three parameters:

- The Diffusion coefficient of the resin D_r ,
- The Diffusion coefficient of the fibres D_f ,
- The volume fraction of fibres V_f ,

In the case of an unidirectional material, it is assumed that $D_x = D_y = D_{\perp}$, which are the diffusion coefficients transverse to the fibres, and $D_z (= D_{\parallel})$ is the coefficient along the fibres

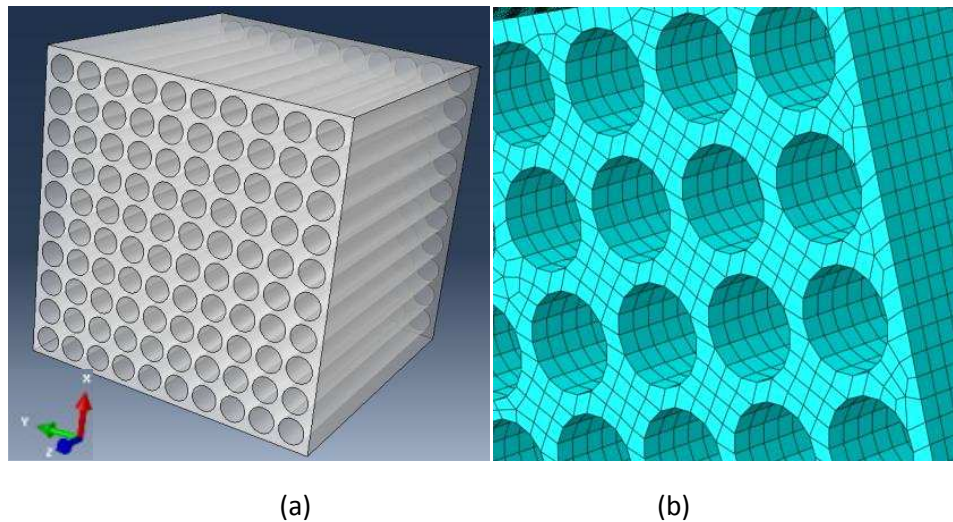


Figure 151: (a) Representation of the 3D model using for diffusion in Abaqus™ and (b) the associated mesh.

Using Abaqus™ and entering the water diffusion coefficient, density, specific heat of the matrix and the composite fibre fraction, it is possible to determine for an UD laminate the diffusion through the thickness and in the fibre direction. In the specific case of carbon/epoxy we will consider that carbon fibres do not participate in water diffusion.

To complete these calculations an analogy was made between water diffusion and heat transfer. Then this analogy allows the following Eq.53 to be established, between the heat diffusivity

K_x and water diffusion coefficient, where ρ is the density, C is the specific heat of the considered material.

$$K_x = \rho \cdot C \cdot D_x \quad \text{Eq. 53}$$

Two steps were necessary for modelling diffusion: The first one with an increment size of 50 seconds from 2000 to 4000 seconds (depending on the temperature of diffusion) and the second one a larger step representing the saturation plateau with a time period of 30000 to 90000 seconds with increments of 1000 seconds. The first step is very important specifically to determine the transition between the linear part of the diffusion curve and the plateau. These diffusion parameters and time condition were applied to a specific geometry representing an UD composite.

In this 3D model an elementary geometry can be defined using composite parameters, volume fraction of fibres and diameter of carbon fibres, as presented in Figure 4 (a). We assume that this geometry reflects a global fibre content and a perfect fibre distribution with a tetragonal arrangement, which can influence the diffusion process. To reduce computation time, the size of the geometry was limited to a volume of approximately $60 \times 60 \times 60 \mu\text{m}^3$ (with fibres of 5 for the Infused material or $7 \mu\text{m}$ diameter for the RTM). The sensitivity of the mesh was studied and an optimal mesh size was chosen with hex elements, as shown in Figure 4 (b). The sensitivity of the mesh has been studied in the following section.

In order to determine diffusion coefficients in the longitudinal and transverse directions to the fibres, two different simulations were performed.

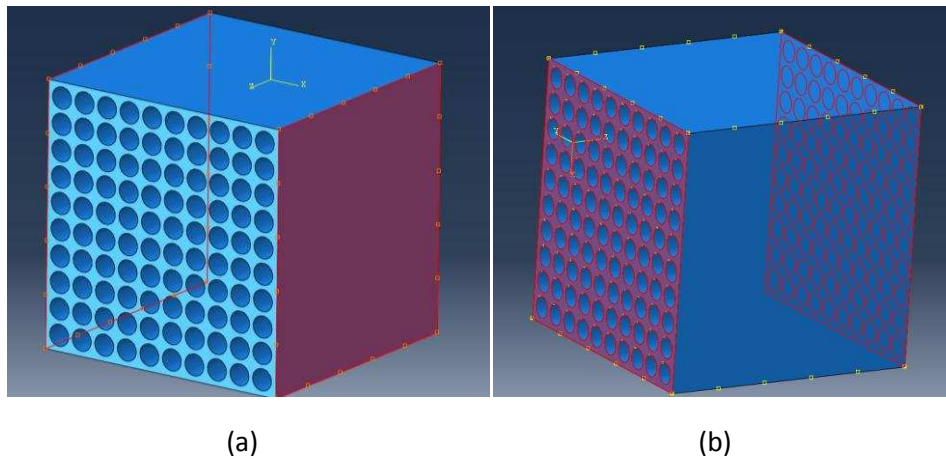


Figure 152: Representation of boundary conditions applied on the 3D model for transverse (a) and longitudinal (b) diffusion through composite.

In the first case, concentration conditions of diffusion were applied to the parallel surfaces of the cube, as shown on Figure 152 (a). In this case diffusion will occur perpendicular to the fibres. In the second case, a concentration was applied to the surfaces perpendicular to the fibres, as presented in Figure 152 (b). In both cases the applied temperature concentration was 1°C, as a consequence the temperature will evolve between 0 and 1 in the model, as the normalized water content.

The post processing of the FE calculation was performed with a Python script. This script averages the water concentration for the whole model at each time step (to simulate the gravimetric measurement of sea water diffusion in composite samples). Thus the global evolution of water concentration is plotted as a function of the square root of time normalized by the thickness.

1.2 Identification of model parameters

For the simulation of the diffusion, the parameters of the model were either determined experimentally or taken from the literature. Previously density of composites and the epoxy resin were determined. It was also necessary to determine the specific heat (C) of the epoxy resin using DSC analysis. As described in Appendix 25 representing a DSC analysis of the epoxy resin, C has been identified and is equal to 1500 J.Kg⁻¹.°C⁻¹ (±100). It known that the value has a dependence on temperature, but here for all calculations it will be fixed at 1500 J.Kg⁻¹.°C⁻¹ (for RTM and Infused simulation). As the epoxy resin diffusion was described in the previous chapter for different temperatures, Figure 153, is it now possible to determine its diffusion coefficient.

The water diffusion coefficient of the resin (and for each composite) D can thus be determined (Eq.54) from the slope of the relative mass uptake, M_t/M_∞ as a function of square root of time, \sqrt{t}/e :

$$D = \frac{\pi}{16} \left(\frac{dy}{d\sqrt{t}/e} \right)^2 \quad \text{Eq. 54}$$

For all the materials of the study these diffusion coefficients were identified in the Fickian part of the diffusion curve, after water ingress has reached a saturation plateau. Diffusion coefficient and slope of the curves have been determined between 0 and 50% ±10% of the maximum water uptake

in order to have enough points to analyze. Figure 154 represents the experimental diffusion curves allowing the slopes to be identified for each temperature.

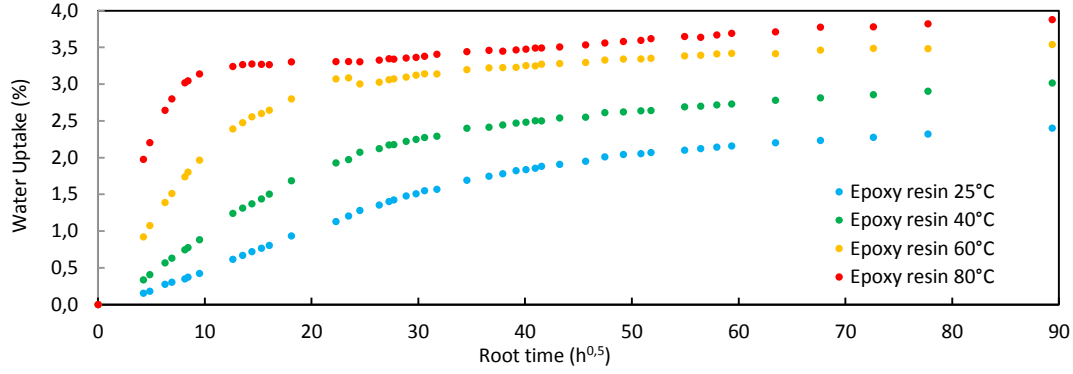


Figure 153: Plots of mean measured weight gains for pure epoxy resin immersion at the different temperatures.

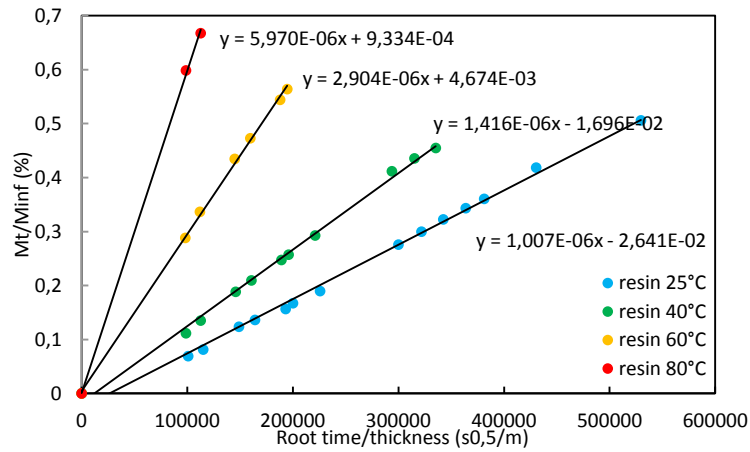


Figure 154: Determination of the slopes for each relative mass uptake for the unreinforced epoxy resin.

As specimen edges were not sealed, water could diffuse through the edges of the resin sample. As a consequence there is a need to apply an edge correction in order to determine the diffusion coefficient in one direction. A correction has been proposed in [176], and will be applied for both resin and composites in order to correct this phenomena, according to Eq.55:

$$D_x^{corr} = D_{exp} \cdot \left(1 + \frac{h}{l} + \frac{h}{n}\right)^{-2} \quad \text{Eq. 55}$$

Here h is the thickness of the sample (2.55mm in resin case), and l and n are the length and width of the specimen ($l=n=50\text{mm}$). The experimental sea water coefficient D_{exp} and the corrected coefficient D_x are presented in Table 23 for the epoxy resin at the different ageing temperatures.

Ageing temperature Epoxy resin 2.55	Experimental diffusion coefficient D_{exp} ($\text{m}^2.\text{s}^{-1}$)	Experimental diffusion coefficient corrected D_x ($\text{m}^2.\text{s}^{-1}$)
25°C	1.99E-13	1.64E-13
40°C	3.93E-13	3.22E-13
60°C	16.5E-13	13.5E-13
80°C	69.9E-13	57.6E-13

Table 23: Sea water diffusion coefficients determined experimentally for the epoxy resin.

These diffusion coefficients will be used in the model with the objective to simulate water diffusion behavior for Infused and RTM materials.

In order to compare the results of the model with the experimental results the same identification of water diffusivity was made for each composite material at each temperature. For each composite material an estimation of the fibre content was obtained based on pycnometry density measurements. Thus the carbon fibre contents in RTM, Infused and Pre-preg materials, are respectively 50, 54 and 58%. These fibre contents will be recreated in the geometry of the model.

Ageing temperature Infused UD 1.7	Experimental diffusion coefficient D_{exp} ($\text{m}^2.\text{s}^{-1}$)	Experimental diffusion coefficient corrected D_x^{cor} ($\text{m}^2.\text{s}^{-1}$)
25°C	5.6E-14	4.6-14
40°C	9.5E-14	8.3-14
60°C	48.8E-14	42.8E-14

Table 24: Sea water coefficient diffusion determined experimentally for the Infused composite ($V_f=54\%$).

Ageing temperature RTM 2.8	Experimental diffusion coefficient D_{exp} ($\text{m}^2.\text{s}^{-1}$)	Experimental diffusion coefficient corrected D_x^{cor} ($\text{m}^2.\text{s}^{-1}$)
25°C	8.8E-14*	7.13-14
40°C	14.8E-14*	11.9-14
60°C	52.9E-14	43.0E-14
80°C	257.9E-14	208.5E-14

Table 25: Sea water diffusion coefficients determined experimentally for the RTM composite ($V_f=50\%$) * for these temperatures material is not clearly saturated.

Ageing temperature Pre-preg 1.29	Experimental diffusion coefficient D_{exp} ($\text{m}^2.\text{s}^{-1}$)	Experimental diffusion coefficient corrected D_x^{cor} ($\text{m}^2.\text{s}^{-1}$)
25°C	4.28-14	3.76-14
40°C	11.2E-14	10.0-14
60°C	32.6E-14	29.3E-14
80°C	73.1E-14	65.7E-14

Table 26: Sea water diffusion coefficients determined experimentally for the Pre-preg 1.29 mm (fibre content 56.7%).

Ageing temperature Pre-preg 2.07	Experimental diffusion coefficient D_{exp} ($\text{m}^2.\text{s}^{-1}$)	Experimental diffusion coefficient corrected D_x^{cor} ($\text{m}^2.\text{s}^{-1}$)
80°C	49.4E-14	42.1E-14

Table 27: Sea water diffusion coefficients determined experimentally for the Pre-preg 2.07 mm (fibre content 58.3%).

Ageing temperature Epoxy resin	Experimental diffusion coefficient D_x ($\text{m}^2.\text{s}^{-1}$)	Specific heat ($\text{J.Kg}^{-1}.\text{°C}^{-1}$)	Thermal Conductivity K_x ($\text{J.s}^{-1}.\text{m}^{-1}.\text{°C}^{-1}$)
25°C	1.63E-13	1500	2.86E-7
40°C	3.22E-13	1500	5.65E-7
60°C	13.5E-13	1500	23.7E-7

Table 28: Epoxy matrix parameters used in the FE diffusion model for the different temperatures, K_x the thermal conductivity determined based on D_x .

Based on the parameters identified experimentally or taken from the literature, it will be thus possible to model the diffusion in composite materials in different material directions and for different temperatures.

1.3 Sensitivity study of the model

As presented previously the diffusion model used different parameters, such as K_x , C , ρ and which can also depend on the geometry of the specimen, the fibre content and the mesh of the geometry. In order to study the sensitivity of the model to these parameters, different simulations with different mesh sizes, fibre contents, and different diffusion coefficients have been tested and will be presented in this section. Then in the next section model and experimental results will be compared.

1.3.1 Influence of mesh size on diffusion model

As introduced in the model presentation, the diffusion process is applied to a specific geometry. This cubic geometry represents a simplified composite micro-structure, taking into account its fibre content and the carbon fibre diameter. As the distance between each fibre is quite small it requires an appropriate size of mesh. Thus three different mesh sizes have been tested on a geometry with a fibre content of 54% (fibre diameter of 5 μm): 0.001, 0.0005 and 0.0002 mm with hex elements (elements used for heat transfer). Figure 155 presents the diffusion kinetics results for each mesh. As a first conclusion it seems that mesh does not greatly influence the diffusion kinetics. Table 29 presents more details about this comparison, including the thermal diffusion coefficient, number of elements in the model and calculation durations. Using the diffusion curves, transverse diffusivities were identified for each type of mesh.

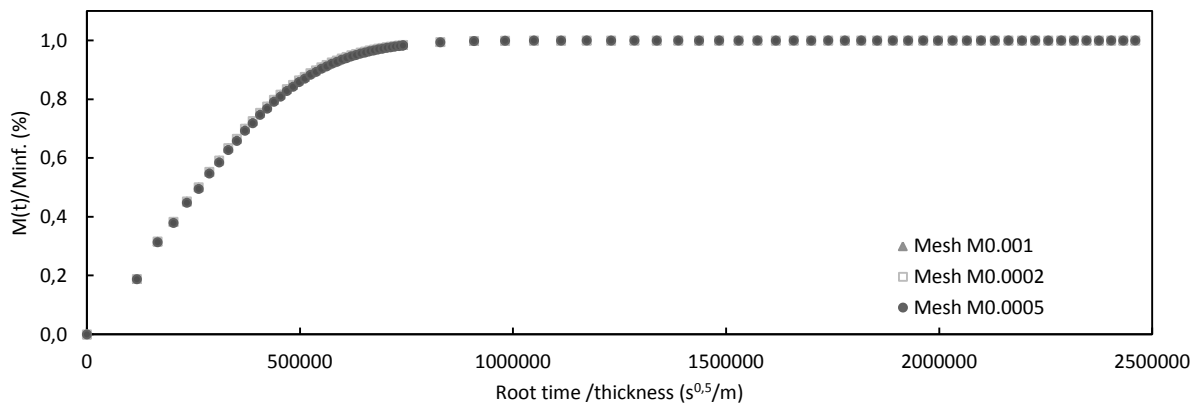


Figure 155: Influence of mesh size on transverse diffusion kinetics.

These transverse sea water diffusivities are presented in Table 29, and are slightly influenced by the mesh size. But due to the large number of elements in this mesh, the calculation times became very long. To allow faster calculation and in spite of the slight influence of the mesh on final diffusivity, for future simulations a mesh of 0.001 mm has been chosen.

Mesh size (mm)	Number of elements	Average calculation time (h)	K_x used in the model ($\text{J.s}^{-1}.\text{°C}^{-1}$)	Water diffusion coefficient obtained D_x ($\text{m}^2.\text{s}^{-1}$)
0.001	123240	1	2.31E-6	7.45E-13
0.0005	995225	5	2.31E-6	7.28E-13
0.0002	15167390	13	2.31E-6	7.45E-13

Table 29: Influence of mesh size on calculation time and water diffusion coefficient obtained.

1.3.2 Influence of fibre content on diffusion model

The second model geometry parameter which could have a major influence is the fibre content of the model. In order to evaluate the influence of fibre content on the diffusion model and the resulting diffusivities, three geometries were considered. These geometries with different fibre contents are presented in Figure 156. All cubes have the same dimension, $60.28\mu\text{m}$ (except (b)), only the number of fibres differs. According to Figure 156, in (a) and (b) there are 81 fibres, (c) 100 fibres, (d) 121 fibres, which represents respectively a fibre content of 44, 47, 54 and 65%.

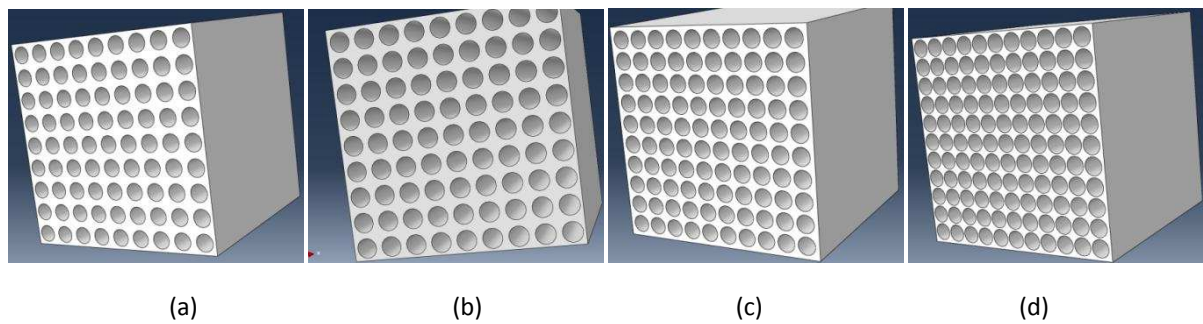


Figure 156: Representation on the geometries used to model diffusion with different fibre contents, (a) $V_f=44\%$, (b) $V_f=47\%$, (c) $V_f=54\%$ and (d) $V_f=65\%$.

The results of this comparison are presented in the Figure 157. As shown in this figure, the kinetics of transverse diffusion are only slightly influenced by fibre content, except for the 65% fibre content case.

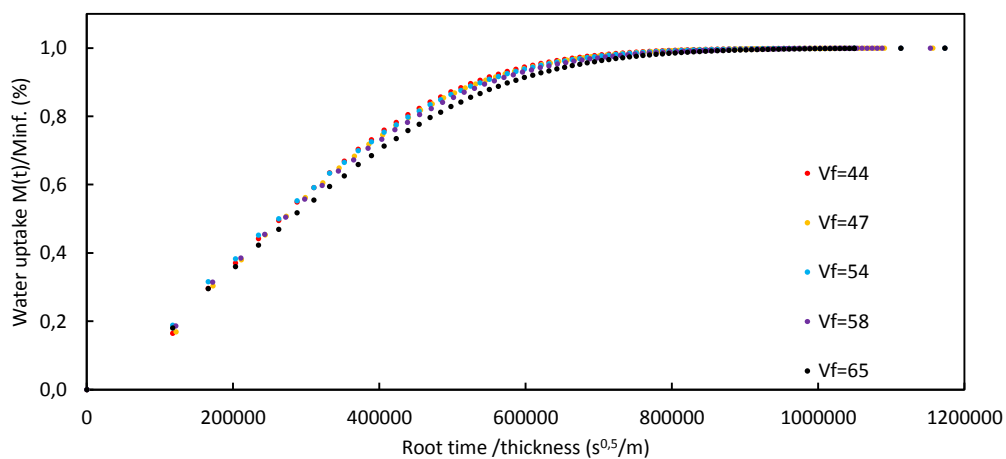


Figure 157: Influence of model fibre content on transverse diffusion kinetics.

Transverse diffusion coefficients were also determined. These coefficients are presented in Table 30. Thanks to the determination of this diffusion coefficient it is possible to see that for high fibre contents such as 58 and 65% where the distance between each fibre is much reduced, the diffusion process slows down. For 44%, 47% and 54% only small differences are perceptible, the perfect arrangement in those cases increased the diffusion rate in the model.

Fibre content (%)	Water diffusion coefficient obtained D_x (m^2s^{-1})
43.7	7.45E-13
47.2	7.44E-13
54.0	7.33E-13
58.3	7,06E-13
65.4	6.57E-13

Table 30: Influence of fibre content on transverse water diffusion coefficient.

In this section it has been shown that the diffusion model is not influenced by the size of the mesh. The model allows the influence of fibre content on diffusion kinetics to be described, but it seems that the fibre arrangement plays a role in diffusion modelling. The last parameter to study is the influence of the resin diffusion coefficient, which is the main input parameter of the model, this coefficient changes as a function of the temperature. As a consequence in the following section the diffusion model results will be compared to the experimental results obtained on the different materials of the study.

1.4 Validation and optimisation of the model

In this section the model will be compared to the experimental results obtained previously on the composite materials. For RTM and Infused materials the diffusion coefficients used in the model will be the experimental ones determined in Table 23 (converted to thermal diffusivity). Each temperature of ageing will be modelled and predictions will be compared to experimental results.

1.4.1 A first comparison between FE calculation and experimental results

In a first step the model has been tested on the Infused material. For this material the geometry of the model was defined using fibres of 5 μm diameter, a fibre content of 54% and the

edge of the cube was 60.28 μm . The modelling of the transverse diffusion has been performed for 60°C and 40°C using the diffusion coefficients identified on the epoxy resin. First results from the diffusion model are presented in Figure 158. For both temperatures the model overestimates the kinetics of diffusion. The transverse diffusion coefficients have been determined from the model.

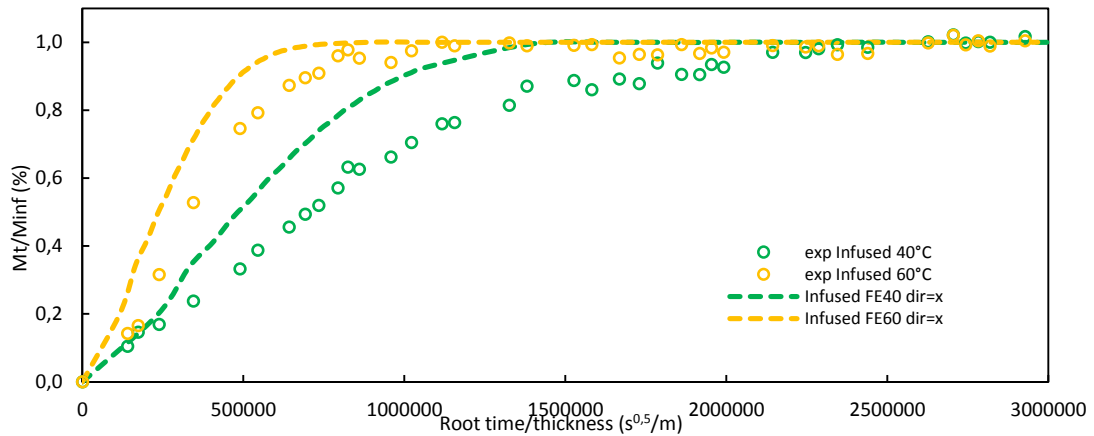


Figure 158: First comparison between diffusion model (FE) and experimental (exp) results on Infused materials at 40°C and 60°C.

These coefficients are presented in Table 31, they are compared to the experimental ones. For each temperature the model predicts diffusion coefficient which are approximately double the measured values. This result reinforces the hypothesis formulated previously about the role of the fibre arrangement in the model of diffusion. As a consequence there is a need to understand the influence of the arrangement of the fibres on the diffusion kinetics of the FE model.

Diffusion temperature (°C)	Experimental water diffusion coefficient D ($\text{m}^2\cdot\text{s}^{-1}$)	Experimental diffusion coefficient corrected D_x^{cor} ($\text{m}^2\cdot\text{s}^{-1}$)	Model diffusion coefficient D_x^m ($\text{m}^2\cdot\text{s}^{-1}$)
40	9.5E-14	8.3-14	21.6-14
60	48.8E-14	42.8E-14	89.9-14

Table 31: First results of the diffusion model for infused material at 40°C and 60°C, the model coefficients are compared to experimental ones.

1.4.2 Investigation of fibre arrangement

In order to examine the influence of the fibre arrangement on the model simulation, four types of fibre arrangement were studied using the parameter previously used for the Infused

material, as presented on Figure 159 and Figure 160. The first three examples have the same fibre content, size, mesh, number of fibres and diffusion coefficient. Only the distribution of the fibres has been changed. Figure 159, (a) represents the reference studied previously with a perfect fibre distribution. Geometry (b) is composed of three zones of fibre arrangement, the zone in the middle has a fibre content of 62% while the two other zones have a fibre content of 49%. In the last geometry (c) the same three zones have been created but the fibres were distributed manually in the zone with a fibre content of 49%. For all these models the mesh size has been reduced to 0.004 mm.

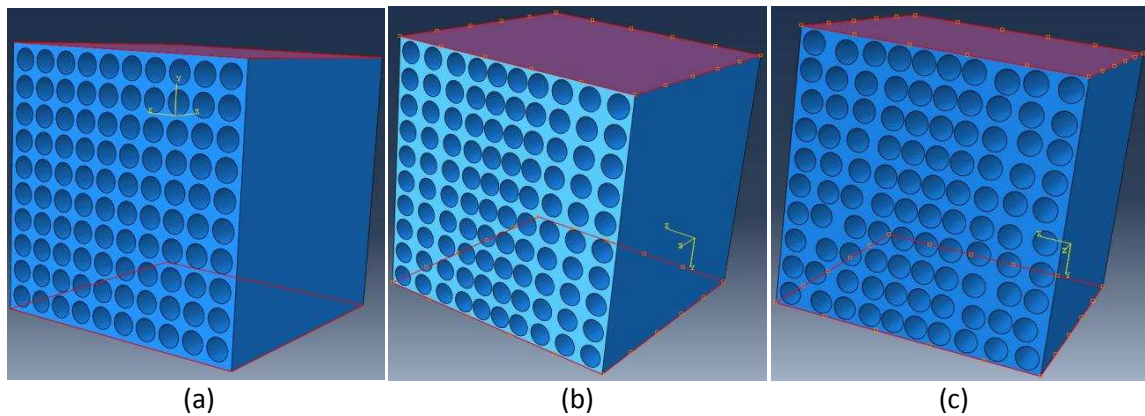


Figure 159: Three different type of fibre arrangement tested with the diffusion model, transverse boundary conditions of diffusion are represented in red.

The fourth example is based on the observed micro-structure of the Infused material. The aim of this geometry is to reproduce resin-rich and fibre-rich regions. The local fibre content in the fibre bundles of this Infused composite has been estimated to be 65% ($\pm 2\%$), based on the micrographs analyzed in Chapter II (see section 4. Chapter II). Thus this specific geometry was created with matrix rich regions with 0% of fibres and fibre bundle regions with 63.4% fibres, as presented in Figure 160 (red rectangle). Average thicknesses of each region have been reproduced in accordance with the observed structure of the Infused material. In order to reduce calculation time the width and depth of the geometry were reduced (they do not influence diffusion through the thickness). In order to model water diffusion in the transverse direction to fibres, boundary conditions have been applied on each side of the geometry, as presented in Figure 160 with the red arrows. For this specific case the mesh has been reduced to a size of 0.0004 mm (4 657 416 elements).

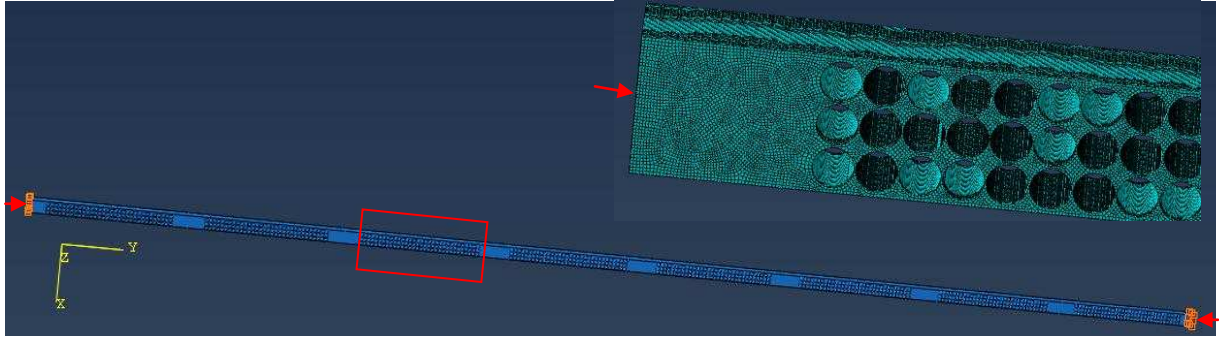


Figure 160: Fourth case of diffusion “8 plies” (d) with specific fibres distribution aiming to recreate the micro structure of the Infused materials.

The results for transverse diffusion for each geometry are presented in Figure 161 and Figure 162. For the first three examples with different fibre distributions, the fibre arrangement modifies the diffusion kinetics, as presented in Figure 161.

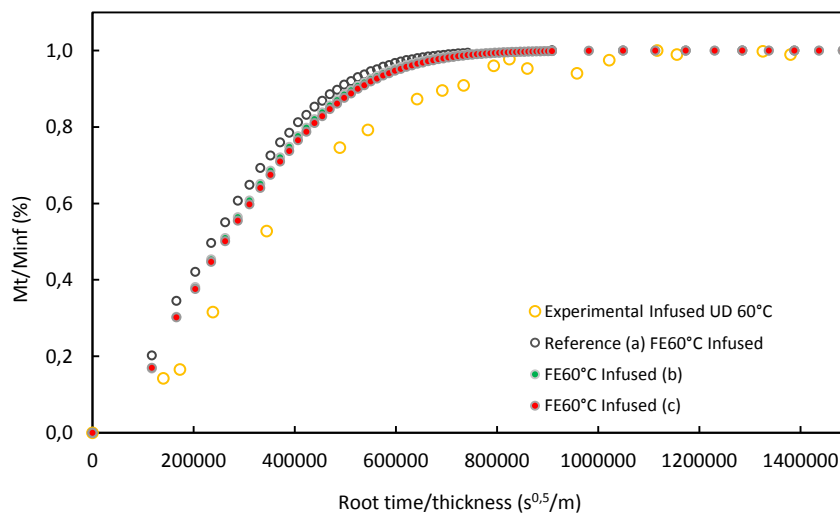


Figure 161: Transverse diffusion results for the geometries (a), (b) and (c) with different fibre arrangements. These results are compared to experimental ones (orange circles).

For the last geometry (d), the model and experimental results show a better agreement as presented in Figure 162, suggesting that it is important to introduce a fibre distribution which is as realistic as possible.

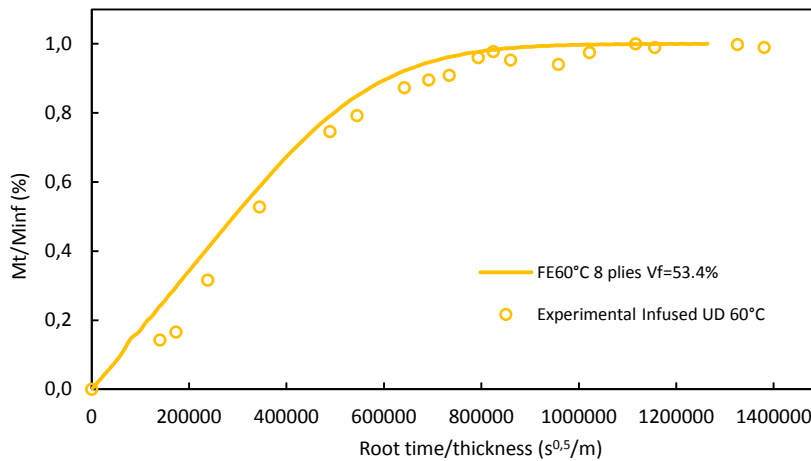


Figure 162: Transverse diffusion results for the geometry (d). These results are compared to experimental ones (orange circles).

These examples of diffusion allow the transverse diffusion coefficients to be determined, Table 32. This table provides an overview of the effect of fibre distribution on the model. It is clearly shown that the fibre arrangement in the model has a strong influence on diffusion kinetics. But this type of simulation requires a finer mesh size, due to the complexity of the geometry, which leads to longer calculation time. As stated in the introduction of this chapter, the aim here is to develop a simple model able to determine sea water diffusion coefficients in different material directions and then to estimate the water profiles in a real structure. A second aim is to take into account the effect of the damage on diffusion. As a consequence it is necessary to introduce a correction coefficient in order to correct the effect of fibre arrangement that the first (simple) model proposed is not taking into account. It has been shown previously that the model overestimates transverse diffusion coefficient, this coefficient was nearly doubled compared to experimental one. A correction coefficient will therefore be applied on the diffusivity of the resin (Table 28), which will be multiplied by $1/c$ for each temperature of diffusion (with $c=2$).

Some comparisons have also been made for the diffusion in the fibres direction. The geometry (d) and the reference (a) (with and without correction) have been compared with diffusion applied in the fibre direction. These investigations are presented in Appendix 26, as a result the longitudinal diffusion in composites is not influenced by the fibres arrangement, as presented in Table 32. As a consequence it will be not necessary to apply a correction to determine D_z in future modelling.

Model geometry	Average calculation time (h)	Model diffusion coefficient D_x^m ($\text{m}^2\cdot\text{s}^{-1}$)	Model diffusion coefficient D_z^m ($\text{m}^2\cdot\text{s}^{-1}$)
Reference FE60°C Infused (a)	14	89.4E-14	12.0E-14
FE60°C Infused (b)	14	77.6E-14	-
FE60°C Infused (c)	14	74.9E-14	-
FE60°C 8 plies (d)	20	57.3E-14	11.8E-14

Table 32: Results for transverse diffusion coefficients obtained on the different geometries of the diffusion model (mesh size was 0.0004 mm for all geometries).

1.4.3 Modelling diffusion on Infused and RTM materials at different temperature

The numerical model provides information on parameters affecting the diffusion in unidirectional composite materials. In the following simulation of water diffusion, two materials were studied: the Infused and the RTM composites. Geometries of the models have been adapted in order to respect fibre content and fibre diameter for each composite, (Infused: $V_f=54\%$ $\phi_f=5\ \mu\text{m}$, RTM: $V_f=50\%$ $\phi_f=7\ \mu\text{m}$). The transverse diffusion of each material has been examined at 60, 40 and 25°C.

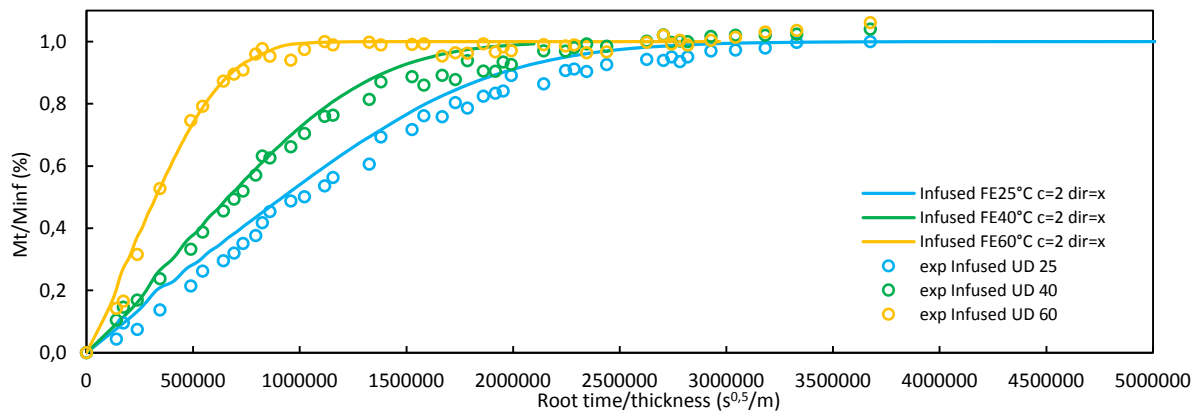


Figure 163: Comparison between modelling of diffusion and experimental results for Infused materials at 60, 40 and 25°C.

Ageing temperature Infused	Experimental diffusion coefficient D_x ($\text{m}^2\cdot\text{s}^{-1}$)	Model estimation of D_x ($\text{m}^2\cdot\text{s}^{-1}$)	Model estimation of D_z ($\text{m}^2\cdot\text{s}^{-1}$)
25°C	4.6E-14	5.62E-14	15.4E-14
40°C	8.3E-14	11.4E-14	28.9E-14
60°C	42.8E-14	48.2E-14	120.7E-14

Table 33: Comparison between model estimation of transverse diffusion and measured values for the Infused material.

The results obtained are presented for the Infused material in Figure 163 and in Figure 164 for the RTM. A good agreement between the model and experimental results has been found for all temperatures in the case of Infused material. The correction coefficient determined previously provides a good description of the diffusion process for each temperature. The diffusion coefficients determined with the model are in accordance with the experimental ones for each temperature, as presented in Table 33. For the model of the RTM material the kinetics of diffusion also show a good agreement with the experimental results. But at 40 and 25 °C it is difficult to compare model and experimental results for the moment, because experimental diffusion has not reached a saturation plateau (25°C) or begun the stabilisation of water uptake (40°C). Table 34 presents a comparison between model and measured transverse diffusion coefficients for the RTM material.

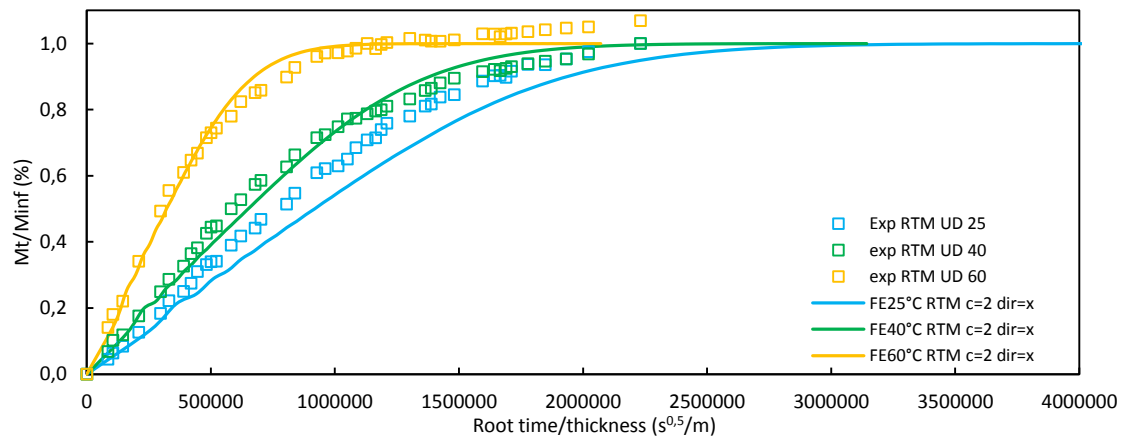


Figure 164: Comparison between modelling of diffusion and experimental results for RTM materials at 60, 40 and 25°C.

Ageing temperature RTM	Experimental diffusion coefficient D_x ($\text{m}^2.\text{s}^{-1}$)	Model estimation of D_x ($\text{m}^2.\text{s}^{-1}$)	Model estimation of D_z ($\text{m}^2.\text{s}^{-1}$)
25°C	7.13E-14	5.84E-14	16.9E-14
40°C	11.9E-14	11.3E-14	29.2E-14
60°C	43.0E-14	49.1E-14	132.6E-14

Table 34: Comparison between model estimation of transverse diffusion for the RTM material.

This last example for RTM composite at lower temperature illustrates the need to predict diffusion with a model, as for lower temperatures the experimental procedures may be very long.

1.4.4 Prediction of sea water diffusion on Infused material for lower temperature

Previously the diffusion model has been used in order to determine transverse diffusion in composites at 60, 40 and 25°C. However the aim of this model is to determine longitudinal and transverse water diffusion coefficients in order to reintroduce them in models of structures such as tidal turbine blades. In the case of the tidal turbines these temperatures of 40°C and 60°C do not reflect the real temperature of their environment during service life. Even 25°C is quite warm for the actual location of tidal turbines such as OpenHydro near Paimpol or Sabella D10 close to Ouessant. As a consequence there is a need to predict sea water diffusion for lower temperatures for instance 20°C and 15 °C. An Arrhenius law has therefore been applied to the diffusion coefficients determined experimentally on the epoxy resin in order to determine resin diffusivities at 20 and 15°C, as presented in Figure 165. The following Table 35 presents the diffusion coefficients obtained extrapolating with an Arrhenius law. For the determination of the thermal diffusion coefficient of the model, the heat capacity has been considered as constant in this range of temperature.

However this estimation of diffusion coefficients at lower temperatures must be considered with care. For polymers, Arrhenius plots of diffusivity against the ratio $1/T$ are often linear. Nevertheless in certain cases, there may be discontinuities in the diffusion coefficient-temperature curves near phase transitions. For instance, the water diffusion rate can increase significantly when the temperature is increased above the T_g .

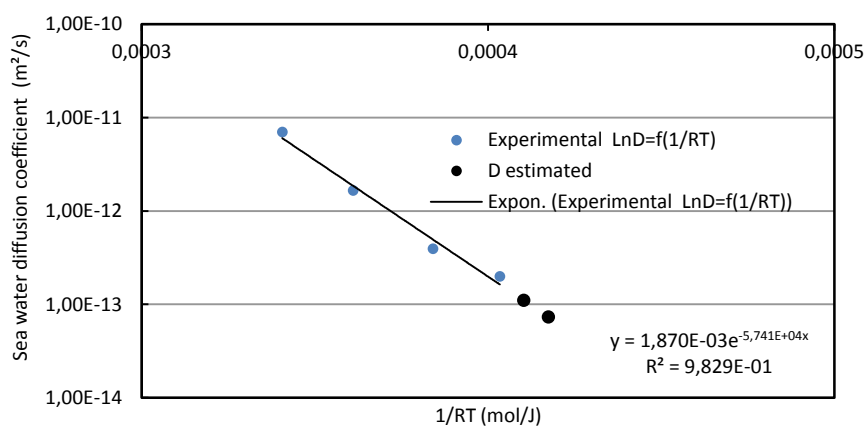


Figure 165: Arrhenius graph of the logarithm of epoxy resin diffusion coefficient as a function of $1/RT$ for 25, 40, 60 and 80°C (blue points). The black points represent the water diffusivity estimated by an Arrhenius law for 20°C and 15°C.

Ageing temperature Epoxy resin	Experimental diffusion coefficient D_x ($\text{m}^2\cdot\text{s}^{-1}$)	Arrhenius estimation of D_x ($\text{m}^2\cdot\text{s}^{-1}$)	K_x ($\text{J}\cdot\text{s}^{-1}\cdot\text{m}^{-1}\cdot^\circ\text{C}^{-1}$)
15°C	-	5.93E-14	10.4E-8
20°C	-	9.05E-14	15.8E-8
25°C	16.3E-14	-	28.6E-8
40°C	32.2E-14	-	56.5E-8
60°C	135.E-14	-	237.2E-8

Table 35: Transverse experimental diffusion coefficients and estimated transverse coefficient for 20°C and 15°C.

The coefficients determined at 20 and 15°C with the Arrhenius law for the resin were then implemented in the diffusion model in order to determine composite diffusivity in each material direction. Figure 166 presents a comparison between modelling of transverse (dotted line) and longitudinal directions to fibres (continuous line) at 15°C and 25°C for the infused materials. Table 36 presents the diffusion coefficient obtained in both directions and for each temperature. In Appendix 27 a comparison is presented of the modelling of transverse diffusion for all temperatures for the Infused material. The figure highlights the influence of the diffusion coefficient and temperature on the time for water to diffuse in the composite. These models allow diffusion coefficients to be estimated rapidly when the experimental procedure requires several years, but they are only estimations, and require validation as further data become available.

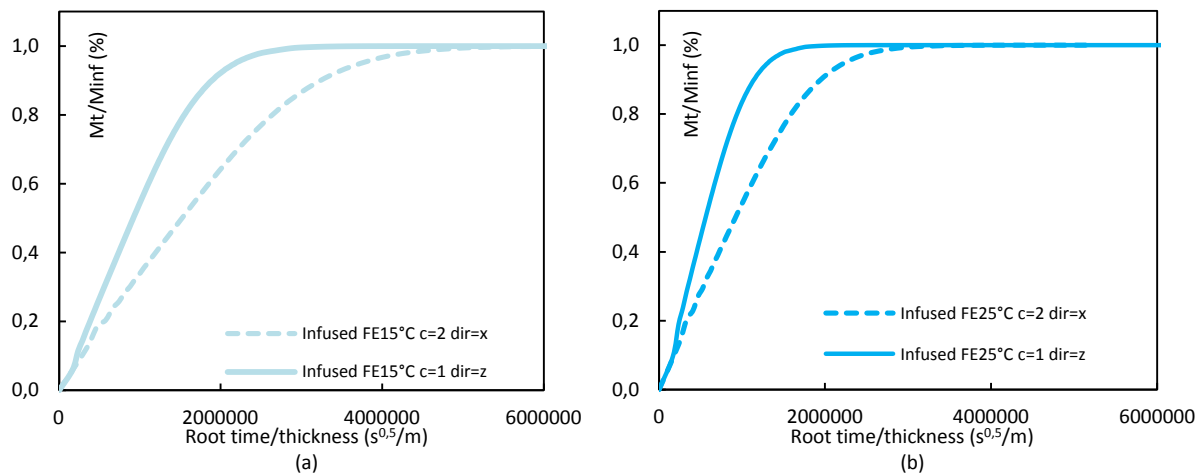


Figure 166: Modelling of both transverse (dotted line) and longitudinal (continuous line) water diffusion for the Infused material at 15°C (a) and 25 °C (b).

This procedure has also been used to determine sea water diffusion coefficients for the RTM material, these coefficients are presented in Appendix 28. Thus it is possible to use these diffusivities to examine how larger structures behave with respect to long term water entry.

Model diffusion temperature	Infused transverse diffusion coefficient D_x ($\text{m}^2.\text{s}^{-1}$)	Infused longitudinal diffusion coefficient D_z ($\text{m}^2.\text{s}^{-1}$)
15°C	2.01E-14	6.15E-14
20°C	3.03E-14	9.26E-14
25°C	5.62E-14	15.4E-14

Table 36: Coefficients of water diffusion determined in longitudinal and transverse direction to the fibres for the Infused material for temperatures close to tidal turbine service life conditions.

1.5 Application to a tidal turbine blade

In the previous section the diffusivities of the different composite materials have been modelled at different temperatures and in different directions of the material. In this section a first study of sea water diffusion in a large tidal turbine blade structure will be described using the method presented above. The aim was to have a first estimation of the timescale for long term water diffusion into a real structure. As sea water ageing has important effects on mechanical properties, it is important to estimate the sea water entry in such structures.

A 3D blade model was used. This model is presented solely as an example, it does not represent a particular blade. For this 3D geometry, only a short section was considered (100 mm). The average dimensions of this section are 1000 mm by 200 mm and the thickness of the composite skin is 20 mm. An illustration of the blade section is presented in Figure 167 (a). The boundary conditions of water concentration were only applied on the outer composite skin of the blade with the composite diffusivity determined at 15°C and 25°C, as presented in Figure 167 (b). Diffusion coefficients used for modelling were presented previously in Table 36.

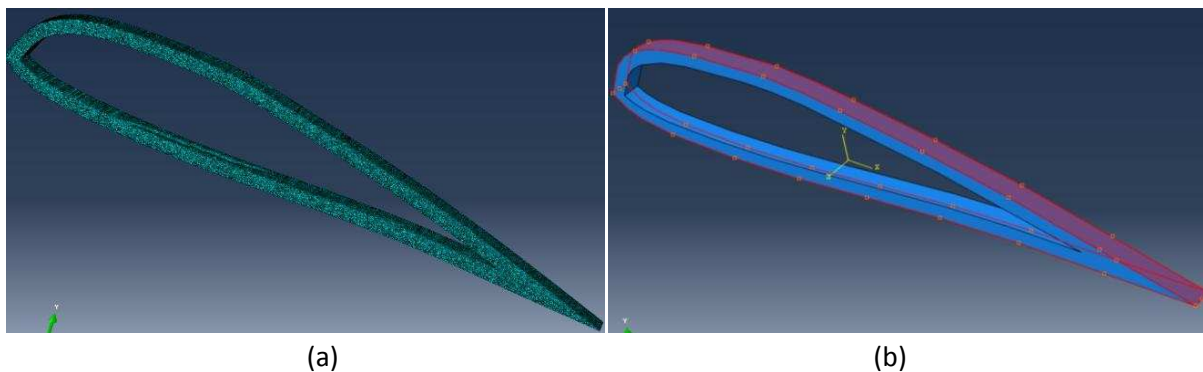


Figure 167: Presentation of blade section geometry (a) and the associated boundary conditions of diffusion (b).

The water concentration profiles in the blade section are presented in Figure 168 for two cases, immersion at 15°C and 25°C. In these figures the predicted kinetics of diffusion on the blade section until saturation are presented. The service life of tidal turbines is given by some manufacturers as 25 years, so this time period has been taken as a reference. For this immersion time the models estimate that the composites of the blade reach an average concentration of water of 0.22 at 15°C and 0.36 at 25°C (for this geometry and thickness). The difference of slopes observed in Figure 168 (b) could be explained by the variation of thickness on the trailing and leading edges.

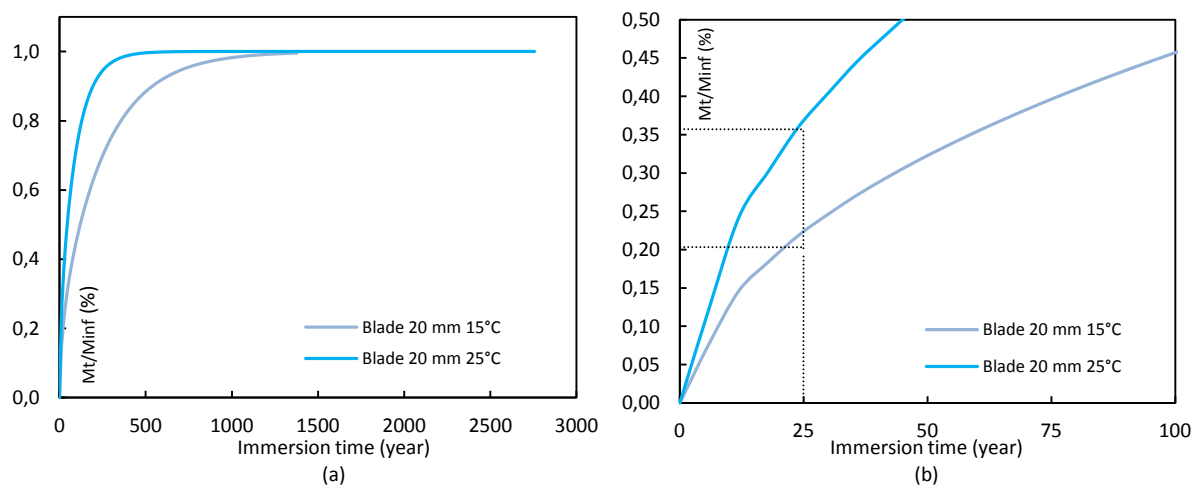


Figure 168: Diffusion curves obtained after modelling sea water entry on the blade section at 15°C and 25°C (a). Focus on first 25 years of water diffusion through the blade.

After 25 years of immersion at these temperatures the 20 mm thick blade will not be fully saturated by the seawater, but some outer composite layers will be fully saturated, as shown in Figure 167. For instance at 15°C, 4% of the thickness of the blade is fully saturated after 25 years, and 20% of this thickness has a water content between 90% and 50%. Diffusion at 25°C is more severe, in this case 5% of the thickness of the blade is fully saturated after 25 years, and 30% of the blade thickness has a water content between 90% and 50%.

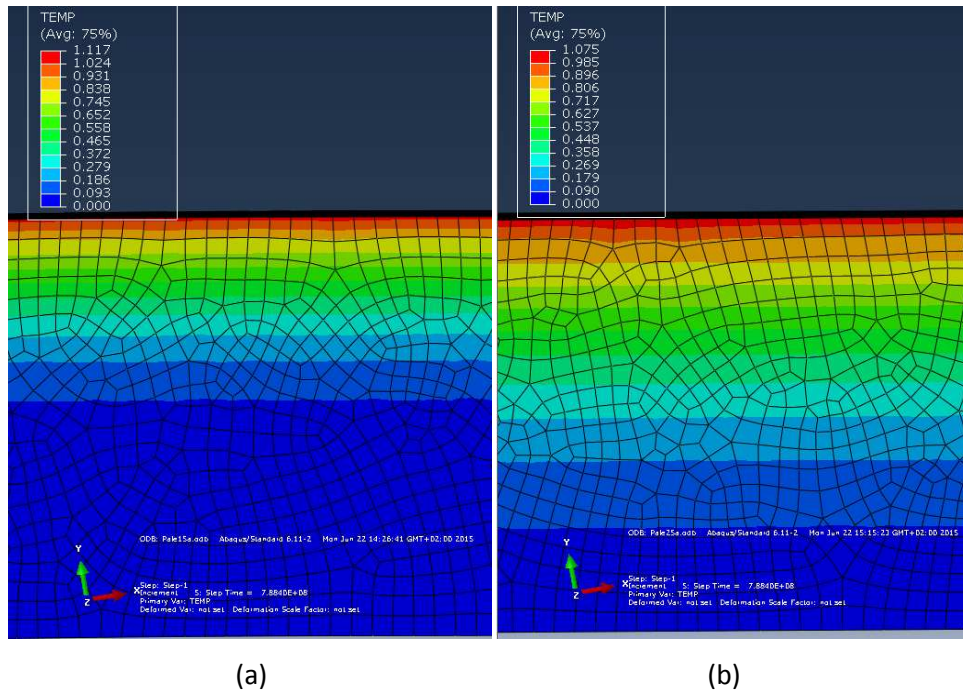


Figure 169: Water diffusion modelling results at 15°C (a) and 25°C (b), figures present local diffusion of water in the blade section after 25 years of immersion.

These previous examples have been taken in a section of the blade where thickness is constant. However in some regions like the trailing edge of the blade, composite layers can be much thinner. As a consequence the water concentration in these regions is more important, as presented in Figure 170.

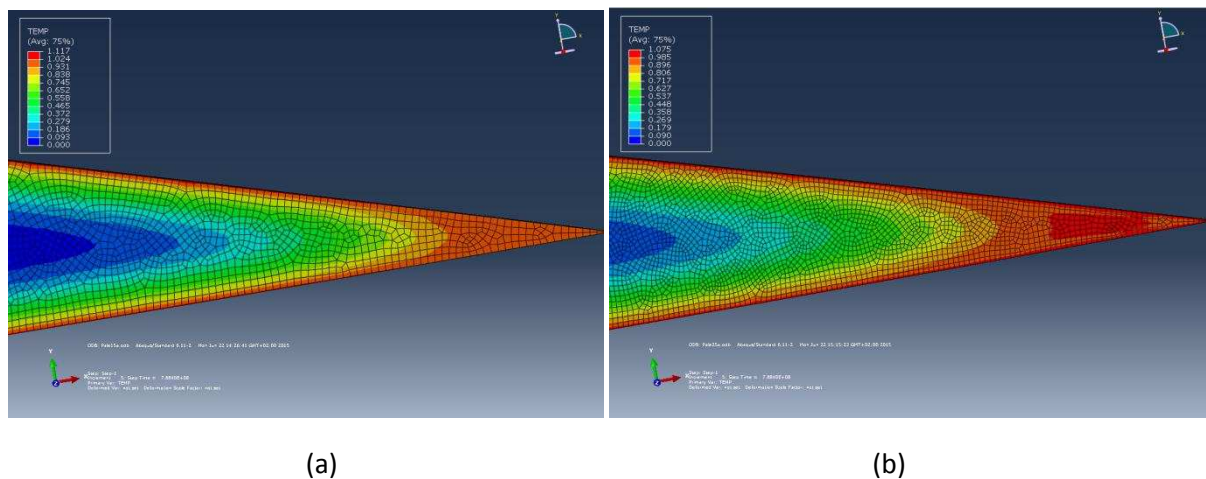


Figure 170: Water diffusion modelling results at 15°C (a) and 25°C (b), figures present local diffusion of water in the blade trailing edge after 25 years of immersion.

Water ingress into tidal turbine blades is strongly dependent on the temperature of the environment, but a significant part of even thick composites will be affected by water. In these composite layers a weakening of the mechanical strengths by between 20 to 40% will appear, as presented in the previous chapter. It is worth mentioning that in this modelling, the influences of the static (and cyclic) loads were not taken into account. However, it has been shown that before ageing, damage may appear above a certain loading threshold. Damage in the form of intra-laminar cracks can create new pathways for water, which will accelerate the diffusion kinetics in the damaged composites.

2. Modelling of damage after sea water ageing

In Chapter II, a model taking account of the crack development in composite materials has been presented and applied to the carbon/epoxy materials of the study. It has been shown that before sea water ageing the model allows a good description of damage initiation and propagation in composites, thanks to identified physical material parameters. During sea water ageing, the evolution of these parameters has been investigated. The influence of sea water ageing on inter-laminar crack propagation behaviour has also been investigated. The aim of this section is to use the physical parameters identified experimentally at the different ageing times in the model, in order to predict damage development after ageing.

2.1 Model key elements after sea water ageing

The damage model is based on two key elements, both of which could be affected by sea water ageing. The first of these is the threshold of damage which is based on a failure criterion which is a function of the strength and the toughness. The second key point of the model concerns the kinetics of damage development, which are described by a finite fracture approach. It has been shown that the potential of energy between two steps of loading mainly depends on the toughness of the ply. This has been identified previously using the threshold of damage on a laminate with a thin 90° ply, and gives correct results.

Based on the experimental tests performed on the Infused material at different steps of ageing, it has been shown that the strengths of the material are severely affected by ageing but the toughness remained quasi constant, as presented in Table 17. We will suppose that the toughness of the ply $G_I^{C,ply}$ is also not influenced by the absorption of water.

Ageing time	E_{11} (GPa)	E_{22} (GPa)	ν_{12} *	X_t (GPa)	Y_t (MPa)	G_I^c (N.mm ⁻¹)
T0	136	6.8	0.4	2.2	45	0.57
T1	141	6.0	0.4	1.8	27	0.47
T2	131	5.9	0.4	1.6	23	0.51

*not measured, chosen equal to a common acceptable values for this kind of material

Table 37: Materials physical properties determined previously and used in the model for the ageing conditions.

2.2 Comparison between modelling and experimental results

Using the elements presented in the previous section, the model has been implemented with aged material parameters. First, the case of the infused materials has been studied, on cross ply Infused laminate $[0_2,90_2]_s$.

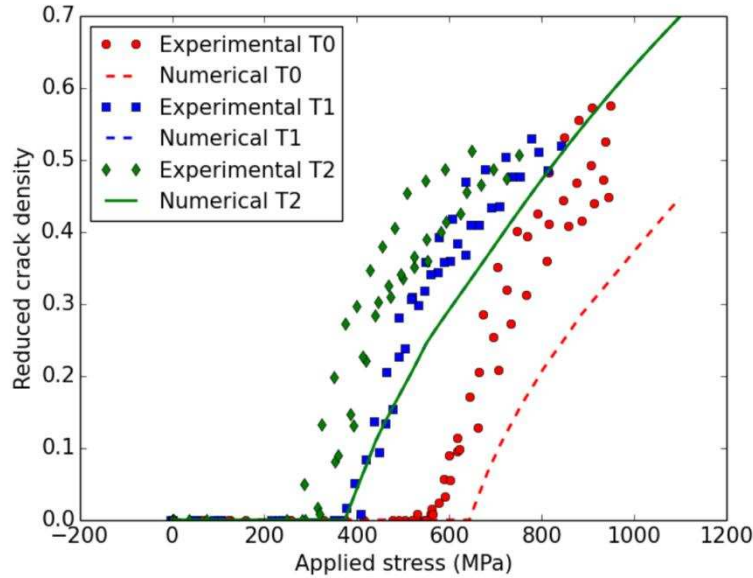


Figure 171: Evolution of the crack density in the 90° plies as a function of the loading for a $[0_2,90_2]_s$ Infused laminate. Comparison between model (line) and experimental results (points) at different ageing times (T0: un-aged; T1: aged 37 days, T2: aged 67 days).

A comparison between model prediction and experimental results is presented in Figure 76. The results provided by the model are reasonably close to the experimental ones. As the tenacity is constant as a function of the immersion time, the kinetics of the damage remain un-changed according to the modelling prediction. It is observed experimentally that the evolution of the crack density curves is only shifted to lower stress after sea water ageing, but keeps the same shape. Long immersion in water has only an influence on the threshold of damage. The procedure developed in Chapter II (Eq.20) has allowed changes in the in-situ strength to be calculated as a function of sea water exposure time. Due to the loss of transverse strength of the UD ply Y_t , the strength Y_t^{stress} decreases as a function of ageing time, as shown in Figure 75. However Y_t^{energy} remains constant during sea water ageing immersion, because this parameter depends on $G_I^{c,ply}$ (which is constant during ageing). After saturation by water (T1 and T2) in the composites the threshold of damage

does not evolve further. This could be explained by the fact that $G_I^{c,ply}$ remains constant, as a consequence in-situ strength is controlled by the toughness (with Y_t^{energy}).

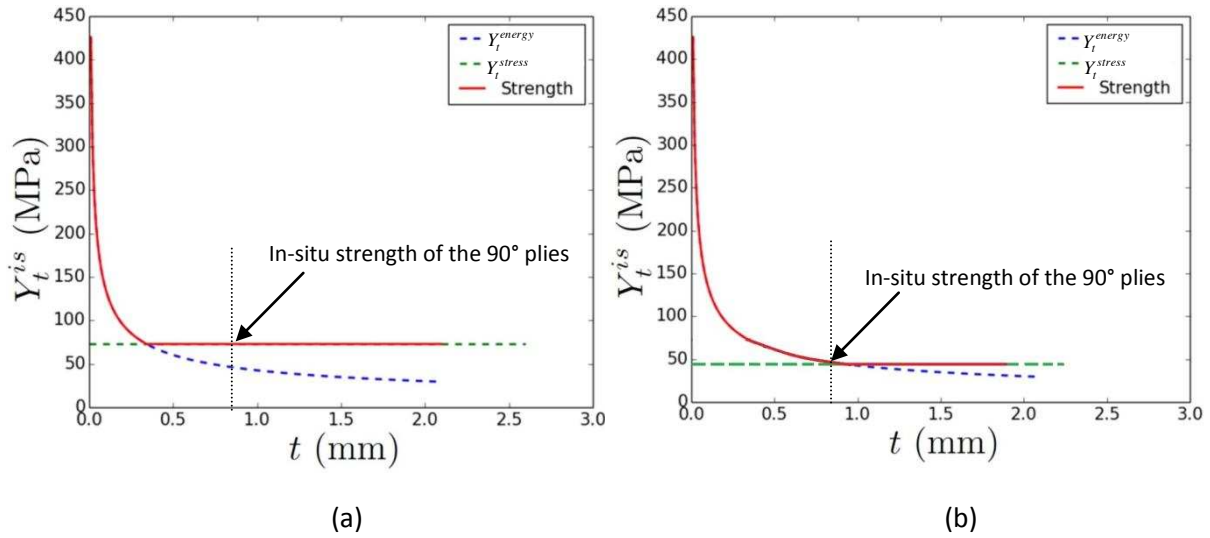


Figure 172: Criterion evolution before (a) and after (b) sea water ageing, Y_t^{stress} decreases as a function of sea water ageing time.

The damage model has shown that is possible to predict the effect of water ageing on damage threshold and kinetics. Due to the reduction in in-situ strengths after saturation, the threshold of damage is simply shifted while the kinetics of damage remain unchanged. As a consequence, damage will appear earlier in these composite materials when they are subjected to loads and sea water ageing.

3. **Modelling of damage/diffusion coupling**

The study of damage in these composites has revealed that sea water ageing induces some changes, causing an earlier appearance of damage. As a consequence, intra-laminar cracks will appear more quickly in aged composite structures, creating new pathways for water entry with which may in turn accelerate water ingress. In the past some authors have investigated the interaction between composite damage and diffusion. It has been shown that water diffusion and damage are intricately coupled phenomena, which may reinforce each other to the detriment of the composite durability [207],[208]. The evolution of moisture content and kinetics of diffusion as a function of the applied load have been studied by Weitsman in [209]. Perreux and Suri have proposed an approach to predict how the presence of damage affects absorption [210],[211]. Finally, experimental and theoretical investigations on the mechanics of moisture diffusion in damaged composites have been proposed by Roy [212],[52].

In this section a first approach to the coupling between diffusion and damage will be presented using the diffusion model developed in the preceding section. Then some preliminary experimental investigations of the interaction of damage and water ageing on composite materials will be presented.

3.1 **Modelling of damage/diffusion coupling**

The aim here is simply to speculate on how the coupling between damage and water diffusion might be introduced in the numerical model. The diffusion model previously developed has been used to model water diffusion on a composite laminate where a crack density has been introduced. For this first investigation a [0,90,0] composite laminates has been studied. Different crack densities have been introduced into the 90° ply, in order to model the appearance of cracks as previously studied in section 2.

The 3D geometry of this model is based on the Infused material, as a consequence each ply of the model has a thickness of 0.21 mm, as shown in Figure 173 (a). The length and number of cracks have been changed in order to investigate diffusion for different crack densities (between 0 and 1.16). The crack width has been measured experimentally during the previous optical measurements, a width of 0.02 mm was used for each intra-laminar crack as presented in Figure 173 (a).

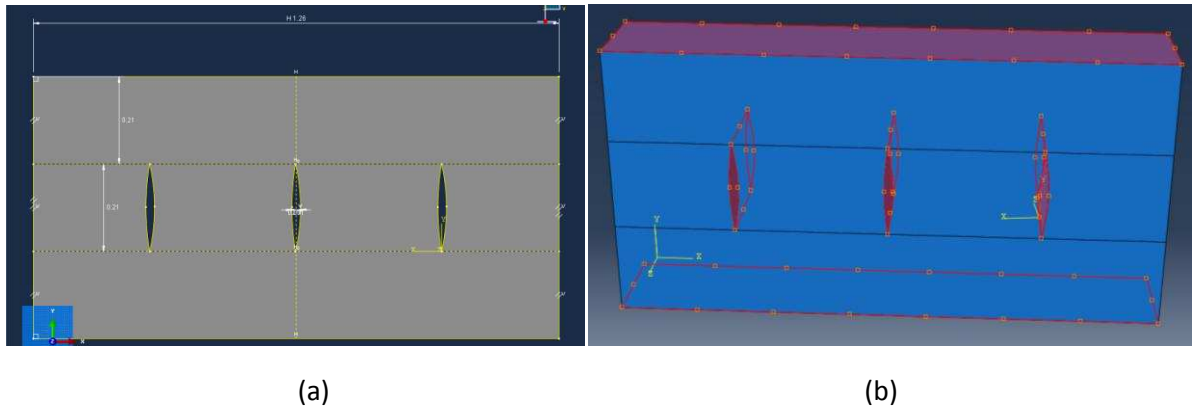


Figure 173: Example of 3D geometry generated to model diffusion in damaged composite, presenting dimension of composite layers (a). The boundary conditions applied on the model (red) (b).

To model water diffusion in this geometry, the diffusion coefficients (longitudinal and transverse) of the Infused material at 25°C have been used. The boundary conditions of diffusion have been applied on the edge of the geometry and at each surface of the cracks, as presented in the example Figure 173 (b). In applying these boundary conditions in the cracks we consider that the cracks are fully open and filled with water, which is an extreme case. As diffusivities are different and depend on the orientation of the material, orientation has been assigned in order to account for the orientation of each ply in the model.

Figure 174 shows some illustrations of the diffusion geometries with different crack densities after 10^5 seconds of water diffusion. As a first conclusion, it seems that damage has a strong influence on the kinetics of water diffusion into these composite laminates. Appendix 29 presents the diffusion curves for each model with different crack densities.

Using the results obtained with the different configurations of the model, it is possible to determine the transverse diffusion coefficient of the composite laminate as a function of the normalized crack density, as presented in Figure 175 (red points). However this coefficient represents the homogenised diffusion coefficient because diffusivity in the 0° plies remains constant as these plies are not subjected to damage. As a consequence it is necessary to determine the diffusion coefficient of the 90° ply, which is subjected to changes in diffusion as cracks appear.

To determine the local diffusion coefficient in the 90° ply an inverse identification has been applied based on the diffusion coefficient of the undamaged laminate and the volume fraction of each ply. In this way the transverse diffusion coefficient of the 90° ply has been determined as a function of the crack density and this is presented in Figure 175 (blue points).

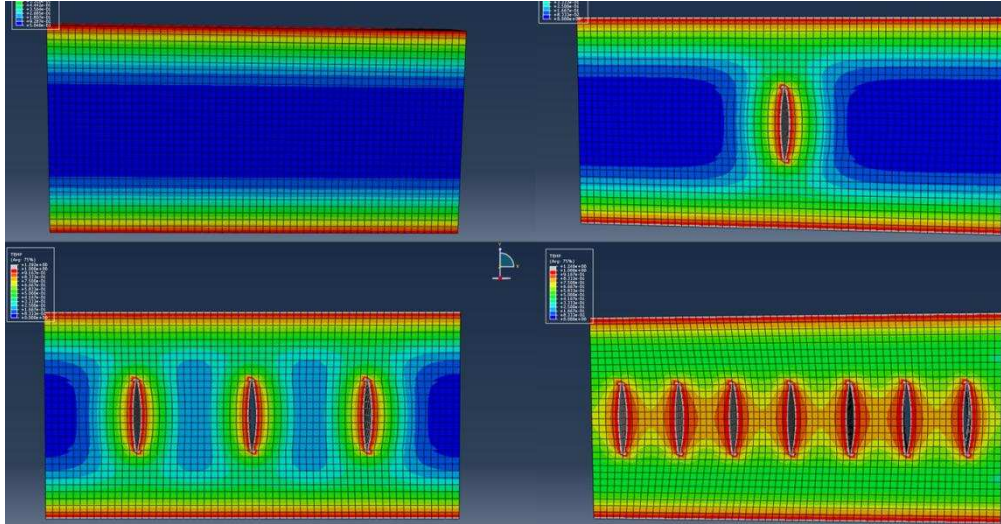


Figure 174: Different 3D geometry configurations of damaged and un-damaged composite. The results presented were taken after 10^5 seconds of diffusion.

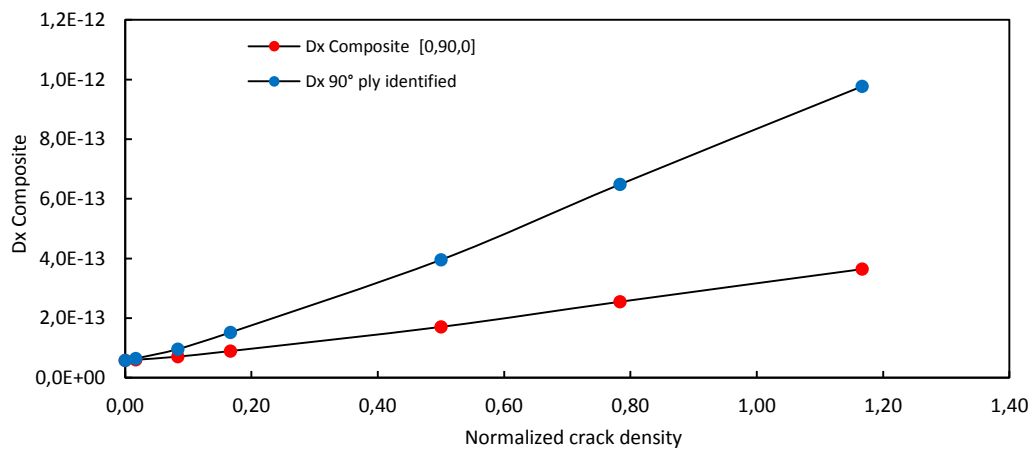


Figure 175: Evolution of composite [0,90,0] diffusion coefficient and the identified diffusion coefficient of the 90° ply as a function of the normalized crack density.

This first investigation has shown that damage development can influence the water diffusion kinetics in laminated composites. This approach has allowed changes in the diffusion coefficient of the 90° ply to be followed as a function of the crack density (for these conditions and this specific material). This new coupled parameter can be applied in a blade diffusion model.

3.2 First experimental approach on damage/diffusion coupling

In the previous section the effect of damage on diffusion has been investigated in a first modelling approach. It has been shown that damage could increase the rate of water entry inside composites. Some preliminary tests were also performed, in order to examine whether water ageing under load reduces the final strengths of the material. One would expect a damaged composite to degrade faster in water compared to un-damaged one.

3.2.1 Experimental procedure

The aim of these experimental tests is to characterize the effect of damage and diffusion on the final strength of the material. As kinetics of damage are now known before and after ageing on the Infused material, it is possible to introduce a controlled level of damage in this material by tensile loading. An Infused material with a stacking sequence of $[0_2, 90_2]_s$ was chosen for these tests.

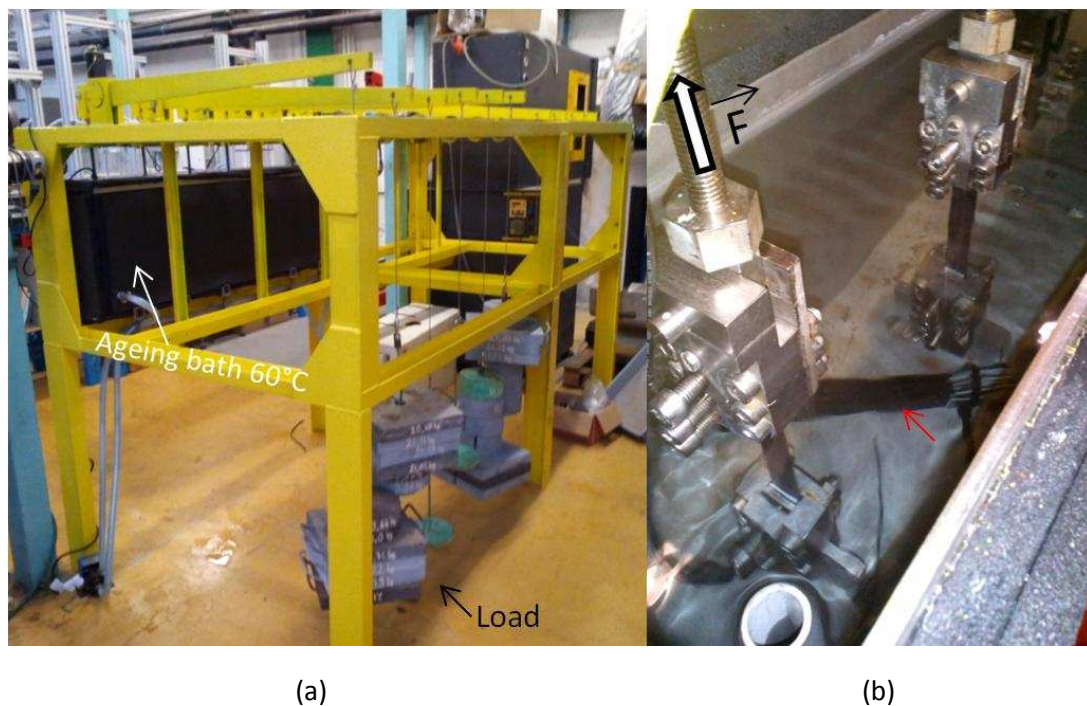


Figure 176: Ifremer test bed for coupled diffusion and tensile loading.

Ifremer disposes of a special test bed with renewed water bath and the possibility to apply tensile loading on specimens as presented on Figure 176. Figure 176 (a) shows the test bed, the yellow frame, and loading arms allow different loads up to 1 Ton to be applied. The tensile apparatus used in the bath is presented in Figure 176 (b), the water is continuously renewed and maintained at 60°C. The specimen width is limited to 18 mm. As a consequence it is only possible to apply a load of 327 MPa on the specimen of Infused material. As presented previously in Chapters II and III, the threshold of damage for this un-aged material (in the considered stacking sequence) is approximately 550 MPa. As the present test bed does not allow a sufficient load to initiate damage, the specimens were pre-damaged using an Instron electromechanical tensile machine. A pre-load of 700 MPa was applied on certain specimens.

It is thus possible to distinguish four types of specimen tested in this preliminary study of coupling between damage and diffusion. The different specimens are presented in Figure 177. For type A, specimens have been pre-damaged to a normalized crack density of approximately 0.25 (700 MPa preload). These specimens were loaded on the test bed (327MPa) in the water bath at 60°C. In this case we consider that cracks in the 90° plies are open due to the applied load. Open cracks can induce faster diffusion and degradation. For the specimen type B, specimens were also pre-loaded under the same conditions as type A. However, the specimens were not loaded but they were placed in the water bath, as presented in Figure 176 (b) by the red arrow. Type C specimens were not pre-damaged and not loaded but they were also placed in the water bath to age. The last set of specimens, Type D, were the same as Type C but they were stored in dry conditions at 20°C and 50% RH. All these specimens were aged in these specific conditions for 30 days. Specimens of types C and D have been used as a reference.

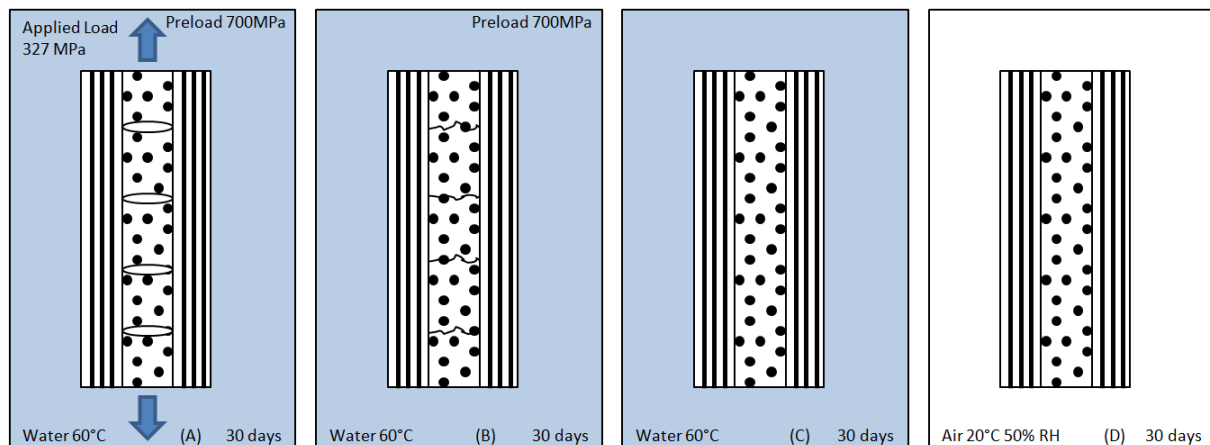


Figure 177: Different test conditions applied to the Infused $[0_2,90_2]_s$ specimens for 30 days (water immersion time, pre-loading and loading).

3.2.2 First results and additional investigations

After applying these different conditions for 30 days, each type of specimen has been tested in tension in order to compare the influence of applied conditions on the final strength. The results are presented in Table 38. Obviously the fact that the specimens are pre-damaged (A and B types) induces an early failure compared to C. However, ultimate strengths obtained in cases A and B are quite close. These first results suggest that coupling between damage and diffusion does not have as much influence as expected on the final strength of the material. Specimens A and B were aged for 30 days in water at 60 °C. It has been shown that 37 days are necessary to saturate un-damaged Infused material. As these two times of ageing are quite close, and despite the fact that the cracks were open, specimens in both cases were nearly saturated and showed the same reduction in strength. As a consequence it is necessary to perform other tests, for a period over which the sample is not saturated in water but sufficiently long to allow ageing to affect the material.

Procedure	A	B	C	D
Preload (MPa)	700	700	No	No
Immersion Water 60°C	30 Days	30 Days	30 Days	No
Load during immersion (MPa)	327	No	No	No
Ultimate strength(MPa)	1058 (61)	1064 (29)	1156 (26)	1273 (3)

Table 38: Summary of ageing conditions for each specimen type and ultimate tensile strength after 30 days.

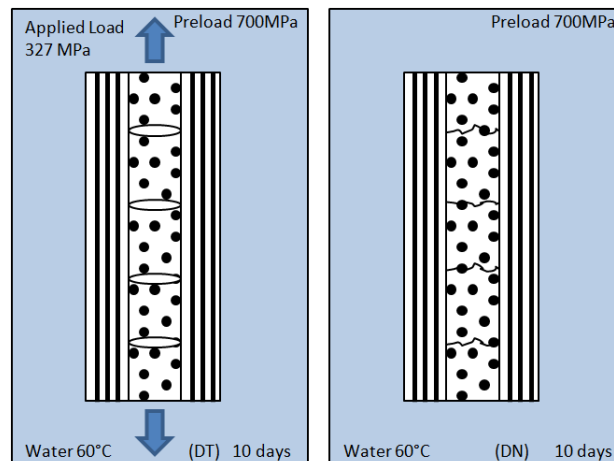


Figure 178: Different test conditions applied to the Infused $[0_2,90_2]_s$ specimens during 10 days.

The same procedure presented above has therefore been repeated, as for specimen type A and B, but the specimens DT and DN were only immersed in water at 60°C for 10 days, (under

tension or not, after pre-damage, as shown in Figure 178). Then after 10 days the specimens were tested in tension. The results obtained are presented in Table 39. Once again the difference between specimens under loading and without loading is not significant.

Procedure	DT	DN
Preload (MPa)	700	700
Immersion Water 60°C	10 Days	10 Days
Load during immersion (MPa)	327	No
Ultimate strength(MPa)	1103 (75)	1116 (87)

Table 39: Summary of ageing conditions for each specimen type, and ultimate tensile strength after 30 days.

Based on the results from these first investigations on the coupling between damage and diffusion, it is difficult to conclude. No significant effect of this coupling has been observed on the final strength of the material after 10 and 30 days. This suggests that pre-damage did not accelerate degradation of the material during water ageing.

To investigate this hypothesis the 3D diffusion model has been used. Based on the previous development of coupling between damage and diffusion (see section 3.1), the experimental samples used for the test have been modelled (type A and type C, see Figure 177). This modelling took into account the real dimension of the specimen and an average normalized cracks density of 0.25. The model geometries are presented in Appendix 31. Diffusion boundary conditions have been applied on the both faces of the specimen model and in whole cracks surfaced (making the hypothesis that all cracks are open for A).

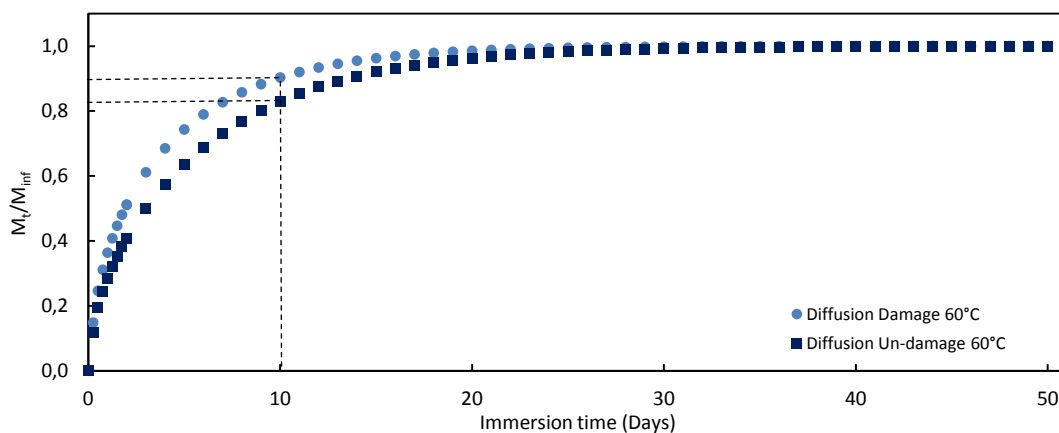


Figure 179: Model results of water diffusion comparison, between un-damage (blue squares) and damage (blue points) sample after immersion in water at 60°C. Samples were representatives of Infused $[O_2, 90_2]_s$ with an average normalized cracks density of 0.25.

The results obtained for the modelling of water diffusion on the different samples are presented on the Figure 179. This first comparison obtained from the model show that after 10 days of immersion the quantity of water absorbed in the different cases are similar, 83% of M_{∞} for the un-damage infused material and 90% M_{∞} for the damage infused material. This can explain why the pre-damage procedure did not accelerate degradation of the material during water ageing.

However, it has not been verified whether under a load of 327 MPa the cracks of the pre-damaged specimens were open. If this stress, which was the maximum possible on the test bed, was not sufficient to open the cracks that could explain the very similar results. A larger capacity test frame is being constructed to allow higher stress levels to be applied.

In this chapter different models have been developed or have been used to predict the effect of sea water ageing on materials. A first approach to model anisotropic diffusion in composites using the matrix diffusion coefficient has been presented. The damage model presented in Chapter II has then been used in order to predict damage initiation and development in these composite materials. It has been shown that the model can predict the threshold of damage after sea water ageing. The kinetics of the damage are also well described after long immersion in water. The diffusion model developed has been used in order to couple the effect of damage with diffusion kinetics. Diffusion kinetics of a damaged ply have been identified, and could be implemented in a larger diffusion model. Finally, results from first investigations into coupling between damage and diffusion have been presented. For the test conditions presented in this study, no significant effect of coupling between diffusion and damage has been observed on strength for these materials, but further work is needed to confirm this.

Dans ce chapitre différents modèles ont été développés et utilisés pour prédire l'effet du vieillissement en eau de mer sur les matériaux. Une première approche a été présentée pour modéliser la diffusion anisotrope dans les composites en utilisant les coefficients de diffusion de la résine. Le modèle d'endommagement présenté dans le Chapitre II a été utilisé dans le but de prédire l'apparition et la propagation de l'endommagement dans ces matériaux composites. Il a été montré que le modèle peut prédire le seuil d'endommagement après vieillissement en eau de mer. La cinétique d'endommagement est également bien décrite après une longue immersion dans l'eau. Le modèle de diffusion développé a été utilisé dans le but de coupler les effets de l'endommagement et de la diffusion. La cinétique de diffusion d'un pli endommagé a été identifiée, et peut être

implémentée dans un modèle plus important. Finalement, les résultats de cette première investigation sur le couplage entre la diffusion et l'endommagement ont été présentés. Pour les conditions d'essais présentées dans cette étude, aucun d'effet significatif du couplage diffusion/endommagement n'a été observé sur la résistance des composites.

Chapter V. **General conclusion**

Table of contents

<i>Chapter V. General conclusion.....</i>	<i>214</i>
1. Conclusion	215
1.1 Effect of accelerated sea water ageing on different composites	215
1.2 Modelling composite long term behaviour.....	216
1.3 Material choice for tidal turbine blades.....	217
2. Perspectives.....	218
2.1 Sea water ageing at lower temperature	218
2.2 Interface degradation and diffusion	218
2.3 Coupling diffusion under loading/damage/diffusion	219
2.4 Sea water ageing and fatigue	219
2.5 Composites protection, abrasion, impact, shock.....	220

1. Conclusion

Renewable marine energies are emerging, especially tidal turbines, and these structures are subjected to complex loads and will be immersed in sea water for 25 years or more. For these applications and this type of environment composite materials are good candidates. However, these materials are not insensitive to sea water. Glass fibre reinforced polyester, vinylester and epoxy materials have been used in applications such as yachting and offshore, so the long term behaviour of these composites is now quite well known. Nevertheless, for new highly loaded applications such as tidal turbines, most blade developers have preferred to use carbon/epoxy composites, and in this specific application, the sea water ageing studies on carbon/epoxy are very rare. For this reason, in this study, three carbon/epoxy composites, which are all candidates for tidal turbine blades have been studied and compared. These materials have been manufactured using different processes, pre-preg autoclave, RTM and vacuum infusion process. The aim is to provide the data necessary for understanding the influence of marine ageing on these materials and to contribute to predicting long term behaviour. No previous studies have been found which provide these data.

1.1 Effect of accelerated sea water ageing on different composites

The first step is to understand the diffusion process for the three different composites in order to predict water profiles. Gravimetric studies of the epoxy resin used to manufacture the RTM and the Infused materials, and the three composites have been performed at different temperatures of immersion in sea water, 25°C, 40°C, 60°C and 80°C. For the epoxy resin and its composites (RTM, and Infused), it has been highlighted that the diffusion processes are dependent on the water temperature, while diffusion in Pre-preg composites with a higher T_g remains independent of temperature. As tidal turbine blades are thick and as their thickness and orientation may change along the blade section, it has been necessary to characterise the influence of composites thickness and orientation on sea water diffusion process. It has been shown for the different composites, that sea water diffusion process is independent of fibre orientation and thickness. Finally, the normalized kinetics of diffusion are very similar for the three materials, even though the water content in the RTM material was significantly higher due to higher porosity content compared to the Pre-preg and Infused materials.

Based on this first step it was decided to age RTM and Infused specimens for mechanical property characterization at 60°C and the Pre-preg at 80°C in order to accelerate this sea water ageing process.

The three composites of the study have been characterised with different mechanical and physico-chemical tests before and after sea water ageing (until saturation of water and then after saturation plus one and two months). For the Infused and RTM composites it is the plasticization of the epoxy matrix which dominates long term properties. While moduli change little strengths drop, both in the longitudinal and transverse directions. One exception is interlaminar fracture toughness, for which no significant changes have been found. However the validity of the test to characterise composite toughness in these conditions is questionable due to the influence of stitching and multiple crack development after ageing. These phenomena may increase artificially the composite toughness, hiding a possible change during sea water ageing, and indeed when initiation values are determined these follow the same trend as strengths. An original study was performed on 0/90° laminates to evaluate damage initiation and propagation. It has been found that damage initiation is also a function of ageing, sea water ageing causes a shift of the threshold of damage to lower loads.

1.2 Modelling composite long term behaviour

Two modelling aspects have been examined, in order to provide tools to contribute to the evaluation of long term tidal turbine blade performance. The first concerns the modelling of damage propagation in composites. This model is not new, there have been many previous developments to simulate damage in composites. However, in the present study the model is based on physical properties, which can be easily identified and followed at the different stages of sea water ageing, using standardized tests. The proposed damage model is thus based on two physical criteria, a strength criterion which provides the initiation of damage and an energetic criterion describing the kinetics of damage development.

The model has been applied before and after sea water ageing. The developed criteria simulate the shift of the threshold of damage after saturation time well, while the kinetics of damage remain the same after long immersion in water. After longer immersion time no more changes appear (threshold or kinetics), as was indicated by results from the experimental tests.

The second modelling tool developed was a diffusion model, in order to predict water ingress into composite blades in a marine environment. The aim of this model was to describe anisotropic

diffusion in composite materials in a simple manner, it uses a commercial FE code. Model parameters, resin diffusion kinetics and composite fibre diameter and content can be easily identified or found in the literature. Thanks to this development, it is possible to model diffusion in the transverse and longitudinal directions to fibres and then to determine composites diffusivities at lower temperatures, which are more realistic for the final application. As service life for tidal turbine blades is expected to be 25 years, it is important to be able to estimate how the blade will be affected by water after this period. This information is not available so a first model of diffusion in such a large structure has been proposed. Results indicate that after 25 years' immersion at 15°C of a 20 mm thick blade (one side exposure) the blade is not fully saturated, though in some regions like the trailing edge (thinner region), saturation may be reached. This approach does not take into account the influence of mechanical loads on the diffusion process, and the possibility of damage development in the composite during the blade service life, which may result in faster diffusion.

For this reason some preliminary studies of coupling between water and mechanical damage have been performed. It has been possible to identify the diffusivities of the damaged plies and in future modelling it will be possible to use these new diffusion coefficients in tidal turbine blade calculations.

1.3 Material choice for tidal turbine blades

Three candidate materials for tidal turbine blades have been studied and compared before and after accelerated ageing. These materials have been manufactured under different conditions and with different materials. While Pre-preg manufacturing requires specific tools, materials, time and an important cost impact on final price, the RTM is more adapted for production in series but still requires specific tools and equipments; finally infusion uses a simpler mold with a vacuum bag. It has been shown that the three materials have similar diffusion kinetics and globally similar losses of mechanical properties after sea water ageing. As a consequence, if we consider a choice criterion cost/durability it seems that due to the Pre-preg cost, this material is unlikely to be competitive compared to the others.

2. Perspectives

Based on the results from a large experimental programme, some first conclusions about the durability of three carbon/epoxy composites for tidal turbine blades have been proposed. However there is a need for further investigations. The following section will propose some possible perspectives for future work to improve predictions of durability for composites used in renewable marine energy structures.

2.1 Sea water ageing at lower temperature

This study has revealed the limitations of accelerated sea water ageing procedures for materials such as RTM and Infused composites. Accelerated ageing at 60°C induced transitions in these materials and invalidates accurate quantitative prediction of the evolution of the properties, yielding only a conservative estimation. It seems more reasonable to age this type of materials at lower temperature, for instance at 40°C (or 25°C). However the acceleration factor to age the material then reduces. There is an acceleration factor of 4 between 60°C and 40°C but at 25°C it requires 10 times longer than at 60°C to saturate the sample in water. As presented in Chapter III, the time needed to age 2 mm thick samples at 25°C is 500 days, but for 1 mm only 150 days are needed. However reducing the thickness presents some limits. When thin samples are manufactured, there is a need to have a microstructure, fibre content, ply thickness and void content still representative of thicker material and the final application.

2.2 Interface degradation and diffusion

While matrix changes dominate the long term behaviour micrographic observations suggest that the fibre/matrix interface is also affected by sea water. First the matrix is degraded until saturation in water and composites properties drop. But after saturation in water it is possible to observe further loss of properties. This may be due to the slower process of interface degradation. As a consequence there is a need to study the influence of sea water on interface degradation during ageing, especially for carbon/epoxy. It is possible to modify carbon fibres surface treatments to improve long term durability of the interface, [213],[214],[215],[216]. Modifying the interface may also affect diffusion phenomena locally. Measuring interface diffusion is not a simple task but more information on this region is required to improve confidence in long term behaviour.

2.3 Coupling diffusion under loading/damage/diffusion

The perspectives of coupling under loading or with damage are numerous. However, it is important to have more feedback about the real loading cases for this application. This type of data is really critical but due to confidentiality few published results are available even though some tidal turbine projects in the water have been equipped with data loggers and instrumentation.

The study of the coupling between moisture and mechanical stress is a large subject and is being addressed in another PhD [217]. It requires special equipment and in the present work only a few preliminary tests have been performed.

However, in this study two models have been developed, one to predict damage in composites subjected to water ageing and the other to predict water diffusion in composites. A future study could focus on coupling the two models. However, the nature of the models are different, and more work is needed in order to achieve this coupling, involving the nature of the meshes used, and optimizing the time step.

2.4 Sea water ageing and fatigue

For tidal turbine blades applications, fatigue loading must be considered, and, it is also important to investigate the influence of sea water ageing on carbon/epoxy composite fatigue behaviour. Very few published data are available and this is an area which requires further work. Some preliminary tests have been performed in this project, in four point flexure, and an example of test results is given below, Figure 180. Details of the test procedure are given in appendix O.

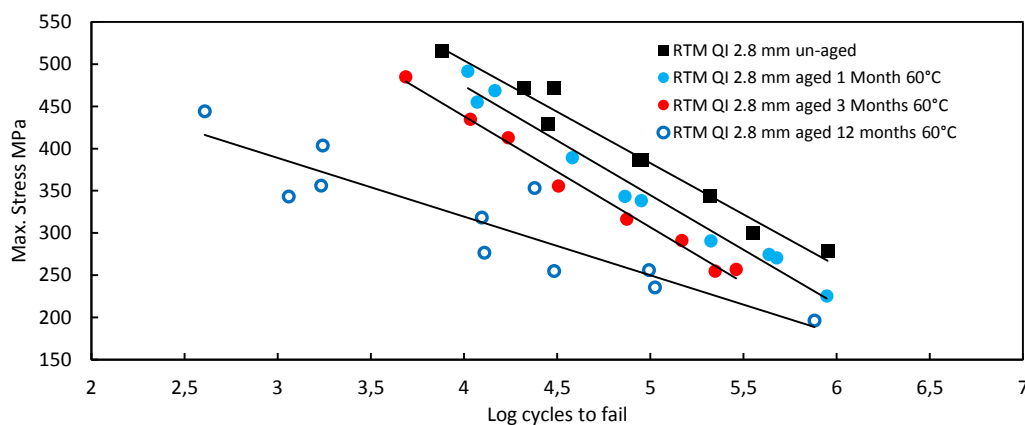


Figure 180: Example of fatigue results for RTM QI samples before and after seawater ageing.

The un-aged specimens fail in compression but after ageing 90° damage and delamination occur. This might be expected, given the influence of ageing on 90° tensile strength, and suggests that there is scope for optimization of material selection with respect to fatigue lifetimes (see figures in Appendix 32). This is critical aspect for long term reliability, and must be investigated further.

It is also possible that fatigue loads may induce some changes in the kinetics of diffusion. It would be interesting to couple water uptake measurements with fatigue tests in further investigations.

2.5 Composites protection, abrasion, impact, shock

Finally, the question of composite protective coatings has not been examined during this study. However tidal turbine blades are generally protected during their immersion in water. This can involve protective layers for instance, an epoxy primer, paint, but also specific coatings to limit bio fouling. These coatings will act as a barrier for water diffusion, some work has been performed on this subject for racing boat applications [218]. Moreover it is possible to take into account this barrier effect in a multi-layer diffusion model, after measuring the diffusivity of the coating. However, the long term durability of such coatings is questionable, at sea bed level and in high tide locations the abrasion and impacts are likely to damage coatings (and the underlying composites), and this is another area requiring further study.

The Figure 181 below summarizes the work performed in the present study and the further studies required.

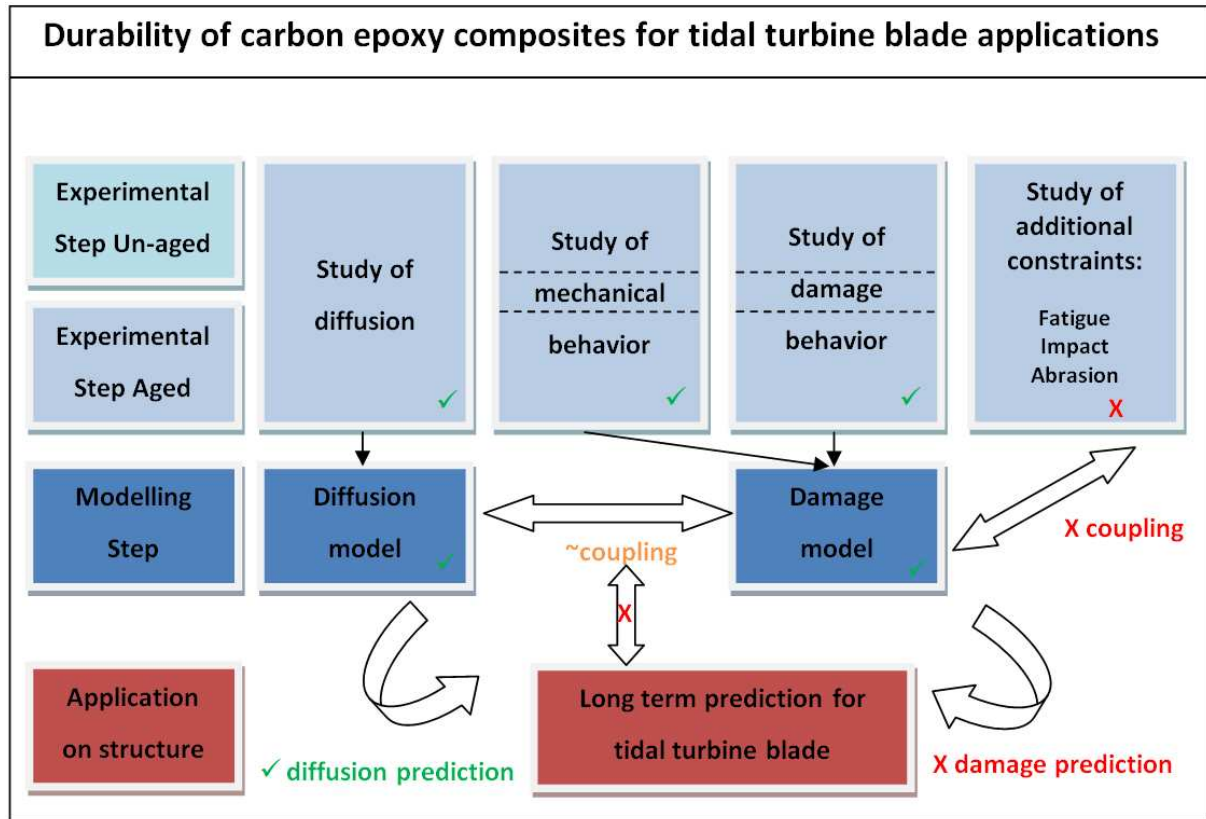


Figure 181: Overview of work performed (green tick) and required (✗).

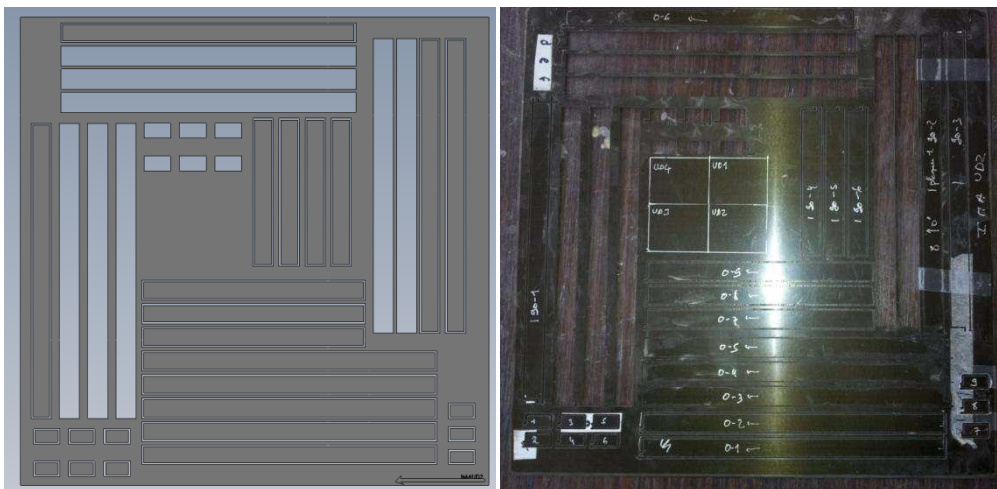
Appendix Chapter II

A. Appendix: Specimen preparation

This section presents the procedure applied in order to prepare samples after receiving composites panels.

In The figure in Appendix 1 shows the cutting steps applied for each composite panel. The figure in Appendix 2 is divided into steps numbered between 1 and 7.

The step number 1 is the cutting of the composite panels. As the specimen cutting method can affect composite mechanical and water diffusion properties [219], all specimens tested were cut using the same high pressure water jet cutting method and parameters. All plates have been cut at the GMP department of the IUT in Brest. The figure in Appendix 1 (a) shows a pre-preg panel after water jet cutting. A number has been assigned for each specimen to know its location in the plate after cutting. Due to low quantity of certain materials and the cost of production of some composites panels, an optimisation of space and cutting was performed, to allow an adequate quantity of specimens for tests. The figure in Appendix 1 shows an example of a cut panel and the optimisation of the space on composite panel using design tool software.

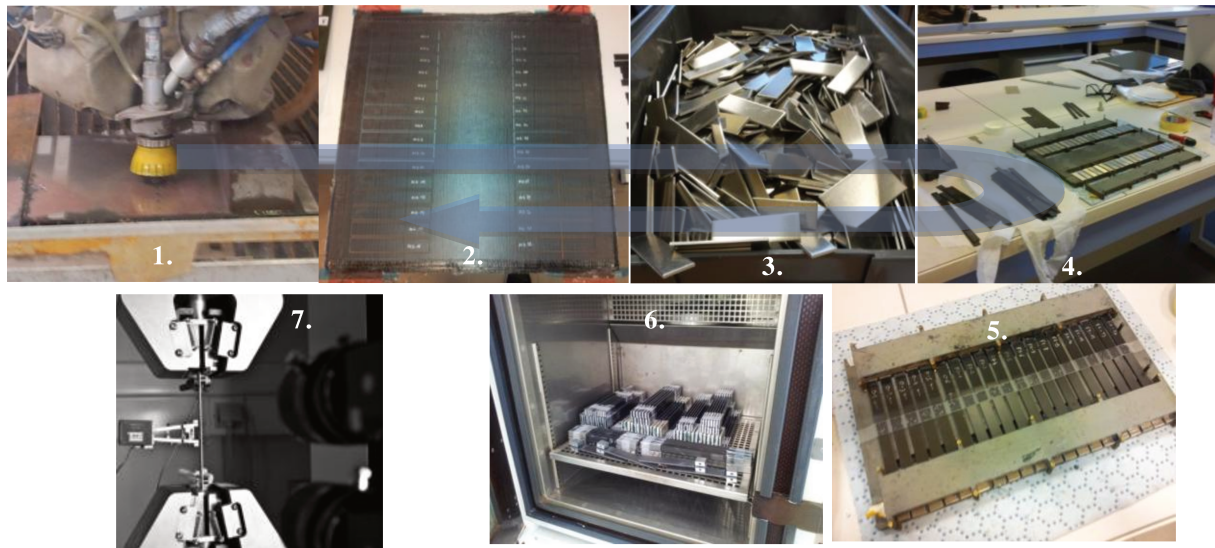


(a)

(b)

Appendix 1: Optimisation of the space using design tool (a), and Pre-preg panel after water jet cut (b).

Then step 2 consists of giving each specimen a unique reference as a function of its ageing process and test type. This step provides traceability in case of problems during the tests.

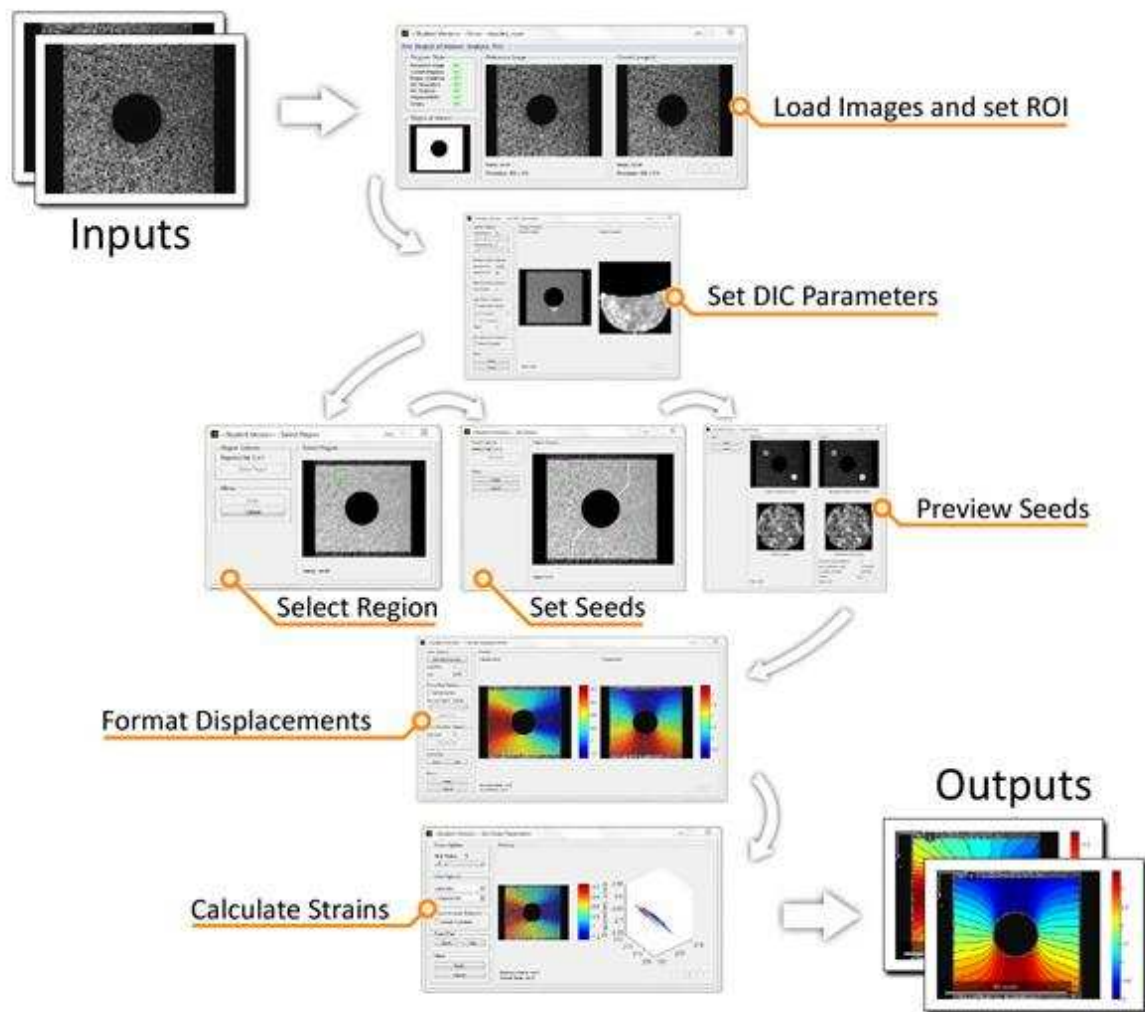


Appendix 2: Preparation procedure for all specimens.

Steps 3, 4 and 5 concern the bonding of aluminium tabs on specimens (for tensile and DCB tests). For tensile tests and other tests using tensile machine, the average tab dimensions were a length of 50 mm, 25 mm width (this size could change depending on materials and specimen size) and a thickness of 2 mm. The tabs were in marine aluminium alloy. Both specimens and tab surfaces were sanded with 120 grade paper and then cleaned with acetone. Finally tabs and specimens were bonded using Huntsman Araldite 420 A/B, which is widely used in structural marine applications and known to have a good tolerance of sea water exposure. The penultimate step 6, was curing the Araldite 420 AB, to ensure a good polymerisation state of this adhesive. Specimens underwent a short low temperature cure, below their T_g , so as not to modify the T_g of the composites. Thus a curing step of 2 hours at 50°C was used to cure the adhesive.

B. Appendix: Ncorr

This flowchart presents the Ncorr procedure allowing composite strains to be determined using digital image correlation.

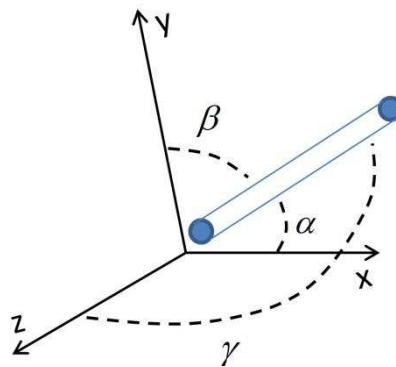


Appendix 3: Digital Image Correlation process for strains determination using Ncorr code.

Appendix Chapter III

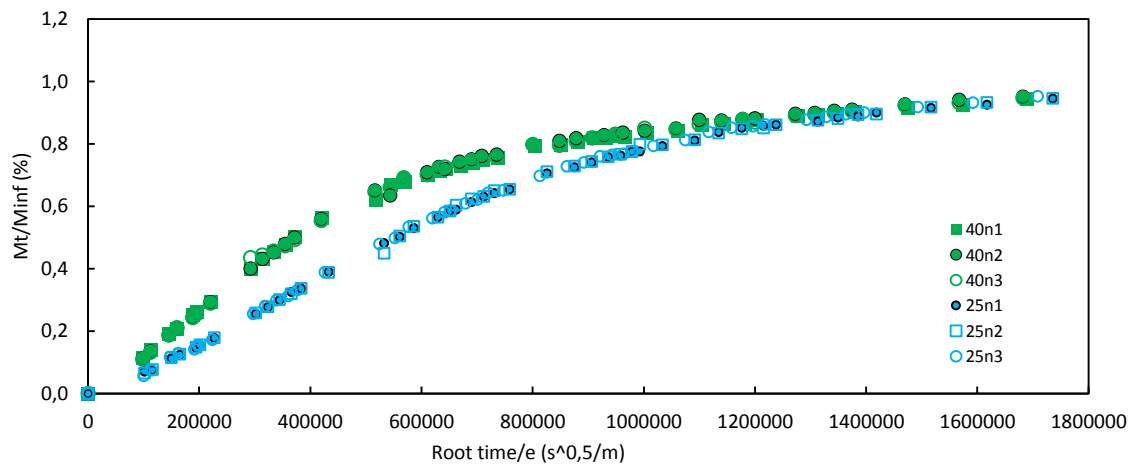
C. Appendix: Diffusion

This appendix gives additional information about diffusion in the composites of the study. The first figure, Appendix 2, presents the fibre orientation and the corresponding angles which are used in order to estimate diffusion coefficient as function of diffusion direction and fibre orientation.



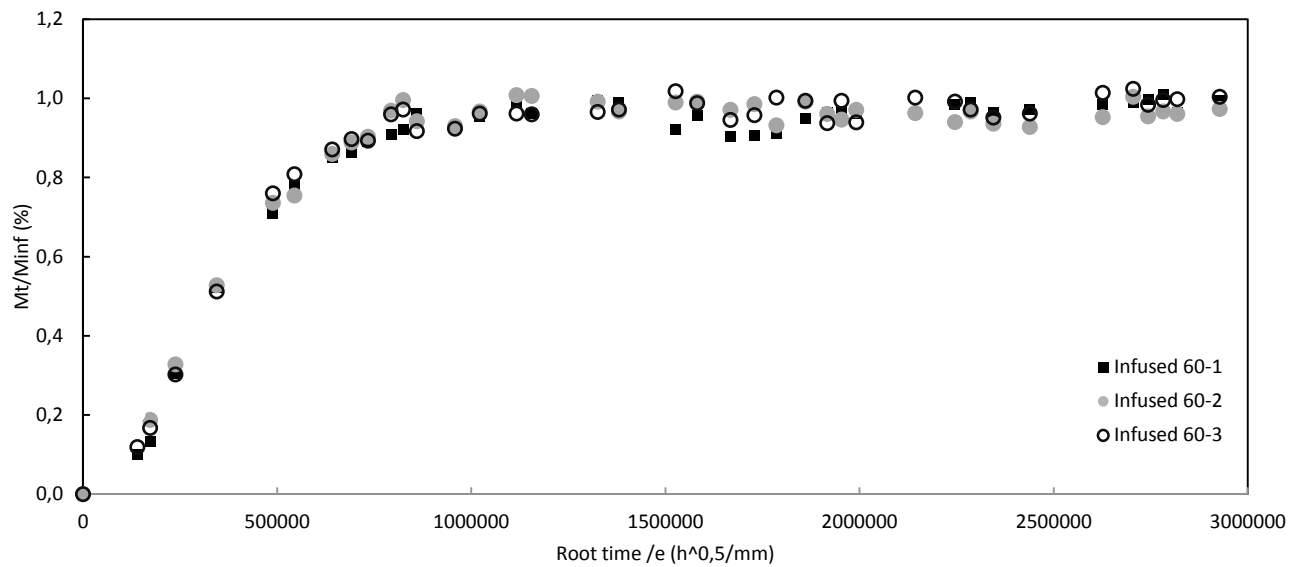
Appendix 4: Fibre orientation and corresponding angles.

The figure, Appendix 5, gives an example of the scatter in weight gain measurements for the epoxy resin at 40°C and 25°C. Results show little dispersed.



Appendix 5: Example of measurement variability on the epoxy resin at 40°C and 25 °C.

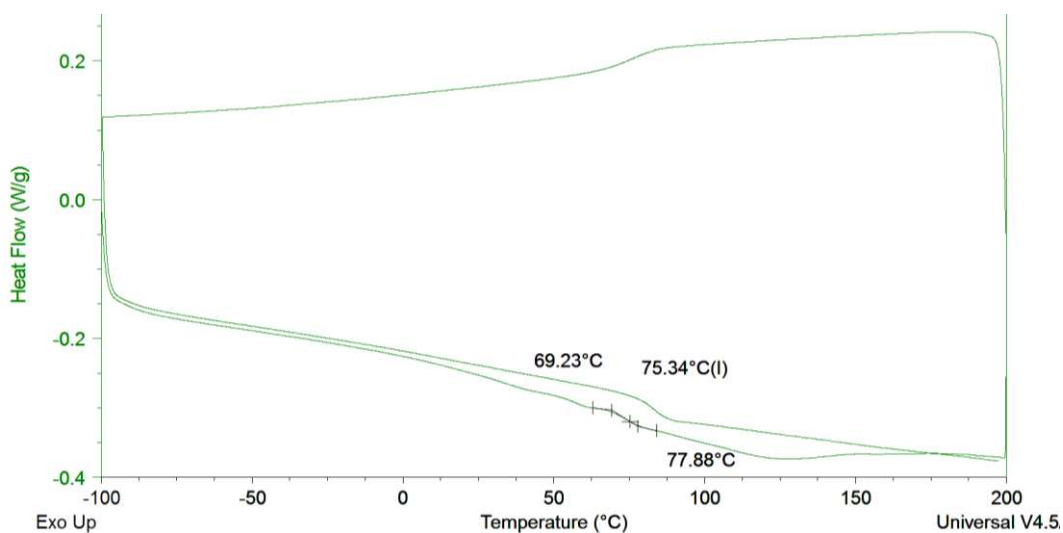
The Appendix 6, gives an example of the scatter in weight gain measurements for the Infused carbon/epoxy at 60°C. Measurements again present little variability.



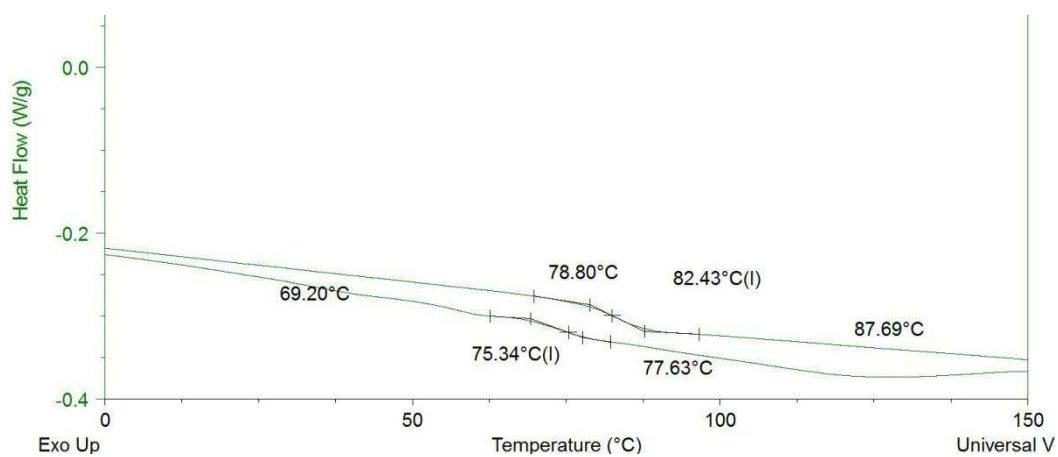
Appendix 6: Example presenting the scattering of gravimetric measurement for three samples of Infused UD material at 60°C.

D. Appendix: Differential Scanning Calorimetry

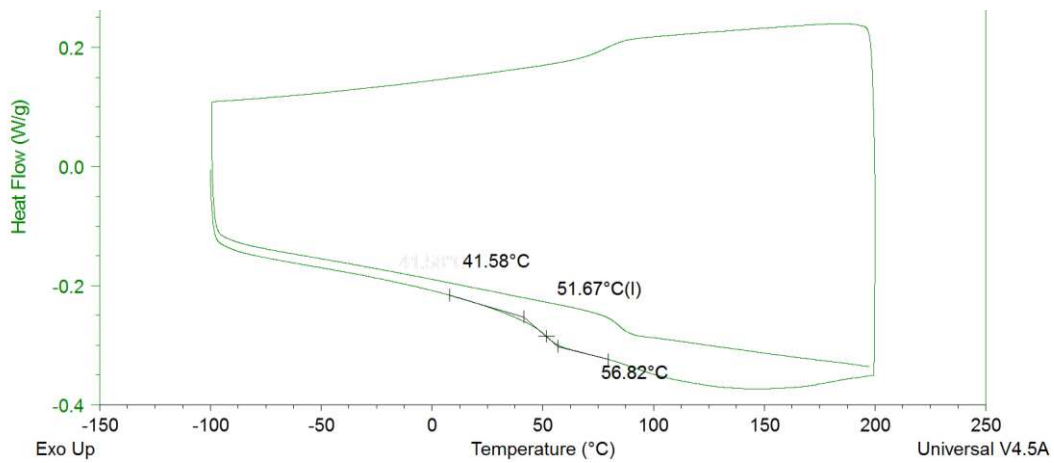
In this appendix section different DSC analyses are presented on the three materials of the study before and after sea water ageing.



Appendix 7: Glass transition measurement for un-aged Infused material.

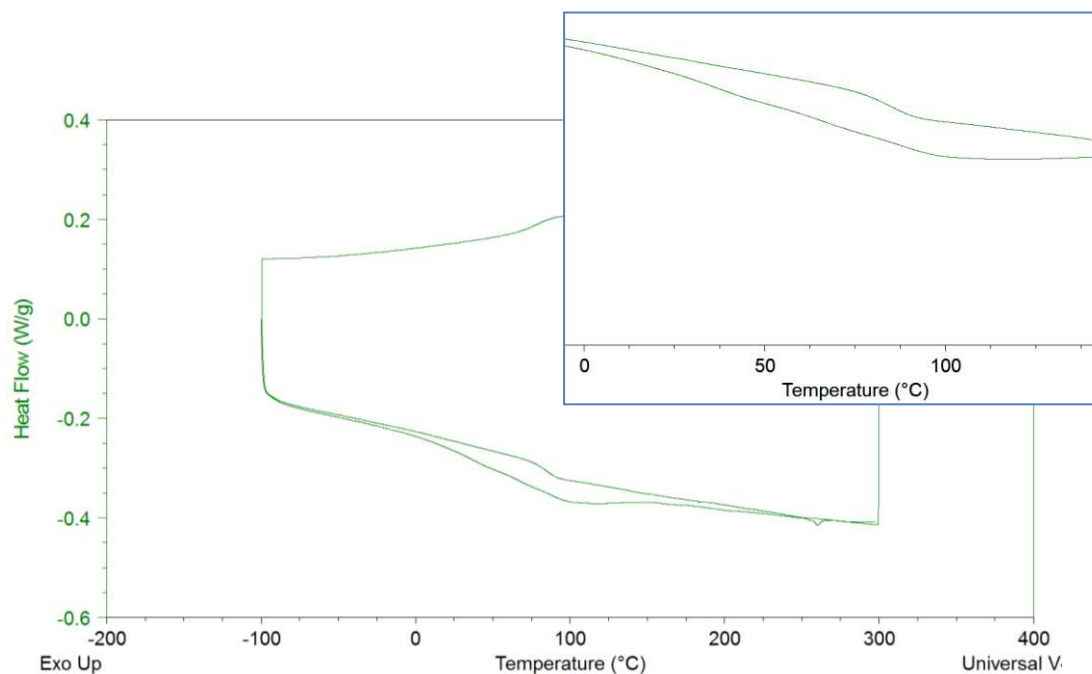


Appendix 8: Glass transitions measurement for un-aged Infused material, this focus presents the difference of Tg after the first and second DSC run.



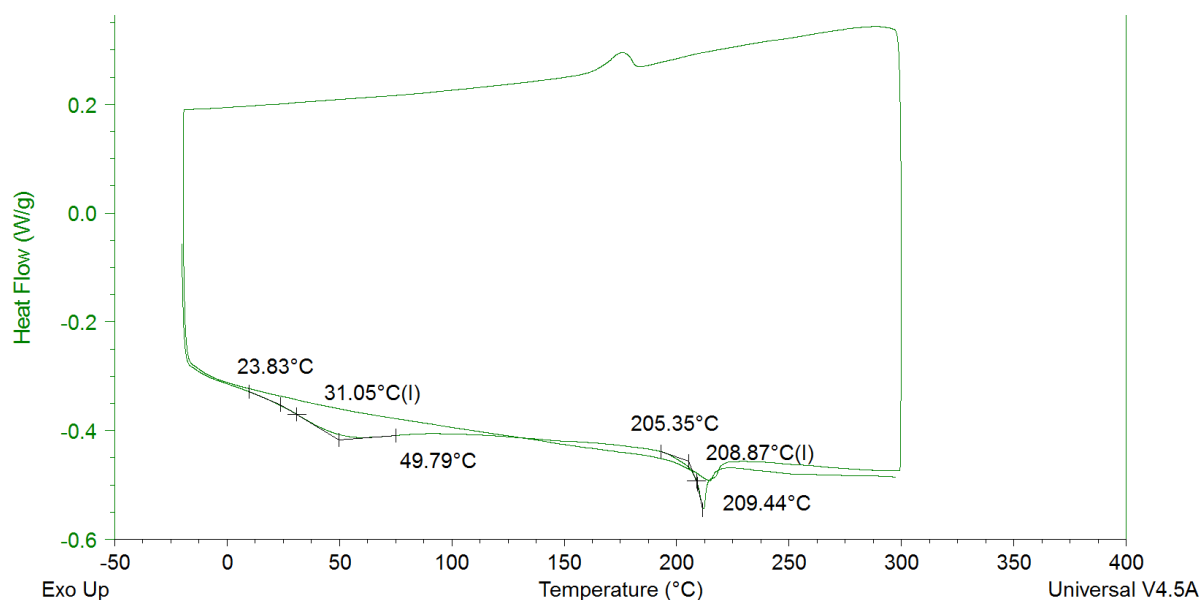
Appendix 9: Glass transition measurement for Infused material at saturation time.

The figure on the Appendix 10 presents a DSC analysis performed on the RTM materials after saturation time plus one month. During the first run it was difficult to identify clearly the glass transition which could be superposed on water evaporation phenomena. Due the important quantity of water in this material it was difficult to follow T_g evolution during ageing

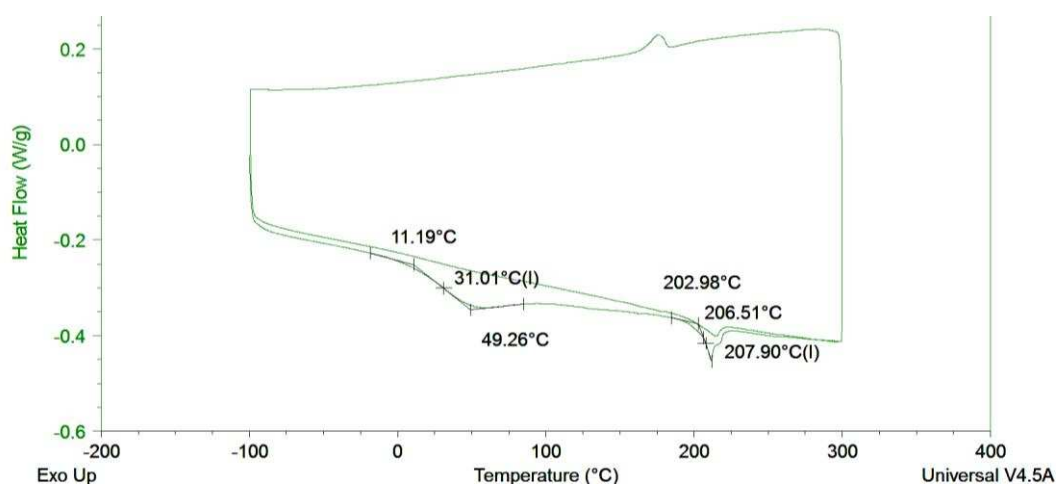


Appendix 10: Glass transition measurement for RTM material at T₂.

The DSC analysis in Appendix 11 and Appendix 12 show that sea water ageing does not affect the glass transition of the Pre-preg material. The first transition at 31°C remains constant, but this transition has not been clearly identified, it may be related to nodules



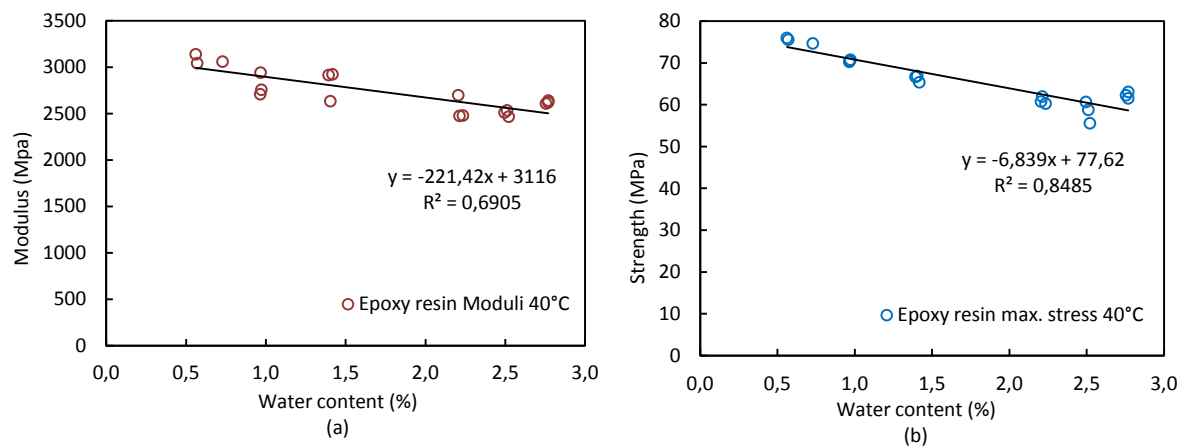
Appendix 11: Example of glass transition measurement for Pre-preg material before ageing.



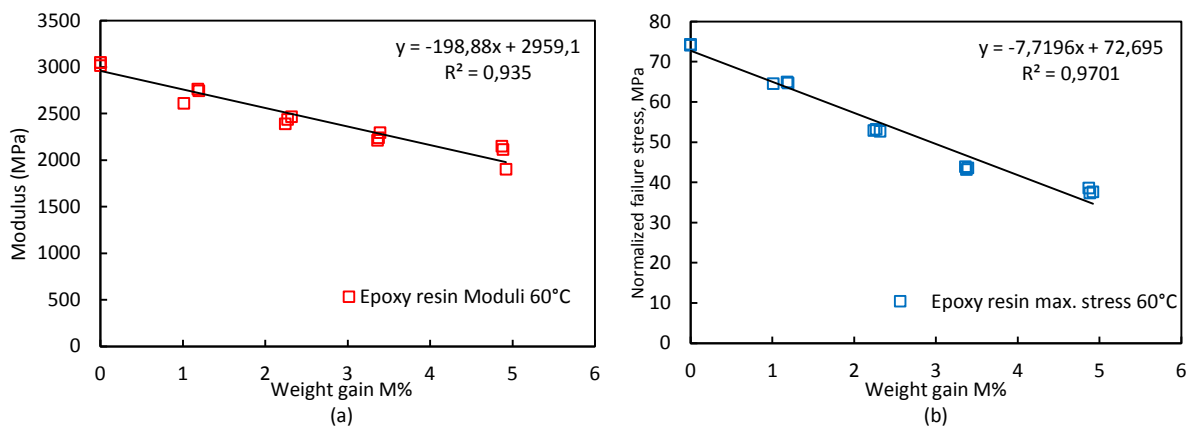
Appendix 12: Glass transition measurement for Pre-preg material at T3 (saturation time + 2 months). First transition linked to the thermoplastic nodules second to composites Tg.

E. Appendix: Tensile tests on epoxy resin

The figures of this section are related to tensile tests on pure epoxy samples. The aim of this part was to study the effect of accelerated ageing at 60°C and 40°C on matrix tensile strength and modulus. The figures in Appendix 13 present the loss of epoxy tensile modulus and strength as a function of water content during sea water ageing at 40°C. In Appendix 14 the figures represent the same procedure at 60°C.



Appendix 13: Evolution of pure resin tensile modulus (a) and strength (b) versus water content, aged at 40°C.



Appendix 14: Evolution of pure resin tensile modulus (a) and strength (b) versus water content, aged at 60°C.

F. Appendix: Tensile properties estimation

In this appendix, the method allowing composites stiffness to be estimated before and after ageing is presented. The table below presents the fibre and matrix properties used for this estimation. Additionally the next table compares this estimation and the experimental results. This estimation is based on a composite law of mixtures presented in the following equations.

Infused matrix and carbon fibres properties	T0	T1
E_f (GPa)	290	290
E_m (MPa)	3.05*	2.5*
V_f (%)	54*	54*

**Properties experimentally measured*

Appendix 15: Fibre and matrix properties for the infused materials, before and after saturation time.

Infused UD Properties	Theoretical T0	Experimental T0	Theoretical T1	Experimental T1
E_{11} (GPa)	158.0	136.9	157.7	141.2
E_{22} (MPa)	6.5	7.1	5.38	6.0

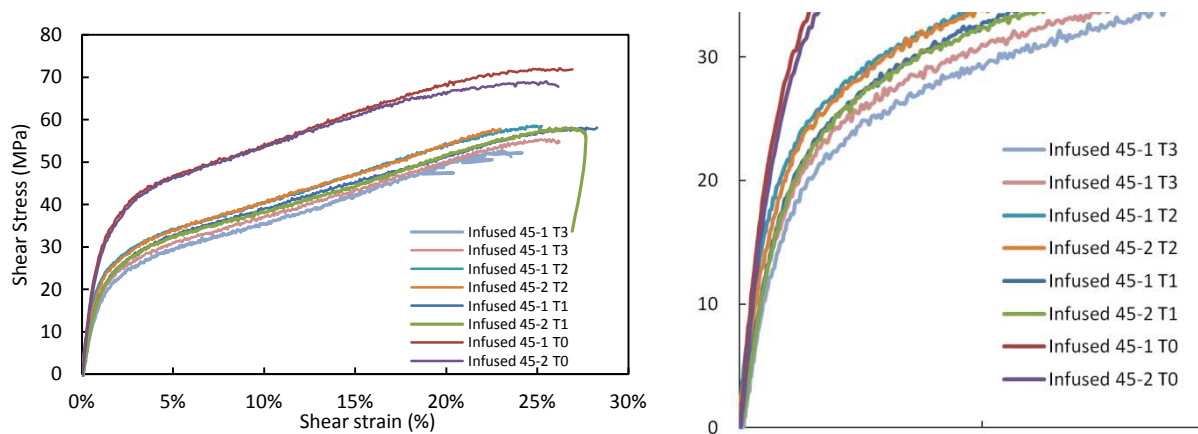
Appendix 16: Comparison between the properties estimated by micromechanics and experimental values before and after saturation time for the Infused material.

$$E_{11} = V_f \times E_f + V_m \times E_m \quad \text{and} \quad \frac{1}{E_{22}} = \frac{V_f}{E_f} + \frac{V_m}{E_m}$$

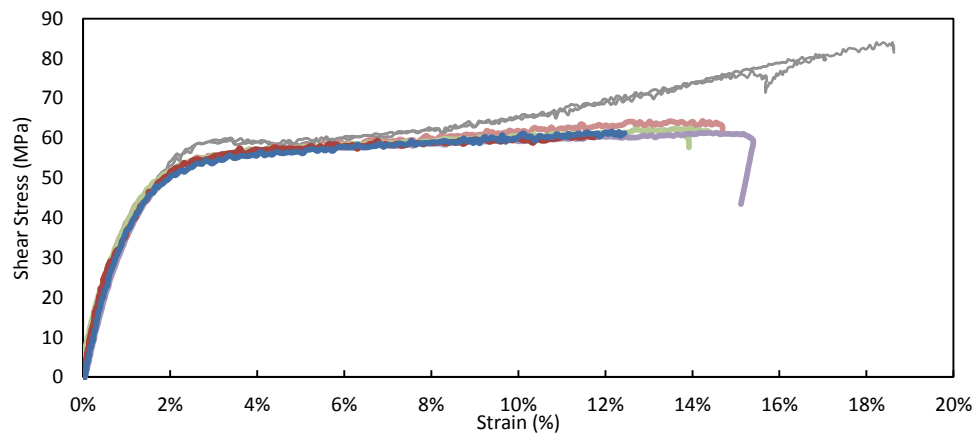
Appendix 17: Equations based on composite mixture law used to estimate longitudinal and transverse moduli.

G. Appendix: In-plane shear test by tension on $\pm 45^\circ$ specimens

In this appendix section, some results are presenting on the effect of sea water ageing on the in-plane shear response in tension for the Infused and Pre-preg materials. Samples have been tested in the un-aged state and after saturation in water. The stacking of the samples was $[\pm 45^\circ]_{8s}$.



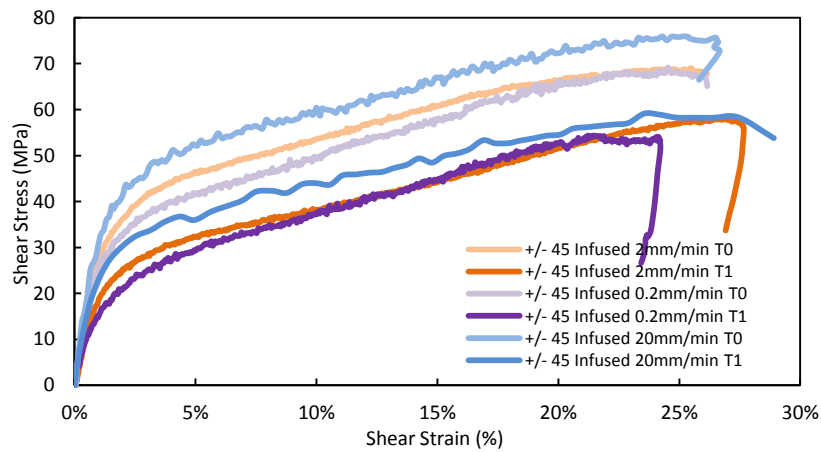
Appendix 18: Shear stress response of the Infused carbon/epoxy materials before ageing and after ageing.



Appendix 19: Shear stress response of the Pre-preg carbon/epoxy materials before ageing (grey) and after ageing.

H. Appendix: Tensile test on $\pm 45^\circ$ specimens at different loading rates

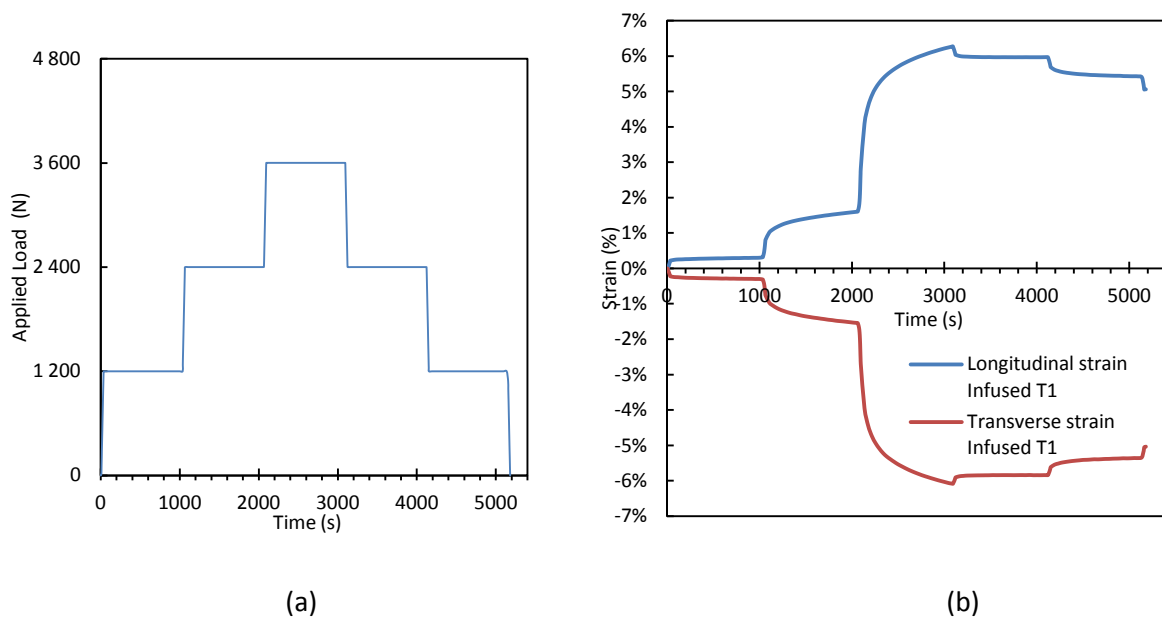
The graph below presents the different results for the effect of load rate applied on un-aged Infused material samples and specimens saturated in water. The stacking sequence of the samples was $[\pm 45^\circ]_{8s}$.



Appendix 20: Effect of different load rates on un-aged and aged Infused material.

I. Appendix: Creep test

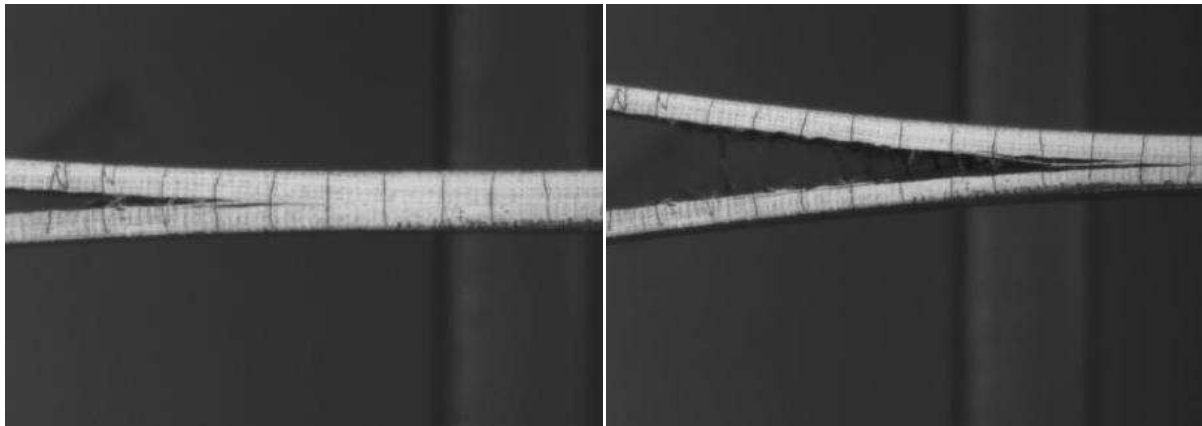
In this section more details are given concerning the loading steps applied during creep test (a). A second graph (b) presents results obtained on Infused material after saturation. Longitudinal and transverse strains are plotted as a function of time. The stacking of the samples was $[\pm 45^\circ]_{8s}$.



Appendix 21: Creep test at the different loading steps applied to the specimens (a) and the observed results at different loading steps (b) for the Infused material.

J. Appendix: DCB test

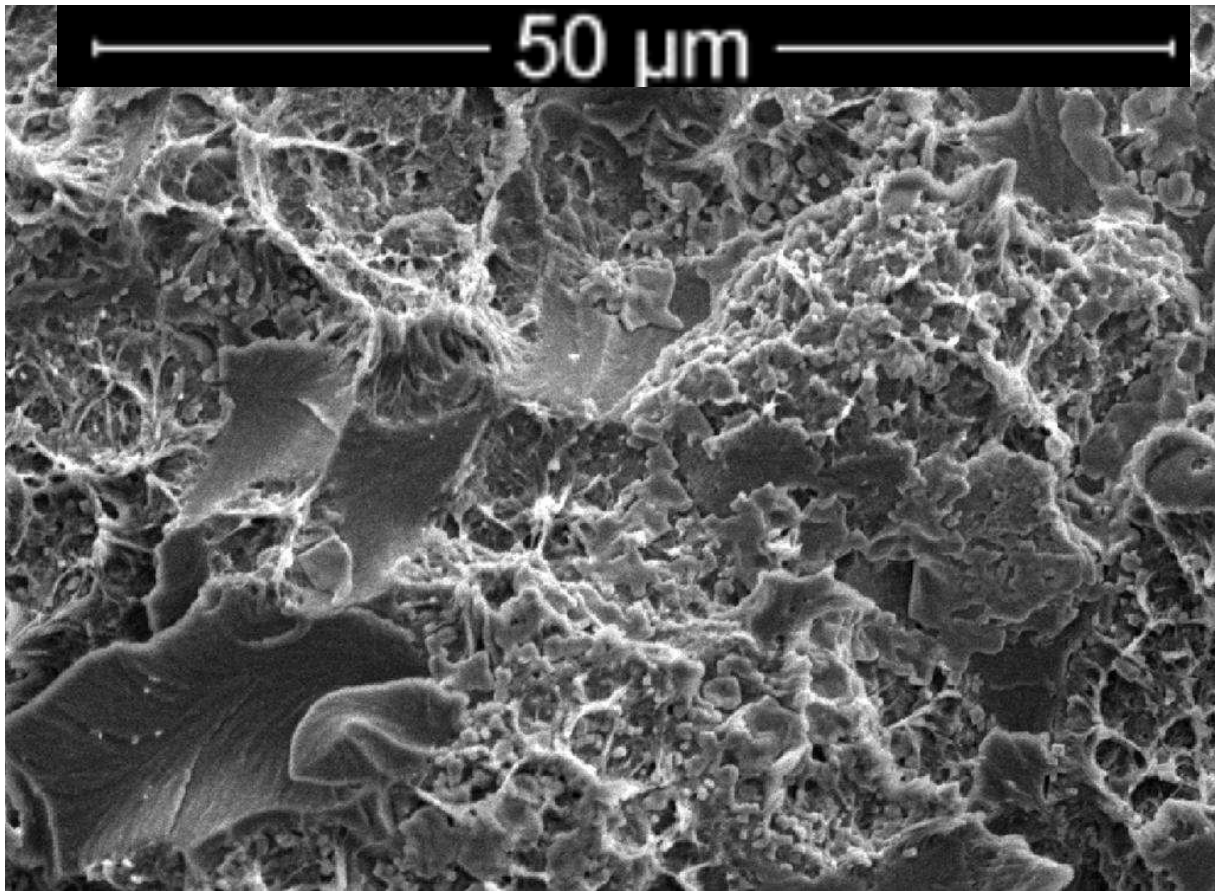
The figure below presents an example of multiple crack development during a DCB test on an RTM specimen after sea water ageing. This multiple crack development would invalidate the use of DCB tests to characterize composites propagation toughness in mode I. The thickness of the specimen is approximately 5.1 mm.



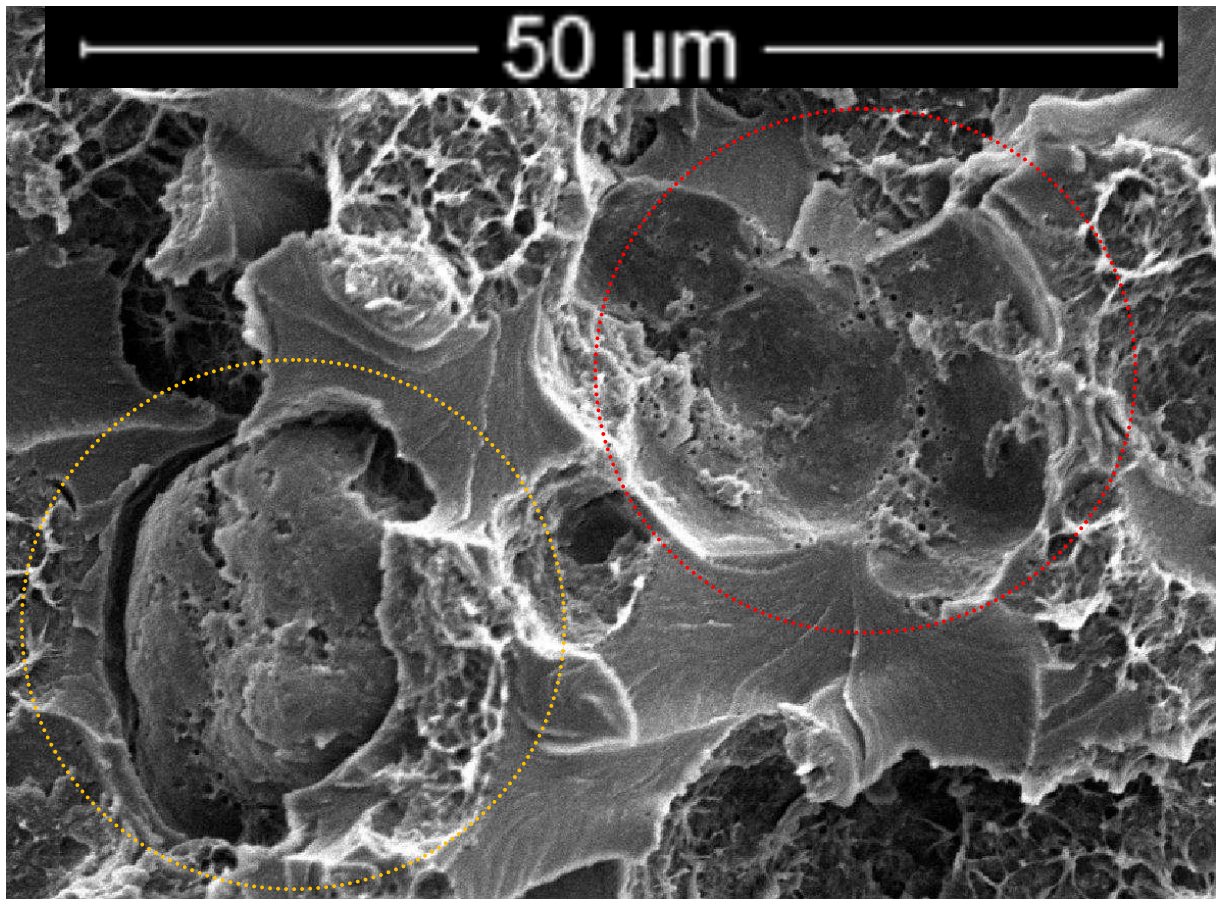
Appendix 22: Examples of multiple crack development after sea water ageing T3 on UD RTM specimen.

K. Appendix: SEM

The following figures in this appendix present a zoom on DCB fracture surface after crack propagation on Pre-preg material, un-aged and aged T3. The figures are focused on the thermoplastic nodules, showing the difference in fracture around these nodules.



Appendix 23: Focus on nodules in un-aged Pre-preg material after DCB test. Approx size of the nodule is 20μm.

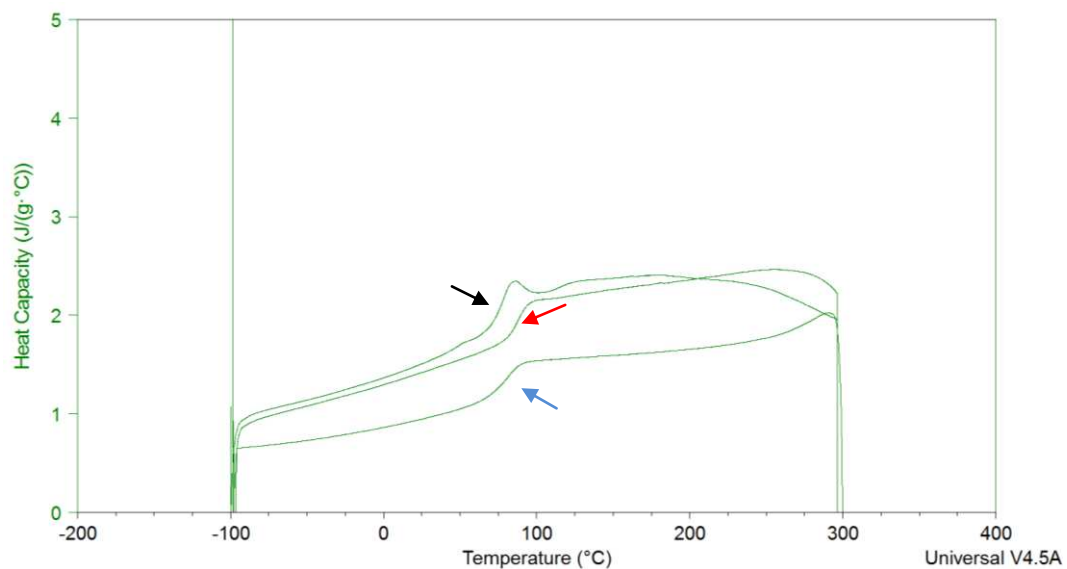


Appendix 24: Focus on nodules in Pre-preg material after DCB test. Sample was aged T3. Approx size on the nodule is 20μm.

Appendix Chapter IV

L. Appendix: Diffusion parameters

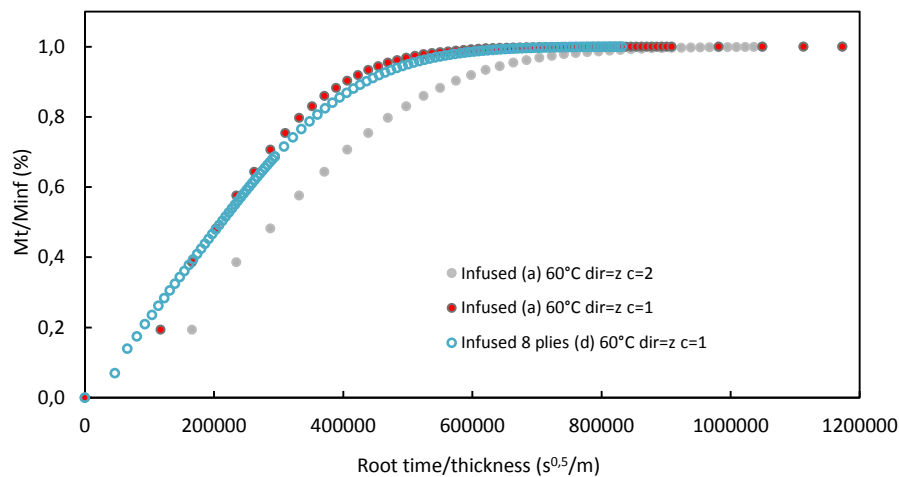
In order to determine diffusion parameters to implement the model, DSC analysis has been performed in order to determine the heat capacity of the epoxy resin. DSC analysis was performed on a neat epoxy sample. In the following appendix the evolution of the heat capacity as a function of the temperature is presented, black arrow shows the first temperature scan, red arrow the second, and the blue arrow shows the cooling after the first scan.



Appendix 25: Heat Capacity determination for the epoxy resin using DSC.

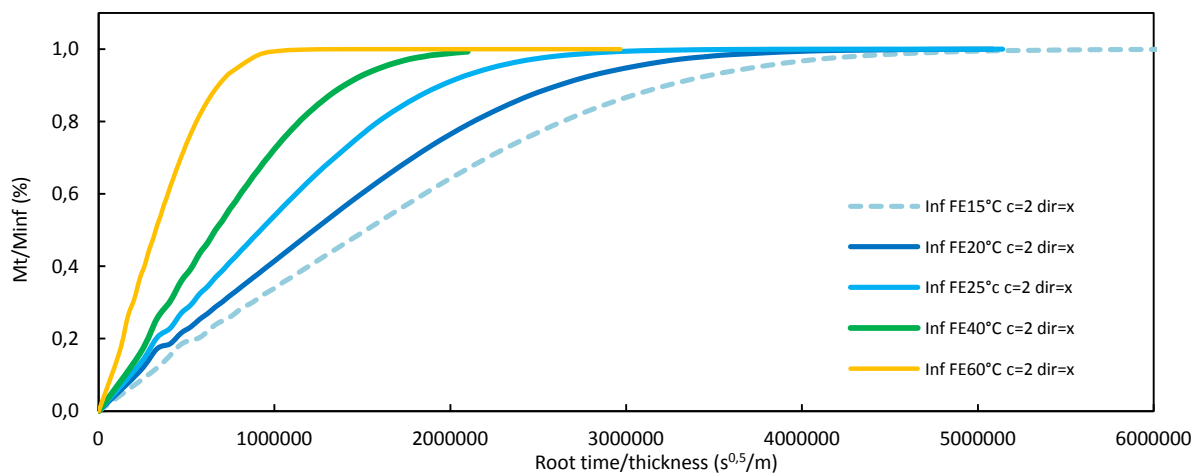
M. Appendix: Diffusion model

In the figure below, two different geometries have been used in order to see if the fibre arrangement in the model has an impact on longitudinal diffusion. Using the geometry (a) which is the simplest one, allow the longitudinal diffusion through fibres to be determined without any correction.



Appendix 26: Comparison between geometry model (a) and (d) for Infused longitudinal direction.

In the following figure and table, more comparisons are provided for the model results at different temperatures for the Infused material (modelling diffusion in transverse direction to fibres). As presented in the following appendix.



Appendix 27: Modelling of transverse water diffusion in Infused material at 15, 20, 25, 40 and 60°C.

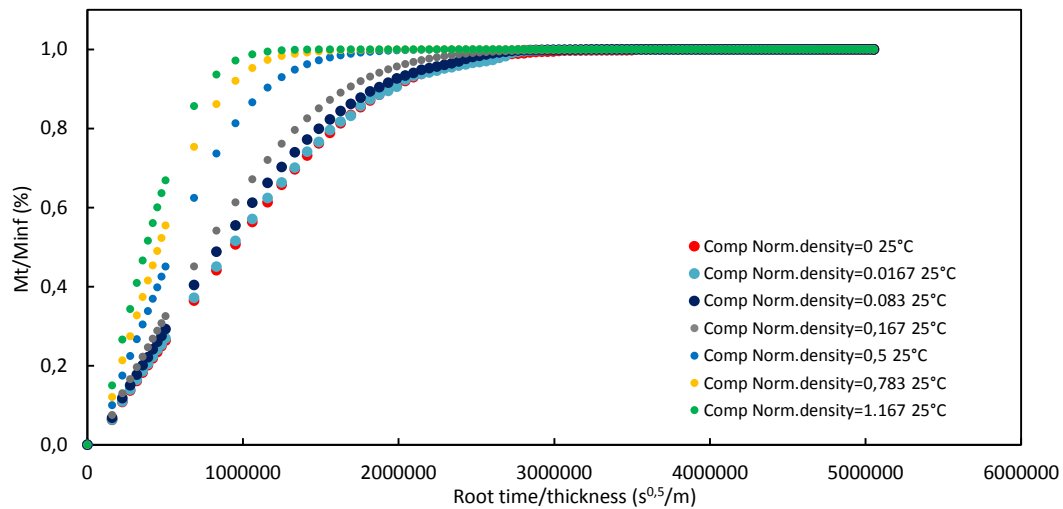
Modelling has been also performed on the RTM material at more realistic temperatures for the final application. These diffusion coefficients are presented in the following table.

Model diffusion temperature	RTM transverse diffusion coefficient D_x (m².s⁻¹)	RTM longitudinal diffusion coefficient D_z (m².s⁻¹)
15°C	2.02E-14	6.43E-14
20°C	3.13E-14	9.50E-14
25°C	5.84E-14	16.9E-14

Appendix 28: Coefficients of water diffusion determined in longitudinal and transverse direction to the fibres in the case of the RTM material for temperatures close to tidal turbine service conditions.

N. Appendix: Coupling diffusion/damage

Investigations into the effect of cracks on diffusion have been performed and modelled for different crack densities in the case of Infused material. The following graph represents the diffusion curves for the damaged 3D model.



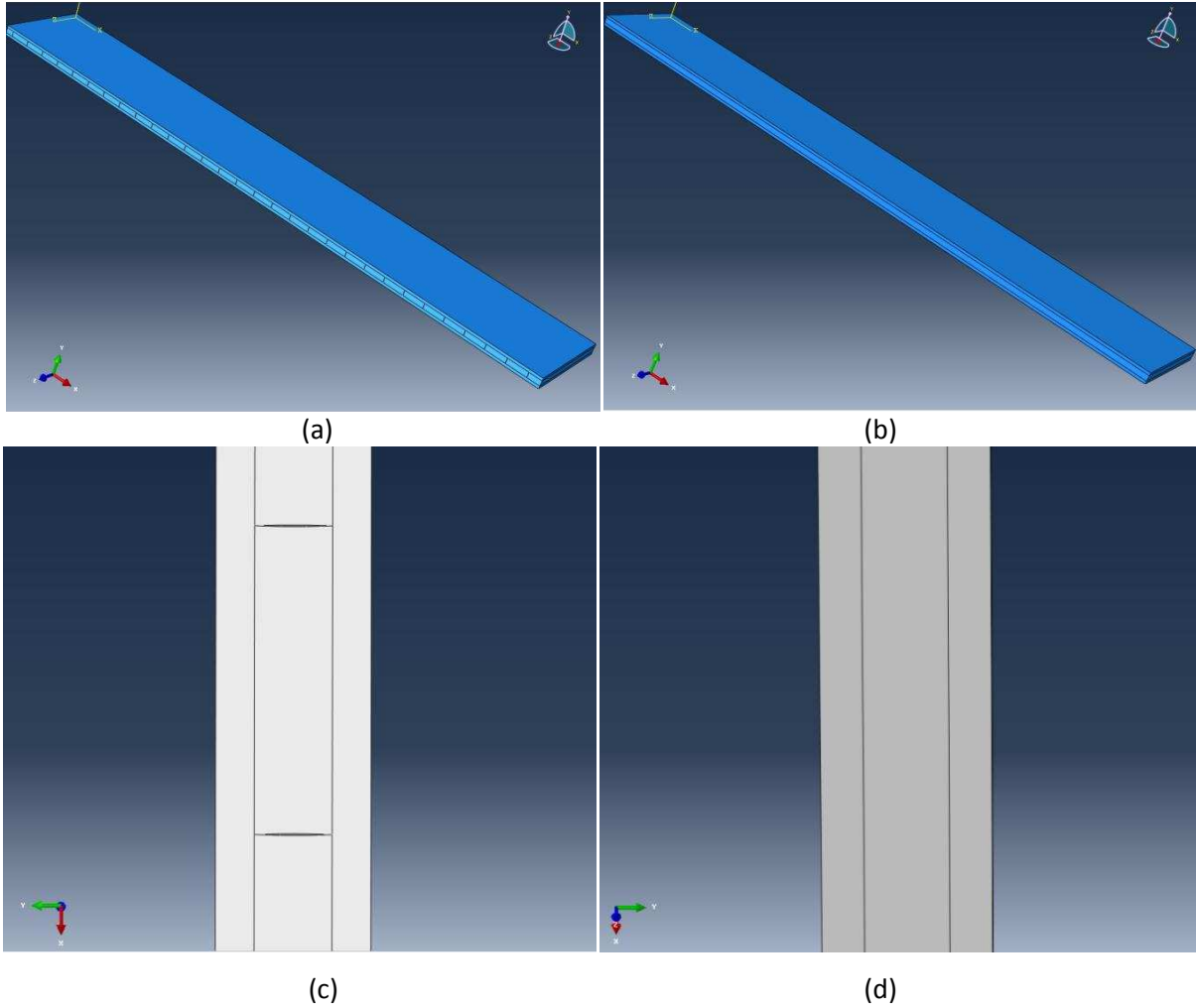
Appendix 29: Kinetics of diffusion for the each model with different normalized crack densities.

According to the previous diffusion curves, the diffusivities of the composite laminate [0,90,0] and for the 90° ply have been identified. The following table presents the diffusion coefficient obtained in perpendicular direction to the thickness (and the fibres).

Normalized crack density	Homogenised diffusion coefficient composite [0,90,0] D_x (m ² .s ⁻¹)	Identified diffusion coefficient on 90° ply D_x (m ² .s ⁻¹)
0.000	5.83E-14	5.83E-14
0.016	6.04E-14	6.47E-14
0.083	7.09E-14	9.61E-14
0.167	8.96E-14	15.2E-14
0.500	17.1E-14	39.6E-14
0.783	25.5E-14	64.9E-14
1.167	36.5E-14	97.7E-14

Appendix 30: Comparison between the homogenised diffusion coefficients of the composite obtained from the model and the identified diffusion coefficient of the damaged 90° ply as a function on the normalized density of this ply.

In order to understand the previous results (experimental coupling between diffusion and damage), some other investigations have been performed to compare the influence of damage on diffusion process. Thus damage model has been used in the two different cases presented on the Appendix 31 below. It is possible to distinguish the cracks in the 90° plies on the damaged sample represented in Appendix 31 (a) and (b). These 3D models are representative of the specimens tested.



Appendix 31: Illustration of the models used to determine the influence of damage on diffusion process on $[0_2 90_2]_s$ Infused material, for the case of pre-damage sample (a),(c) and for the un-damage sample (b),(d).

Appendix Chapter V

O. [Appendix: Fatigue tests](#)

In order to access preliminary fatigue tests on carbon epoxy materials, four point bending test has been chosen in order to apply cyclic loading on composites. For these first results RTM material has been chosen with a quasi-isotropic stacking sequence (same material as presented in Chapter II section 3.1.3 a). The average thickness of the tested samples was 2.77 (0.04) mm. For the four point bending test apparatus, distance between upper supports was 50 mm and 100 mm for lower ones. Cyclic loads have been applied with a hydraulic test machine at a frequency of 2Hz and $R=0.1$. Samples have been both tested before and after immersion in water at 60°C. The figures in the Appendix 32, present two examples of fatigue failure mode after sea water ageing.



Appendix 32: Examples of fatigue failure mode after sea water ageing on RTM QI 2.8 mm material.

Figure table caption

Figure 1: Illustration of possible technologies used for horizontal and vertical axis turbines [13].	12
Figure 2: Sabella D10 Tidal turbine (a) and CoRMat tidal turbine with 4 m RTM blades, courtesy of Airborne Marine and Nautricity Ltd (b).....	12
Figure 3: Example of open centre tidal turbine blade developed by OpenHydro and DCNS for the EDF project (a) [14] and the Bay of Fundy (b) [15].....	13
Figure 4: Blade cross-section at the root with acting bending moments: M_f – flap wise moment, M_o – in-plane moment and M_t – total moment, [30].....	14
Figure 5: 10 m blade pressure for extreme operating condition [31] (a), and pressure on the blade surface (pressure and suction side) for different tide velocities [25] (b).....	15
Figure 6: Composite reinforcement and matrix used for composite laminates.	16
Figure 7: Example of subtraction Fourier transform infrared spectroscopy after different times of water exposure for epoxy resin [53].	18
Figure 8: Representation of swelling due to water absorption between polymer chains at different steps of absorption, illustration from [62] (water molecules are represented by the black circles). ..	19
Figure 9: Shear fracture surfaces of the dry (a) and saturated specimens (c), saturated carbon/epoxy specimens were aged 37 days in distilled water [73].	20
Figure 10: Schematic illustration of possible moisture sorption locations and mechanisms (readapted from [77] by [53]).	21
Figure 11: Illustration of the different type of damage in laminated composites [84].	22
Figure 12: Possible composition of tidal turbine blade.....	23
Figure 13: Sabella tidal turbine blade during manufacturing, (a) one side of the blade body before vacuum infusion process and (b) final assembly of spar box and blade bodies [86].....	24
Figure 14: Airborne Marine tidal turbine blades for the Tocado turbine, these composites blades have been manufactured using the one shot RTM process [87].....	24
Figure 15: Infusion process [88].	25
Figure 16: RTM process method (a) [89] and the RTM mold developed by Airborne Marine to produce test plates (b) [90].	26
Figure 17: Pre-preg process tooling and components(a) [89] and an example of a part entering the autoclave (b) [91].	27
Figure 18: Overview of the study's methodology.	29
Figure 19 : A pre-preg part under vacuum going into the FMC autoclave, [91].	37

Figure 20 : AMBV (Alkmaar class Mine-hunting vessel) composite propeller and mould engineered by Airborne Marine.	38
Figure 21 : Infusion process (LBMS laboratory).	39
Figure 22 : Three part resin mould (a), gravity moulding process (b).	40
Figure 23 : Resin plate after polymerisation and curing.	41
Figure 24 : Example of density measurements for Pre-preg and Infused material.	44
Figure 25: Tensile test resin specimen dimension (a) and the specimens used for the tests (b).	47
Figure 26: Illustration of tensile modulus determination on the resin (a) and on the composite (b). .	48
Figure 27: Test procedure for the determination of in plane shear response of composites.	50
Figure 28: Definition of specimen and material axes according to ASTM D3518[11].	50
Figure 29: Comparison between normal strains measured by extensometer (doted lines) and image correlation (continuous lines) during tension test on +/-45° Infused laminates.	51
Figure 30: Illustration of shear modulus determination according to ASTM D3518.	52
Figure 31: Example of $\pm 45^\circ$ RTM specimens presenting voids on their surface.	53
Figure 32: Shear stress response of the three carbon/epoxy materials before ageing.	54
Figure 33: Four point bending test configuration according to ASTM D7264 standard.	55
Figure 34: Response of $\pm 45^\circ$ Infused composites at three different loading rates.	58
Figure 35: Creep behaviour of Infused materials, a) Loading sequence, b) creep strains/	59
Figure 36 : Amplitude distribution according to the damage mechanisms in composite materials [126].	61
Figure 37 : Test set-up to measure intralaminar tensile cracking.	61
Figure 38 : Visualization of cracks before (left) and after (right) Matlab™ processing on a $[0_2,90_2]_s$ sample.	62
Figure 39 : Visualization of cracks before (left) and after (right) Matlab™ processing on a $[0,90]_{4s}$ sample putting in exergue possible location of cracks.	62
Figure 40: Comparison between automatic counting (a) and manual (b) methods on $[0_2,90_2]_s$	63
Figure 41: Evolution of normalized crack density as a function of applied stress for Pre-preg (a) and Infused (b) materials. Pre-preg $[0_2,90_2]_s$: blue triangles, Pre-preg $[0_2,90_{1/2}]_s$: red squares, Infused $[0_2,90_2]_s$: grey squares, Infused $[0,90,0,90]_s$: blue circles for centre 90_2 and purple circles for single 90° plies on specimen sides.	64
Figure 42 : Fracture test loading modes.	65
Figure 43: Double Cantilever Beam Specimen.	66
Figure 44: Delamination length measurement using Measure Tool.	67
Figure 45: DCB test set-up.	67
Figure 46: Load displacement trace from DCB test [133].	68

Figure 47 : Modified Beam Theory (a) and Compliance calibration (b) for DCB test.	69
Figure 48: DCB initial and artificial delamination (a), pre-delamination and process zone initiation (b), growing of the delamination (c).	70
Figure 49: Pre-crack and crack propagation on pre-preg material.	71
Figure 50: Examples of DCB test on Infused (a) and RTM (b) materials.	71
Figure 51: Crack propagation in mode I into Pre-preg, Infused and RTM materials (left to right).	72
Figure 52 : ILSS loading configuration.	73
Figure 53: Out-of-plane compression mechanism in unidirectional composite. Shear ILSS test leads to τ_{13} if 0° plies are oriented in (y,z) plan or leads to τ_{23} if 90° are oriented in (y,z) plan.	74
Figure 54: Illustration of inter-laminar shear failure in composites samples.	74
Figure 55: Optical microscope observation of UD samples, left to right, Infused, RTM and Pre-preg materials (dimension A is approximately 1.5 mm, for all three materials).	76
Figure 56: Microscope optical observation of Infused UD (scale bars: (a) 1.5 mm, (b) 0.38 mm).	77
Figure 57: Microscope optical observation of RTM UD (average scales: (a) and (b) 1.5mm).	77
Figure 58: Microscope optical observation of RTM UD (average scales: (a) 0.38mm (b) 20 μ m).	78
Figure 59: Microscope optical observation of Pre-preg UD (average scales: (a) 1.5 mm, (b) 0.38 mm).	78
Figure 60: Example of optical microscope observation (a) and ImageJ treatment (b) for UD 2.5 mm RTM material (perpendicular to fibres, fibre diameter is approximately 5 μ m).	79
Figure 61: Fracture surfaces of a crack initiation region for mode II ENF glass/epoxy specimens, (a) dry specimen, (b) specimen immersed in distilled water at 50°C for 5 months, [139].	80
Figure 62: Interlaminar shear fracture surface of carbon/epoxy material dry (a) and exposed to sea water for 11 years (b), [146].	81
Figure 63: Crack at a carbon/epoxy composite surface after 15 days exposure to water at 90°C, [147]	81
Figure 64: SEM observation on tensile fracture surface on UD Infused laminates in transverse direction, before ageing.	82
Figure 65: SEM observation on tensile fracture surface on UD Infused laminates loaded in the fibre direction, before ageing.	83
Figure 66: SEM observation on tensile fracture surface on UD RTM laminates loaded in the fibre direction, before ageing. Global surface of the specimen (a), focus between two plies of the laminate (b).	84
Figure 67: SEM observation on tensile fracture surface on UD RTM laminates loaded in the fibre direction, before ageing. Region on specimen surface (a), focus on fibres (b).	84

Figure 68: SEM observations on tensile fracture surface on UD RTM laminates tested in the transverse direction, before ageing.	85
Figure 69: SEM observation on tensile fracture surface of UD Pre-preg laminates in transverse direction, before ageing.	85
Figure 70: SEM observation on tensile fracture surface on UD Pre-preg laminates in transverse direction, before ageing. Focus on interface region between matrix and fibres.....	86
Figure 71: Evolution of the in-situ strength as a function of the thickness.	91
Figure 72: Representation of the surface S_f^{2+} corresponding to a single crack.	93
Figure 73: Flowchart presenting the different processes in the model allowing the crack density to be predicted as a fonction of the loading.	95
Figure 74: Evolution of crack density in 90° ply as a function of the loading for two Pre-preg laminates $[0_2,90_{1/2}]_s$ and $[0_2,90_2]_s$	97
Figure 75: Evolution of the crack density in the 90° ply as a function of the loading for a $[0,90,0,90]_s$ Infused laminate. The threshold of damage in the double central ply is used to identify the toughness of the ply. The experimental results correspond to two tests.	98
Figure 76: Evolution of the crack density in the 90° plies as a function of the loading for a $[0_2,90_2]_s$ Infused laminate. Comparison between model (line) and experimental results (points)	98
Figure 77: Representation of water diffusion through polymer material as a function of time.	105
Figure 78: Diagram presenting the difference of constituent concentration in sea water and river water.	106
Figure 79: Kinetics of diffusion according to Fick's law.	110
Figure 80: Kinetics of diffusion expected from the Langmuir model.	112
Figure 81: Schematic representation of diffusion through (a) homogeneous material (e.g. epoxy resin) and (b) heterogeneous material (e.g. composite carbon/epoxy).	112
Figure 82: Illustration of diffusion in composites representing the diffusion in normal and fibres directions for an UD composite.	114
Figure 83: Ifremer sea water ageing tanks with natural and renewed sea water from the bay of Brest.	118
Figure 84: Accelerated test characteristic times for testing superposed on a Fickian diffusion law, T_0 , T_1 , T_2 and T_3	119
Figure 85: Plots of mean measured weight gains for pure epoxy resin.....	121
Figure 86: Plots of mean measured weight gains versus the associated Fickian law for an ageing temperature of 60°C.....	121
Figure 87: Plots of mean measured weight gains versus the associated Fickian law for an ageing temperature of 40°C.....	122

Figure 88: Epoxy resin samples used for weight measurement at 80, 60, 40 and 25°C (left to right) suggesting oxidation of the resin.	123
Figure 89: Plot of mean measured weight gains for the UD Infused material immersed in sea water at different temperatures.	124
Figure 90: Comparison between experimental diffusion results and the Fickian law of diffusion at 40 and 60°C for the Infused material.	124
Figure 91: Plot of mean measured weight gains for the UD RTM material immersed in sea water at different temperatures.	125
Figure 92: Comparison between experimental diffusion results and Fickian law of diffusion at 60°C for the RTM material.....	126
Figure 93: Plot of mean measured weight gains for the UD Pre-preg material immersed in sea water at different temperatures.	126
Figure 94: Comparison between experimental diffusion results and Fickian law of diffusion at 80°C for the Pre-preg material.	127
Figure 95: UD Infused specimens with different geometries and orientations.....	127
Figure 96: Comparison of diffusion process at 60°C, between UD Infused material with different orientations and geometries.....	128
Figure 97: Comparison of diffusion process between RTM UD and QI samples, immersed in sea water at 60°C.	128
Figure 98: Influence of sample thickness. Comparison of mean measured weight gains for Pre-preg UD 1.3, 2.06 and 3.12 mm 80°C.	129
Figure 99: Influence of sample thickness. Comparison of mean measured weight gains for RTM UD 2.5mm and UD 5mm at 60°C.....	129
Figure 100: Evolution of glass transition for Infused materials during sea water ageing at 60°C.	131
Figure 101: Evolution of epoxy resin tensile properties during sea water ageing at 40°C (strength and modulus).....	132
Figure 102: Evolution of epoxy resin tensile properties during sea water ageing at 60°C (strength and modulus).....	132
Figure 103: Comparison of the effect of sea water ageing temperature (40 and 60°C) on epoxy resin modulus (a) and strength (b).....	133
Figure 104: Plots of the evolution of mean longitudinal (E_{11}) (a) and transverse (E_{22}) (b) moduli for the three materials during accelerated sea water ageing.....	134
Figure 105: Plots of the evolution of mean longitudinal (X_t) (a) and transverse (Y_t) (b) tensile strengths for the three materials during accelerated sea water ageing. Scatter bars show standard deviations.	134

Figure 106: Plots of the change in mean tensile shear strength (a) and tensile shear modulus (b) for the Infused and Pre-preg materials during accelerated sea water ageing. Scatter bars show standard deviations.	136
Figure 107: Response of $\pm 45^\circ$ Infused composites at three different loading rates 0.2, 2 and 20mm/min (left to right) before ageing (T0) and after ageing (T1).	137
Figure 108: Creep response of Infused material before(dotted line) and after sea water ageing (continuous line).....	137
Figure 109: Evolution of normalized crack density for infused composite $[0_2, 90_2]_s$ before ageing (red square), at saturation (blue triangle) and at saturation time plus one month (green circle) (3 specimens per condition).	138
Figure 110: Evolution of normalized crack density for infused composite $[0, 90, 0, 90]_s$ before ageing (purple round for the doubled 90° plies and purple doted circles for the single 90° plies), at saturation (red round for the doubled 90° plies and red doted circles for the single 90° plies), 3 specimens per condition.	139
Figure 111: Evolution of normalized crack density as a function of applied stress for Pre-preg $[0_2, 90_2]_s$, before (blue points) and after ageing (green points T1, red points T2).....	140
Figure 112: Evolution of critical strain energy release rate G_{Ic} in carbon/epoxy Pre-preg, Infused and RTM materials during sea water ageing.....	141
Figure 113: Initiation fracture energies from film insert, Infused composite during sea water ageing.	141
Figure 114: Changes in mean ILSS shear stress strength during sea water ageing for three different UD (a) and QI (b) materials. Scatter bars show standard deviations.	142
Figure 115: Illustration on reversibility of ageing process for tensile modulus (a) and tensile strength (b) of the epoxy resin aged (blue) and aged and dried (red) at 60°C	143
Figure 116: SEM observation of Infused UD cross section immersed during 6 months. (edge region).	146
Figure 117: SEM observation of Infused UD cross section immersed during 6 months, (a) presents a region between two plies where stitching fibres are located, (b) presents the whole thickness of the specimen and highlights a crack.....	146
Figure 118: SEM observation of Pre-preg UD cross section immersed during 6 months, (a) presents a region between two plies where are located nodules, (b) presents a focus in interply region.	147
Figure 119: SEM observation of RTM UD cross section immersed during 6 months, (a) presents a region between two plies, (b) presents a focus on an interply region and stitching fibres.....	148
Figure 120: SEM observation of Infused UD fracture surface after longitudinal tensile test, (a), (c) for un-aged material, (b), (d) for specimen aged T3.....	149

Figure 121: SEM observation of Infused UD fracture surface after longitudinal tensile test T3, (a) edge specimen region, (b) interply region.	150
Figure 122: SEM observation of RTM UD fracture surface after longitudinal tension test, (a) T0 and (b) T3 compare edge observations, (c) and (d) compare interply regions.	151
Figure 123: SEM observation of RTM UD fracture surface after longitudinal tension test, (a) T0 and (b) T3 are focused on the fibres fracture surfaces.	151
Figure 124: SEM observations of Infused UD after transverse tensile test, observations are focused on intra-ply region. (a) before ageing T0, and (b) after ageing T3. (c) and (d) present a focus on carbon fibres.....	153
Figure 125: SEM observations of RTM UD after transverse tensile test, observations are focused in intraply region. (a) before ageing T0, and (b) after ageing T3. (c) and (d) present a focus on carbon fibres.....	153
Figure 126: SEM observation of RTM UD after transverse tensile test, (a) presents a region between two plies at T0, (b) presents a focus in interply after sea water ageing T3.	154
Figure 127: SEM observations of Pre-preg UD after transverse tensile test, observations are focused in edge region before (a) and after sea water ageing (b).	154
Figure 128: SEM observations of Pre-preg UD after transverse tensile test, observations are focused on interply regions, before (a) and after sea water ageing (b).	155
Figure 129: SEM observations of Pre-preg UD after transverse tensile test, observations are focused in intraply region, before (a) and after sea water ageing (b).	155
Figure 130: SEM observation of Infused material after crack propagation using DCB test, observations present a large view on the specimen fracture surface, arrows show the direction of the propagation. (a) T0, (b) T3.	156
Figure 131: SEM observation of Infused material after crack propagation using DCB test, observations present a detail on the specimen fracture surface, (a) T0, (b) T3.....	157
Figure 132: SEM observation of Infused material after crack propagation using DCB test, observations focus on carbon fibres ((a) T0 and (b) after saturation time plus 2 months).....	157
Figure 133: SEM observation of RTM material after crack propagation using DCB test, observations present a large view on the specimen fracture surface, arrows show the direction of the propagation.	158
Figure 134: SEM observation of RTM material after crack propagation using DCB test, (a) T0 and (b) T3.....	159
Figure 135: SEM observation of RTM material after crack propagation using DCB test, observations present a large view on the specimen fracture surface, arrows show the direction of the propagation. (a) T0, (b) T3.	159

Figure 136: SEM observation of Pre-preg after crack propagation during DCB test, (a) T0, (b) T3.	160
Figure 137: SEM observation of Pre-preg after crack propagation during DCB test, (a) T0, (b) T3.	161
Figure 138: SEM observation of Pre-preg after crack propagation during DCB test. Observations are focused on fibre imprints, (a) T0, (b) T3.....	161
Figure 139: SEM observations of Pre-preg after crack propagation during DCB test, observations are focused on interply crack propagation, (a) T0, (b) T3.	162
Figure 140: Illustration of crack propagation phenomena (mode I) in un-aged and aged states.	163
Figure 141: Weight gain as a function of the square root of time normalised by the thickness for the three types of materials used in this study.	165
Figure 142: Comparison of weight gains for RTM UD and QI samples, immersed in sea water at 60°C. The water content is plotted as a function of the square root of time.	165
Figure 143: Evolution of the water content normalised by the maximum content of water as a function of the square root time normalised by the thickness for the three types of materials used in this study.	166
Figure 144: Evolution or normalised longitudinal tensile strength X_t , during sea water ageing for the three materials.	167
Figure 145: Evolution of normalised transverse strength Y_t , during sea water ageing for the three materials.....	167
Figure 146: Evolution of normalised in-plane shear strength τ_{12} , during sea water ageing for Infused and Pre-preg materials.....	168
Figure 147: Evolution of normalised tensile shear modulus G_{12} , during sea water ageing times for Infused and Pre-preg materials.....	169
Figure 148: Evolution of normalised ILSS strength, during sea water ageing times for the three UD materials.....	170
Figure 149: Evolution of normalised ILSS strength, during sea water ageing times for the RTM and Pre-preg QI materials.	170
Figure 150: Time needed to saturate composites sample in water as a function of ageing temperature and thickness.....	172
Figure 151: (a) Representation of the 3D model using for diffusion in Abaqus™ and (b) the associated mesh.....	180
Figure 152: Representation of boundary conditions applied on the 3D model for transverse (a) and longitudinal (b) diffusion through composite.	181
Figure 153: Plots of mean measured weight gains for pure epoxy resin immersion at the different temperatures.....	183

Figure 154: Determination of the slopes for each relative mass uptake for the unreinforced epoxy resin.....	183
Figure 155: Influence of mesh size on transverse diffusion kinetics.....	186
Figure 156: Representation on the geometries used to model diffusion with different fibre contents, (a) $V_f=44\%$, (b) $V_f=47\%$, (c) $V_f=54\%$ and (d) $V_f=65\%$	187
Figure 157: Influence of model fibre content on transverse diffusion kinetics.	187
Figure 158: First comparison between diffusion model (FE) and experimental (exp) results on Infused materials at 40°C and 60°C.....	189
Figure 159: Three different type of fibre arrangement tested with the diffusion model, transverse boundary conditions of diffusion are represented in red.....	190
Figure 160: Fourth case of diffusion “8 plies” (d) with specific fibres distribution aiming to recreate the micro structure of the Infused materials.	191
Figure 161: Transverse diffusion results for the geometries (a), (b) and (c) with different fibre arrangements. These results are compared to experimental ones (orange circles).	191
Figure 162: Transverse diffusion results for the geometry (d). These results are compared to experimental ones (orange circles).....	192
Figure 163: Comparison between modelling of diffusion and experimental results for Infused materials at 60, 40 and 25°C.	193
Figure 164: Comparison between modelling of diffusion and experimental results for RTM materials at 60, 40 and 25°C.	194
Figure 165: Arrhenius graph of the logarithm of epoxy resin diffusion coefficient as a function of $1/RT$ for 25, 40, 60 and 80°C (blue points). The black points represent the water diffusivity estimated by an Arrhenius law for 20°C and 15°C.	195
Figure 166: Modelling of both transverse (dotted line) and longitudinal (continuous line) water diffusion for the Infused material at 15°C (a) and 25 °C (b).....	196
Figure 167: Presentation of blade section geometry (a) and the associated boundary conditions of diffusion (b).	197
Figure 168: Diffusion curves obtained after modelling sea water entry on the blade section at 15°C and 25°C (a). Focus on first 25 years of water diffusion through the blade.	198
Figure 169: Water diffusion modelling results at 15°C (a) and 25°C (b), figures present local diffusion of water in the blade section after 25 years of immersion.....	199
Figure 170: Water diffusion modelling results at 15°C (a) and 25°C (b), figures present local diffusion of water in the blade trailing edge after 25 years of immersion.	199

Figure 171: Evolution of the crack density in the 90° plies as a function of the loading for a [0 ₂ ,90 ₂] _s Infused laminate. Comparison between model (line) and experimental results (points) at different ageing times (T0: un-aged; T1: aged 37 days, T2: aged 67 days).	202
Figure 172: Criterion evolution before (a) and after (b) sea water ageing, Y_t^{stress} decreases as a function of sea water ageing time.	203
Figure 173: Example of 3D geometry generated to model diffusion in damaged composite, presenting dimension of composite layers (a). The boundary conditions applied on the model (red) (b).	205
Figure 174: Different 3D geometry configurations of damaged and un-damaged composite. The results presented were taken after 10 ⁵ seconds of diffusion.	206
Figure 175: Evolution of composite [0,90,0] diffusion coefficient and the identified diffusion coefficient of the 90° ply as a function of the normalized crack density.	206
Figure 176: Ifremer test bed for coupled diffusion and tensile loading.	207
Figure 177: Different test conditions applied to the Infused [0 ₂ ,90 ₂] _s specimens for 30 days (water immersion time, pre-loading and loading).....	208
Figure 178: Different test conditions applied to the Infused [0 ₂ ,90 ₂] _s specimens during 10 days.....	209
Figure 179: Model results of water diffusion comparison, between un-damage (blue squares) and damage (blue points) sample after immersion in water at 60°C. Samples were representatives of Infused [0 ₂ ,90 ₂] _s with an average normalized cracks density of 0.25.	210
Figure 180: Example of fatigue results for RTM QI samples before and after seawater ageing.	219
Figure 181: Overview of work performed (green tick) and required (x).....	221

Table caption

Table 1: Materials, process, resin and fibre compositions, (*IMS: intermediate modulus).	41
Table 2: Nominal fibre and matrix tensile properties from technical data sheets.	42
Table 3: Technical data about UD carbon fabric composition.	42
Table 4: Curing process and glass transition (T _g) temperature resulting for each material. The numbers between brackets are the coefficient of variation (the same notation is used for all tables in the document).....	43
Table 5 : Density measurements and estimated fibre content of studied materials, mean (standard deviation), UD (unidirectional) and QI (quasi-isotropic) and pure resin.....	44
Table 6: Average specimen dimensions for tensile tests on the three different materials and the pure resin.	47
Table 7: Tensile test results on Infused, RTM, Pre-preg material and pure resin.....	48
Table 8: Average specimen dimension for +/-45 tensile test on Pre-preg and Infused materials.....	49
Table 9: Results of in plane shear strength and modulus for the three materials.....	53
Table 10: Four point bending test specimens average dimensions and stacking sequences.	55
Table 11: Flexural strength and stiffness for RTM and Pre-preg materials.	57
Table 12 : Specimen information for intralaminar tensile cracking tests.	60
Table 13: DCB specimen average dimensions for the three materials.	66
Table 14 : DCB results of re-initiation using CC method.	72
Table 15: Inter-laminar shear strength (ILSS) values, S_{13}^{C*} , S_{23}^{C**} , and specimen dimensions for the three materials.	75
Table 16: Comparison between local (in the ply) and global fibre volume fractions of the UD materials. Global fibre contents have been determined by pycnometry measurements.....	79
Table 17: Materials physical properties determined previously and used in the model.....	96
Table 18: Comparison between T _g and temperature for accelerated ageing for the materials of the study.....	118
Table 19: Comparison between an estimation of tensile properties degradation based classical mixture law and the experimental measurement after saturation time (for the Infused UD). The composite mixture law is based on infused matrix and fibres properties at T ₀ and T ₁	135
Table 20: Illustration on reversibility of the ageing process, presented on RTM QI 5 mm flexural strength (T ₀ : un-aged, T ₁ : saturated in water, T ₁ dried: saturated in water and then dried).	143
Table 21: Comparison between effects of sea water ageing and thermal ageing on RTM UD 2.8 mm after transverse tensile test, (SW: sea water).	144

Table 22: Sea water diffusion coefficients determined experimentally for the different materials of the study. These coefficients have not been corrected with an edge coefficient of correction.	166
Table 23: Sea water diffusion coefficients determined experimentally for the epoxy resin.....	184
Table 24: Sea water coefficient diffusion determined experimentally for the Infused composite (Vf=54%).	184
Table 25: Sea water diffusion coefficients determined experimentally for the RTM composite (Vf=50%) * for these temperatures material is not clearly saturated.	184
Table 26: Sea water diffusion coefficients determined experimentally for the Pre-preg 1.29 mm (fibre content 56.7%).	185
Table 27: Sea water diffusion coefficients determined experimentally for the Pre-preg 2.07 mm (fibre content 58.3%).	185
Table 28: Epoxy matrix parameters used in the FE diffusion model for the different temperatures, K_x the thermal conductivity determined based on D_x	185
Table 29: Influence of mesh size on calculation time and water diffusion coefficient obtained.	186
Table 30: Influence of fibre content on transverse water diffusion coefficient.	188
Table 31: First results of the diffusion model for infused material at 40°C and 60°C, the model coefficients are compared to experimental ones.	189
Table 32: Results for transverse diffusion coefficients obtained on the different geometries of the diffusion model (mesh size was 0.0004 mm for all geometries).	193
Table 33: Comparison between model estimation of transverse diffusion and measured values for the Infused material.	193
Table 34: Comparison between model estimation of transverse diffusion for the RTM material.	194
Table 35: Transverse experimental diffusion coefficients and estimated transverse coefficient for 20°C and 15°C.	196
Table 36: Coefficients of water diffusion determined in longitudinal and transverse direction to the fibres for the Infused material for temperatures close to tidal turbine service life conditions.	197
Table 37: Materials physical properties determined previously and used in the model for the ageing conditions.	201
Table 38: Summary of ageing conditions for each specimen type and ultimate tensile strength after 30 days.....	209
Table 39: Summary of ageing conditions for each specimen type, and ultimate tensile strength after 30 days.....	210

References

- [1] International Energy Agency. <http://www.iea.org/publications/>.
- [2] M. S. Güney and K. Kaygusuz, "Hydrokinetic energy conversion systems: A technology status review," *Renew. Sustain. Energy Rev.*, vol. 14, no. 9, pp. 2996–3004, Dec. 2010.
- [3] S. Walker, R. Howell, P. Hodgson, and A. Griffin, "Tidal energy machines: A comparative life cycle assessment study," *Proc. Inst. Mech. Eng. Part M J. Eng. Marit. Environ.*, vol. 229, no. 2, pp. 124–140, May 2015.
- [4] D. Magagna and A. Uihlein, "Ocean energy development in Europe: Current status and future perspectives," *Int. J. Mar. Energy*, vol. 11, pp. 84–104, Sep. 2015.
- [5] J. Twidell and T. Weir, *Renewable Energy Resources*. Routledge, 2015.
- [6] L. S. Blunden and A. S. Bahaj, "Tidal energy resource assessment for tidal stream generators," *Proc. Inst. Mech. Eng. Part J. Power Energy*, vol. 221, no. 2, pp. 137–146, Mar. 2007.
- [7] R. F. Nicholls-Lee and S. R. Turnock, "Tidal energy extraction: renewable, sustainable and predictable," *Sci. Prog.*, vol. 91, no. 1, pp. 81–111, Mar. 2008.
- [8] R. H. Charlier, "A 'sleeper' awakes: tidal current power," *Renew. Sustain. Energy Rev.*, vol. 7, no. 6, pp. 515–529, Dec. 2003.
- [9] S. C. Bhatia, "13 - Tide, wave and ocean energy," in *Advanced Renewable Energy Systems*, S. C. Bhatia, Ed. Woodhead Publishing India, 2014, pp. 307–333.
- [10] C. Lang, "Harnessing tidal energy takes new turn," *IEEE Spectr.*, vol. 40, no. 9, p. 13–, Sep. 2003.
- [11] J. Hardisty, *The Analysis of Tidal Stream Power*. John Wiley & Sons, 2009.
- [12] Une brève histoire de La Rance : de l'époque romaine à Charles De Gaulle. <http://pulse.edf.com/fr/une-breve-histoire-de-la-rance-de-lepoque-romaine-charles-de-gaulle>.
- [13] M. J. Khan, G. Bhuyan, M. T. Iqbal, and J. E. Quaicoe, "Hydrokinetic energy conversion systems and assessment of horizontal and vertical axis turbines for river and tidal applications: A technology status review," *Appl. Energy*, vol. 86, no. 10, pp. 1823–1835, Oct. 2009.
- [14] OpenHydro, a DCNS company. <http://www.openhydro.com/>.
- [15] OpenHydro gets \$6.3m from Ottawa for Fundy tidal project, *The Chronicle Herald*, 15-Apr-2015. <http://thechronicleherald.ca/novascotia/1280765-openhydro-gets-6.3m-from-ottawa-for-fundy-tidal-project>.
- [16] Les principaux enjeux et perspectives de développement des énergies marines renouvelables," *ENEA Consulting*. <http://www.enea-consulting.com/publication-sur-les-energies-marines-renouvelables/>.
- [17] A. I. Winter, "Differences in fundamental design drivers for wind and tidal turbines," in *OCEANS, 2011 IEEE - Spain*, 2011, pp. 1–10.
- [18] I. Bryden and G. T. Melville, "Choosing and evaluating sites for tidal current development," *Proc. Inst. Mech. Eng. Part J. Power Energy*, vol. 218, no. 8, pp. 567–577, Dec. 2004.
- [19] S. Gooch, J. Thomson, B. Polagye, and D. Meggitt, "Site characterization for tidal power," in *OCEANS 2009, MTS/IEEE Biloxi - Marine Technology for Our Future: Global and Local Challenges*, 2009, pp. 1–10.
- [20] G. McCann, M. Thomson, and S. Hitchcock, "Implications of site-specific conditions on the prediction of loading and power performance of a tidal stream device," in *2nd International Conference on Ocean Energy, Brest, France*, 2008.
- [21] A. S. Bahaj, "Generating electricity from the oceans," *Renew. Sustain. Energy Rev.*, vol. 15, no. 7, pp. 3399–3416, Sep. 2011.
- [22] A. Small and G. Cook, "Overcoming seabed design obstacles," *Renew. Energy Focus*, vol. 15, no. 3, pp. 34–35, May 2014.
- [23] G. Marsh, "Tidal turbines harness the power of the sea," *Reinf. Plast.*, vol. 48, no. 6, pp. 44–47, Jun. 2004.

- [24] W. M. J. Batten, A. S. Bahaj, A. F. Molland, and J. R. Chaplin, "The prediction of the hydrodynamic performance of marine current turbines," *Renew. Energy*, vol. 33, no. 5, pp. 1085–1096, May 2008.
- [25] C. C. Chen, Y. D. Choi, and H. Y. Yoon, "Blade design and performance analysis on the horizontal axis tidal current turbine for low water level channel," *IOP Conf. Ser. Mater. Sci. Eng.*, vol. 52, no. 5, p. 052020, Dec. 2013.
- [26] J. A. Clarke, G. Connor, A. D. Grant, and C. M. Johnstone, "Design and testing of a contra-rotating tidal current turbine," *Proc. Inst. Mech. Eng. Part J. Power Energy*, vol. 221, no. 2, pp. 171–179, Mar. 2007.
- [27] C. Faudot and O. G. Dahlhaug, "Prediction of Wave Loads on Tidal Turbine Blades," *Energy Procedia*, vol. 20, pp. 116–133, 2012.
- [28] A. Boisseau, P. Davies, and F. Thiebaud, "Sea Water Ageing of Composites for Ocean Energy Conversion Systems: Influence of Glass Fibre Type on Static Behaviour," *Appl. Compos. Mater.*, vol. 19, no. 3–4, pp. 459–473, Jun. 2012.
- [29] A. Boisseau, P. Davies, and F. Thiebaud, "Fatigue Behaviour of Glass Fibre Reinforced Composites for Ocean Energy Conversion Systems," *Appl. Compos. Mater.*, vol. 20, no. 2, pp. 145–155, Apr. 2013.
- [30] D. V. Val, L. Chernin, and D. V. Yurchenko, "Reliability analysis of rotor blades of tidal stream turbines," *Reliab. Eng. Syst. Saf.*, vol. 121, pp. 26–33, Jan. 2014.
- [31] G. S. Bir, M. J. Lawson, and Y. Li, "Structural Design of a Horizontal-Axis Tidal Current Turbine Composite Blade," pp. 797–808, Jan. 2011.
- [32] W. C. Tucker and T. Juska, "Marine Applications," in *Handbook of Composites*, S. T. Peters, Ed. Springer US, 1998, pp. 916–930.
- [33] D. W. Chalmers, "The Potential for the use of composite materials in marine structures," *Mar. Struct.*, vol. 7, no. 2–5, pp. 441–456, 1994.
- [34] C. S. Smith, *Design of marine structures in composite materials* /. London ; Elsevier Applied Science, c1990.
- [35] A. P. Mouritz, E. Gellert, P. Burchill, and K. Challis, "Review of advanced composite structures for naval ships and submarines," *Compos. Struct.*, vol. 53, no. 1, pp. 21–42, Jul. 2001.
- [36] G. Pritchard, *Reinforced Plastics Durability*. Elsevier, 1998.
- [37] R. F. Nicholls-Lee, S. R. Turnock, and S. W. Boyd, "Performance prediction of a free stream tidal turbine with composite bend-twist coupled blades," presented at the 2nd International Conference on Ocean Energy (ICOE 2008), 2008.
- [38] B. Harris, *Fatigue in Composites: Science and Technology of the Fatigue Response of Fibre-reinforced Plastics*. Woodhead Publishing, 2003.
- [39] D. M. Grogan, S. B. Leen, C. R. Kennedy, and C. M. Ó Brádaigh, "Design of composite tidal turbine blades," *Renew. Energy*, vol. 57, pp. 151–162, Sep. 2013.
- [40] K. Uzawa, K. Kageyama, H. Murayama, I. Ohsawa, M. Kanai, T. Nishiyama, and A. Shichiri, "Study of the Characteristic and Possibility for Applying Composite Materials to the Blades of Tidal Power Generation," pp. 721–728, Jan. 2008.
- [41] R. F. Nicholls-Lee, S. W. Boyd, and S. R. Turnock, "Development of high performance composite bend-twist coupled blades for a horizontal axis tidal turbine," presented at the 17th International Conference on Composite Materials, 2009.
- [42] C.-H. Shen and G. S. Springer, "Effects of Moisture and Temperature on the Tensile Strength of Composite Materials," *J. Compos. Mater.*, vol. 11, no. 1, pp. 2–16, Jan. 1977.
- [43] G. S. Springer, *Environmental effects on composite materials*. Technomic Pub. Co., 1981.
- [44] P. Davies, F. MazÉas, and P. Casari, "Sea Water Aging of Glass Reinforced Composites: Shear Behaviour and Damage Modelling," *J. Compos. Mater.*, vol. 35, no. 15, pp. 1343–1372, Aug. 2001.
- [45] A. Kootsookos and A. P. Mouritz, "Seawater durability of glass- and carbon-polymer composites," *Compos. Sci. Technol.*, vol. 64, no. 10–11, pp. 1503–1511, Aug. 2004.

- [46] H. S. Choi, K. J. Ahn, J.-D. Nam, and H. J. Chun, "Hygroscopic aspects of epoxy/carbon fiber composite laminates in aircraft environments," *Compos. Part Appl. Sci. Manuf.*, vol. 32, no. 5, pp. 709–720, May 2001.
- [47] R. Martin, "Introduction," in *Ageing of Composites*, R. Martin, Ed. Woodhead Publishing, 2008, pp. xix–xxiii.
- [48] X. Colin and J. Verdu, "Humid Ageing of Organic Matrix Composites," in *Durability of Composites in a Marine Environment*, P. Davies and Y. D. S. Rajapakse, Eds. Springer Netherlands, 2014, pp. 47–114.
- [49] ASTM International, "ASTM D5229/D5229M-92(2010) Standard Test Method for Moisture Absorption Properties and Equilibrium Conditioning of Polymer Matrix Composite Materials." ASTM International, 2010.
- [50] O. Gillat and L. J. Broutman, "Effect of an external stress on moisture diffusion and degradation in a graphite-reinforced epoxy laminate," *ASTM Spec. Tech. Publ.*, no. 658, pp. 61–83, 1978.
- [51] S. Roy and W. Xu, "Modeling of diffusion in the presence of damage in polymer matrix composites," *Int. J. Solids Struct.*, vol. 38, no. 1, pp. 115–126, Jan. 2001.
- [52] C. E. Browning, G. E. Husman, and J. M. Whitney, "Moisture effects in epoxy matrix composites," *ASTM STP*, vol. 617, pp. 481–496, 1977.
- [53] P. Musto, M. Galizia, G. Scherillo, and G. Mensitieri, "Water Sorption Thermodynamics in Polymer Matrices," in *Durability of Composites in a Marine Environment*, P. Davies and Y. D. S. Rajapakse, Eds. Springer Netherlands, 2014, pp. 15–45.
- [54] M. K. Antoon, J. L. Koenig, and T. Serafini, "Fourier-transform infrared study of the reversible interaction of water and a crosslinked epoxy matrix," *J. Polym. Sci. Polym. Phys. Ed.*, vol. 19, no. 10, pp. 1567–1575, Oct. 1981.
- [55] E. Morel, V. Bellenger, and J. Verdu, "Structure-water absorption relationships for amine-cured epoxy resins," *Polymer*, vol. 26, no. 11, pp. 1719–1724, Oct. 1985.
- [56] V. Bellenger, J. Verdu, and E. Morel, "Structure-properties relationships for densely cross-linked epoxide-amine systems based on epoxide or amine mixtures," *J. Mater. Sci.*, vol. 24, no. 1, pp. 63–68, Jan. 1989.
- [57] C. Grave, I. McEwan, and R. A. Pethrick, "Influence of stoichiometric ratio on water absorption in epoxy resins," *J. Appl. Polym. Sci.*, vol. 69, no. 12, pp. 2369–2376, Sep. 1998.
- [58] Y. Diamant, G. Marom, and L. J. Broutman, "The effect of network structure on moisture absorption of epoxy resins," *J. Appl. Polym. Sci.*, vol. 26, no. 9, pp. 3015–3025, Sep. 1981.
- [59] E. L. McKague, J. D. Reynolds, and J. E. Halkias, "Swelling and glass transition relations for epoxy matrix material in humid environments," *J. Appl. Polym. Sci.*, vol. 22, no. 6, pp. 1643–1654, Jun. 1978.
- [60] Y. J. Weitsman, *Fluid Effects in Polymers and Polymeric Composites*. Springer Science & Business Media, 2011.
- [61] B. De'Nève and M. E. R. Shanahan, "Water absorption by an epoxy resin and its effect on the mechanical properties and infra-red spectra," *Polymer*, vol. 34, no. 24, pp. 5099–5105, Dec. 1993.
- [62] M. Gordon, "The Physics of Rubber Elasticity (Third Edition). L. R. G. Treloar, Clarendon Press, Oxford. 1975 pp. xii + 370. Price: £14.00," *Br. Polym. J.*, vol. 8, no. 1, pp. 39–39, Mar. 1976.
- [63] D. Cohn and G. Marom, "A proposal for a coefficient of hygroelasticity," *Polym. Eng. Sci.*, vol. 18, no. 13, pp. 1001–1005, Oct. 1978.
- [64] S. Gazit, "Dimensional changes in glass-filled epoxy resin as a result of absorption of atmospheric moisture," *J. Appl. Polym. Sci.*, vol. 22, no. 12, pp. 3547–3558, Dec. 1978.
- [65] O. Ishai, "Environmental effects on deformation, strength, and degradation of unidirectional glass-fiber reinforced plastics. II. Experimental study," *Polym. Eng. Sci.*, vol. 15, no. 7, pp. 491–499, Jul. 1975.
- [66] U. Gaur and B. Miller, "Effects of environmental exposure on fiber/epoxy interfacial shear strength," *Polym. Compos.*, vol. 11, no. 4, pp. 217–222, Aug. 1990.

- [67] H. H. Y. Kim, "Swelling of composite laminates," *Adv. Compos. Mater.-Environ. Eff.*, no. 658, p. 98, 1978.
- [68] H. T. Hahn and R. Y. Kim, "Swelling of Composite Laminates.," Dec. 1977.
- [69] R. De Iasi and J. B. Whiteside, "Effect of moisture on epoxy resins and composites," *Adv. Compos. Mater. Eff.*, pp. 2–20, 1978.
- [70] B. C. Ray, "Temperature effect during humid ageing on interfaces of glass and carbon fibers reinforced epoxy composites," *J. Colloid Interface Sci.*, vol. 298, no. 1, pp. 111–117, Jun. 2006.
- [71] A. Sérier, J. P. Pascault, and L. T. My, "Modeling of interphase in composite materials: Characterization of epoxy resin/aminosilane system," *Makromol. Chem. Macromol. Symp.*, vol. 25, no. 1, pp. 85–90, Jan. 1989.
- [72] K. Hoh, H. Ishida, and J. L. Koenig, "The diffusion of epoxy resin into a silane coupling agent interphase," *Compos. Interfaces*, pp. 251–263, 1986.
- [73] H. L. Luo, J. J. Lian, Y. Z. Wan, Y. Huang, Y. L. Wang, and H. J. Jiang, "Moisture absorption in VARTMed three-dimensional braided carbon-epoxy composites with different interface conditions," *Mater. Sci. Eng. A*, vol. 425, no. 1–2, pp. 70–77, Jun. 2006.
- [74] K. Komai, K. Minoshima, and S. Shiroshita, "Hygrothermal degradation and fracture process of advanced fibre-reinforced plastics," *Mater. Sci. Eng. A*, vol. 143, no. 1–2, pp. 155–166, Sep. 1991.
- [75] R. Selzer and K. Friedrich, "Influence of water up-take on interlaminar fracture properties of carbon fibre-reinforced polymer composites," *J. Mater. Sci.*, vol. 30, no. 2, pp. 334–338, Jan. 1995.
- [76] F. U. Buehler and J. C. Seferis, "Effect of reinforcement and solvent content on moisture absorption in epoxy composite materials," *Compos. Part Appl. Sci. Manuf.*, vol. 31, no. 7, pp. 741–748, Jul. 2000.
- [77] D. A. Bond and P. A. Smith, "Modeling the Transport of Low-Molecular-Weight Penetrants Within Polymer Matrix Composites," *Appl. Mech. Rev.*, vol. 59, no. 5, p. 249, 2006.
- [78] G. Z. Xiao and M. E. R. Shanahan, "Irreversible effects of hygrothermal aging on DGEBA/DDA epoxy resin," *J. Appl. Polym. Sci.*, vol. 69, no. 2, pp. 363–369, Jul. 1998.
- [79] G. Z. Xiao and M. E. R. Shanahan, "Water absorption and desorption in an epoxy resin with degradation," *J. Polym. Sci. Part B Polym. Phys.*, vol. 35, no. 16, pp. 2659–2670, Nov. 1997.
- [80] M. L. Costa, M. C. Rezende, and S. F. M. de Almeida, "Effect of Void Content on the Moisture Absorption in Polymeric Composites," *Polym.-Plast. Technol. Eng.*, vol. 45, no. 6, pp. 691–698, Jul. 2006.
- [81] J. L. Thomason, "The interface region in glass fibre-reinforced epoxy resin composites: 2. Water absorption, voids and the interface," *Composites*, vol. 26, no. 7, pp. 477–485, Jul. 1995.
- [82] P. Davies and Y. D. S. Rajapakse, *Durability of Composites in a Marine Environment*. Springer Science & Business Media, 2013.
- [83] R. Martin, *Ageing of Composites*. Elsevier, 2008.
- [84] Duplessis, H. MALLARD Du, and A. Thionnet Renard, *Dimensionnement des structures en composite stratifiés à fibres longues*. ENSMP, 2005.
- [85] A. Boisseau, "Long term durability of composites for ocean energy conversion systems," PhD Thesis, Université de Franche-Comté, Ifremer Brest, 2011.
- [86] Sabella - Engineering and project management firm in the field of marine energies. <http://www.sabella.bzh/>.
- [87] Composite blades for tidal turbines," *Airborne Marine*. <http://airborne-marine.com/reliable-tidal-blades/composite-blades-for-tidal-turbines/>
- [88] Vacuum infusion, *Kevra Oy*. .
- [89] Composite Manufacturing, Aerospace Engineering Blog.
- [90] Materials and processes," *Airborne Technology Centre*. <http://airborne-technologycentre.com/materials-and-processes/>.
- [91] FMC Florian Madec Composites. <http://www.fmc-composites.com/pre-impregne>.

- [92] P. Coppens, "Tidal energy – an emerging market for composites," *Reinf. Plast.*, vol. 58, no. 3, pp. 26–27, May 2014.
- [93] C. Binetruy and F. Boussu, *Recent Advances in Textile Composites: October 26-28, 2010, Lille Grand Palais, Lille, France*. DEStech Publications, Inc, 2010.
- [94] C. A. Douglas, G. P. Harrison, and J. P. Chick, "Life cycle assessment of the Seagen marine current turbine," *Proc. Inst. Mech. Eng. Part M J. Eng. Marit. Environ.*, vol. 222, no. 1, pp. 1–12, Mar. 2008.
- [95] R. Stewart, "New prepreg materials offer versatility, top performance," *Reinf. Plast.*, vol. 53, no. 5, pp. 28–33, Jun. 2009.
- [96] Airborne Marine, "Customer base for reliable tidal blades." <http://airborne-technologycentre.com>
- [97] ASTM D3039 / D3039M - 14 Standard Test Method for Tensile Properties of Polymer Matrix Composite Materials," ASTM International, 2014.
- [98] ISO 527-2:2012 Determination of tensile properties -- Part 2: Test conditions for moulding and extrusion plastics.
- [99] ISO 527-5:2009 Determination of tensile properties -- Part 5: Test conditions for unidirectional fibre-reinforced plastic composites." 2009.
- [100] D. E. Walrath and D. F. Adams, "The Iosipescu shear test as applied to composite materials," *Exp. Mech.*, vol. 23, no. 1, pp. 105–110, Mar. 1983.
- [101] H. Ho, J. Morton, and G. L. Farley, "Non-linear numerical analysis of the Iosipescu specimen for composite materials," *Compos. Sci. Technol.*, vol. 50, no. 3, pp. 355–365, 1994.
- [102] H. Ho, M. Y. Tsai, J. Morton, and G. L. Farley, "A comparison of three shear test methods for composite materials," presented at the International Conference on Composite Materials, July 15-19, 1991, United States, 1991.
- [103] T. Dickson, M. Munro, and S. Lee, "Selection of an in-plane shear test method based on the shear sensitivity of laminate tensile modulus," *Composites*, vol. 26, no. 1, pp. 17–24, 1995.
- [104] P. H. Petit, "A Simplified Method of Determining the Inplane Shear Stress-Strain Response of Unidirectional Composites," in *Composite Materials: Testing and Design*, S. Yurenka, Ed. 100 Barr Harbor Drive, PO Box C700, West Conshohocken, PA 19428-2959: ASTM International, 1969, pp. 83–83–11.
- [105] M. Kawai, M. Morishita, H. Satoh, S. Tomura, and K. Kemmochi, "Effects of end-tab shape on strain field of unidirectional carbon/epoxy composite specimens subjected to off-axis tension," *Compos. Part Appl. Sci. Manuf.*, vol. 28, no. 3, pp. 267–275, 1997.
- [106] ASTM D3518/D 3518M-94 Standard Test Method for In-Plane Shear Response of Polymer Matrix Composite Materials by Tensile Test of a 45 Laminate, ASTM International, 2001.
- [107] B. W. Rosen, "A Simple Procedure for Experimental Determination of the Longitudinal Shear Modulus of Unidirectional Composites," *J. Compos. Mater.*, vol. 6, no. 3, pp. 552–554, Jul. 1972.
- [108] Ncorr open source 2D digital image correlation MATLAB program. <http://www.ncorr.com/>.
- [109] R. Harilal and M. Ramji, "Adaptation of Open Source 2D DIC Software Ncorr for Solid Mechanics Applications," presented at the 9th International Symposium on Advanced Science and Technology in Experimental Mechanics, New Delhi, India, 2014.
- [110] D. J. O'Brien, P. T. Mather, and S. R. White, *Viscoelastic Properties of an Epoxy Resin during Cure*. 2001.
- [111] G. C. Papanicolaou, T. V. Kosmidou, A. S. Vatalis, and C. G. Delides, "Water absorption mechanism and some anomalous effects on the mechanical and viscoelastic behavior of an epoxy system," *J. Appl. Polym. Sci.*, vol. 99, no. 4, pp. 1328–1339, Feb. 2006.
- [112] D. A. Dillard, M. R. Straight, and H. F. Brinson, "The nonlinear viscoelastic characterization of graphite/epoxy composites," *Polym. Eng. Sci.*, vol. 27, no. 2, pp. 116–123, Jan. 1987.
- [113] A. Chateauminois, L. Vincent, B. Chabert, and J. P. Soulier, "Study of the interfacial degradation of a glass-epoxy composite during hygrothermal ageing using water diffusion measurements and dynamic mechanical thermal analysis," *Polymer*, vol. 35, no. 22, pp. 4766–4774, Oct. 1994.

- [114] J. Z. Wang, H. Parvatareddy, T. Chang, N. Iyengar, D. A. Dillard, and K. L. Reifsnider, "Physical aging behavior of high-performance composites," *Compos. Sci. Technol.*, vol. 54, no. 4, pp. 405–415, 1995.
- [115] M. Nakada, S. Hara, and Y. Miyano, "Effect of Water Absorption on Time-Temperature Dependent Strength of CFRP," in *Challenges In Mechanics of Time-Dependent Materials and Processes in Conventional and Multifunctional Materials, Volume 2*, B. Antoun, H. J. Qi, R. Hall, G. P. Tandon, H. Lu, C. Lu, J. Furmanski, and A. Amirkhizi, Eds. Springer International Publishing, 2014, pp. 121–128.
- [116] D. Colombini, J. J. Martinez-Vega, and G. Merle, "Dynamic mechanical investigations of the effects of water sorption and physical ageing on an epoxy resin system," *Polymer*, vol. 43, no. 16, pp. 4479–4485, Jul. 2002.
- [117] D. A. Dillard, "Viscoelastic behavior of laminated composite materials," *Fatigue Compos. Mater.*, vol. 4, pp. 339–384, 1991.
- [118] F. Laurin, N. Carrère, and J.-F. Maire, "A multiscale progressive failure approach for composite laminates based on thermodynamical viscoelastic and damage models," *Compos. Part Appl. Sci. Manuf.*, vol. 38, no. 1, pp. 198–209, Jan. 2007.
- [119] K. KOMAI, K. Minoshima, and T. SHIBUTANI, "Investigations of the Fracture Mechanism of Carbon/Epoxy Composites by AE Signal Analyses," *JSME Int. J. Ser 1 Solid Mech. Strength Mater.*, vol. 34, no. 3, pp. 381–388, Jul. 1991.
- [120] S. Barré and M. L. Benzeggagh, "On the use of acoustic emission to investigate damage mechanisms in glass-fibre-reinforced polypropylene," *Compos. Sci. Technol.*, vol. 52, no. 3, pp. 369–376, 1994.
- [121] Y. Z. Pappas, A. Kontsos, T. H. Loutas, and V. Kostopoulos, "On the characterization of continuous fibres fracture by quantifying acoustic emission and acousto-ultrasonics waveforms," *NDT E Int.*, vol. 37, no. 5, pp. 389–401, Jul. 2004.
- [122] R. L. Mehan and J. V. Mullin, "Analysis of Composite Failure Mechanisms Using Acoustic Emissions," *J. Compos. Mater.*, vol. 5, no. 2, pp. 266–269, Apr. 1971.
- [123] R. Gutkin, C. J. Green, S. Vangrattanachai, S. T. Pinho, P. Robinson, and P. T. Curtis, "On acoustic emission for failure investigation in CFRP: Pattern recognition and peak frequency analyses," *Mech. Syst. Signal Process.*, vol. 25, no. 4, pp. 1393–1407, May 2011.
- [124] D. Valentin, P. Bonniau, and A. R. Bunsell, "Failure mechanism discrimination in carbon fibre-reinforced epoxy composites," *Composites*, vol. 14, no. 4, pp. 345–351, Oct. 1983.
- [125] S.-E. Mechraoui, A. Laksimi, and S. Benmedakhene, "Reliability of damage mechanism localisation by acoustic emission on glass/epoxy composite material plate," *Compos. Struct.*, vol. 94, no. 5, pp. 1483–1494, Apr. 2012.
- [126] P. P. Camanho, C. G. Dávila, S. T. Pinho, L. Iannucci, and P. Robinson, "Prediction of in situ strengths and matrix cracking in composites under transverse tension and in-plane shear," *Compos. Part Appl. Sci. Manuf.*, vol. 37, no. 2, pp. 165–176, Feb. 2006.
- [127] A. C. Garg, "Delamination—a damage mode in composite structures," *Eng. Fract. Mech.*, vol. 29, no. 5, pp. 557–584, 1988.
- [128] T. K. O'Brien, "Characterization of delamination onset and growth in a composite laminate," *Damage Compos. Mater. ASTM STP*, vol. 775, no. 2, pp. 140–167, 1982.
- [129] V. V. Bolotin, "Delaminations in composite structures: Its origin, buckling, growth and stability," *Compos. Part B Eng.*, vol. 27, no. 2, pp. 129–145, 1996.
- [130] T. E. Tay, "Characterization and analysis of delamination fracture in composites: an overview of developments from 1990 to 2001," *Appl. Mech. Rev.*, vol. 56, no. 1, pp. 1–32, 2003.
- [131] J. R. Reeder, "A bilinear failure criterion for mixed-mode delamination," *Compos. Mater. Test. Des. Elev. Vol. ASTM STP*, vol. 1206, pp. 303–322, 1993.
- [132] ASTM D5528 - 01 Standard Test Method for Mode I Interlaminar Fracture Toughness of Unidirectional Fiber-Reinforced Polymer Matrix Composites, 2007.
- [133] ISO 15024:2001-12, Fibre-reinforced plastic composites - Determination of Mode I interlaminar fracture toughness, GIC, for unidirectionally reinforced materials.

- [134] ASTM D6671 / D6671M - 13 Standard Test Method for Mixed Mode I-Mode II Interlaminar Fracture Toughness of Unidirectional Fiber Reinforced Polymer Matrix Composites.
- [135] R. Selzer and K. Friedrich, "Mechanical properties and failure behaviour of carbon fibre-reinforced polymer composites under the influence of moisture," *Compos. Part Appl. Sci. Manuf.*, vol. 28, no. 6, pp. 595–604, 1997.
- [136] B. Blackman, A. Brunner, and P. Davies, "Delamination fracture of continuous fiber composites: mixed-mode fracture," Elsevier, 2001, pp. 335–359.
- [137] A. J. Brunner, B. R. K. Blackman, and P. Davies, "A status report on delamination resistance testing of polymer–matrix composites," *Eng. Fract. Mech.*, vol. 75, no. 9, pp. 2779–2794, Jun. 2008.
- [138] EN ISO 14130:1997, Fibre reinforced plastic composites: Determination of apparent interlaminar shear strength by short beam-method.
- [139] P. Davies, F. Pomiès, and L. A. Carlsson, "Influence of water and accelerated aging on the shear fracture properties of glass/epoxy composite," *Appl. Compos. Mater.*, vol. 3, no. 2, pp. 71–87, Mar. 1996.
- [140] K. Liao, C. R. Schultheisz, and D. L. Hunston, "Effects of environmental aging on the properties of pultruded GFRP," *Compos. Part B Eng.*, vol. 30, no. 5, pp. 485–493, Jul. 1999.
- [141] J. Charrier, "Développement de méthodologies dédiées à l'analyse robuste de la tenue de structures composites sous chargements complexes tridimensionnels," Thèse, École Nationale Supérieure d'Arts et Métiers, 2013.
- [142] D. Tilbrook, D. Blair, M. Boyle, and P. Mackenzie, "Composite materials with blend of thermoplastic particles."
- [143] D. Purslow, "Some fundamental aspects of composites fractography," *Composites*, vol. 12, no. 4, pp. 241–247, Oct. 1981.
- [144] D. Purslow, "Matrix fractography of fibre-reinforced epoxy composites," *Composites*, vol. 17, no. 4, pp. 289–303, Oct. 1986.
- [145] R. E. Robertson, V. E. Mindroiu, and M.-F. Cheung, "Fracture in epoxy matrix resins," *Compos. Sci. Technol.*, vol. 22, no. 3, pp. 197–207, 1985.
- [146] A. Mazor, L. J. Broutman, and B. H. Eckstein, "Effect of long-term water exposure on properties of carbon and graphite fiber reinforced epoxies," *Polym. Eng. Sci.*, vol. 18, no. 5, pp. 341–349, Apr. 1978.
- [147] M. C. Lee and N. A. Peppas, "Water transport in graphite/epoxy composites," *J. Appl. Polym. Sci.*, vol. 47, no. 8, pp. 1349–1359, 1993.
- [148] J. A. Nairn and S. Hu, "The initiation and growth of delaminations induced by matrix microcracks in laminated composites," *Int. J. Fract.*, vol. 57, no. 1, pp. 1–24, Sep. 1992.
- [149] N. Carrère, N. Tual, T. Bonnemains, E. Lolive, and P. Davies, "Coupled modelling of damage and sea-water absorption in carbon/epoxy laminates."
- [150] A. S. Kaddour, M. J. Hinton, P. A. Smith, and S. Li, "A comparison between the predictive capability of matrix cracking, damage and failure criteria for fibre reinforced composite laminates: Part A of the third world-wide failure exercise," *J. Compos. Mater.*, vol. 47, no. 20–21, pp. 2749–2779, Sep. 2013.
- [151] A. S. Kaddour and M. J. Hinton, "Maturity of 3D failure criteria for fibre-reinforced composites: Comparison between theories and experiments: Part B of WWFE-II," *J. Compos. Mater.*, vol. 47, no. 6–7, pp. 925–966, Mar. 2013.
- [152] M. J. Hinton, A. S. Kaddour, and P. D. Soden, "A comparison of the predictive capabilities of current failure theories for composite laminates, judged against experimental evidence," *Compos. Sci. Technol.*, vol. 62, no. 12–13, pp. 1725–1797, Sep. 2002.
- [153] Z. Hashin, "Finite thermoelastic fracture criterion with application to laminate cracking analysis," *J. Mech. Phys. Solids*, vol. 44, no. 7, pp. 1129–1145, Jul. 1996.
- [154] N. Carrere, F. Laurin, and J.-F. Maire, "Micromechanical-based hybrid mesoscopic three-dimensional approach for non-linear progressive failure analysis of composite structures—Part B: Comparison with experimental data," *J. Compos. Mater.*, p. 0021998312460558, Sep. 2012.

- [155] F. Laurin, N. Carrere, C. Huchette, and J.-F. Maire, "A multiscale hybrid approach for damage and final failure predictions of composite structures," *J. Compos. Mater.*, p. 0021998312470151, Jan. 2013.
- [156] S. O. Nobuo Takeda, "Microscopic fatigue damage progress in CFRP cross-ply laminates," *Composites*, vol. 26, no. 12, pp. 859–867, 1995.
- [157] S. Ogiwara and N. Takeda, "Interaction between transverse cracks and delamination during damage progress in CFRP cross-ply laminates," *Compos. Sci. Technol.*, vol. 54, no. 4, pp. 395–404, 1995.
- [158] Z. Hashin, "Failure Criteria for Unidirectional Fiber Composites," *J. Appl. Mech.*, vol. 47, no. 2, pp. 329–334, Jun. 1980.
- [159] N. Carrere, E. Martin, and D. Leguillon, "Comparison between models based on a coupled criterion for the prediction of the failure of adhesively bonded joints," *Eng. Fract. Mech.*
- [160] P. Moy and F. E. Karasz, "Epoxy-water interactions," *Polym. Eng. Sci.*, vol. 20, no. 4, pp. 315–319, Mar. 1980.
- [161] J. (John) Crank, *The Mathematics of Diffusion*, First Edition. Oxford University Press, 1956.
- [162] J. Crank, *The Mathematics of Diffusion*. 1979.
- [163] N. L. Thomas and A. H. Windle, "A theory of case II diffusion," *Polymer*, vol. 23, no. 4, pp. 529–542, Apr. 1982.
- [164] A. Fick, "Ueber Diffusion," *Ann. Phys.*, vol. 170, no. 1, pp. 59–86, Jan. 1855.
- [165] J. (John) Crank, *The mathematics of diffusion / by J. Crank*. Oxford [England]: Clarendon Press, 1975.
- [166] M. R. Vanlandingham, R. F. Eduljee, and J. W. Gillespie, "Moisture diffusion in epoxy systems," *J. Appl. Polym. Sci.*, vol. 71, no. 5, pp. 787–798, Jan. 1999.
- [167] J. S. Vrentas and C. M. Vrentas, "Fickian diffusion in glassy polymer-solvent systems," *J. Polym. Sci. Part B Polym. Phys.*, vol. 30, no. 9, pp. 1005–1011, Aug. 1992.
- [168] W. P. De Wilde and P. Frolkovic, "The modelling of moisture absorption in epoxies: effects at the boundaries," *Composites*, vol. 25, no. 2, pp. 119–127, Feb. 1994.
- [169] T. C. Wong and L. J. Broutman, "Moisture diffusion in epoxy resins Part I. Non-Fickian sorption processes," *Polym. Eng. Sci.*, vol. 25, no. 9, pp. 521–528, Jun. 1985.
- [170] H. G. Carter and K. G. Kibler, "Langmuir-Type Model for Anomalous Moisture Diffusion In Composite Resins," *J. Compos. Mater.*, vol. 12, no. 2, pp. 118–131, Jul. 1978.
- [171] The analytical theory of heat: Fourier, Jean Baptiste Joseph, baron, 1768-1830 : <https://archive.org/details/analyticaltheory00fourrich>.
- [172] S. C. George and S. Thomas, "Transport phenomena through polymeric systems," *Prog. Polym. Sci.*, vol. 26, no. 6, pp. 985–1017, Aug. 2001.
- [173] J. Zhou and J. P. Lucas, "The effects of a water environment on anomalous absorption behavior in graphite/epoxy composites," *Compos. Sci. Technol.*, vol. 53, no. 1, pp. 57–64, 1995.
- [174] L.-W. Cai and Y. Weitsman, "Non-Fickian Moisture Diffusion in Polymeric Composites," *J. Compos. Mater.*, vol. 28, no. 2, pp. 130–154, Jan. 1994.
- [175] R. M. Barrer, "Diffusion and permeation in heterogeneous media," New York, 1968.
- [176] C.-H. Shen and G. S. Springer, "Moisture Absorption and Desorption of Composite Materials," *J. Compos. Mater.*, vol. 10, no. 1, pp. 2–20, Jan. 1976.
- [177] G. S. Springer and S. W. Tsai, "Thermal Conductivities of Unidirectional Materials," *J. Compos. Mater.*, vol. 1, no. 2, pp. 166–173, Apr. 1967.
- [178] K. Kondo and T. Taki, "Moisture Diffusivity of Unidirectional Composites," *J. Compos. Mater.*, vol. 16, no. 2, pp. 82–93, Mar. 1982.
- [179] M. T. Aronhime, S. Neumann, and G. Marom, "The anisotropic diffusion of water in Kevlar-epoxy composites," *J. Mater. Sci.*, vol. 22, no. 7, pp. 2435–2446, Jul. 1987.
- [180] C. D. Shirrell and J. Halpin, "Moisture absorption and desorption in epoxy composite laminates," *ASTM Spec. Tech. Publ.*, no. 617, pp. 514–528, 1977.
- [181] J. C. H. Afdl and J. L. Kardos, "The Halpin-Tsai equations: A review," *Polym. Eng. Sci.*, vol. 16, no. 5, pp. 344–352, May 1976.

- [182] E. R. Long, "Moisture Diffusion Parameter Characteristics for Epoxy Composites and Neat Resins.," Aug. 1979.
- [183] H. Ramezani Dana, A. Perronnet, S. Fréour, P. Casari, and F. Jacquemin, "Identification des paramètres de diffusion d'humidité des matériaux composites à matrices organiques," in *17èmes Journées Nationales sur les Composites (JNC17)*, Poitiers-Futuroscope, France, 2011, p. 77.
- [184] S. Roy, "Modeling of Anomalous Moisture Diffusion in Polymer Composites: A Finite Element Approach," *J. Compos. Mater.*, vol. 33, no. 14, pp. 1318–1343, Jul. 1999.
- [185] S. Roy and S. Singh, "Analytical modeling of orthotropic diffusivities in a fiber reinforced composite with discontinuities using homogenization," *Compos. Sci. Technol.*, vol. 69, no. 11–12, pp. 1962–1967, Sep. 2009.
- [186] K. Derrien and P. Gilormini, "The effect of moisture-induced swelling on the absorption capacity of transversely isotropic elastic polymer–matrix composites," *Int. J. Solids Struct.*, vol. 46, no. 6, pp. 1547–1553, Mar. 2009.
- [187] S. P. Pilli and L. V. Smith, "The Effect of Pressure on Moisture Diffusion in Polymer Matrix Composites," *Int. J. Thermophys.*, vol. 33, no. 8–9, pp. 1715–1725, Nov. 2012.
- [188] D. Choqueuse and P. Davies, "18 - Ageing of composites in underwater applications," in *Ageing of Composites*, R. Martin, Ed. Woodhead Publishing, 2008, pp. 467–498.
- [189] P. Davies and D. Choqueuse, "12 - Ageing of composites in marine vessels," in *Ageing of Composites*, R. Martin, Ed. Woodhead Publishing, 2008, pp. 326–353.
- [190] A. C. Loos and G. S. Springer, "Moisture Absorption of Graphite-Epoxy Composites Immersed in Liquids and in Humid Air," *J. Compos. Mater.*, vol. 13, no. 2, pp. 131–147, Apr. 1979.
- [191] J. B. Sturgeon, "Creep, repeated loading, fatigue and crack growth in $\pm 45^\circ$ oriented carbon fibre reinforced plastics," *J. Mater. Sci.*, vol. 13, no. 7, pp. 1490–1498, Jul. 1978.
- [192] A. B. de Moraes, "A new fibre bridging based analysis of the Double Cantilever Beam (DCB) test," *Compos. Part Appl. Sci. Manuf.*, vol. 42, no. 10, pp. 1361–1368, Oct. 2011.
- [193] P. Davies, W. Cantwell, C. Moulin, and H. H. Kausch, "A study of the delamination resistance of IM6/PEEK composites," *Compos. Sci. Technol.*, vol. 36, no. 2, pp. 153–166, 1989.
- [194] F.-H. Leroy, "Rupture des composites unidirectionnels à fibres de carbone et matrice thermodurcissable: approche micro–macro," Université de Bordeaux I, Bordeaux France, 1996.
- [195] D. Lévêque, A. Schieffer, A. Mavel, N. Chemineau, and J.-F. Maire, "Analyse multiéchelle des effets du vieillissement sur la tenue mécanique des composites à matrice organique," *Rev. Compos. Matér. Avancés*, vol. 12, no. 1, pp. 139–162, Apr. 2002.
- [196] J. M. Augl and A. E. Berger, "The Effect of Moisture on Carbon Fiber Reinforced Epoxy Composites. 1. Diffusion," DTIC Document, 1976.
- [197] A. P. Mouritz, K. H. Leong, and I. Herszberg, "A review of the effect of stitching on the in-plane mechanical properties of fibre-reinforced polymer composites," *Compos. Part Appl. Sci. Manuf.*, vol. 28, no. 12, pp. 979–991, 1997.
- [198] G. Pritchard and S. D. Speake, "The use of water absorption kinetic data to predict laminate property changes," *Composites*, vol. 18, no. 3, pp. 227–232, Jul. 1987.
- [199] K. Kondo and T. Taki, "Moisture Diffusivity of Unidirectional Composites," *J. Compos. Mater.*, vol. 16, no. 2, pp. 82–93, Mar. 1982.
- [200] L.-R. Bao and A. F. Yee, "Moisture diffusion and hygrothermal aging in bismaleimide matrix carbon fiber composites—part I: uni-weave composites," *Compos. Sci. Technol.*, vol. 62, no. 16, pp. 2099–2110, Dec. 2002.
- [201] L.-R. Bao and A. F. Yee, "Moisture diffusion and hygrothermal aging in bismaleimide matrix carbon fiber composites: part II—woven and hybrid composites," *Compos. Sci. Technol.*, vol. 62, no. 16, pp. 2111–2119, Dec. 2002.
- [202] B. Dewimille and A. R. Bunsell, "The modelling of hydrothermal aging in glass fibre reinforced epoxy composites," *J. Phys. Appl. Phys.*, vol. 15, no. 10, p. 2079, Oct. 1982.
- [203] M. Blikstad, P. O. W. Sjöblom, and T. R. Johannesson, "Long-Term Moisture Absorption in Graphite/Epoxy Angle-Ply Laminates," *J. Compos. Mater.*, vol. 18, no. 1, pp. 32–46, Nov. 1984.

- [204] J. Mercier, A. Bunsell, P. Castaing, and J. Renard, "Characterisation and modelling of aging of composites," *Compos. Part Appl. Sci. Manuf.*, vol. 39, no. 2, pp. 428–438, Feb. 2008.
- [205] N. Roe, Z. Huo, K. Chandrashekhara, A. Buchok, and R. Brack, "Advanced moisture modeling of polymer composites," *J. Reinf. Plast. Compos.*, vol. 32, pp. 437–449, Apr. 2013.
- [206] L. P. Canal and V. Michaud, "Micro-scale modeling of water diffusion in adhesive composite joints," *Compos. Struct.*, vol. 111, pp. 340–348, May 2014.
- [207] Y. WEITSMAN, "Chapter 9 - Moisture in Composites: Sorption and Damage," in *Composite Materials Series*, vol. 4, K. L. Reifsnider, Ed. Elsevier, 1991, pp. 385–429.
- [208] Y. J. Weitsman, "Anomalous fluid sorption in polymeric composites and its relation to fluid-induced damage," *Compos. Part Appl. Sci. Manuf.*, vol. 37, no. 4, pp. 617–623, Apr. 2006.
- [209] Y. Weitsman, "Coupled damage and moisture-transport in fiber-reinforced, polymeric composites," *Int. J. Solids Struct.*, vol. 23, no. 7, pp. 1003–1025, 1987.
- [210] C. Suri and D. Perreux, "The effects of mechanical damage in a glass fibre/epoxy composite on the absorption rate," *Compos. Eng.*, vol. 5, no. 4, pp. 415–424, 1995.
- [211] D. Perreux and C. Suri, "A study of the coupling between the phenomena of water absorption and damage in glass/epoxy composite pipes," *Compos. Sci. Technol.*, vol. 57, no. 9–10, pp. 1403–1413, 1997.
- [212] S. Roy and T. Bendorawalla, "Modeling of Diffusion in a Micro-Cracked Composite Laminate Using Approximate Solutions," *J. Compos. Mater.*, vol. 33, no. 10, pp. 872–905, May 1999.
- [213] H. R. Dana, F. Jacquemin, P. Casari, S. Fréour, and A. Perronnet, "Caractérisation du comportement hydro-thermo-mécanique de composite à matrice organique instrumenté par fibre optique: étude de l'adhérence interfaciale."
- [214] L. T. Drzal, M. Madhukar, and M. C. Waterbury, "Adhesion to carbon fiber surfaces: Surface chemical and energetic effects," *Compos. Struct.*, vol. 27, no. 1–2, pp. 65–71, 1994.
- [215] L. T. Drzal and M. Madhukar, "Fibre-matrix adhesion and its relationship to composite mechanical properties," *J. Mater. Sci.*, vol. 28, no. 3, pp. 569–610, Feb. 1993.
- [216] D. Olmos, R. Lopez-Moron, and J. Gonzalez-Benito, "The nature of the glass fibre surface and its effect in the water absorption of glass fibre/epoxy composites. The use of fluorescence to obtain information at the interface," *Compos. Sci. Technol.*, vol. 66, no. 15, pp. 2758–2768, 2006.
- [217] C. Humeau, P. Davies, and F. Jacquemin, "Moisture diffusion under pressure in composites," presented at the 20th International Conference on Composite Materials, Copenhagen, 2015.
- [218] R. Maurin, C. Baley, and P. Davies, "Influence du vieillissement marin sur l'endommagement en sollicitation hors plan de bordé de bateau de course = Influence of sea water aging on damage development in racing boat hull under inplane shear loading.," presented at the JNC 16, 2009, p. 10 p.
- [219] P. Ghidossi, *Contribution à l'étude de l'effet des conditions d'usinage d'éprouvettes en composites à matrice polymère sur leur réponse mécanique*. Paris, ENSAM, 2003.

Abstract

Composite materials are used in many marine structures and new applications are being developed such as tidal turbine blades. The reliability of these components, in a very severe environment, is crucial to the profitability of tidal current energy systems. These structures are subject to many forces such as ocean tides, waves, storms but also to various marine aggressions, such as sea water and corrosion. A thorough understanding of the long term behavior of the moving parts is therefore essential. The majority of tidal turbine developers have preferred carbon blades, so there is a need to understand how long immersion in the ocean affects these composites. In this study the long term behavior of different carbon/epoxy composites has been studied using accelerated ageing tests. A significant reduction of composite strengths has been observed after saturation of the material in seawater. For longer immersions only small further changes in these properties occur. No significant changes have been observed for moduli nor for composite toughness. Changes in properties are initially due to matrix plasticization, followed by reductions due to fibre/matrix interface changes. Damage can affect the long term behavior of composites structures and create new pathways for water diffusion. As a consequence a damage model has been proposed based on a coupled strength/toughness criterion to describe the threshold of damage and on a toughness criterion to describe the crack development kinetics. It describes in a correct manner the damage threshold and kinetics for the as-received material and for material after sea water ageing. The evolution of the rate of water ingress into composite materials has been followed, in order to develop a diffusion model taking into account the anisotropic nature of composites. Then the diffusion model has been applied on a tidal turbine blade. Finally a first investigation of the coupling between the diffusion model and damage has been performed. This study has contributed to the development of tools to quantify long term durability of composite tidal turbine blades.

Résumé

Les matériaux composites sont utilisés dans de nombreuses structures marines et de nouvelles applications sont en cours de développement telles que les pales d'hydroliennes. La fiabilité de ces composants dans environnement très sévère est cruciale pour la rentabilité de ces systèmes récupérateurs d'énergie des courants marins. Ces structures sont sujettes à de nombreuses forces, telles que les courants marins, les vagues, tempêtes mais également diverses agressions marines telles que l'eau de mer et la corrosion. Une compréhension approfondie du comportement au long terme de ces parties mobiles est donc essentielle. La majorité des développeurs d'hydroliennes ont préféré des pales en carbone. Ainsi il est nécessaire de comprendre comment une longue immersion dans l'océan affecte ces composites. Dans cette étude, le comportement au long terme de différents composites carbone/époxy a été étudié en utilisant des essais de vieillissement accéléré. Une diminution significative des résistances des composites a été observée après saturation en eau de mer. Pour des temps d'immersion plus long, seulement peu de changements des propriétés apparaissent. Peu d'effets significatifs ont été observés tant sur les modules que sur la ténacité. Ces changements de propriétés sont initialement dus à la plastification de la matrice, suivis par un affaiblissement de l'interface fibre/matrice. L'endommagement peut affecter le comportement au long terme des structures composites et créer de nouveaux chemins préférentiels pour la diffusion de l'eau. En conséquence un modèle basé sur un critère couplé résistance/ténacité a été proposé pour décrire le seuil d'endommagement et basé sur un critère en ténacité pour décrire la cinétique d'endommagement. Il permet de reproduire d'une manière correcte le seuil et la cinétique d'endommagement pour des matériaux vieillis et non vieillis. L'évolution de l'entrée d'eau dans les composites a été suivie dans le but de développer un modèle de diffusion prenant en compte la nature anisotrope des composites. Ainsi le modèle de diffusion a été utilisé sur pale d'hydrolienne. Finalement des premières investigations sur le couplage entre le modèle de diffusion et l'endommagement ont été réalisées. Cette étude a contribué au développement d'outils pour quantifier la durabilité au long terme des pales d'hydroliennes en composites.